This is to certify that the
dissertation entitled

A THEORETICAL, EXPERIMENTAL AND CFD ANALYSIS OF REGENERATIVE FLOW COMPRESSORS AND PUMPS FOR MICROTURBINE AND AUTOMOTIVE FUEL APPLICATIONS

presented by

Muhammad Mukarram Raheel

has been accepted towards fulfillment
of the requirements for the

Ph.D. Mechanical Engineering

Major Professor's Signature

09/10/03

Date

A THEORETICAL, EXPERIMENTAL AND CFD ANALYSIS OF REGENERATIVE FLOW COMPRESSORS AND PUMPS FOR MICROTURBINE AND AUTOMOTIVE FUEL APPLICATIONS

By

Muhammad Mukarram Raheel

A DISSERTATION

Submitted to
Michigan State University
in partial fulfillment of the requirements
for the degree of

DOCTOR OF PHILOSOPHY

Department of Mechanical Engineering

2003

ABSTRACT

A THEORETICAL, EXPERIMENTAL AND CFD ANALYSIS OF REGENERATIVE FLOW COMPRESSORS AND PUMPS FOR MICROTURBINE AND AUTOMOTIVE FUEL APPLICATIONS

By

Muhammad Mukarram Raheel

Regenerative flow compressors and pumps, hereafter known as RFC/RFP are rotodynamic machines capable of producing high heads at very low flow rates. They can produce heads equivalent to that of several centrifugal stages from a single rotor with comparable tip speed. The compression process is usually not regarded as efficient. Typically regenerative compressors produce less than 50 % efficiency but still they have found many applications, because they allow the use of fluid dynamic compressors in place of positive displacement compressors for duties requiring high heads at low flow rates. Recently Capstone Turbine Corporation has made use of RFC in low pressure (0.2-15 psig) natural gas compression required by its Model C30 microturbine system. Moreover, due to compact size and self priming characteristics of the regenerative pumps, Delphi Automotives has utilized RFP for automotive fuel pumping application.

A detailed discussion of fundamentals, hypothesis of operation, applications, limitations, challenges and future trends in regenerative turbomachines is presented. Experimental data on Capstone single and multistage RFC with radial blades is analyzed in the form of various non-dimensional parameters. A mathematical model to describe the complex three dimensional corkscrew flow pattern in radial and non-radial blade RFC/RFP is presented. Governing equations for blade and channel region are developed and various losses are correlated with geometric and aerodynamic parameters. A performance

prediction code for RFC based on these governing equations and loss models is developed and performance results are compared with test data on Capstone multistage RFC. An extensive sensitivity analysis from the code is performed, based on which some design changes are suggested for performance improvement. Moreover, a generalized design procedure for radial and non-radial blade RFC is proposed in this work.

Application of regenerative turbomachines in automotive fuel pumping is discussed in detail. Delphi Automotives replaced radial blades by non-radial blades to improve performance. Performance of Delphi fuel pump is predicted from the code and compared with test data and some design improvements are suggested after performing a sensitivity analysis on various geometric parameters. Details of CFD analysis on a 3D model of the fuel pump using commercial software "STAR CD" are presented. The regenerative pump with non-radial blades produces hydraulic efficiencies around 40% surpassing all the existing regenerative fuel pump designs in the automotive industry. However, there is still a lot of room for improvement in hydraulic efficiency by employing aerodynamically designed aerofoil blades. Therefore, need was felt to investigate RFC/RFP with aerofoil blades. A compressible flow theory for aerofoil blade RFC is presented in this work. Theoretical performance results are compared with published test data on aerofoil blade RFC. Extensive sensitivity analysis from the code is performed and design changes are suggested for performance improvement. Theoretical analysis shows that aerofoil blading introduced in these turbomachines can enhance isothermal efficiency above 60%. Based on suggested design changes, a new RFC model with aerofoil blades is developed and a CFD analysis is performed. Currently work is in progress to optimize the inlet manifold of aerofoil blade RFC.

To my parents' innumerable sacrifices and untiring support throughout my life

ACKNOWLEDGEMENT

The author is extremely grateful to his thesis advisor, Professor Abraham Engeda for his valuable guidance, support, continuous encouragement and willing attitude throughout this research work. Special thanks go to Professor Tom Shih, Professor Harold Schock and Professor Charles MacCluer for their advice, discussion and interest in this work. The author would like to thank Douglas Hamrin, Greg Rouse, Greg Priddie and Murali Chinta at Capstone Turbine Corporation, CA for initiating this work and providing useful discussions. Special interest taken by Mohammed Aslam and Partab Jeswani at Delphi Energy and Engine Management System, MI in this work is highly appreciated. The author is grateful to Dr. David Nye and Dr. Yunbae Kim at Dresser-Rand Turbo products division, NY for their encouragement and keen interest in this work. Moreover, the author is thankful to Dr. Herbert Sixsmith and Walter Swift at Creare Inc, for their useful suggestions towards completion of this work. The author also appreciates technical assistance, productive discussions and great friendship with Jae Wook Song, who was extremely helpful in completion of this work. Author would like to express special thanks to all the members of Turbomachinery lab including Dr. Norbert Mueller, Jae Wook Song, Faisal Mahroogi, Zeyad Alsuhaibani, Donghui Zhang, Yinghui Dai, Pezhman Akbari, Amir Kharazi, Toshiyuki Sato, Devon Washington, Umar Farooq and Saqib Riaz. Moreover, it is my duty to mention the contribution of all my instructors in the National University of Sciences and Technology (NUST), Pakistan who taught and encouraged me to reach this point. Last but not the least, the author is grateful to members of his family: his father, Ch. Mohammad Altaf, his mother Mrs. Parveen Altaf, elder brother Khurram Adeel and endless love and continuous support of his wife Saddaf Raheel.

TABLE OF CONTENTS

LIST OF TABLES

LIST OF FIGURES

(Images in this dissertation are presented in color)

NOMENCLATURE

a_c	Shear area of casing
a_i	Shear area of impeller
A_b	Area of blade
A_c	Channel area
A_R	Area at any radial location R_p
b	Blade depth
BF	Blade blockage factor
c_a	Axial clearance
c_r	Radial clearance
C_c	Shear stress coefficient of casing
C_D	Orifice discharge coefficient
C_i	Shear stress coefficient of impeller
C_p	Specific heat at constant pressure
d_A, d_B	Channel depth at station A and B
dX_G	Peripheral distance
D_h	Hydraulic diameter
e	Impeller blade height
f_R, f_C	Rotor and Casing friction factor
F_s	Fraction of periphery occupied by impeller seal

g	Acceleration due to gravity
H	Head
H_b	Aerofoil blade height
H_1, H_2	Total enthalpy of fluid at inlet and exit of impeller blade
k_b	Blade turning loss coefficient
k_{in}, k_{out}	Inlet and discharge port loss coefficients
k_s	Blade mixing loss
k_{se}	Sudden expansion loss
k_t	Channel turning loss coefficient
K_t	Head loss coefficient
l	Aerofoil blade chord length or Flow path length
L_1, L_2	Length of blading at inlet and outlet edges
$\dot{m}$	Mass flow rate
M_{OT}	Impeller tip Mach number
$\dot{M}_A$	Mass flow rate through annular channel
$\dot{M}_B$	Mass flow rate through blading
N_B	Number of passages of fluid between inlet and outlet ports
N_s	Specific speed
p	Pressure
p_{in}, p_{out}	Inlet and discharge pressure
$\dot{P}_{decomp.}$	Decompression power

$\dot{P}_{disk}$	Disk friction loss power
$\dot{P}_{hyd}$	Hydraulic power
P	Power
PC	Pitch to cord ratio
$\dot{q}$	Non-dimensional heat transfer rate $\left(\dot{Q}/\rho_{00}\, a_{00}^{3} H_{b2}^{2}\right)$
Q	Volume flow rate
Q_c	Circulatory flow rate
Q_{leak}	Leakage flow rate
Q_s	Flow rate based on solid body rotation
$\dot{Q}$	Heat transfer rate
r_G	Centroidal radius
r_2, r_e	Impeller tip and hub radius
R	Gas constant
Re	Reynolds number
S	Transverse component of path length
t	Blade thickness
T	Torque, Temperature
T_1, T_2	Absolute temperature of fluid at inlet and exit port
U_1, U_2	Tangential velocity of impeller at hub and tip
V_c	Circulatory velocity
V_θ	Tangential velocity

V_m	Mean tangential fluid velocity
$V_{\theta 1}, V_{\theta 2}$	Tangential velocity of fluid at inlet and exit of impeller
W_1, W_2	Relative velocities of fluid with respect to blading
Z	Number of impeller blades
Z_s	Number of blades in stripper

Symbols

α	Shock loss coefficient
β	Blade angle
β_1, β_2	Fluid angles at inlet and outlet edges of blading
γ	Ratio of specific heats
Υ	Power coefficient
η	Efficiency
ρ_1 , ρ_2	Density at inlet and outlet edges of blading
ρ_M	Mean density of fluid in annular channel
ω	RPM
θ	Tangential angle
θ_p, θ_s	Pumping and stripper angle respectively
σ	Slip factor
Ψ	Head coefficient
λ	Flow coefficient
Π	Pressure ratio
Φ	Specific mass flow rate

CHAPTER 1

INTRODUCTION

1.1 Turbomachinery

Turbomachinery is the science of using working fluids to boost output, either increase or decrease pressure by using machinery. The original meaning of turbo is "spins or whirls around". The term turbomachinery applies to rotating (as opposed to reciprocating) machinery that either extracts or adds energy to fluids by the dynamic action of one or more moving blade rows. The rotor changes the stagnation enthalpy, kinetic energy and stagnation pressure of the fluid. This broad definition covers everything from a classic Dutch windmill to the space shuttle main engine turbopumps. Turbomachinery is a major component in aerospace and marine vehicle applications, land propulsion systems, energy applications, hydraulic, gas and steam turbines, industrial pipeline and processing equipment such as gas, petroleum and water pumping plants. Moreover, turbomachinery has a wide variety of other applications (e.g. heart-assist pumps, industrial compressors and refrigeration plants).

Turbomachines can be of different types depending on application. Turbines are turbomachines which produce power by expanding a continuously flowing fluid to a lower pressure or head. Pumps are turbomachines which increase the pressure or head of a flowing liquid. Fans is term used for turbomachines imparting only a small pressure rise

to a continuously flowing gas, usually with a density ratio across the machine of less than 1.05 such that the gas may be considered to be incompressible. Compressors are turbomachines imparting a large pressure rise to a continuously flowing gas with a density ratio in excess of 1.05. The fundamentals and operating principle of pumps and compressors is very similar. Pumps are used primarily for pumping the liquid media and compressors are employed for gas compression. Due to close resemblance in pumps and compressors, this dissertation discusses regenerative flow pumps and compressors in tandem.

1.2 Classification of Compressors

A compressor converts shaft power to a rise in enthalpy of a fluid. The fluid, often a gas, enters the compressor at a low pressure (low enthalpy) and exits at a high pressure (high enthalpy). The rotating shaft is attached to a blade assembly. The rotating blades push on the gas and increase the pressure, thereby increasing the enthalpy. The earliest compressors were bellows, used by blacksmiths to intensify the heat in their furnaces. The first industrial compressors were simple reciprocating piston-driven machines powered by a water wheel.

There are various types of compressors being used in industry because of the almost infinite range of service requirements. Before a compressor type can be selected for a particular application, certain basic information relating to its performance requirements should be at hand. This includes: pressure ratio, flow rate, efficiencies desired and could include other special characteristics. One can then consider the type of machine desired from a range of types of compressors available, as shown in Figure 1.1. Broadly

speaking there are two basic compressor types: positive displacement compressors and continuous flow compressors.

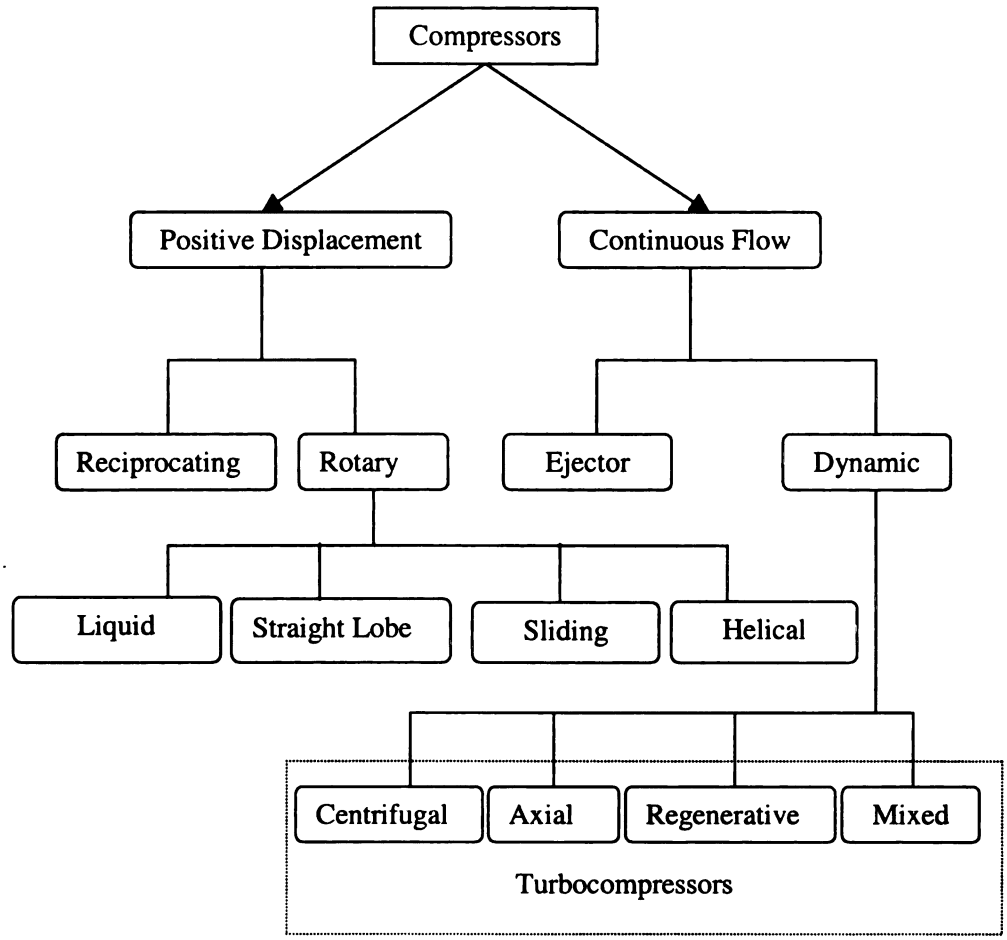

Figure 1.1 Classification of compressors

In the positive displacement type, a given quantity of air or gas is trapped in a compression chamber and the volume which it occupies is mechanically reduced, causing a corresponding rise in pressure prior to discharge. At constant speed, the air flow remains essentially constant with variations in discharge pressure. These compressors are

available in two types: reciprocating and rotary. Reciprocating compressors work like bicycle pumps. A piston, driven through a crankshaft and connecting rod by an electric motor reduces the volume in the cylinder occupied by the air or gas, compressing it to a higher pressure. Single-acting compressors have a compression stroke in only one direction, while double-acting units provide a compression stroke as the piston moves in each direction. Large industrial reciprocating air compressors are double-acting and water-cooled. Multistage double-acting compressors are the most efficient compressors available, and are typically larger, noisier and more costly than comparable rotary units. Reciprocating compressors are available in sizes from less than 1 hp to more than 600 hp. Rotary compressors have gained popularity and are now the "workhorse" of American industry. They are most commonly used in sizes from about 30-200 hp. The most common type of rotary compressor is the helical twin screw-type (also known as rotary screw or helical lobe). Male and female screw-rotors mesh, trapping air and reducing the volume of the air along the rotors to the air discharge point. Rotary screw compressors have low initial cost, compact size, low weight and are easy to maintain. Rotary screw compressors are available in sizes from 3-600 hp and may be air or water-cooled. Less common rotary compressors include sliding vane, liquid piston and straight lobe. Both Reciprocating and rotary compressors will not be considered further in this dissertation.

Continuous flow compressors work by the principle of accelerating the fluid to a high velocity and then converting this kinetic energy into potential energy, manifested by an increase in pressure by decelerating the gas in diverging channels. The continuous flow compressors are categorized into ejector and dynamic type compressors. The dynamic compressors are subdivided into axial, centrifugal, mixed type and regenerative

compressors. These four categories are also called Turbocompressors. They can be further classified into three broad categories based on the path of flow through the machine as discussed below.

1.3 Turbocompressors

Turbcompressors can be classified based on the nature of flow path through the passages of the rotor. When the meridional flow path is axial, the compressors are called axial compressors. They are composed of several rows of airfoil cascades. Some of the rows, called rotors, are connected to the central shaft and rotate at high speed. Other rows, called stators, are fixed and do not rotate. The job of the stators is to increase pressure and keep the flow from spiraling around the axis by bringing the flow back parallel to the axis. The second category is radial or centrifugal compressors, which have predominantly radial flow path. In axial compressors the deceleration takes place in the stator blade passages and in centrifugal compressors it takes place in the diffuser. One obvious difference between these two types of compressors is that, in axial compressors, the flow leaves the compressor in the axial direction, whereas, in centrifugal compressors, the flows leaves the compressor in a direction perpendicular to the axis of the rotating shaft. The third category is called the mixed flow compressors in which the flow path is partially axial and partially radial. Mixed flow compressors have impellers and rotors which combine the characteristics of both axial and centrifugal compressors.

The regenerative flow compressors and pumps, hereafter known as RFC/RFP are rotodynamic turbomachines capable of developing high pressure ratios in a single stage. They permit a head equivalent to that of several centrifugal stages obtained from a single rotor with comparable tip speeds. The fluid in a regenerative flow compressor moves

helically in the casing and reenters the impeller many times in its peripheral path from inlet to discharge. This repetitive action of the impeller blading on fluid is, in effect, "multistaging" and accounts for the high head per stage characteristic of this type of turbomachines. The regenerative flow pumps are also known as Peripheral pump, Side channel pump. Turbine pump, Drag Pump, Traction pump, Tangential pump and Vortex pump in literature. The main characteristics of regenerative turbomachines are their ability to generate high heads at low flow rates. They have a very low specific speed and share some of the characteristics of positive displacement machines such as a roots blower, but without problems of lubrication and wear. In addition to self priming characteristics, the main advantage offered by a RFP/RFC is the ability to develop much higher heads than any other type of turbomachine with the same tip speed. When a regenerative flow turbomachine is applied as a gas compressor, there is further advantage of no surge or stall instability.

1.4 Objective of research

The objective of present study is to improve existing designs of regenerative turbomachines and improve the efficiency. During last twenty years, there has not been much research done on RFC/RFP to improve the efficiency. With the development of commercial softwares and advanced manufacturing techniques over last few years, the industry has shown interest to modify the conventional designs of regenerative turbomachines with aerodynamically improved designs. There are no reliable theoretical models to forecast performance of regenerative turbomachines using geometric parameters as input. Most of the available theoretical models need extensive experimental support to predict the performance. Therefore, it is not easy to make design changes and

improve the performance. Most of the researchers carried out experimental analysis to study the effect of various geometric and aerodynamic parameters on performance. Experimentation is always very expensive and time consuming. Therefore, the objective of current research is to develop theoretical means to predict the performance of existing regenerative turbomachines. After predicting the performance, extensive sensitivity analysis is performed to study which design changes are effective for performance improvement. Design guidelines for improved performance are proposed from the sensitivity analysis. Some design criteria are developed in this work, which can be very useful for designers and engineers working in regenerative turbomachinery. Proposed design changes need validation by CFD before prototype models can be built. There is not much evidence available in the literature about CFD analysis on regenerative turbomachines using commercially available CFD softwares. Therefore, it is one of the objectives of this dissertation to introduce and motivate industry to use CFD analysis to get a better insight in the complicated flow mechanism in regenerative turbomachines.

This research is carried out in association with two organizations. Capstone Turbine Corporation, CA has made use of a multistage RFC for low pressure (0.2-15 psig) natural gas compression for its C30 microturbine system. The compressor design builds required pressure ratio but with very low isothermal efficiency in the range of 15-20% at the design point. These efficiency levels are very low and there is significant room for improvement. Thus, experimental data on Capstone single and multistage RFC is analyzed to study the performance characteristics of the compressor. Correlations among various non-dimensional parameters are developed from experimental data to make this discussion attractive for designers and engineers working in regenerative turbomachinery.

A theory to describe the complex helical fluid flow in radial and non-radial blade RFC/RFP is presented. Governing equations are derived and loss models are proposed, based on which a performance prediction code is developed. This code takes compressor geometry information and inlet conditions as input and predicts the performance. The theoretical results are matched with the test data to verify the proposed model. After overlapping theoretical results and test data, a design sensitivity analysis is performed on various geometric parameters to study which design changes affect compressor performance. A new and improved design for Capstone multistage RFC is proposed based on sensitivity analysis results.

Delphi Automotives, MI utilizes regenerative fuel pumps for raising head of gasoline contained in the fuel tank and delivering it to fuel injectors at sufficient flow rate and pressure. The present design of Delphi fuel pump comprises of non-radial blades producing hydraulic efficiency around 40%, making it best available RFP design in automotive industry at the moment. However, there seems a lot of room for improvement by replacing the non-radial impeller blades by aerodynamically designed aerofoil blades. The performance prediction code for RFC/RFP is used to predict the performance of non-radial blade automotive fuel pump. After predicting the performance with the code and performing a sensitivity analysis on various geometrical elements of the pump, few design suggestions are proposed. However, it is observed that there is not much increase in hydraulic efficiency expected by keeping the traditional non-radial blades. This motivated the researcher to investigate the possibility of employing aerofoil blades to the regenerative turbomachines and proposing an entirely new design. There is not much evidence available in literature on aerofoil blade RFP. However, it is found from

literature that aerofoil blade RFC can produce isothermal efficiencies in excess of 55%. Some experimental data and geometry information on two aerofoil blade RFC designs is available in literature.

A compressible flow theory is proposed which enables to predict the performance of aerofoil blade RFC/RFP. The compressible flow theory is used to develop another performance prediction code, specifically to predict performance of aerofoil blade RFC/RFP. Excellent agreement between theoretical prediction and experimental data on available RFC designs is observed. This led the researcher to perform a sensitivity analysis for various geometric parameters of aerofoil blade design to improve the performance. The idea of decompression ducts is used to reduce the power consumption which results in significant performance improvement. Based on findings from the theory, a new RFC model with aerofoil blades is developed in "UNIGRAPHICS". A CFD analysis is performed in "STAR CD" to validate the theoretical prediction of efficiencies in excess of 55%. Currently work is in progress to optimize the inlet manifold of aerofoil blade RFC for better performance.

1.5 Outline of thesis

This dissertation consists of ten chapters starting with a detail discussion of fundamentals, hypothesis of operation, applications, limitations and challenges faced by regenerative turbomachines in chapter 2. Chapter 3 deals with previous research work done on RFC/RFP. The literature survey presented in chapter 3 consists of previously presented theoretical models, experimental investigations, blade designs, loss analysis and CFD work performed on regenerative turbomachines. Chapter 4 discusses application of RFC in microturbine systems. Non-dimensional geometry and experimental data of Capstone

single and multistage RFC is presented and analyzed. Chapter 5 discusses a theoretical analysis of complex helical flow in regenerative turbomachines. Governing equations and loss models are developed in chapter 5. Chapter 6 presents results of design sensitivity analysis from the performance prediction code along with suggestions for improved design of multistage RFC for Capstone C30 microturbine system.

Chapter 7 opens up a new subject and discusses application of regenerative turbomachines in automotive fuel pumping. Performance prediction of Delphi regenerative fuel pump is compared with experimental data along with some suggestions for design improvement. Moreover details of CFD analysis on Delphi fuel pump are also presented in this chapter. Chapter 8 targets on development of aerofoil blade regenerative compressors with the idea of decompression ducts to reduce the power requirement. A compressible flow theory for aerofoil blade RFC is presented. Theoretical and available test data are compared and suggestions for design improvement are provided. Chapter 9 discusses CFD analysis on aerofoil blade RFC design. In chapter 10, attempts are made to draw conclusions focusing mainly on performance improvement of regenerative turbomachines. Suggestions for future research in this area are provided at the end of dissertation.

CHAPTER 2

THE REGENERATIVE TURBOMACHINES

The unique design and operational features of regenerative turbomachines have excited many researchers to investigate their characteristics. They are identified by the application of combined radial and toroidal flow. They are partly axial and partly radial in design and function. A typical regenerative turbomachine is shown in Figures (2.1 and 2.2). In contrast to other popular types of continuous flow compressors and pumps in which the fluid passes through the impeller once, regenerative turbomachines have the fluid exposed to the impeller many times. The flow through a RFC/RFP resembles a corkscrew flow pattern as illustrated in Figure 2.1 by the help of a streamline passing through the impeller. To visualize the path which the fluid follows, imagine a spring that has been stretched too far, so that the coils no longer touch. Take that stretched spring, form it into a circle, and lay it on the impeller blade. This situation is depicted in Figure 2.1. As the coiled spring is followed, the progression of movement from one blade to the trailing blade is seen. Depending on how far the spring has been stretched (the distance between coils could be large relative to the coil diameter) the pitch of one loop may span more than the distance between adjacent blades. As the discharge pressure increases, the pitch of the loops in the helix gets smaller in a manner analogous to compression of the spring. It has been visually confirmed that as the discharge pressure increases, the helical pitch of the fluid becomes shorter. There is additional energy imparted to the fluid each

time it passes through the blades of the impeller, allowing substantially more motive force to be added which enables much higher pressures to be achieved in a more compact design. Each passage through the vanes may be regarded as a conventional stage of compression. It is due to the repeated flow through impeller blades that has made a regenerative compressor capable of replacing a 7 or 8 stage centrifugal compressor, producing the same head. Thus the equivalent of several stages of compression may be obtained from a single impeller in a relatively smaller compressor. This is because the head coefficient obtainable from this machine is of an order of magnitude higher than obtainable from a centrifugal machine. This compression process, however, cannot be regarded as efficient. Typically the regenerative compressors have less than 50% efficiency, but still they have found many applications because they allow the use of fluid dynamic compressors in place of positive displacement compressors for duties requiring high head and low flow rates. The efficiency limitation of regenerative turbomachinery is shown in Figure 2.3, which shows the comparative efficiency of low specific speed compressors of centrifugal type and various regenerative designs as a function of specific speed. It can be seen that the regenerative machine has tended to peak at about 50% efficiency in the low specific speed range, while centrifugal picks up from this point. Also, it can be noted that in very low specific speed ranges, the regenerative is more efficient than the centrifugal compressors. Although, regenerative turbomachines are widely used in the industry but there is still a need to study and make design changes in their geometry to improve the performance.

2.1 Elements of a Regenerative Turbomachine

The essential elements of a regenerative turbomachine are shown in Figure 2.4. Typically, they have an impeller, inlet port, discharge port, stripper, flow passage and a casing. These components are discussed below:

2.1.1 Impeller

Regenerative turbomachines utilize a free rotating impeller just like other types of continuous flow compressors and pumps. The impeller has vanes machined into each side at its periphery, which produce a series of helical flows, returning the fluid repeatedly through the vanes for additional energy as it passes through an open annular channel. Thus the rotation of the impeller causes a helical corkscrew flow pattern of the fluid. The fluid does not discharge freely from the tips of the blades but circulates back to blades many times before leaving the impeller. This motion is composed of a peripheral motion induced in the peripheral stator channel by the rotation of the wheel, superimposed by a circulatory motion in the rotor pockets and stator caused by the centrifugal pressure gradient. The effect of these motions is a gradual increase of air pressure in peripheral direction. It is from this internal "multistaging" or "regeneration" that these turbomachines derive their name. The action of impeller blades operating in series instead of parallel to each other makes them different from centrifugal turbomachines. The impeller is fitted with blades to promote the toroidal flow pattern, consisting of a combined impeller-to-side channel circulation and an annular flow from inlet to outlet. This complex flow regime is not readily amendable to detailed theoretical flow analysis. The fluid is in contact with the fluted portion of the impeller. The impeller, through centrifugal forces, propels the fluid radially outward. The enclosing chambers conduct

the fluid into twin vortices around the impeller blade as shown in Figure 2.5. A very small pressure rise occurs in the vicinity of each impeller blade. Regenerative turbomachines are also designed in multistage configurations to meet certain design requirements. A two stage regenerative compressor is shown in Figure 2.6.

2.1.1.1 Classification of Impeller blades

The impeller of RFC/RFP can have blades of different shapes. Some of the widely used types are radial blades, non-radial blades, semi-circular blades and aerofoil blades. Some examples of these blade shapes are given in Figures 2.7, 2.8 and 2.9. Usually regenerative compressors with the aerofoil blades are fitted with a core. The core serves to guide the circulation through the blading and to minimize the loss due to formation of vortices at the tips of blades. The core can be fixed to the blades and rotate with them or be fixed to machine casing. The blades or vanes are usually cast into the face of the impeller or machined at the periphery. The blades can be constructed as a single row, or as two rows side by side to provide parallel contrarotating paths.

2.1.2 Inlet and Discharge Ports

Inlet and discharge ports connect the external system piping to the flow channel. The fluid enters the flow channel via the inlet port, which is shaped to set up spiral flow around the annular channel. The fluid at high pressure is discharged to the piping from the discharge port. The inlet and outlet ports are shown in Figure 2.4.

2.1.3 Stripper

Between discharge and inlet, the casing clearance is reduced to block the high pressure discharge from the low pressure inlet. In this region, which is also known as stripper or septum, the open channel closes to within a few thousandths of an inch of the sides and

tip of the rotor and allows only the fluid within the impeller to pass through the suction. Clearances between the impeller disk and the casing are kept to a minimum to prevent leakage from the high pressure side back to the low pressure side. The stripper forces the fluid to go out through the discharge port. The stripper also helps to cause the establishment and maintenance of the regenerative flow pattern.

2.1.4 Flow channel

Around greater portion of the periphery, the vanes project into an annular channel in which the cross sectional area is greater than that of the impeller vanes. The casing contains a flow channel or raceway. It is this annular flow channel through which the fluid circulates repeatedly through the impeller vanes. The fluid between the vanes is thrown out and across the annular channel. A violent mixing occurs and the angular momentum acquired by the fluid in its passage between the vanes is transferred to the fluid in this annular channel. The mixing process is accompanied by production of a great deal of turbulence, and this implies an undesirable waste of power.

2.2 Working principle

In conventional fluid dynamic compressors and pumps, the predominant direction of flow through the machine is at right angles to the velocity of the blades, whereas in RFC/RFP the predominant direction of flow through the machine is parallel to the velocity of the blades. Superimposed on the parallel flow is a circulation through the blades and around the core of the annular channel. Every time the fluid passes through the rotor, work is done on it and its stagnation pressure and tangential velocity are increased. The tangential velocity is removed, not by a row of stator blades as in a conventional turbomachine, but

by the action of tangential pressure gradient around the periphery of the machine between the exit conditions and the inlet conditions. Thus by the time the fluid re-enters the blade row, the magnitude of its tangential velocity will be reduced and its direction will be reversed. Hence during each loop of the spiral, the fluid is accelerated in the tangential direction as it passes through the blades and is decelerated by the tangential pressure gradient as it passes round the unbladed part of the channel. Because the flow passes through the same blade row several times between the entry and the exit, the work done on it and hence the pressure rise is considerably greater than that which can be obtained from a conventional turbomachine with the same tip speed. The specific speed is therefore low and the machines operate in the usual range of positive displacement machines. Pressure variation of the fluid as it circulates through the pump for several flow rates is shown in Figure 2.10. These curves suggest five regions in the pump operation, which are also marked in Figure 2.4.

- Inlet region (A): The flow experiences some pressure loss through the inlet region.
- Acceleration region (A-B): The flow enters the working section of pump with a velocity and pressure dependent largely on the inlet region.
- Linear region (B-C): The pressure gradient is constant as indicated in the diagram. This region is referred to as the working section of the pump where the flow pattern is fully developed.
- Deceleration region (C-D): In this region, a deceleration occurs and the kinetic energy of the circulatory velocity is changed as a pressure rise. Therefore, there is a little pressure rise as shown in Figure 2.10.

- Outlet region (D): A loss similar to that at the inlet region occurs at the outlet region.

The head, power, and efficiency relationships as a function of flow rate for a typical regenerative turbomachine are shown in Figure 2.11. It indicates that comparatively high heads can be obtained at low flow rates. This is due to the fact that circulatory velocity is higher at lower flow rate resulting in higher pressure rise. However, the power requirement is also higher at low flow rates. The maximum efficiencies in regenerative turbomachines occur at comparatively large flow rates as shown in Figure 2.11.

2.3 Comparison of regenerative and centrifugal Compressors

The regenerative compressors are frequently in competition with centrifugal compressors for meeting application requirements. Therefore, it is interesting to mention the relative merits of the two operationally different compressors being widely used in the industry. Some of the characteristics of both compressors are discussed below.

1. Centrifugal compressors take in the fluid at center of the impeller and push it radially outward with no axial component of velocity, however regenerative compressors impart both radial and an axial component to fluid flow.
2. In centrifugal compressors, fluid passes through the impeller only once while in regenerative compressors, fluid is exposed to impeller many times, thus adding more energy to the fluid.
3. One of the most significant structural advantages of the regenerative type compressors is that no complex flow passages or vaning is required. They are

simple and easy to machine and there is no need of diffusers and scrolls. Regenerative compressors tend to have more internal components than the centrifugal compressors, and we can cast the centrifugal compressor impeller with the outside diameter machined, however regenerative compressor impeller is completely machined.

4. Centrifugal compressors have large axial length per stage and large overall diameter because of diffusers and scrolls. On the other hand, in the regenerative compressors, the suction and discharge nozzles are at periphery, thus the axial and radial dimensions are small compared to centrifugal compressor. Regenerative compressors provide much more pressure rise in a more compact compressor design.
5. Performance wise, while it is true that centrifugal compressors are inherently more efficient than regenerative compressor types, this may not be true under many conditions. The regenerative compressor is considered a low specific speed machine, and in its normal range of specific speeds, its efficiency compares favorably with that of centrifugal compressors.
6. The power requirement of a regenerative compressor decreases with increasing flow rate, whereas the power requirement increases with increasing flow rate in case of a centrifugal compressor. Moreover, the head and flow rate characteristics of the two machines are also significantly different.
7. The centrifugal compressor surges at low flow rate, sometimes at flow rate as great as 50% of maximum flow rate. In a regenerative compressor, the flow can be shut off without surging; however, there will be a temperature rise. The

regenerative compressors have advantages of stability, since they have a stable operation throughout the flow range (a regenerative compressor will not surge under any condition).

8. Since the regenerative compressor does not surge even at zero flow, stage matching is less critical and off-design operation less restricted than with the centrifugal.
9. Higher rotative speeds and/or a large number of stages are usually required with centrifugal compressors. Regenerative compressors produce heads several times greater for a given impeller tip speed. Head coefficients greater than 5 have been measured on the regenerative types, compared to about 0.7 to 0.8 for the centrifugal. (The maximum theoretical head coefficient for a radial bladed centrifugal compressor with zero prerotation is 1.0).
10. The head vs. flow rate graph for a centrifugal compressor is flatter than for a regenerative compressor. This means that a regenerative compressor can have more ability to deliver fluid at a variable (desired) flow rate, which is something a centrifugal compressor lacks. The volume of fluid in a centrifugal compressor is generally much higher than in a comparable regenerative compressor.
11. Another difference between a regenerative compressor and a centrifugal compressor is that in the centrifugal compressor, gain in pressure is proportional to the square of the peripheral velocity of the impeller, whereas in a regenerative compressor it is the relative velocity to the blades that depends on the pressure gradient.

12. The clearances for regenerative compressors are held to closer tolerances than for the centrifugal compressors.
13. The radial positioning is important in some centrifugal compressor designs; axial positioning should be within about 0.05 inch. In a regenerative compressor, however the axial positioning is within 0.01 to 0.03 inch; radial clearance of 0.01 to 0.020 inch (depends on machine size).
14. The centrifugal compressors have no radial shaft loading except gravitational, but with usual design there can be high axial loading. However, in a regenerative compressor there are no axial shaft loadings with usual design, but there is a radial loading due to pressure difference around periphery.
15. The regenerative compressors have an advantage on centrifugal compressors in quietness and problems due to wear are minimal.

2.4 Applications

Although the efficiency of RFC/RFP is not very high, being usually less than 50%, still they have found many applications in industry because they allow the use of rotodynamic action in place of positive displacement actions. They are being used in increasing number of applications that require high delivery head at low flow rates. The relative simplicity of construction and stable operating characteristics of the regenerative flow compressors are making them more and more attractive to users in several areas, including chemical, petroleum, and nuclear industries. The regenerative gas compressors and liquid pumps have important applications as gas circulators and liquid pumps in accessory systems to the above mentioned activities. RFCs have been proposed for use in hydrogen gas pipelines and as helium compressors for cryogenic applications in space

vehicles. If hydrogen comes into widespread use as a synthetic fuel, large scale pipeline transmission of gaseous hydrogen becomes necessary. Compressor stations along these pipelines will be required to boost the pressure, as is now the practice in natural gas industry. Utilization of regenerative compressor as a hydrogen pipeline compressor offers several advantages as discussed by Hollenberg [30]. RFCs can also be used as natural gas pipeline compressors; in fact, they can be designed to handle both natural gas or hydrogen or any mixture of the two. Further, it may be possible to accomplish this in a single design, which can be adjusted to handle a varying mixture by speed control or other means. Crowe and Schwarz [18] developed a helium regenerative compressor operating on hydrodynamic gas bearings. It was designed for use in Ultra High Temperature Reactor Experiment (UHTREX) because of the highly radioactive system contamination resulting from the investigation of unclad fuel elements. Moreover, RFCs are advantageous for incorporation in small closed cycle helium refrigerators. Gessner [25] reported the development of a four stage regenerative compressor, which was employed in the development of a highly reliable, long life cryogenic refrigerator for space vehicle application. One of the recent applications is in accessory loops and auxiliary systems for nuclear pile operation. They have been considered for pneumatic control drive mechanisms for reactor control systems. Grindell [26] developed a regenerative compressor for gas cooled in-pile loops. Another application of RFCs is in plants, which can be used to separate isotopes of gases whose speeds of sound are in the 300-600 ft/sec range. This takes the compressor operation in the compressible flow range. Because of the reliability, compact size and low maintenance, recently there is an increasing use of regenerative compressors in low pressure (0.2 - 15 psig) natural gas

compression required by microturbine systems. Other applications of RFC include boosting and recycling of hydrogen mixtures and hydrocarbon gases, gas phase reactor recycling, molecular sieve regeneration in gas drying processes, vent/purge gas recovery, fuel gas boosting for GT feed and gas compression in many other industrial processes.

Regenerative blowers are also getting popular in industry. There have been various publications describing different applications of regenerative blowers in industry. Figure 2.12 gives the typical operating range of certain type of blowers. One advantage of regenerative blowers is that relatively simple design changes can produce significant changes in shape of the pressure-flow curves as shown in the Figure 2.13. Pressure is proportional to the square of impeller diameter, and flow is proportional to the cross sectional area swept by the impeller. Therefore, special blowers matched to a particular application may be only a little more costly than standard blowers. Manufacturers can tailor the characteristics of a particular model by varying impeller diameter, impeller cross sectional area, and clearance between impeller and casing.

Cundari and Nuti [19] described the use of regenerative blowers in scavenging of small S.I power plants. The regenerative blower was found to be the most suitable option since it was able to match the engine air breath demand all over its utilization range. Regenerative blowers have found many industrial applications in solids conveying systems. Historically, the pressure and flow rates demanded by many solids conveying systems made roots or vaned-type blowers the almost automatic choice despite their limitations. Some conveying systems operate during severely restricted hours because of the noise of roots type blowers normally used. Many packaging and paper handling jobs were historically beyond the regenerative blowers capability, but now with increasing

emphasis on working environment, the low noise regenerative blowers are welcomed in these areas. Regenerative blowers also find use in sewage treatment and anti-icing services, both of which require considerable volume to be blown against a head of water. There is increasing interest in customers for use of regenerative blowers to provide air for fluidizing powder products in bag filling machines; in pressure and vacuum conveying machinery and for use in the textile industry to provide vacuum for removing stray fibers and lint from knitting machines. Regenerative blowers are also used for powder coating recovery applications, plating, cleaning and rinse tank agitation. Since regenerative blowers provide high airflow capacities at low pressure differentials, they become excellent for air moving applications, such as agitation of bath or aeration of a pond.

RFPs find applications in automotive and aerospace fuel pumping, booster systems, water supply, agriculture industry, shipping and mining, chemical and foodstuff industries and regulation of lubrication and filtering. One of the advantages of regenerative pump is that operation under cavitation does not generally lead to mechanical failure. More advantages of RFP are discussed in chapter 7.

2.5 Limitations and Challenges

Main limitations of regenerative turbomachines are:

1) Low efficiency levels in regenerative turbomachines compared to those levels enjoyed by centrifugal compressors and pumps.
2) Low range of specific speed.

Some of the vital challenges faced by regenerative turbomachines are discussed below:

1) The biggest challenge faced by regenerative turbomachines is to raise the efficiency beyond the levels reached already. This can be achieved by means of improving flow guidance in the compressor.
2) The specific speed range can be extended by designing for higher flow rate through improvement in the inlet and outlet ports, creating a better match of the blading geometries. As a side benefit, this may also contribute to the raising of efficiency if the inlets and outlets can also be designed to provide some turning for the flow.
3) Most of the performance data available in literature dealt with relatively low Mach numbers. Performance data are much needed where compressibility effects must be considered.
4) Research on multistaging presents a big challenge in regenerative turbomachinery.
5) Investigation of flow passage geometry (shape and channel area distribution along the periphery) is a critical factor for performance.
6) Improvement in geometry of the impeller vanes (bending radius, height, penetration and angle) is another challenging area.
7) Improvement in location, orientation and area of inlet/outlet ports can create huge difference in efficiency.
8) Investigation of axial and radial clearances can improve performance.

2.6 Conclusions

The detail insight in regenerative compressors and pumps gives an idea of the hidden potential in these turbomachines for duties requiring high head and low flow rates. The compact size, high reliability and low noise of regenerative turbomachines make them

attractive in certain applications. Better efficiency at low specific speeds makes them a tough competitor of centrifugal turbomachines in low specific speed applications. Thus, there is a need to do research and make design changes in RFC/RFP to improve their performance and make them more attractive to industry.

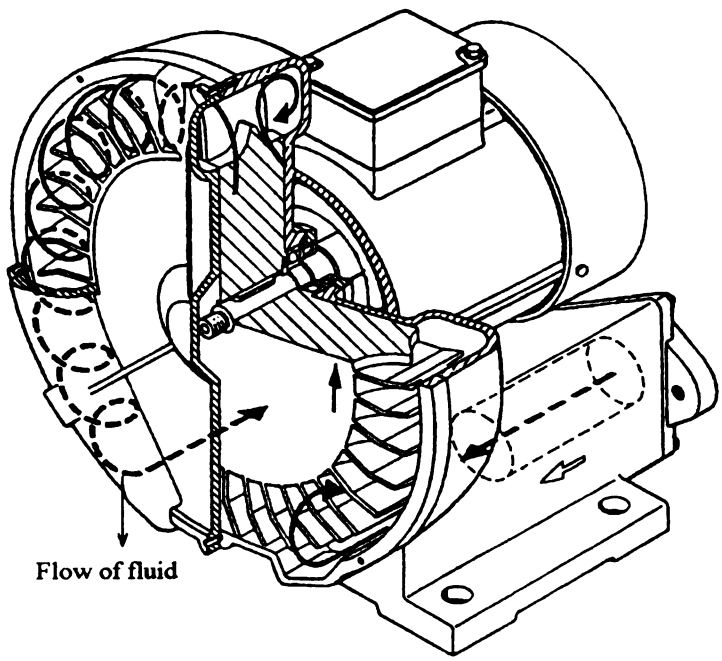

Figure 2.1 A regenerative turbomachine (After Mugele [42])

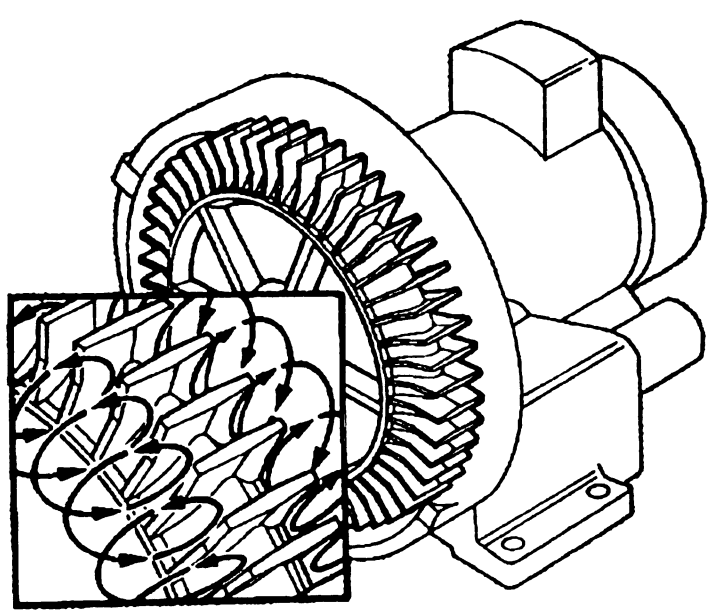

Figure 2.2 A regenerative turbomachine (after Moffat [41])

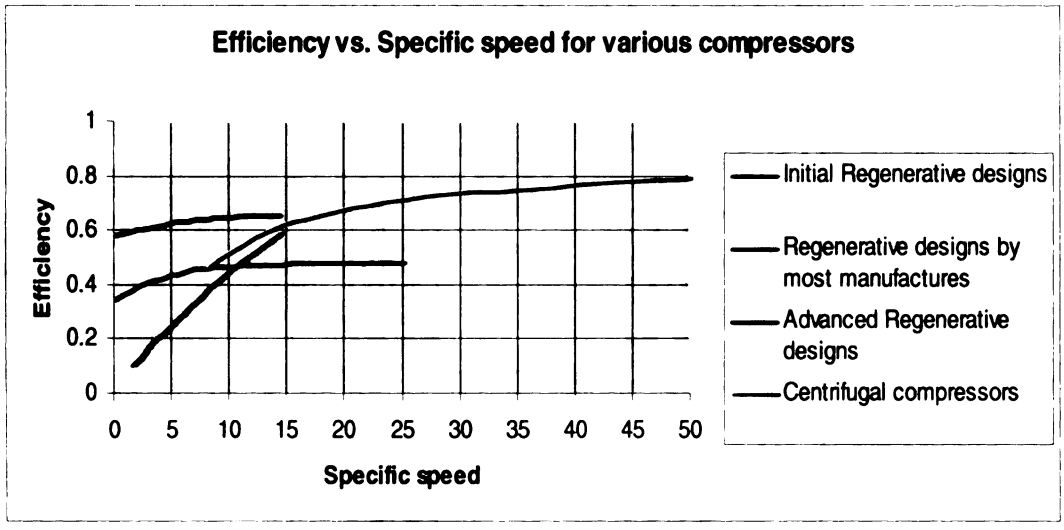

$$Specific\ Speed\ = N_s = \frac{\sqrt{Q}\omega}{H^{\frac{3}{4}}}$$

where, Q (ft^3/sec), ω (rpm), H (ft)

Figure 2.3 Efficiency vs. specific speed for various compressors

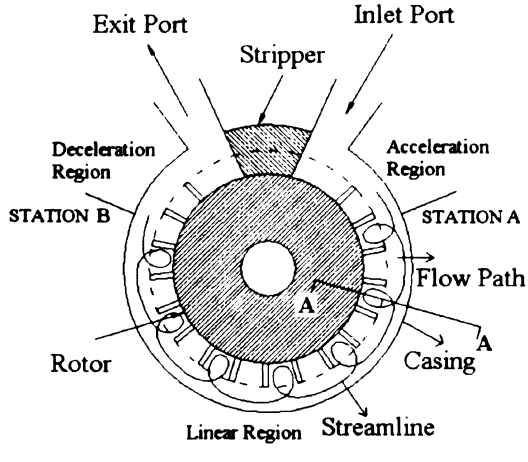

Figure 2.4 Schematic of a regenerative turbomachine

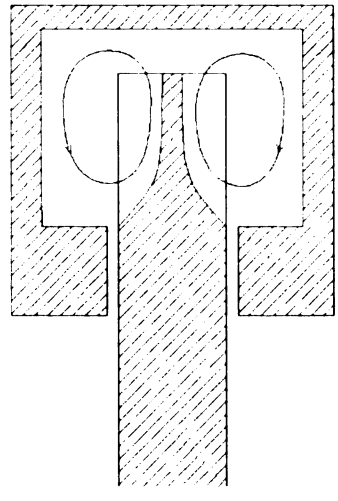

Figure 2.5 Section A-A Enlarged (Radial Blade)

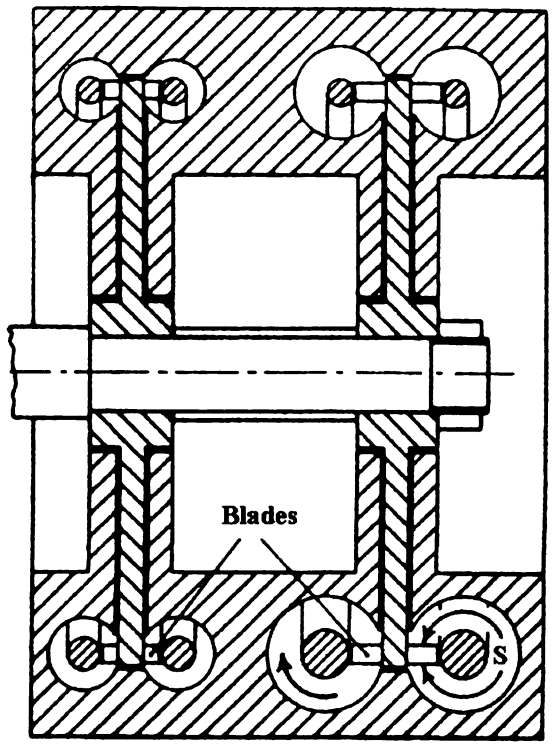

Figure 2.6 Layout of a two-stage regenerative compressor (after Sixsmith [60])

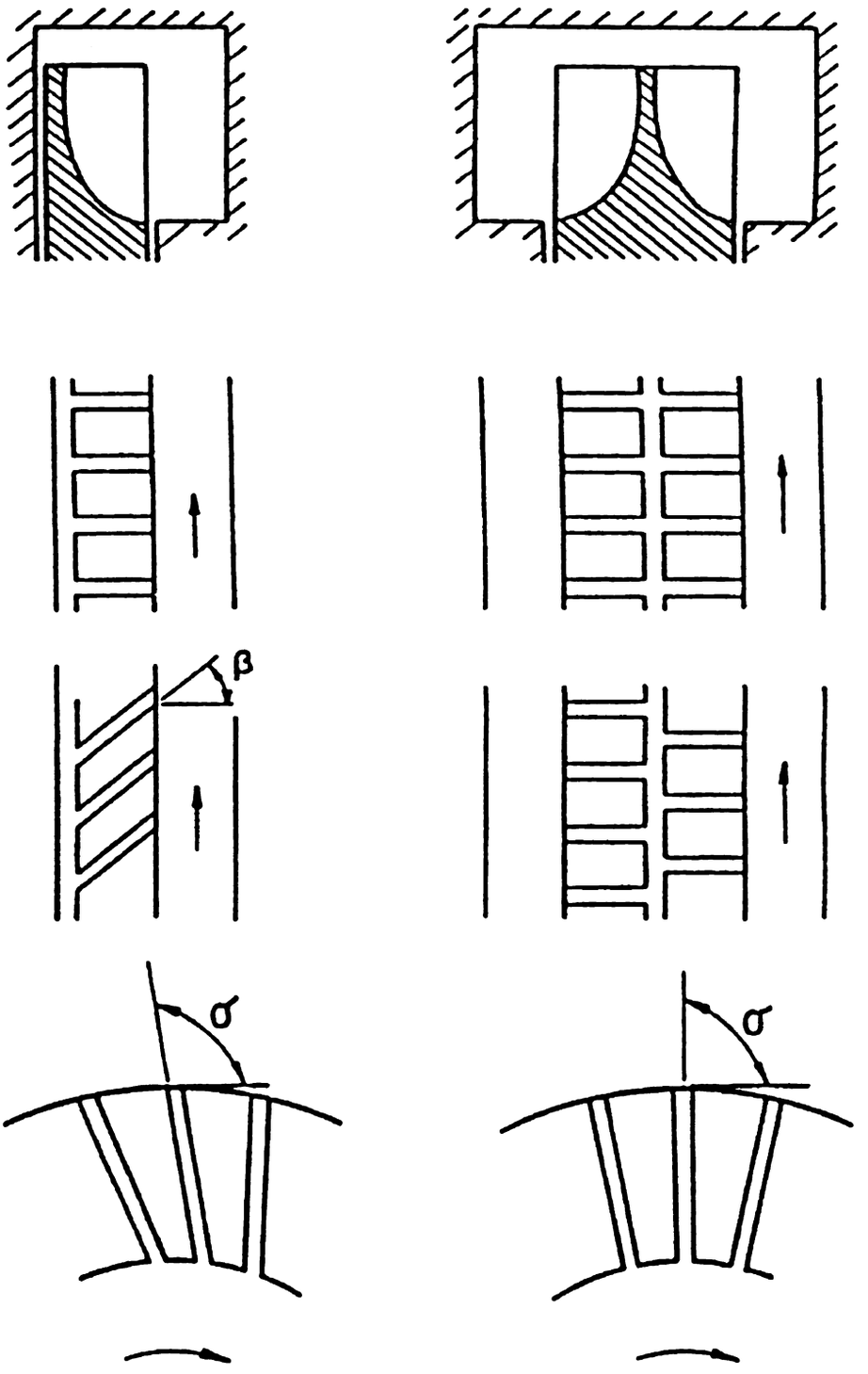

Figure 2.7 Regenerative turbomachines with radial and non-radial blades (after Abdallah [1])

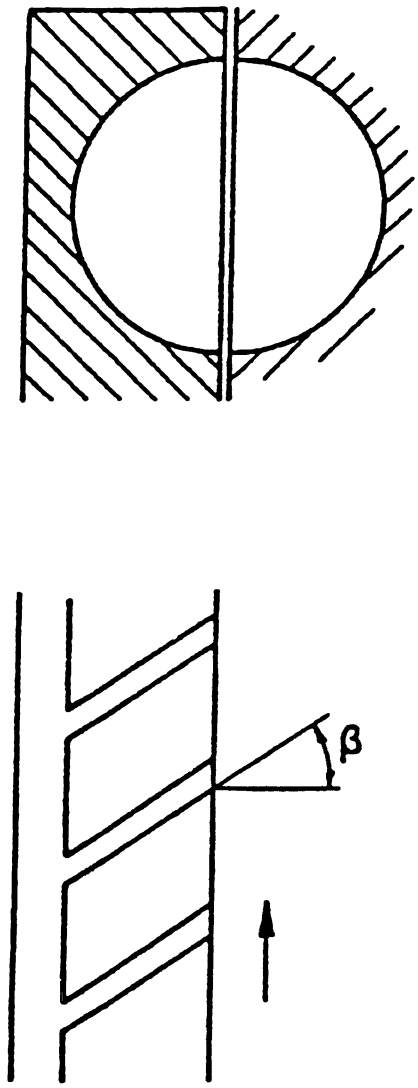

Figure 2.8 Regenerative turbomachines with semi-circular blades (after Abdallah [1])

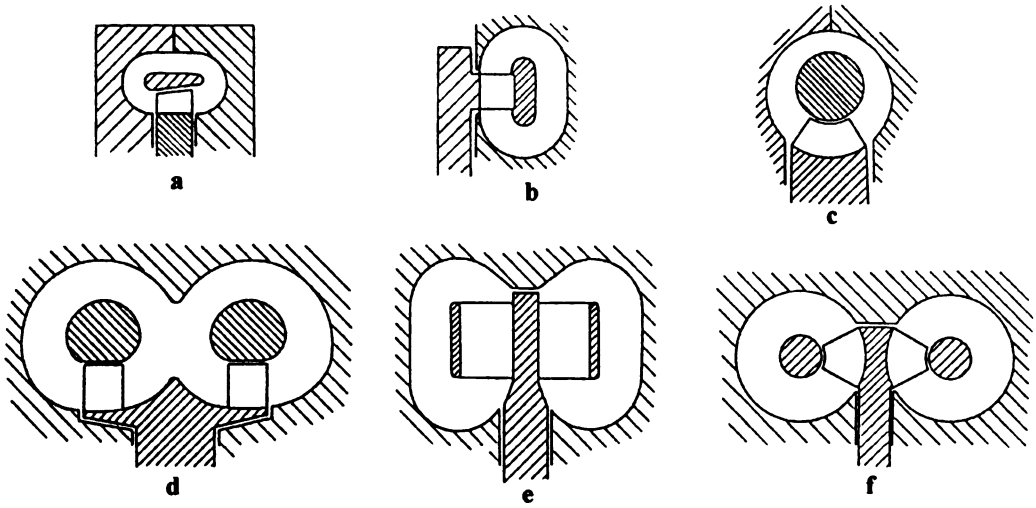

Figure 2.9 Regenerative compressors with aerofoil blades (after Abdallah [1])

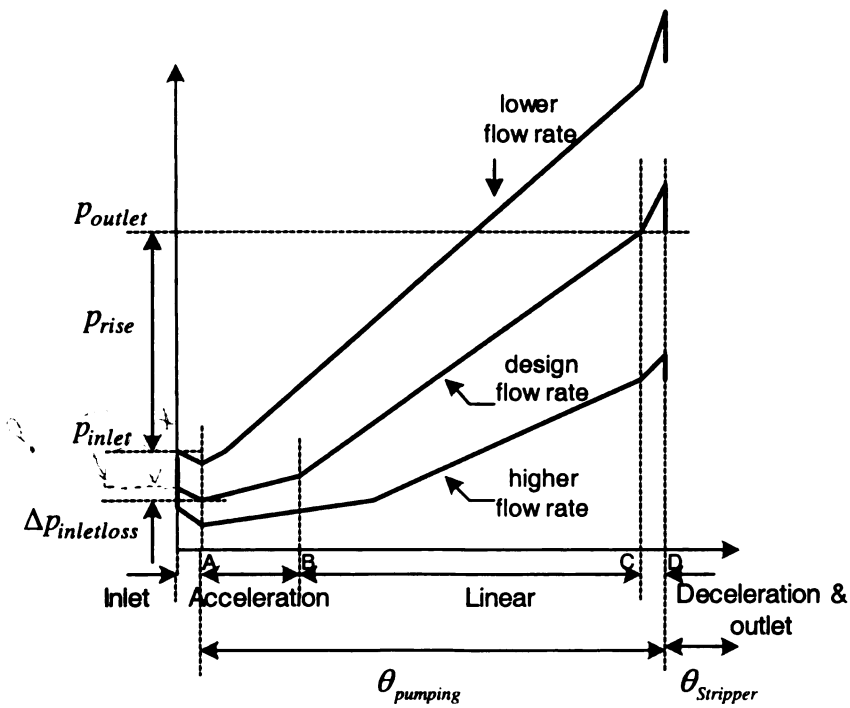

Figure 2.10 Tangential pressure variation in a regenerative turbomachine

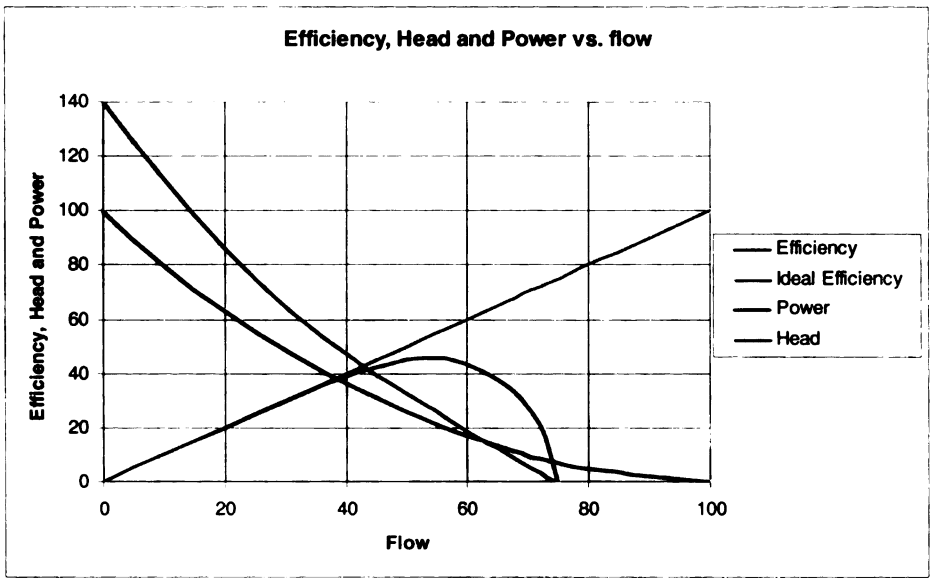

Figure 2.11 Performance characteristics of regenerative turbomachines

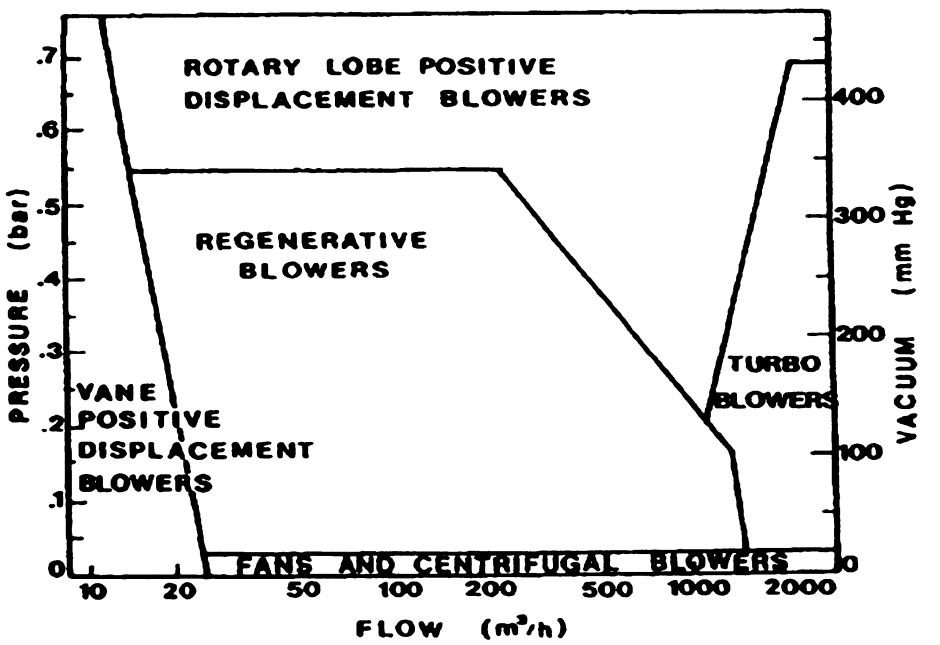

Figure 2.12 Blowers typical operating range (after Roppenecker [51])

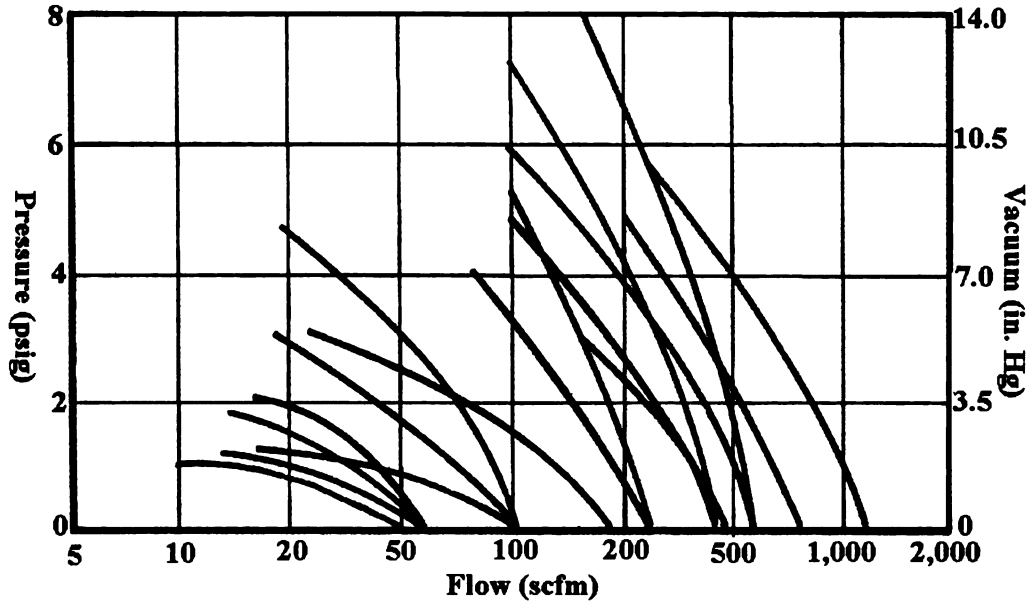

Figure 2.13 Pressure flow curves of Regenerative Blowers (after Roppenecker [51])

CHAPTER 3

LITERATURE SURVEY

3.1 Introduction

Regenerative turbomachines have appeared to originate in either Germany or Holland after the First World War. Although they have found many applications in industry, still they are the most neglected in the family of dynamic turbomachines. The number of publications existing in literature is very small compared to the large number of papers about the centrifugal and axial turbomachines. After there origin, they became the subject of a number of doctoral theses at German technical universities during the period between the wars. Regenerative turbomachines have been studied as pumps, turbines, blowers and compressors. Most of the existing literature can be broken down into five broad areas of regenerative turbomachine research:

1) Theoretical Models
2) Experimental work
3) Impeller blade Profile
4) Loss categorization
5) CFD Analysis

The literature survey presented in this chapter is based on work done in regenerative turbomachines in the above mentioned five areas. The idea behind discussing both RFC

and RFP together is due to the very close resemblance in the operating principle of the two machines.

3.2 Theoretical Models

Some investigators after the Second World War attempted to develop rational theories for the type of flow developed within a regenerative turbomachine. Various theoretical models have been used in attempts to describe the flow in regenerative turbomachinery. One school of thought, the leading exponents of which were Crewdson [17] and Iverson [34] postulated the essential flow mechanism as being one of drag induced by the impeller on the stationary fluid in the side channel. Iverson put forward a viscous model for the performance. He analyzed the performance of regenerative pump in terms of shear stresses imparted to the fluid by the impeller. The performance equations were derived by considering a linear system with a linear motion of rough surface as shown in Figure 3.1. A force balance on the fluid in the horizontal flow channel was applied to derive performance equations. The resulting expressions included two shear coefficients and an average impeller velocity, which were determined experimentally. The output head, power and efficiency of the pump were given as

$$gH = \frac{C_i a_i U^2}{2A}\left[\left(1-\frac{Q}{UA}\right)^2 - \frac{C_c a_c}{C_i a_i}\left(\frac{Q}{UA}\right)^2\right] \tag{3.1}$$

$$P = \frac{C_i a_i \rho U^3}{2}\left(1-\frac{Q}{UA}\right)^2 \tag{3.2}$$

$$\eta = \frac{\rho Q g H}{P} = \frac{Q}{UA}\left[1-\frac{C_c a_c}{C_i a_i}\left(\frac{Q/UA}{1-Q/UA}\right)^2\right] \tag{3.3}$$

The shapes of the head, power, and efficiency curves as a function of flow were predicted as shown in Figure 3.2. The shear coefficients and pump performance were shown to be functions of impeller roughness and flow area. This gave a characteristic of increasing pressure with decreasing flow rate with a concave form. Thus, the predicted maximum flow rate was some 23% higher than was practically found, probably due to losses. The predicted shapes of performance curves were found to be in reasonable agreement with the test curves as reported in Iverson [34]. Certain explanations of observed performance were obtained by means of this hypothesis which however proved to be limited in explaining complete features of performance. The procedure outlined by Iverson is not directly applicable to the prediction of performance of any selected pump geometry due to the unknown magnitudes of the shear coefficients and effective vane velocity, but at least it provides a simple representation of the performance of regenerative pumps.

Balje [8] examined the regenerative turbomachines using a simplified approach analogous to Iverson. He concluded that the optimum efficiency of a regenerative turbine, based on experiment is 35%, which is less for regenerative pumps. Theory presented by Balje enabled fair prediction of regenerative turbomachine performance for compressible as well as incompressible media, accounting for the influence of design geometries on performance range and peak efficiency.

Wright disagreed with theories presented by Iverson and Balje indicating that they did not take any account of the blade shape, which is of great importance [34]. Wright suggested an alternative theory in his discussion of Iverson's work based upon a momentum transfer between the blade row and the fluid in the channel. The major finding of Wright's theory was his suggestion that it is possible to increase the pump rpm

without increasing the shutoff pressure rise, if the blades were given a suitable backward curvature. Thus he found that by increasing the speed of such a device and by curving the blades backwards, the same pressure rise was possible, demonstrating the inadequacy of a purely viscous Iverson and Balje model.

Wilson, Santalo and Oelrich [69] presented a hypothesis of regenerative pump operation by considering a helical flow and made various allowances for losses and provided experimental corroborations of their results. Theory presented by Wilson was based on the idea that the fluid gains angular momentum in the impeller and then imparts it to the slower moving fluid in the casing channel. The fluid re-enters the impeller with a lower angular momentum. The rate of change of angular momentum is the torque exerted by the impeller upon the fluid. An analysis based on the hypothesis led to a series of expressions for pump performance over the entire operating range in terms of only three empirical constants. The basic model developed by Wilson [69] was to represent the phenomenon in the linear region as shown in Figure 2.10. He made several assumptions and applied fluid dynamic equations to arbitrary control volumes of the pump. The entire pump flow was characterized by the tangential velocities V_t and circulatory velocity V_c along a mean streamline. The overall head rise, net power input and efficiency of the pump were given as

$$gH = \frac{\Delta p}{\rho} = \frac{Q_c}{Q_s}\left(\sigma U_2^2 - \alpha U_1^2\right) - K_t\left(\frac{Q}{(2r_2)^2}\right)^2 \tag{3.4}$$

$$P = \rho Q_s\left[gH + K_t\left(\frac{Q}{(2r_2)^2}\right)^2\right] \tag{3.5}$$

$$\eta = \frac{\rho Q g H}{P} = \frac{\frac{Q}{Q_s}}{1 + \frac{K_1 Q^2}{gH(2r_2)^4}} \tag{3.6}$$

The dimensionless performance characteristics of STA-RITE TH 7 regenerative pump were tested and reported by Wilson [69]. The experimental plots of flow versus head were obtained at seven different speeds with air as working fluid. The calculated and experimental performance curves were compared and excellent agreement was observed. Qualitatively, the relations presented by Wilson satisfied the major details of the observed flow phenomena, but it was only limited to predict the head-flow characteristics in the linear region of the pump. His model assumed incompressible flow, thus unable to predict performance of compressors producing high pressure ratio. Moreover, Wilson's model lacked in correlation of losses with geometric and aerodynamic parameters. The most remarkable aspect of the design was that it only required three performance parameters to describe performance of the regenerative pump throughout its operating range.

The circulatory flow mechanism on which Wilson's theory was based was recorded by Burton [13] using an experimental machine with Perspex walls. Small energized beads were introduced into the stream and their path was recorded photographically. Burton presented a theoretical and experimental analysis of regenerative pumps and regenerative turbines. His analysis led to expressions for turbomachine performance over entire operating range in terms of empirical constants. The coefficients of the theoretical equations were chosen to give the best overall match to their experimental results.

The characteristics obtained by Wilson [69] were not dissimilar to those found by Whitehead [68], although both authors used machines considerably different

geometrically. Therefore direct comparison was not possible between their works. Whitehead experimentally investigated the performance of a Reavell RC50 regenerative compressor. He found a maximum aerodynamic efficiency of 44% occurring at a specific speed of 0.05. The mechanical losses were significant and reduced the efficiency to 30% at maximum speed. A theoretical model of the internal fluid mechanics was presented in his paper which assumed that the blades are unstalled and circulation is zero at inlet to the machine. The assumptions in the model were poor, since the blades were stalled most of the time. The predictions were not in good agreement with the experimental results. Another finding by Whitehead was that the performance is affected to some extent by Mach number effects, however Reynolds number effects were found to be negligible.

Many authors have reported simplified theoretical models for regenerative pump with different blade designs. Grabow [23] developed a theoretical model for both radial and semicircular blades. Abdallah [1] extended Grabow model to develop a theoretical model for the regenerative compressor with aerofoil blades. This model included inlet effect which was neglected in most theories. The correlation between theoretical and experimental pump performance showed close agreement.

Wilson et al. [69], Burton [13] and Abdallah [1] developed theoretical models to correlate the performance of the machines on the basis of the recirculating flow pattern. However, all these methods suffer from two basic defects which severely limit their use as a design tool. The first of these is that they contain empirically derived loss coefficients which are not directly related to geometric and aerodynamic parameters. Therefore, they give no indication of how the design might be modified to reduce the losses and cannot be used to evaluate designs which differ significantly from those on which the models are based.

The second defect is that they are mainly useful for incompressible pump flow, thus making them inaccurate for compressible flow in RFC. Thus these models are unable to provide any design guidelines.

El Hag [22] developed a theoretical analysis of regenerative pumps. He derived flow equations for regenerative turbomachines revealing that the familiar Euler equation for the head across rotordynamic machines has to be supplemented by an extra term accounting for the tangential pressure gradient so that it can be applied to regenerative turbomachines. Thus, in order to compute head rise, the tangential displacements of flow in the rotor have to be computed. In his analysis, a section of pump circumference was defined and it was assumed that tangential pressure gradient is essentially constant. In this section, flow was modeled such that when the principles of fluid mechanics were applied to it, the resulting flow equations were solvable by numerical methods with the aid of a digital computer. The flow equations derived in his work enabled detailed calculations of the flow in the linear section of these machines. He gave the net increase in the fluid head between any two points 1 and 2 at the same streamline in the impeller by,

$$\Delta(gH) = (U_2 V_{\theta 2} - U_1 V_{\theta 1}) + \frac{1}{\rho}\frac{\partial p}{\partial \theta}\Delta\theta - gH_L \qquad (3.7)$$

The first term on the RHS of equation 3.7 is the familiar Euler's head. The second term is the energy added to the fluid because of its angular displacement $(\theta_2 - \theta_1)$ in a field in which there is a tangential energy gradient $\partial H/\partial\theta$. El Hag [22] showed the variation of fluid energy along a flow cycle on energy gH -angular displacement (θ) plane as shown in Figure 3.3. He considered flow along a streamline, which starts just inside the impeller, passes through the impeller exit, goes through the channel and reaches just inside of the

impeller for next circulation. The losses experienced by this streamline were compared with the ideal flow cycle as shown in Figure 3.3. In Figure 3.3, actual flow cycle is indicated by 123'3 and the ideal cycle is represented by path 145. The increase in the fluid specific energy is given by

$$\Delta(gH)_a = (gH_3 - gH_1) \tag{3.8}$$

Analysis by El Hag did not involve empirical factors which are needed to be determined experimentally from tests on the pumps like in the case of Wilson [69]. However, well established loss empirical parameters, such as the friction loss factors of flows in conduits were used to estimate losses where appropriate in the analysis. The proposed method predicts the performance of a given pump, provided shape and dimensions of impeller, the dimensions of the channel, the number of blades, the stripper angle and clearances are known. However, the model presented by El-Hag is also limited to regenerative pumps.

Hollenberg [29] did an experimental and theoretical analysis on regenerative pumps and blowers and reported the parameters controlling their efficiency. He presented a correlation between torque, pressure and flow rate which was dependent only on one experimental parameter. This correlation was used to examine the variation in efficiency-specific speed characteristics of regenerative turbomachines over the range of their probable designs. The maximum efficiency was shown to be a function of radius ratio parameter and a friction head coefficient ratio.

Kupryashin [30] discussed theoretical approaches to design of regenerative pumps. Both approaches adopted by Wilson and Iverson were discussed and proved unsuitable for practical calculations because of the analytically indeterminate coefficients contained in the performance curve equations. He recommended the circular radial section as most

favorable due to its promotion of the secondary circulation. Experimental results were presented showing pump efficiencies close to 50 %.

A more theoretical approach was taken by Jakubowski et al [35]. They analyzed rotational flow of an incompressible, non-viscous fluid in a toroidal enclosure. However, the cumbersome nature of the mathematics involved and the simplifications necessary to obtain a solution limited the usage of the model.

Schively [53] theoretically solved the flow within a regenerative pump assuming a one-dimensional flow model. In his model, all significant variables were given as function of only the radius. He divided the flow in the vortex chamber into three regions and analyzed the flow by applying the Navier Stoke's equations and momentum balance for each region. The performance of a simple regenerative pump was also investigated theoretically and experimentally by Bullough [10], however the model was not able to predict performance of any given pump design.

Senoo [55] reviewed both viscous and momentum exchange theories and found them compatible with the differences occurring only in their assumptions. The theories discussed in his paper were developed for incompressible flow. The experimental data which had been examined till that time showed that none of these theories was broad enough to cover all the influences that the geometry had on the performance. This remains true to this day even though we are now interested in extending the theories and design into compressible flow range.

Theories for the flow of compressible fluid in regenerative turbomachines are rarely found in literature. Burton [11] made an effort in this direction and reported a simplified theory, which took account of area change and compressibility effects in regenerative

turbomachines. He assumed that energy exchange is obtained through shear stress between the impeller and the fluid in casing. Any radial components of flow were ignored. The continuity, momentum and energy equations were applied to a linear control volume and differential equations were obtained. Following differential equations were derived in Burton [11]:

Continuity:

$$\frac{d\rho}{\rho} = -\frac{d(AV_m)}{AV_m + A_R U_p} \tag{3.9}$$

Momentum:

$$\frac{dp}{\rho} = \frac{R_p(2r_2 - 2r_o + 2b + t)}{2Ag} f_R \left[(U_p - V_m)^2 - \lambda V_m^2 \right] d\theta + \frac{A_R U_p V_m}{Ag} \frac{d\rho}{\rho} - \frac{V_m}{g} dV_m \tag{3.10}$$

where,

$$\lambda = \frac{f_c}{f_R} \frac{2b_1 + 2b_2 - t}{2h + t}$$

Energy:

$$\begin{aligned} \frac{dp}{\rho} &= C_p \left(1 + \frac{AV_m}{A_R U_p} \right) dT + \frac{AV_m}{A_R U_p} \frac{V_m}{g} dV_m + \frac{1}{2g} \left(U_p^2 - V_m^2 \right) \frac{d\rho}{\rho} \\ &- \frac{R_p(2r_2 - 2r_1 + 2b + t)}{2gA_R} f_R (U_p - V_m)^2 \, d\theta \end{aligned} \tag{3.11}$$

The equation of state can also be used for gases showing behavior close to perfect gas.

$$p = \rho RT \tag{3.12}$$

The equations presented by Burton comprise a set of equations for determining the performance of a compressor if the speed, gas, and compressor geometry is specified. Burton's model was also based on shear stress theory which was experimentally proven as unable to explain the fluid motion inside regenerative turbomachines.

Given dearth of design information in regenerative turbomachinery, it is hardly surprising to know that most designs of regenerative turbomachines retained a fairly basic geometrical configuration with simple vanes either machined or cast into the impeller. However, the addition of a core in the flow channel to direct the circulating flow together with the provision of aerofoil blades was shown by Sixsmith and Altmann [60] and it resulted in significant improvements in the performance. They replaced the radial vanes by blades with an aerofoil section as shown in Figure 3.4. The blades were designed to transfer momentum to the fluid with a minimum of turbulence and friction. They were designed to turn the fluid through a definite angle, which preferably should be about 90°. The annular channel had the core to assist in guiding the fluid such that it circulates through the blading with a minimum of loss. The core also acted as a shroud to reduce losses due to formation of vortices at the tips of the blades.

The enthalpy transfer by the action of blades on impeller in one blade passage was given as

$$\Delta H_{\circ} = \omega\left(r_2 W_2 \sin\beta_2 + r_{\circ} W_1 \sin\beta_1\right) \tag{3.13}$$

The mass flow rate through the blading was estimated by

$$\dot{M}_B = 2\pi\left(1-F_s\right) r_{\circ} L_1 \rho_1 W_1 \cos\beta_1 \tag{3.14}$$

The forward mass flow rate through the flow channel was estimated by

$$\dot{M}_A = \frac{\rho_M A_c}{2}\left(U_1 + U_2 + W_2 \sin\beta_2 - W_1 \sin\beta_1\right) \tag{3.15}$$

The number of times fluid passes through the blades N was obtained by dividing the mass flow rate through the blading by the mass flow rate through the annular channel, i.e.

$$N = \frac{4\pi\left(1-F_s\right) r_{\circ} L_1 \rho_1 W_1 \cos\beta_1}{\rho_M A_c \left(U_1 + U_2 + W_2 \sin\beta_2 - W_1 \sin\beta_1\right)} \tag{3.16}$$

The pressure ratio was related to the enthalpy of a stream of gas being compressed from H_1 to H_2 in the form of the following equation

$$\dot{M}(H_2 - H_1) = \frac{\dot{M} C_p T_1}{\eta} \left\{ \left(\frac{p_2}{p_1} \right)^{\left(\frac{\gamma-1}{\gamma} \right)} - 1 \right\} \tag{3.17}$$

Relationship between the inlet velocity with respect to the blades, the pressure gradient in the annular channel and the geometry of the annular channel was given as

$$\frac{1}{2}\rho W_1^2 = \frac{(p_2 - p_1)S}{L\left(1 + \frac{\rho_1 L_1}{\rho_2 L_2}\right)\left(\frac{\rho_1 L_1 \sin\beta_2 \cos^2\beta_1}{\rho_2 L_2 \cos\beta_2} + \sin\beta_1 \cos\beta_1 \right)} \tag{3.18}$$

where S is the circulation distance from trailing edges to the leading edges of blades perpendicular to blade motion.

An interesting conclusion drawn by the authors was that the pressure gradient is dependent on velocity of the fluid relative to the blades and not on the velocity of blades themselves. Conversely, and more correctly, it is velocity relative to the blades that depends on the pressure gradient. This is one significant difference between a regenerative compressor and a centrifugal compressor. In a centrifugal compressor, the gain in pressure is proportional to the square of the peripheral velocity of the impeller. Regenerative compressor tends to behave like positive-displacement machines such as a roots blower. The torque is almost directly proportional to the pressure difference across the ports. Sixsmith and Altmann [60] constructed two regenerative compressors with aerodynamic blading to validate the theoretical results. The efficiency was considerably improved compared to the efficiency of regenerative compressor tested by Wilson [69] who employed the radial blades. These authors reported a performance comparison to

illustrate the advantages of aerofoil blade RFC over purely radial blade RFC design as shown in Table 3.1.

3.3 Experimental Work

The earliest investigators on regenerative turbomachines were concerned with exploring over a wide range, the effects of varying geometry on the design of regenerative turbomachines. The experimental work involved varying the proportions of blading to coverage of the side channel over the blading, shape of the side channel and blade profiles. As a result of these investigations, a great deal of information was derived but still not allowing one to reach the optimum proportions for conventional regenerative turbomachinery design.

Bartles tried to experimentally investigate exact flow mechanism in regenerative turbomachines. He tested three rotors in same pump casing. The first rotor was a smooth disc having no grooves or vanes, the second was grooved out to leave the radial vanes of conventional design, and the third had conventional radial vanes plus additional vanes normal to them. He proposed that if the first rotor pumped, it would have to be due to the viscous drag of a smooth metal disc. If the second rotor pumped, it might be due either to the shearing stresses of viscous and turbulent drag or to the mechanism in which the fluid circulates into and out of the impeller along helical paths under the centrifugal forces. If the third rotor produced pumping it would prove that the shearing stresses are the primary force causing the pumping because any possible radial flow was largely prevented by the cross blades. If it did not pump or was largely rendered ineffective, it implies that the pumping was caused mainly due to the centrifugal action because the shearing capacity of the radial blades could hardly be affected by the cross blades. He found that the pump

would only work when the impeller design permitted circulatory motion and centrifugal pumping, thus supporting Wilson's regenerative theory of pumping mechanism in these turbomachines.

Crewdson also examined the role of the circulatory flow or the centrifugal pumping in the process of enthalpy transfer in a regenerative pump. He soldered a thin brass strip along the middle of the side channel so that the side channel was divided into two parts. Thus any circulatory flow which is mainly radially inwards in the channel would be greatly affected and it might have been splitted into two: one in the lower part of the channel and one in the upper part. The effect of this arrangement on the fluid motion inside the impeller could not be easily judged. However, the suggestion was that although greatly hindered, the circulatory flow was not eliminated completely because there were still the centrifugal forces present although the channel was split into two. From the performance curves, it was concluded that the reduction in the circulatory flow greatly reduced the pumping effectiveness.

Pfleiderer summarized early German and Japanese (prior to 1949) experimental work in which the variation of impeller and side channel geometry was examined for its effect on the performance curves of the machine. He also presented a one-dimensional momentum analysis for the head developed and gave a simplified design approach based on this and available experimental data at that time.

Mason [39] carried out an experimental investigation of a regenerative pump with two channel diameters (2 inch and 1.25 inch), each with 40 and 20 blades in the pump impeller. He compared experimental performance characteristics with a theoretical analysis of the fluid dynamic mechanism of regenerative pumps. He aimed to correlate

empirical parameters with pump geometry, however no obvious relation could be found. Bicard [9] designed a new inlet for a regenerative pump based on a proposed model of the fluid dynamic mechanism in the inlet region. He achieved some improvement in inlet design by getting an increase in linear region of the channel and therefore increasing the head across the channel.

Senoo [57] experimentally investigated the influences of the suction port location on the characteristics of a regenerative pump. He established that when the inlet port is very close to the barrier, the fluid enters the pumping passage too far upstream where the impeller effect is not fully realized. A pressure difference is thus needed between the inlet port and the entry region to maintain the incoming flow. Such a pressure drop constitutes a considerable energy loss when the discharge flow rate is high because the necessary acceleration is high. He reported that the pump performance could be improved considerably if the inlet port is appropriately located downstream from the barrier such that fluid entered the pump passage in a region where the impeller effect was reasonably established. He gave the figure of 65° for the angle between the barrier and the inlet port as the optimum angle for the design he considered. However, such a parameter was not correlated with other design parameters.

Shimosaka and Yamazaki [58] investigated the effects of varying the dimensions of the channel, impeller and the clearances. Fixing some of the dimensions, they established the effects of varying the other on performance of the pump. They found that, due to the numerous variables involved, it was not possible to establish a comprehensive scheme for the performance prediction. They concluded that the dimensions of a high efficiency pump can be obtained by systematic experimentation.

There is very limited data available on gases as the working fluids in regenerative turbomachines, resulting in a scarcity of design information. Organizations which have done some experimentation with gases include the United Kingdom Atomic Energy Authority, Mechanical Technology Incorporated, Massachusetts Institute of Technology, the Los Alamos Scientific Laboratory, Compair Ltd., of Ipswich and the Oak Ridge National Laboratory (ORNL); however, most of their work dealt with relatively low Mach numbers. Performance data with compressibility effects considered are needed in many areas that affect performance, including flow passage geometry, impeller blade geometry, nozzle design, radial and axial clearances and multistaging. The research at ORNL was aimed at utilizing the regenerative machine as a light gas compressor and circulator in the gas-cooled reactor designs, which were being developed at ORNL. Oak Ridge gaseous diffusion plant studied performance characteristics of the regenerative compressor on gases covering a wide range in molecular weights from 4 to 400 and speeds from 5000 to 14000 rpm. Cates [15] published a paper and reported the test data of the regenerative compressor with a variety of gases having molecular weights of 4 to 400. He presented general characteristics in Mach numbers extending well into the compressible realm of operation. The regenerative compressor operated satisfactorily without surging or unstable operation with the variety of gases. Compressibility effects had an important influence on performance because lower pressure ratios were measured at impeller tip Mach numbers approaching 1.0. Isentropic efficiencies over 50% were measured at low Mach numbers. Generally, the efficiency was lower at higher Mach number and went down as low as 10% at Mach numbers exceeding 1.1. Performance map of ORGDP-1 regenerative compressor was reported in Cates [15]. The total pressure ratio

was plotted against specific mass flow with tip Mach number as the speed parameter. It was noted that pressure ratio with various gases increased fairly consistently with Mach number up to 0.769, after that there was a detrimental effect to pressure ratio with further increase in Mach number. It is thought that compressibility effects start to appear at such a high Mach number. Cates calculated the compressor efficiencies based on an isentropic process between suction and discharge pressure as ideal. This isentropic efficiency η_s was defined by

$$\eta_s = \frac{H_{OD}^{'} - H_{OD}}{H_{OD} - H_{OS}} \tag{3.19}$$

where H_{OD} , H_{OS} were average total enthalpies at discharge and suction respectively and $H_{OD}^{'}$ was total enthalpy at discharge total pressure along the isentropic path. He treated the test gases as perfect gases with C_P and γ evaluated at an average of the suction and discharge temperatures. The isentropic efficiency can be rewritten as

$$\eta_s = \frac{C_P\left(T_1^{'} - T_1\right)}{C_P\left(T_1 - T_1\right)} \times 100 = \frac{T_1\left[\left(\frac{p_{out}}{p_{in}}\right)^{\frac{\gamma-1}{\gamma}} - 1\right]}{\left(T_2 - T_1\right)} \times 100 \tag{3.20}$$

Efficiency was plotted with specific mass flow rate for several test gases. It was observed that values of η_s greater than 50% were obtained under certain conditions. The efficiency generally decreased with increasing Mach number. Moreover, pressure level or Reynolds number appeared to effect efficiency described by data measured on air at 2, 6 and 10 *psia* which exhibited a decrease in efficiency with an increase in pressure level. Generally speaking, where different gases were tested at the same Mach number, the heavier ones showed lower efficiencies. Also, very low efficiencies were measured when

the tip Mach number exceeded 1.0. The performance of compressor on the various gases in terms of $\Psi - \lambda$ curves is shown in Figure 3.5 with approximate efficiency contours included. The head coefficient Ψ and flow coefficient λ were defined as:

$$\Psi = \frac{gH}{U_2^2} \tag{3.21}$$

$$\lambda = \frac{Q_s}{U_2 A_c} \tag{3.22}$$

where H is developed adiabatic head, Q_s is suction volume flow rate and A_c is cross sectional area of open channel.

It must be noted from Figure 3.5 that at small flows, the efficiency was lower and the delivery head was also found to be reduced. The logarithmic plot of the head coefficient as a function of tip Mach number is given in Figure 3.6 for three values of flow coefficient. At low Mach numbers, Ψ was nearly constant for a given flow, however, when compressibility effects began their influence, Ψ dropped off rapidly. Cates also reported the effects of changes in flow channel geometry on compressor performance. The effects of the geometry changes were quite different at different Mach number levels. Moreover, Cates presented the effect of impeller-to-casing clearances on pressure ratio as shown in Figure 3.7. The regenerative compressors have been described in the literature as machines which require small clearances between the rotating impeller and the stationary casing at the stripper section and sides in order to minimize cross leakage. The conclusion that was reached by the tests performed by Cates indicated that increasing impeller-to-casing clearances had little effect on performance; probably because of the high carry over flow characteristic of this impeller. He also presented a brief comparison

of six regenerative compressors tested by independent organizations as shown in Figure 3.8.

Hollenberg [29] investigated regenerative turbomachines using both air and water as working fluids. He investigated three machines, representing two geometries and developed a non-dimensional correlation, relating pressure and flow to driving torque. This was confirmed by experiments using data from widely separated investigations. He used this information to prepare a study of maximum efficiency as a function of specific speed. A single loss coefficient was found to be the governing parameter. He found that the optimum head and maximum efficiency were adversely affected by increasing the clearance between the impeller and stripper. Moreover, he concluded that improved efficiency might be obtained at higher specific speeds.

Many other authors have investigated the effect of impeller clearance in the regenerative pump using different impeller blade designs. Senoo [56] reported on the theoretical and experimental effects of clearance in the case of radial blades while Hollenberg [29] reported on the experimental effects in the case of semi-circular blades. Senoo [56] developed a theoretical model to study the effect of clearance on the pump performance. He carried out a series of experimental tests using a pump with radial blades. He changed the pump clearance eight to ten times from 0.04 mm to 0.36 mm and clarified the influence of the clearance experimentally and compared it with his theoretical results. He found that the pump head depends considerably on the value of pump clearance. In his experiment the shut-off head at large clearance was only one fourth of that at the small clearance. Hollenberg [29] carried out a series of experimental tests using regenerative blower of semi-circular blades. He changed the clearance from 0.25mm to 0.5 and 0.7.

He found that the shut-off head at large clearance was only 0.4 of that at the small clearance value. The maximum efficiency at 4500 rpm at large clearance was 0.28 compared to 0.43 at small clearance value. He examined the effect of specific speed on the maximum efficiency of regenerative turbomachines. Moreover, in another publication he determined the effect of Reynolds number on a typical regenerative pump.

The effect of stripper is studied by Sixsmith [60] and he suggested that the regenerative pump performance might be improved if the solid stripper were modified to form a row of stationary blades to allow flow between the blades to continue in a toroidal rather than a peripheral path only. This suggestion was taken by Abdallah [1] in his thesis in which he explored aerofoil blade RFC.

Sixsmith and Altmann [60] tested two regenerative compressors with aerofoil blading by blowing air through them. MK1 regenerative compressor was designed to run up to 10,000 rpm and deliver 250 liter/sec at a pressure of 2 atm. It had an impeller of 300 mm diameter with a single row of blades. The performance of MK1 compressor is given in Figure 3.9. The characteristics resembled to those of a positive displacement compressor and the efficiency was maintained over a wide range of operating conditions. The torque was almost directly proportional to the back pressure and the compressor could be operated from maximum to zero flow without surging or stalling. The authors also tested a second MK2 regenerative compressor with the same basic layout but with two blade rows. The performance curves for MK2 RFC are shown in Figure 3.10. The main features of its performance compared to that of the first compressor were the increased peak efficiency to 52%, the lower pressure ratio at which this efficiency occurred, the gentler slope of pressure-volume curves, the lower efficiency at high pressure ratio, and

the large volume flow at low pressure, i.e., approximately 2.5 times greater than before. The authors retested the MK2 regenerative compressor by making the blading symmetric and the improved performance characteristics are shown in Figure 3.11. When compared to Figure 3.10, the gain in efficiency was particularly marked at high pressure ratios. For example at 4000 rpm, the efficiency increased by 10 percent at a pressure ratio of 1.5.

Sixsmith and Watson [62] constructed an experimental helium regenerative compressor having four stages yielding an overall pressure ratio of 10.5:1. Tests were carried out with 0.5 mm clearance between stripper seal and rotor. A pressure ratio of 1.3 for single stage was achieved with volumetric flow rate of 0.14 m^3/s yielding a maximum isothermal efficiency of 31%. Further testing carried out on reduced clearance of 0.25 mm yielded a pressure ratio of 1.3 at volumetric flow rate of 0.31 m^3/s with a maximum isothermal efficiency of 42%.

Swift et al [66] developed a regenerative compressor with aerodynamically shaped blades primarily for use in cryogenic helium systems. Test data demonstrated a pressure ratio of 1.5 at a flow rate of 12 g/s with measured isothermal efficiencies in excess of 30%. Authors developed a performance prediction model of the compressor to support the design of prototype machine. The model incorporated important performance and loss mechanisms that related pressure rise, flow rate and speed to geometry of the machine. The model was used to predict performance and to assess the relative importance of basic geometric features, such as blade angles, inlet and exit port sizes, internal clearances etc. Important loss mechanisms were incorporated in the model.

Crowe [18] reported the overall performance curve of a UHTREX gas bearing regenerative blower developed by Mechanical Technology Incorporated for Los Alamos

Scientific Laboratory. This blower design was selected for use in the Ultra High Temperature Reactor Experiment (UHTREX) because of highly radioactive system contamination resulting from the investigation of unclad fuel elements. Figure 3.12 shows the pressure rise versus flow rate curve and Figure 3.13 gives overall efficiency versus flow coefficient curve for the regenerative blower. It must be noted that this blower was capable of producing a pressure rise of 30 psi at design flow rate and temperature, but the overall efficiency was just about 10% at the design conditions.

A four stage regenerative compressor was adopted by Gessner [25] for the compression of helium gas in the development of a highly reliable, long life cryogenic refrigerator for space vehicle application. The advantage of RFC is due to its ability to produce high pressure ratio at low flow rate with a small overall size of machine. Further advantages are oil-free operation and freedom from stall or surge instability. These characteristics are advantageous in compressors intended for incorporation in small closed cycle helium refrigerators.

3.4 Impeller blade Profile

Many authors have studied regenerative turbomachines with radial blades, e.g., Senoo [54, 55, 56, 57], Iverson [34], Wilson [69], Shimosaka [59], Burton [13], Gessner [25] and Grabow [23]. Iverson [34] reported the experimental effect of blade number on regenerative pump performance. He tested impellers with 31, 36 and 39 blades and found that the pump head and efficiency were increased with an increase in the number of blades within the tested range. The optimum number of blades for the greatest head at a given flow rate was not reached. Burton [13] reported that the pump performance could be improved by using a non-radial blade. The shut-off head coefficient obtained by using

a 47° blade angle was nearly twice of that obtained by using the straight blade. Yamazaki [72, 73, 74] studied non-radial blades and Grabow [23] and Hollenberg [29) studied the semi-circular blade shapes. Sixsmith and Altmann [60], Sixsmith [61] and Abdallah [1] studied the regenerative compressor with aerofoil blades. Grabow [23] reported theoretical and experimental effects of the blade angle for both radial and semi-circular blades. He tested the pump in both cases with different blade angles in the range of ±60° with a step size of 20°. He found from the theoretical research that the optimum shut off head was reached for the blade angle in the range of $40° - 55°$, whereas experimental study resulted in optimal blade angle in the range of $40° - 45°$. Abdallah found from the theoretical study of the blade angle effect on the shut-off head that optimum range of aerofoil blade angle is 55-61 degree.

3.5 Loss categorization

It is thought that more than 40% of the input power in a regenerative turbomachine is consumed in overcoming losses. The regenerative pump operation is affected by different types of losses including

- Losses due to slip
- Hydraulic losses in the circulation process between impeller and free channel
- Shock losses at the blade inlet
- Peripheral friction loss in the flow channel
- Inlet and outlet losses

- Leakage losses between the impeller face and the pump casing and between the inlet and outlet ports through the stripper

Sixsmith and Altmann [60] concluded that the major source of loss of efficiency is due to slip. The slip loss represents the flow rate down the pressure gradient that is needed to maintain the circulation through the annular channel in the presence of losses due to turbulence, fluid friction and the blade drag. All these losses, for a range of pressure ratios, are shown in Figure 3.14. True corresponding flow rates for various blade designs are also plotted. The slip loss is by far the greatest and efforts to raise the efficiency should be directed towards its reduction. In addition to the slip, these authors pointed out various types of leakage losses and carryover loss of compressed gas between the blades as they pass through the stripper. The flow rate delivered by the compressor was reduced by leakage through the clearances from the high pressure region to the low pressure region of the annular channel. Estimates of these leakage losses were made for a compressor speed of 4500 rpm and a pressure ratio of 2.0 as shown in Figure 3.14. A clearance between the faces of the rotor and the casing of 0.25 mm was reported to allow a leakage rate of about 4%. A clearance of 0.305 mm between the profiled edge of the impeller and the stripper allowed a leakage rate of about 3%. The leakage rate past the edges and tips of the blades in the stripper was about 3%. A small but significant fraction of the compressed gas was found to be carried through the stripper from the high pressure region and expanded down to the inlet pressure as the blade pockets between the blades open into the annular channel at the inlet end. This is usually referred to as carry over loss and it represents a loss of efficiency. When a regenerative compressor operates with an

incompressible fluid, the stripper seal plays an entirely passive role except for a certain amount of leakage. However, under compressible flow conditions, the small seal will become a major factor in machine performance. Large quantities of compressible fluid near the exit port are taken through the seal to mix in a highly irreversible process with the fluid entering the machine. This mixing process places a limit on pressure ratio as the Mach number increases. The seal plays a decisive role in reducing the overall efficiency of the machine.

Sixsmith and Altmann replaced the usual straight radial vanes on the rotor by the aerodynamic blading and also redesigned the annular channel in order to reduce the losses due to slip. They proposed a circular cross section annular channel to promote vortex circulation and a minimum of turbulence. They suggested that the blade angles should be designed to match fluid angles to ensure smooth entry to the blades. The angles depend on the rate of variation of the circulation component of velocity with respect to the radius of a streamline. When the effects of fluid friction are allowed, the actual vortex should lie somewhere between a free vortex and a constant linear velocity vortex. This led to blading in which the deflection increases with radius, the tangent of the inlet and outlet angles being proportional to the square of radius. The adoption of this type of blading improved the performance and extended the range of applicability of regenerative turbomachinery.

Burton [12] pointed out that the carryover loss might be reduced by extracting some of the compressed gas passing through the stripper and feeding it back at an intermediate pressure to the annular channel. Thus instead of being deposited inefficiently near the suction, the stripper carry over gas would be made to expand some of its energy inducing

the incoming supply. This idea is further explored in this dissertation by employing decompression ducts to feed high pressure flow entrapped in the stripper blades to various locations in the flow channel.

3.6 CFD Work

Computational Fluid Mechanics (CFD) has been widely used for the flow analysis of various turbomachines in last few years. The computational methods seem very attractive to be applied to RFC/RFP because they provide a possibility of calculating the flow in order to predict the likely effects of design modifications and in the hope of gaining a clearer insight into some of the losses. An attempt to calculate the flow in regenerative turbomachines was undertaken by Abdallah [1], who applied an incompressible version of time marching scheme to the flow outside the blade row of a regenerative compressor with aerofoil blades. However, he took no account of losses and because the solution did not include the blade row, it suffered from an uncertainty in the correct specification of the boundary conditions. Andrew [2], by contrast proposed a method based on an adaptation of the streamline curvature technique commonly used for axisymetric throughflow calculations in conventional axial and radial flow turbomachines. Although this method did not calculate the details of the blade-to-blade flow, his work seems very attractive. There is a potential of extending the calculation through a blade row in which the mean flow angles can be specified, and it is also relatively easy to incorporate loss models into the basic scheme presented by Andrew.

3.7 Conclusions

In this chapter, a summary of previous research on regenerative turbomachines is presented. After reviewing the literature, need was felt to do a theoretical, experimental and CFD analysis on these turbomachines to improve the performance. Although, there are few mathematical models available in literature, but none of them is general enough to predict performance without experimental support. Wilson's incompressible flow theory seems very attractive, however it lacks in correlation of losses with geometric and aerodynamic parameters. Therefore, in this work, Wilson's incompressible flow theory is extended to incorporate compressibility effects. Loss correlations are introduced to predict the performance. Looking at previous experimental work, there are evidences of some good experimental data available in literature. However, most of the data was on single stage pumps. No evidence of test data on multistage turbomachines is available. Moreover, the test data are not used to develop any correlations which can prove useful for designers and engineers. Therefore, need is felt to investigate single and multistage test data on regenerative compressors and develop correlations to quickly estimate the performance characteristics.

Sixsmith's theory [60] seems to be the best effort so far towards designing aerofoil blade RFC. However, there is a further need to theoretically investigate aerofoil blade RFC and perform a sensitivity analysis on various geometric parameters for performance improvement. Therefore, in this work a compressible flow theory for aerofoil blade RFC is put forward. Extensive design sensitivity analysis is performed to find out which geometric parameters have maximum effect on performance. There is little effort done in the past to apply CFD techniques to solve flow details inside regenerative turbomachines.

One reason for this is because most of the research work on these turbomachines was done prior to 1980s during which not many commercial CFD softwares were available. Therefore, it seems very attractive to solve the flow details inside regenerative turbomachines to improve the geometry for better performance. In the present work, CFD analysis on a regenerative automotive fuel pump and an aerofoil blade RFC is performed using commercial software "STAR CD". Details of CFD analysis can be found in chapters 7 and 9.

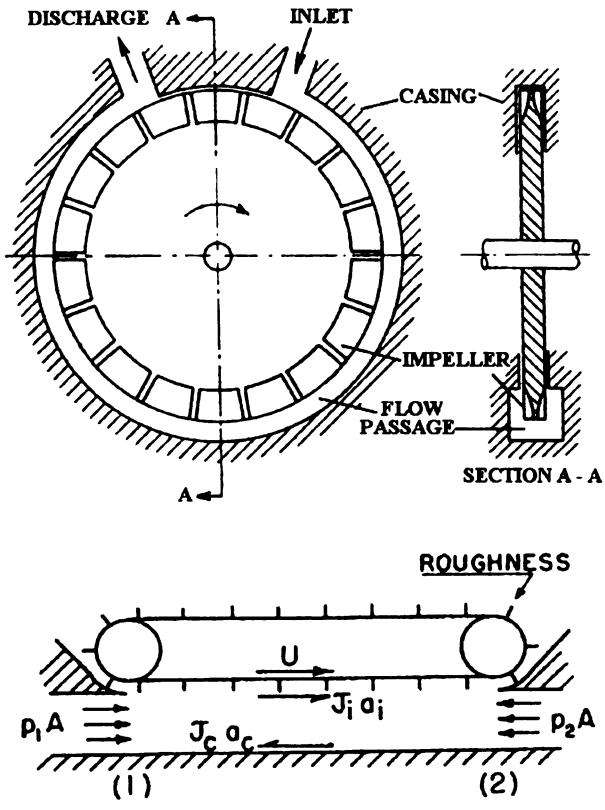

Figure 3.1 Simplified regenerative compressor for force analysis (after Iverson [34])

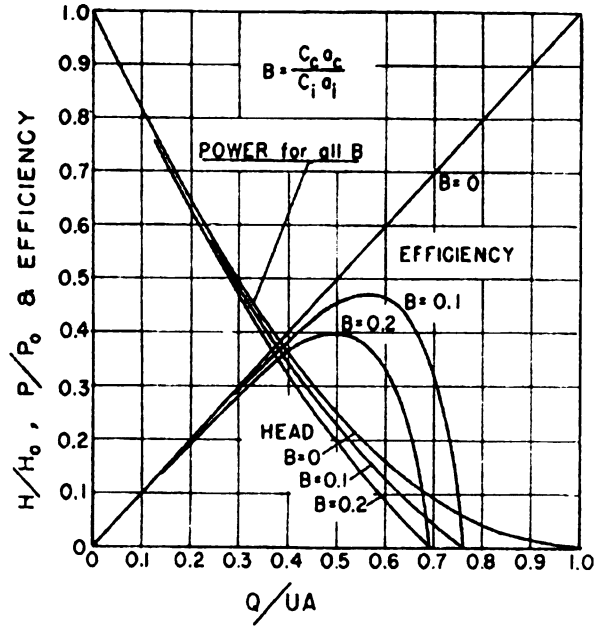

Figure 3.2 Performance characteristics of regenerative compressor (after Iverson [34])

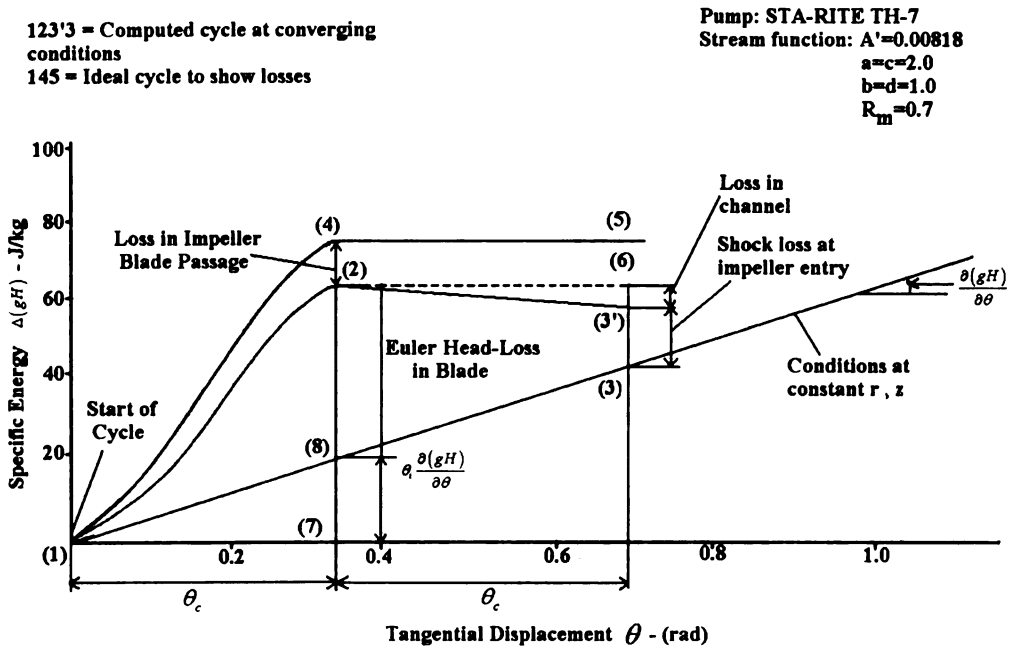

Figure 3.3 Typical flow cycle along a streamline (after, El Hag [22])

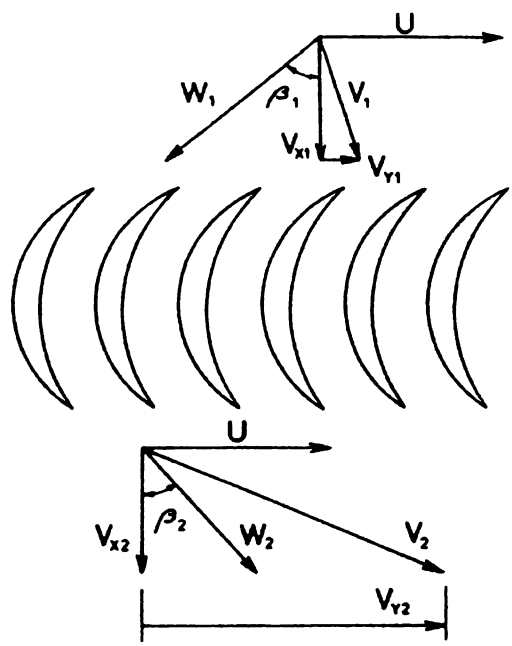

Figure 3.4 Velocity diagrams for compressor blades (after Sixsmith and Altmann [60])

Table 3.1 Performance Comparison at 4000 rpm and pressure ratio of 1.17 (after Sixsmith and Altmann [60])

Performance	Formula	Wilson	Sixsmith and Altmann	Ratio
Efficiency	$\frac{\dot{m} RT \ln \frac{P_2}{P_1}}{\text{Shaft Power}}$	45%	58%	1.29
Specific Speed	$\frac{nQ^{1/2}}{(gH)^{3/4}}$	0.244	0.220	0.90
Head Coefficient	$\frac{gH}{U^2}$	1.5	4.2	2.8
Flow Coefficient	$\frac{Q}{D^2U}$	0.014	0.044	3.14

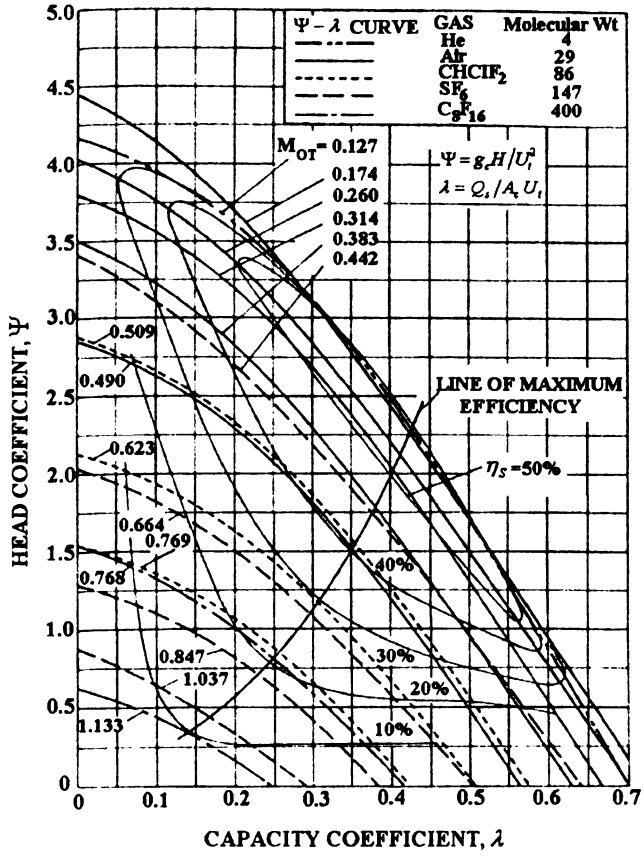

Figure 3.5 Head Coefficients of ORGDP-1 Regenerative Compressor (after Cates [15])

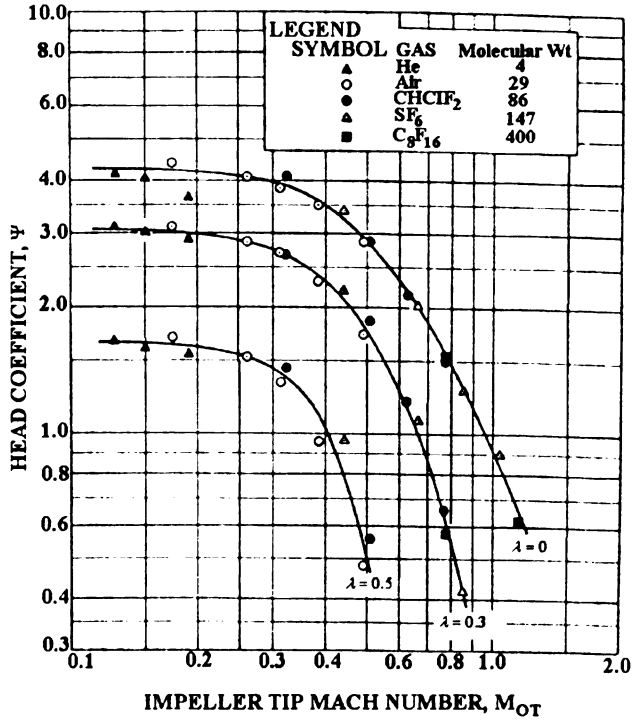

Figure 3.6 Head Coefficients dependence on impeller tip Mach number (after Cates [15])

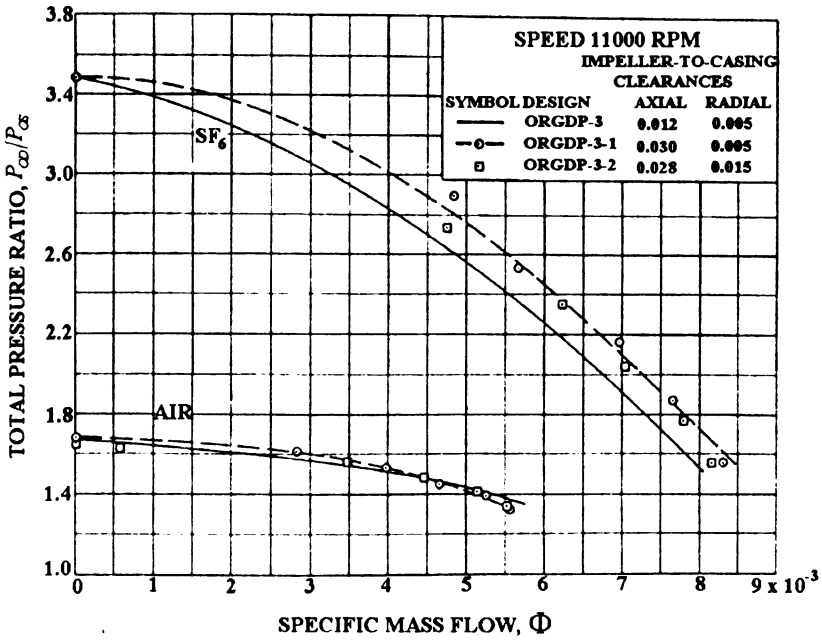

Figure 3.7 Influence of clearances on pressure ratio (after Cates [16])

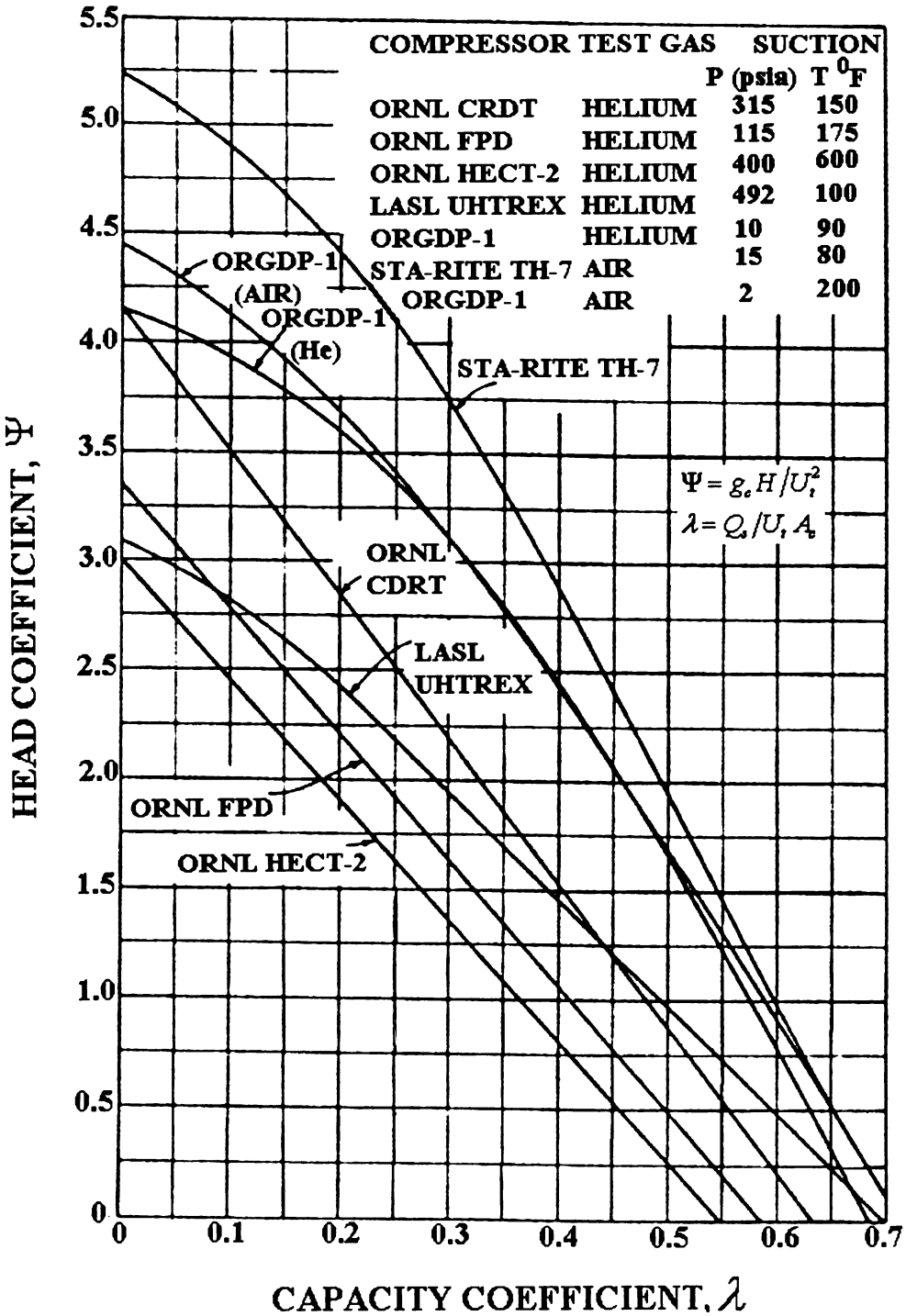

Figure 3.8 Comparison of several regenerative compressors (after Cates [16])

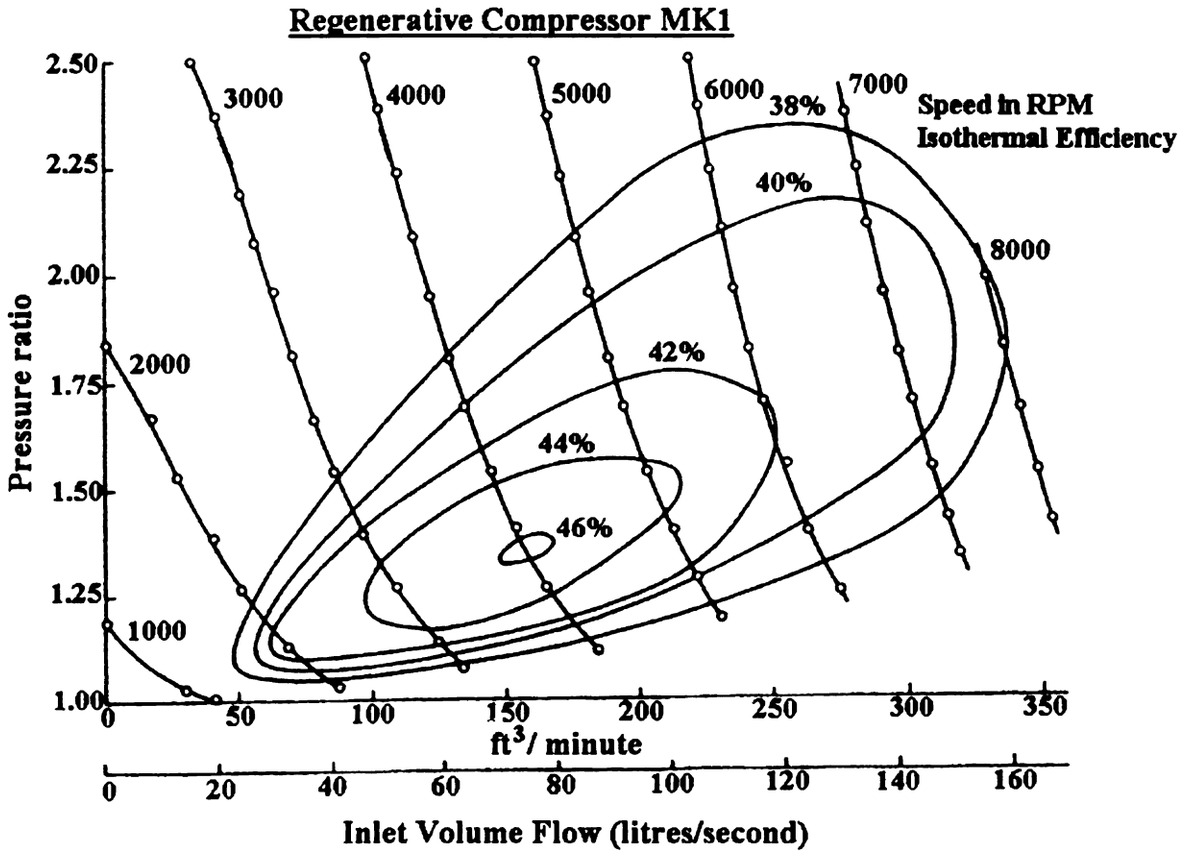

Figure 3.9 Performance of MK1 Compressor (after Sixsmith and Altmann [60])

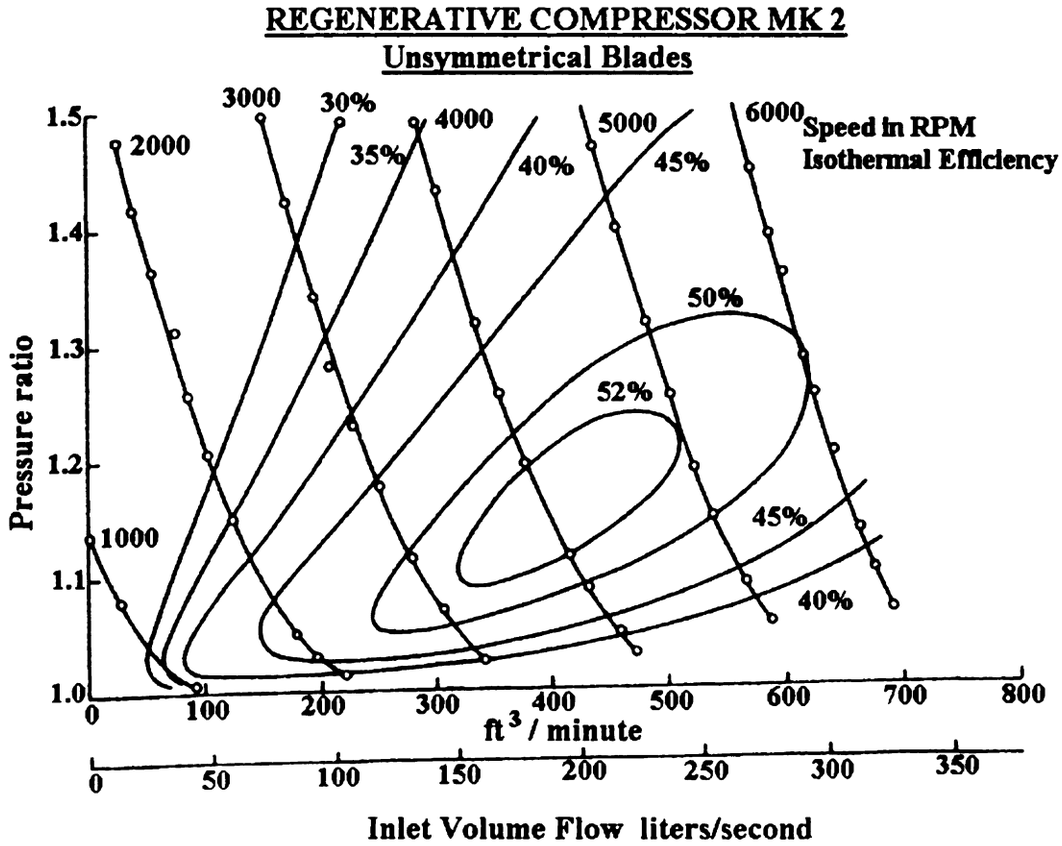

Figure 3.10 Performance of MK2 compressor with unsymmetric blading (after Sixsmith and Altmann [60])

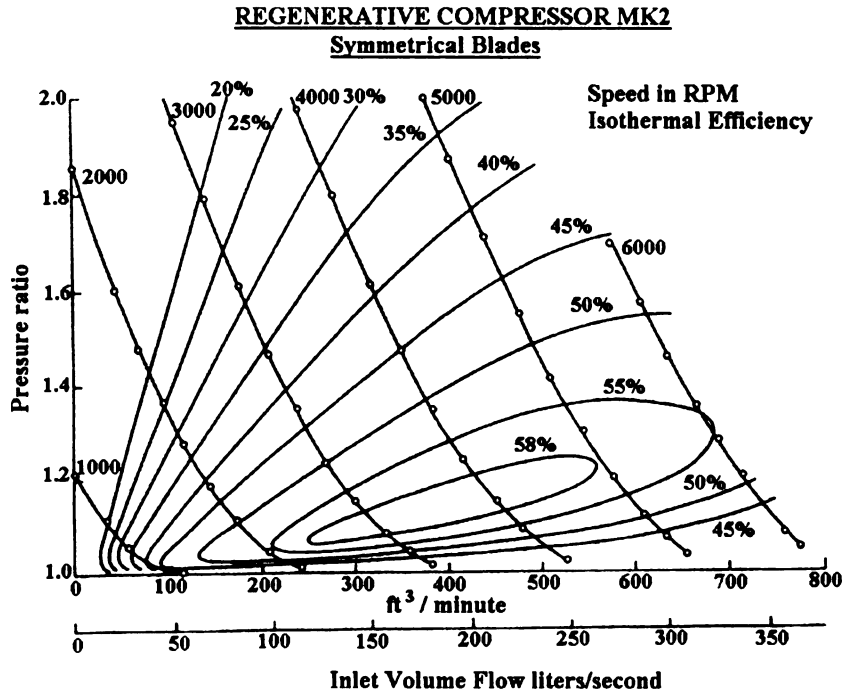

Figure 3.11 Performance of MK2 compressor with symmetric blading (after Sixsmith and Altmann [60])

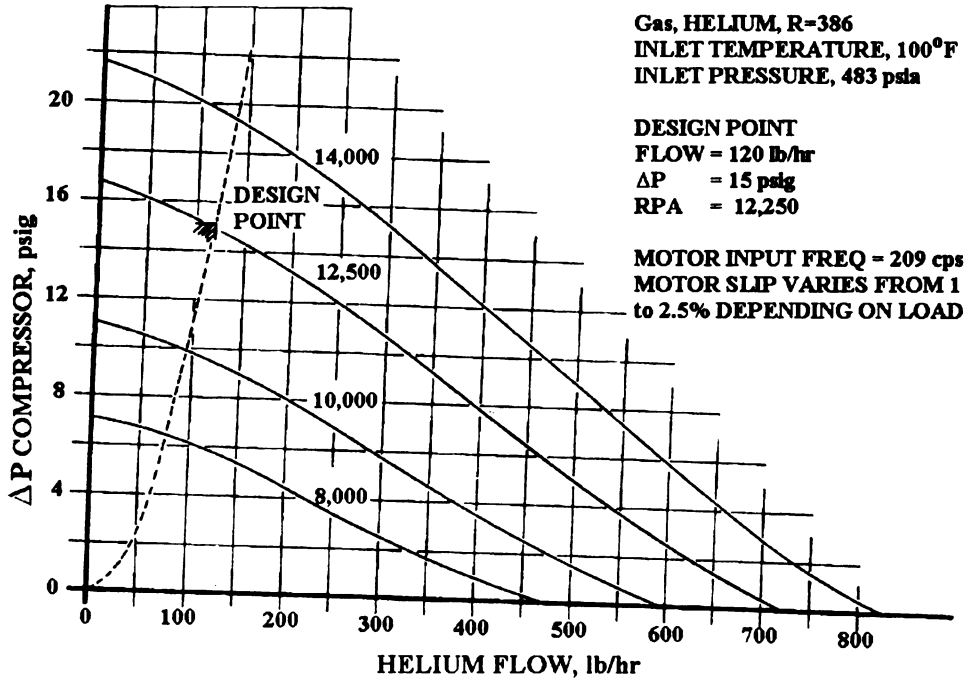

Figure 3.12 Pressure rise vs. flow curve for UHTREX Gas Cleanup System Regenerative Compressor (after Crowe [18])

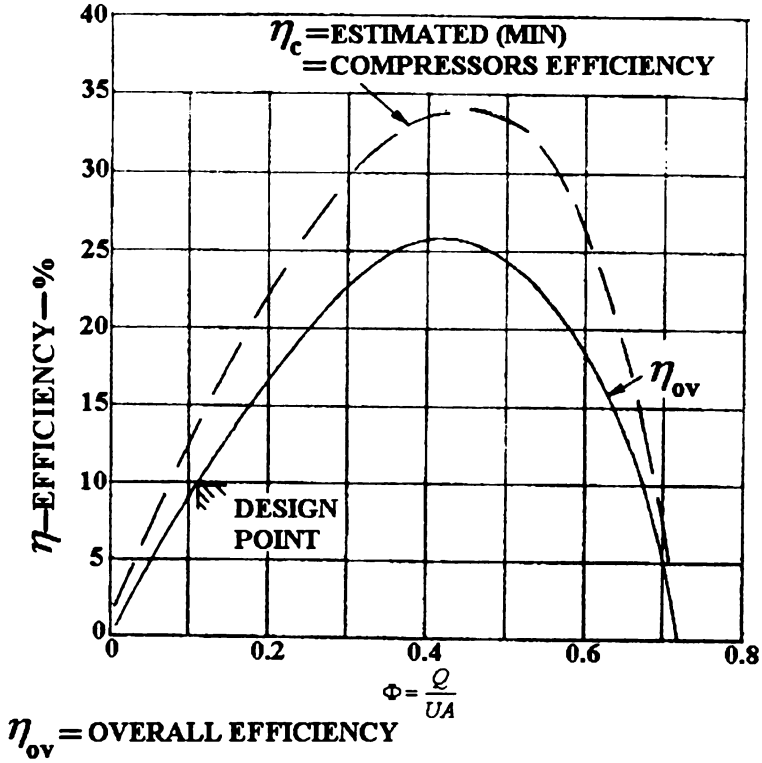

Figure 3.13 Overall efficiency curve for UHTREX gas cleanup system regenerative compressor (after Crowe [18])

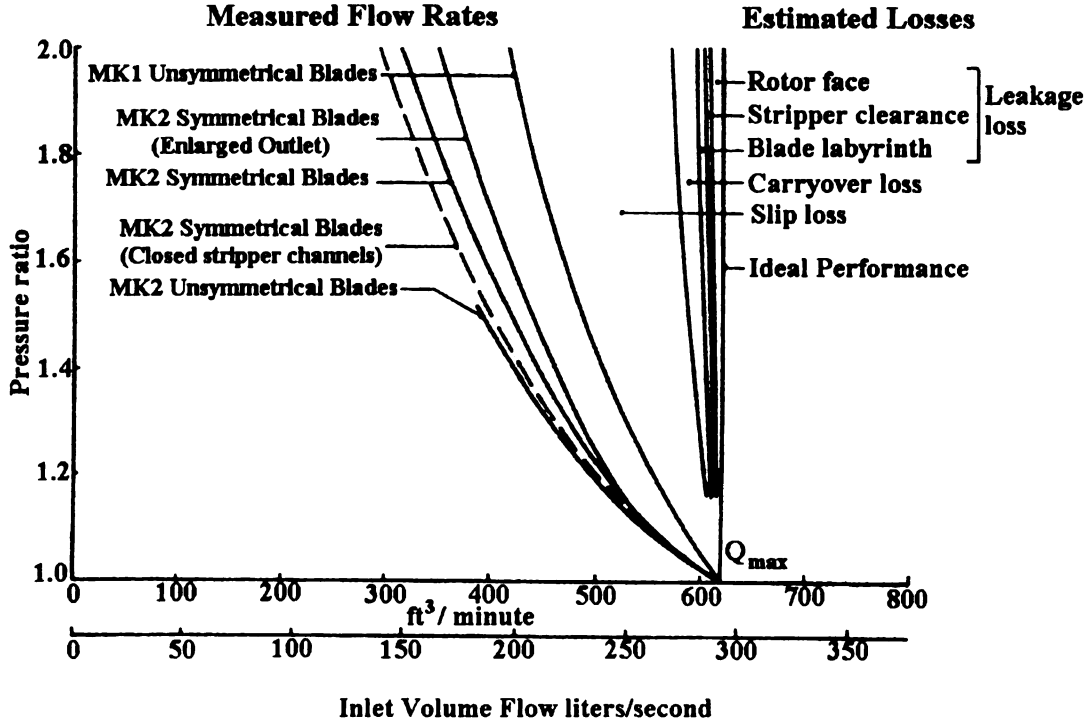

Figure 3.14 Loss analysis based on MK2 regenerative compressor with symmetric blades at 4500 rpm (after Sixsmith and Altmann [60])

CHAPTER 4

APPLICATION OF RFC IN MICROTURBINE SYSTEMS

For small scale power generation, there is currently great interest in microturbines. Microturbines offer a number of potential advantages compared to other technologies for small scale power generation. These advantages include a small number of moving parts, compact size, light weight, greater efficiency, lower emissions, lower electricity costs and opportunities to utilize waste fuels. Waste heat recovery can be used with these systems to achieve efficiencies greater than 80%.

Microturbines can burn various types of fuel, but the most popular microturbine fuel is natural gas. Therefore microturbines require a gaseous fuel compressor to raise a low pressure natural gas supply to that required for injection into the combustion system. Presently, most microturbine manufacturers use high cost and inefficient small compressors for this purpose. This has become one of the weak points of the microturbines despite their other numerous advantages. In microturbine research there is an immediate need for the development of a natural gas pressure booster compressor which is low cost and efficient.

4.1 The need for low cost and efficient gas booster compressor

Microturbines are small combustion turbines with output less than approximately 200 KW and can be located on sites with space limitations for power production. Microturbines are composed of a compressor, combustor, turbine, alternator, recuperator, generator and fuel gas pressure booster compressor. Microturbine application area has recently expanded to include:

- Distributed power generation
- Combined heat and power (co-generation)
- Offshore Rigs
- Hospitals
- Backup Generators
- Vehicle applications: (1) Hybrid vehicle (microturbine connected to high speed alternator) (2) Hybrid vehicle (microturbine and fuel cell together)

The U.S. Department of Energy's Advanced Microturbine Program is working with utilities, energy service companies, industrial manufacturers and equipment suppliers to identify technologies that will improve the energy, environmental, and financial performance of power systems for manufacturing, processing, and commercial applications. The Advanced Microturbine Program is a six-year program for FY 2000-2006 with a Government investment of over $60 million. End use applications for the

program are open and include stationary power applications in industrial, commercial, and institutional sectors.

Planned activities for this program focus on the following performance targets for the next generation of "ultra-clean, high efficiency" microturbine product designs:

- High Efficiency — Fuel-to-electricity conversion efficiency of at least 40%
- Environment — NOx < 7 ppm (natural gas)
- Durability — 11,000 hours of reliable operations between major overhauls and a service life of at least 45,000 hours
- Cost of Power — System costs < $500/kW, costs of electricity that are competitive with the alternatives (including grid) for market applications
- Fuel Flexibility — Options for using multiple fuels including diesel, ethanol, landfill gas, and bio-fuels

With the development of uprated and higher thermal efficiency microturbines, engine design point pressure ratio has been rising. At the same time, the current trend towards more dispersed generation increases the number of occasions when an engine needs to be sited on a lower pressure branch of the natural gas network. This potentially presents a problem in that the gas flow has to overcome engine combustor pressure plus a substantial control/manifold system pressure drop.

Most microturbine manufacturers produce a new range of industrial gas turbine engines, having pressure ratios as high as ten. Experience indicates that, at engine pressure ratios above about 5:1, the chance of having inadequate gas line pressure rises sharply. In such

cases, the gas pressure is boosted by a high cost compressor, comprising of a drive motor, cooler, moisture separator, accumulator and an intercooler (for two-stage units). For example a microturbine may cost about $100, 000 and a typical natural gas pressure booster compressor adds $10,000 - $15,000 to the installation. Therefore it is an urgent need to develop a fuel gas pressure booster compressor which is low cost and efficient. Because of their compact size, relatively low capital costs, low operations and maintenance costs and automatic electronic control, microturbines are expected to capture a significant share of the distributed generation market if improvements both in cost and efficiency of fuel gas pressure booster compressor are achieved.

4.2 RFC in microturbine systems

The power section of a typical microturbine generator includes a compressor, turbine, combustor and permanent magnet generator as shown in Figure 4.1. A schematic diagram of a typical microturbine system is shown in Figure 4.2. Compressor and turbine sections of the system can rotate at speeds as high as 100,000 rpm. Air is compressed in a centrifugal compressor to several atmospheres before it goes to the combustor. Fuel is burnt in the combustor which heats the air which then expands through the turbine wheels. Turbine wheels drive the compressors and through the reduction gear box, the generator. If natural gas is used as fuel in the combustor, it provides the advantage of less cost, no storage problems, cleaner burning, less NO_x emissions and above all it provides higher efficiency and more power output than with any other gaseous fuel. A major problem with the use of natural gas is that it must be compressed enough to enter the combustor and known gas compressors are very expensive and require significant energy to run.

Most of the compressors available are screw type or reciprocating compressors. These are generally equipped with gas coolers, oil separators and accumulators. Due to high costs, it is desirable to provide a cheap method and apparatus for compressing the gas in a manner which eliminates typical problems associated with screw type or reciprocating compressors and also maintains the required concentration of natural gas in the mixture which is injected into the combustor.

Natural gas coming from pipelines in a residential or commercial area is kept at very low pressure ≈ 0.2 psig for fire safety reasons. Natural gas is required to be supplied to the combustor nozzle manifold at pressure as low as 1 psig . Typical gaseous fuel-air requirements are (20:1). Centrifugal compressors meet requirements of oil free operation and no rubbing shafts and seals and no sliding surfaces, however centrifugal compressors operate best (with high efficiencies) when they have a high through flow rate and a low pressure rise relative to their tip speed. These operating conditions are characterized as high specific speed conditions. Highest efficiency is generally achieved at moderate specific speeds. Under these conditions, a centrifugal compressor can operate with efficiency on the order of 78%. However, for the operating conditions needed for microturbine operation, a centrifugal compressor can only provide an efficiency of 20%. Under these low flow and high head conditions, a centrifugal compressor would need as many as 10 stages to produce the same pressure rise for a given tip speed as could single stage RFC can do. RFC provides simple, reliable design with only one rotating assembly. Operation is stable and surge free over a wide range. They have a long life which is mainly dependent on bearing life. They require fewer stages when compared to centrifugal compressors. Moreover they have higher efficiencies when compared to very

low specific speed centrifugal compressors. Regenerative flow compressor operating at low specific speed and at its best operating flow range can have efficiencies of about 55% with aerofoil blades and efficiencies of about 38% with straight radial blades. Requirements of the microturbine systems are low fuel flow and high discharge head. RFCs overcome all the shortcomings of typical compressors which can be used for microturbine operation. This makes RFC a good match for the fuel compression requirements in a microturbine system.

Capstone Turbine Corporation, CA has tested single and multistage RFC with air and natural gas as working fluids. Non-dimensionalized geometry data and non-dimensionalized performance curves for both single and multistage RFCs are presented in this chapter. Such information can be useful for predicting performance of geometrically similar machines.

4.3 Non-dimensional parameters

Six non-dimensional parameters are very critical in analysis of RFC, the impeller tip Mach number, pressure ratio, flow coefficient, specific mass flow rate, power coefficient and isothermal efficiency as defined below.

$$\text{Impeller tip Mach number } M_{OT} = \frac{r_2 \omega}{\sqrt{\gamma R T_{in}}} \tag{4.1}$$

$$\text{Pressure ratio } \Pi = P_{out} / P_{in} \tag{4.2}$$

$$\text{Flow coefficient } \lambda = \frac{Q}{8 \omega r_2^3} \tag{4.3}$$

$$\text{Specific mass flow rate } \Phi = \frac{\dot{m}}{4 r_2^2 P_{in}} \sqrt{\frac{R T_{in}}{\gamma}} \tag{4.4}$$

$$\text{Power coefficient } \Upsilon = \frac{Power\ Draw}{32\rho_{in}\omega^3 r_2^5} \tag{4.5}$$

$$\text{Isothermal efficiency } \eta_{iso} = \frac{\dot{m}RT_{in}\ln\frac{P_{out}}{P_{in}}}{Power\ Draw} \tag{4.6}$$

4.4 Single Stage RFC

Several geometric configurations of single stage RFCs were tested at Capstone. These tests were carried out using air as the working fluid. The impeller of all the single stage configurations consists of straight and radial blades with rectangular flow channel. Channel depth and hence the channel area from inlet to outlet decreases linearly. Stations A and B refer to peripheral locations near inlet and outlet respectively. A schematic diagram of impeller and channel shape is shown in Figure 4.3. Non-dimensionalized geometry data of these configurations is presented in Table 4.1. It must be noted that channel depth at both station A and B is specified in the table for clarity. The single stage configurations were investigated to study the effect of various geometric parameters related to blade and channel on performance. Below is a comparison and discussion of performance characteristics of various configurations.

4.4.1 Design point

Design point refers to the point where RFC is desired to operate for microturbine operation. The design point which is selected yields an impeller tip Mach number of 0.369 and specific mass flow rate of air equal to 1.04×10^{-3}. An attempt is made to compare various configurations and optimize the geometry at the given design point.

Configurations S1, S2, S3 and S4 have different channel inlet and exit areas. We categorize these four configurations in terms of non dimensional channel inlet areas and channel area ratios. Thus, we can say

- S1 (Lower non-dimensional channel inlet area, Normal channel area Ratio)
- S2 (Higher non-dimensional channel inlet area, Normal channel area Ratio)
- S3 (Normal non-dimensional channel inlet area, Higher channel area Ratio)
- S4 (Normal non-dimensional channel inlet area, Lower channel area Ratio)

Where

Higher non-dimensional channel inlet area = 0.0577

Normal non-dimensional channel inlet area = 0.0386

Lower non-dimensional channel inlet area = 0.0283

Higher channel area ratio = 1.309

Normal channel area ratio = 1.179

Lower channel area ratio = 1.0

Test data obtained for these four configurations is plotted in terms of impeller tip Mach number and specific mass flow rate. Figures 4.4 and 4.5 show pressure ratio and isothermal efficiency plotted against specific mass flow rate for configuration S1. It can be seen from Figure 4.4 that higher pressure ratios can be achieved at higher Mach numbers and lower specific mass flow rate. Figure 4.5 shows that a peak efficiency of 12% can be achieved at a Mach number of 0.433 and specific mass flow rate of 1.0×10^{-3}. However, at this operating point, a pressure ratio of 1.36 can be achieved with configuration S1. The data is correlated to obtain an approximate efficiency and pressure

ratio at the design point under consideration. From the correlation, a peak efficiency of 8.6% and a pressure ratio of 1.15 is predicted at the design point.

Performance characteristics of configuration S2 can be seen in Figure 4.6 and Figure 4.7. Figure 4.7 suggest that a peak isothermal efficiency of 6% can be obtained at Mach number 0.325 and specific mass flow rate of 9.77×10^{-4}. The corresponding pressure ratio at this operating point is found to be 1.19. Performance at design point is calculated by correlating the test data and it is found that an efficiency of 5.77% and pressure ratio of 1.24 can be achieved using configuration S2.

The channel inlet and exit area are larger for S2 than S1, thus making the ratio A_{in}/r_2^2 and A_{out}/r_2^2 larger. This causes a small effect on pressure ratio but huge detrimental effect on isothermal efficiency. Exactly similar trend was observed by Cates [15] in his experimental data, however no explanation was provided. The reason for this trend is flow separation at the channel walls. If the channel area is too large, the fluid does not attach to the channel walls and hence fails to circulate properly. This flow separation at channel walls results in extreme turbulence. Moreover, the fluid which fails to circulate mixes with incoming stream of fluid coming from compressor inlet and creates a blockage effect, resulting in huge loss of efficiency. In contrast, if there is small channel area, the fluid attaches to the walls and gets proper guidance and circulation. The more the circulations through the impeller, the more energy transferred to the fluid and more is the pressure ratio. Thus, a smaller channel area helps to create better pressure ratio as well. In the case of S2, pressure ratio dropped slightly because not many circulations were lost by increasing channel area, however if channel area is increased further, more pressure drop is expected.

Isothermal efficiency and pressure ratio for configuration S3 can be seen in Figure 4.8 and 4.9. A peak efficiency of 10.57% can be achieved at Mach number of 0.325 and specific mass flow rate of 1.2×10^{-3}. A pressure ratio of 1.18 is achieved at this operating point. For the design point under consideration, test data is correlated and it is found that isothermal efficiency of 9.82% and pressure ratio of 1.33 can be obtained using configuration S3.

Performance characteristics of configuration S4 can be seen in Figure 4.10 and Figure 4.11. Figure 4.10 suggests that a peak isothermal efficiency of 8.1% can be obtained at Mach number 0.325 and specific flow rate of 9.73×10^{-4}. The corresponding pressure ratio at this operating point is 1.19. Performance at design point is calculated by correlating the test data and it is found that an efficiency of 8.13% and pressure ratio of 1.30 can be achieved using configuration S4.

Best performance at the design point is obtained using S3 configuration yielding an efficiency of 9.82% and pressure ratio of 1.33. Thus it can be concluded that for the design point under consideration, S3 is the best geometric configuration for RFC. This means that at least for the design point, we can say that a normal non-dimensional inlet channel area around 0.0386 and a higher channel area ratio around 1.309 is optimal for best performance.

To investigate further, configuration S3 is chosen and pitch to cord ratio is varied. Pitch to cord ratio depends on number of impeller blades and impeller tip and hub radius. Configuration S5 is designed with higher pitch to cord ratio than pitch to cord ratio of S3 by reducing number of impeller blades "Z". Configuration S3 has a pitch to cord ratio of 0.287, while configuration S5 is designed with pitch to cord ratio of 0.418. Performance

map of

efficienc

of 9.25×

isother

efficier

there

hard

still e

Som

can

S6

(r/

is

pre

It

cor

des

We

mas

An

tha

0.4

12.6

map of configuration S5 can be seen in Figure 4.12 and 4.13. A peak isothermal efficiency of 11.08% is obtained at Mach number of 0.433 and specific mass flow rate of 9.25×10^{-4}. However, these figures suggest that as specific mass flow rate increases, the isothermal efficiency decreases significantly. Therefore, at design point, the isothermal efficiency will be much lower than the efficiency obtained using S3 configuration. Thus there is no advantage of reducing the number of impeller blades. However, still it is very hard to conclude that a pitch to cord ratio of 0.287 is optimal for RFC design, because still effect of radius ratio on performance needs to be investigated.

Some single stage test data is available where effect of radius ratio on RFC performance can be studied. Two such configurations are discussed below.

S6 configuration has a smaller radius ratio ($r_c/r_2 = 0.6$) than configuration S3 ($r_c/r_2 = 0.757$) which is considered optimal so far. A peak isothermal efficiency of 10.19% is achieved at Mach number of 0.324 and specific mass flow rate of 2.6×10^{-3} .The pressure ratio corresponding to this operating point is1.21.

It can be seen from Figure 4.14 that a very high pressure ratio can be obtained from S6 configuration, however Figure 4.15 shows that the isothermal efficiency is very low at design point. Such a configuration is good for high specific mass flow rate applications. We can achieve a good pressure ratio and higher isothermal efficiency at higher specific mass flow rates using geometry of configuration S6.

Another interesting configuration tested is S7 with a higher radius ratio of ($r_c/r_2 = 0.840$) than configuration S3 with radius ratio of ($r_c/r_2 = 0.757$). S7 operates best at Mach number 0.433 and specific mass flow rate of 4.82×10^{-4} producing isothermal efficiency of 12.62% and pressure ratio of1.43. However, it can be seen from Figure 4.16 and Figure

4.17 that s

more suit

numbers.

It is very

depende

a lower

radius r

believe

Test da

optima

RFC.

analy

perfo

collal

stage

discu

Singl

opera

requi

and p

4.5

Figur

Caps

4.17 that such a configuration does not give a good performance at our design point. It is more suited with applications of very low specific mass flow rate and high Mach numbers.

It is very hard to draw any precise conclusions from presented experimental data about dependence of RFC performance on radius ratio. However, the above analysis shows that a lower radius ratio is beneficial at high values of specific mass flow rate and higher radius ratio is beneficial at low values of specific mass flow rate. Therefore, authors believe that configuration S3 is better among all single stage configurations investigated. Test data is not enough to establish any design criteria about what sort of radius ratio is optimal. However, the authors have developed a 1-D performance prediction code for RFC. This code has a capability to predict the performance and then do a sensitivity analysis on various design parameters to study what design changes are beneficial for performance improvement. Findings from the performance prediction code are collaborated with single and multistage test data presented in this chapter and with single stage test results published by other authors to establish some design criteria. A detailed discussion of such analysis is presented in next chapter.

Single stage configurations do not produce pressure ratios desirable for microturbine operation. Capstone has developed a multistage RFC to meet fuel compression requirements of Capstone Model C30 microturbine system. Non-dimensional geometry and performance curves for this multistage RFC are discussed below.

4.5 Multistage RFC

Figure 4.18 shows full assembly of four stage RFC used in natural gas compression for Capstone Model C30 microturbine system producing 30 KW power. Lower side in

Figure 4.18 is called the motor side while top side is called the pump side. Impeller mounted on the motor side represents the first stage, while fourth stage impeller is on the pump side. Layout of the four stages can be seen in Figure 4.19. It can be seen that the cross sectional area of channel for the first stage is largest and that of the fourth stage is smallest. The flow enters from the pump side and travels all the way down and enters the impeller of the first stage. The inlet hole has a constant cross sectional area and it takes the fluid entering from the pump side to the first stage inlet. The discharge nozzle is tapered to match the channel areas at discharge of each stage. Figure 4.20 represents the impeller of first stage of RFC containing straight radial blades machined across the periphery. The inlet and discharge ports are separated by stripper which constitutes about 30° of the periphery. Blades of the four stage RFC are straight and radial like those in single stage RFC configurations, however the channel is semi-circular in cross section as shown in Figure 4.21. This figure shows semi-circular flow channel of first stage built in the casing. Channel area from inlet to discharge port decreases linearly.

A schematic diagram of impeller and channel shape is shown in Figure 4.22. At design point, the impeller tip Mach number is 0.369 and specific mass flow rate of natural gas is 1.04×10^{-3}. Although multistage RFC builds required pressure ratio, however very low isothermal efficiency levels $(15-20\%)$ are achieved. When comparing efficiency to historical test results it appears that significant improvements in efficiency could be achieved. Non-dimensionalized geometry of all four stages of RFC can be found in Table 4.2.

Figure 4.23 shows pressure ratio and isothermal efficiency plotted against the impeller tip Mach number using natural gas as the working fluid. Test data is plotted for four inlet

pressures of 0 psig, 5 psig, 10 psig and 15 psig at flow rate of 195 slpm keeping inlet temperature at $70^{\circ}F$. It can be observed that if the inlet pressure is low, the compressor needs to run at higher rpm (higher Mach number) to produce same pressure ratio. A maximum pressure ratio of 4.4 is obtained at a very low efficiency of 14.14%. Maximum efficiency of 38.85% is achieved, however this corresponds to a very low pressure ratio of1.5. Higher Mach numbers produce lower isothermal efficiencies, but higher pressure ratio and vice versa. The pressure ratio increases with the Mach number consistently.

Figure 4.24 is a plot of pressure ratio and isothermal efficiency using natural gas as working fluid at inlet pressures of 0 psig,5 psig,10 psig and15 psig at flow rate of250 slpm keeping inlet temperature at $70^{\circ}F$. It can be observed that higher flow rates produce relatively low head, however they result in better isothermal efficiency. Moreover, at higher flow rates, the peak efficiencies and maximum pressure ratios are obtained at relatively higher Mach numbers. Maximum efficiency of 40% is obtained and maximum pressure ratio of 3.72 is obtained with an isothermal efficiency of 18.43%. Figure 4.25 is performance map of four stage RFC with air as working fluid. The inlet temperature was again kept at $70^{\circ}F$ and through flow rate was 250 slpm. Non-dimensional test data for pressure and isothermal efficiency is presented for four inlet pressures of 0 psig, 5 psig, 10 psig and15 psig. The trends look similar to previous results for natural gas shown in Figure 4.23 and Figure 4.24. Higher pressure ratios and lower isothermal efficiencies are obtained at high Mach numbers. Lower inlet pressures produce higher pressure ratios. The maximum obtainable efficiency increases to almost 45% and maximum pressure ratio of 4.4 is obtained with an isothermal efficiency of 19.25%.

These trends have been validated by many researchers in the past through testing. A good example is testing done by Cates [15], who conducted extensive tests on various gases with molecular weight varying from 4 – 400. Figure 4.26 reproduced from Cates [15] suggests that pressure ratio increases fairly consistently with Mach number until $M_{OT} \approx 0.75$. From that point onward, an increase in Mach number results in decrease in performance indicating a maximum obtainable pressure ratio. The curves depart from a straight line at about $M_{OT} = 0.4$ to 0.6 , where we believe that compressibility effects start to influence. Figure 4.27 shows the pressure ratio plotted against specific mass flow rate for various gases at various tip Mach numbers. Figure 4.28 shows the variation of adiabatic efficiency with specific mass flow rate for various gases at various impeller tip Mach numbers. Exactly same trends are observed for Capstone RFC as were obtained by Cates through testing. There is an interesting difference between regenerative compressors and centrifugal compressors in power coefficient. Centrifugal compressors draw more power at higher flow rates, however regenerative compressors draw more power at low flow rates. The primary reason for that is increased number of circulations through the impeller blades at low flow rate producing very high heads at low flow rates for RFC. However, these large number of circulations through the blades require high amount of power draw. This is the reason why in RFCs we see a high pressure ratio at low flow rates, but very low efficiency.

4.6 Correlations among non-dimensional parameters

The above analysis discussed performance characteristics of Capstone multistage RFC. Extensive test data is presented in the form of various non-dimensional parameters.

However, to make this discussion useful for designers and engineers, a three dimensional representation of performance characteristics of multistage RFC is provided. Various correlations are developed by best fit curve from three dimensional plots to quickly estimate the performance of geometrically similar machines. These correlations are provided in Appendix A.

Figure 4.29 is a three dimensional plot of impeller tip Mach number, flow coefficient and pressure ratio for the four stage RFC. The scattered points were taken at various inlet pressures, various speeds and flow rates using air and natural gas as working fluids. Test data are non-dimensionalized and a best fit curve is drawn to see the overall trend among various non-dimensional variables. A higher pressure ratio is obtained at low flow coefficient and higher Mach number. This is a characteristic of RFC to produce high heads at low flow rates. Isothermal efficiency is plotted against impeller tip Mach number and flow coefficient in Figure 4.30. The test data collected at various operating conditions is non-dimensionalized and plotted in this figure. To see the overall trend, a best fit curve is plotted as shown in the figure. Efficiency initially increases with increasing flow coefficient, but after a certain limit it starts to go down. Similar trends were found by Cates [15] and Wilson [69]. Moreover, it is obvious from Figure 4.30 that isothermal efficiency decreases with increasing Mach numbers at a given flow coefficient. Specific mass flow rate is another non-dimensional parameter plotted against impeller tip Mach number and pressure ratio as shown in Figure 4.31. Scattered test data points are plotted on this curve along with the best fit curve. Higher pressure ratios are obtained at higher Mach number and lower values of specific mass flow rate. Similar trends were observed by Cates [15]. Figure 4.32 represents isothermal efficiency plotted against

impeller tip Mach number and specific mass flow rate. Once again, it is obvious that lower Mach numbers produce higher efficiency. Moreover, the efficiency starts to go up with increasing specific mass flow rate, however after reaching a certain point, it starts to go down. The correlations provided in Appendix A are very useful to study performance characteristics of RFC. Generally, there is a compromise between efficiency and pressure ratio. If a designer strives for higher efficiency, he needs to sacrifice some pressure ratio and vice versa. Thus, these correlations provide the designer with information that what performance characteristics can be obtained at given operating point using geometry similar to the multistage RFC.

4.7 Conclusions

Experimental data on single and multistage RFCs is presented in the form of various non-dimensional parameters. Moreover, a systematic experimental sensitivity analysis on single stage RFC is discussed to get an understanding how various geometric parameters (impeller radius ratio, channel area ratio, channel dimensions and pitch to cord ratio etc) effect RFC performance. The following conclusions can be drawn from this analysis.

- RFCs are capable of producing high pressure ratios at low specific mass flow rates.
- Higher efficiencies are obtained as specific mass flow rate increases, however after a certain point where peak efficiency is achieved, the efficiency starts to go down.
- Higher pressure ratios and lower isothermal efficiencies are obtained at higher tip Mach numbers and vice versa.

- Higher pressure ratios and lower isothermal efficiencies are obtained at lower inlet pressure for a given tip Mach number. As the inlet pressure is increased, pressure ratio goes down but higher efficiency levels can be achieved.
- Correlations for various non-dimensional parameters are provided through experimental analysis. These correlations can be very useful for designers and engineers to estimate performance of geometrically similar regenerative compressors.
- It is difficult to optimize RFC geometry for its full operating range. However, it is possible to use the above test data to optimize the geometry at a given design point.
- A complete analysis of various geometric parameters on performance is very much needed, so that the effect of RFC geometry on performance can be studied. Design criteria need to be established and used to optimize the geometry for best performance. Such a theoretical analysis is presented in next two chapters.

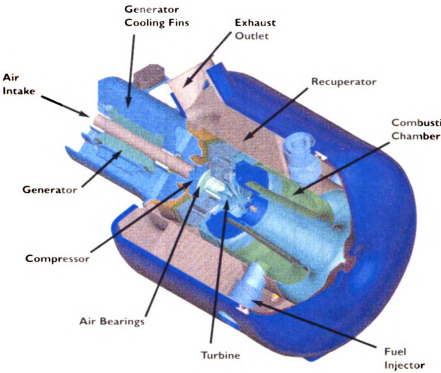

Figure 4.1 The Capstone Model 330 microturbine generator

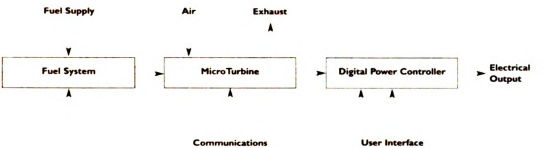

Figure 4.2 Schematic of Capstone Model 330 microturbine system

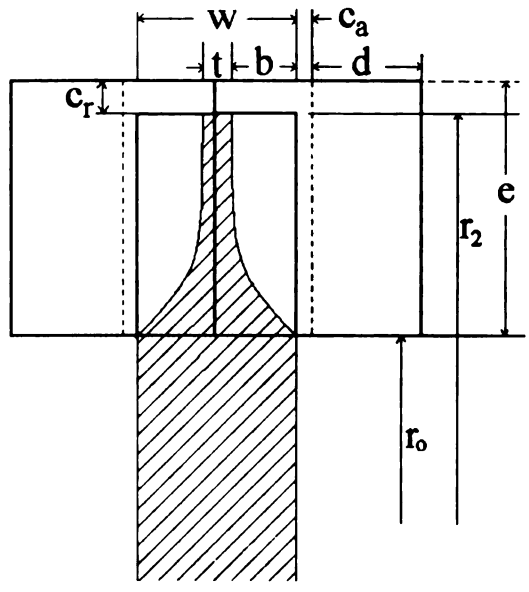

Figure 4.3 Schematic of blade and channel geometry for single stage RFC configuration

Table 4.1 Geometry of various single stage RFC configurations

RFC Config.	Radius Ratio r_o / r_2	Non-Dim Blade Depth b / r_2	Non-Dim Blade Height e / r_2	Non-dim Radial clearance c_r / r_2	Non-dim impeller width $(2b+t) / r_2$	Non-dim Axial clearance c_a / r_2
S1	0.757	0.0606	0.298	0.0566	0.1392	0.00302
S2	0.757	0.0606	0.298	0.0566	0.1392	0.00302
S3	0.757	0.0606	0.298	0.0566	0.1392	0.00302
S4	0.757	0.0606	0.298	0.0566	0.1392	0.00302
S5	0.757	0.0606	0.298	0.0566	0.1392	0.00302
S6	0.6	0.1	0.492	0.0935	0.23	0.005
S7	0.840	0.04	0.196	0.0374	0.092	0.002

Contd

RFC Config.	Non-dim channel depth at inlet d_A / r_2	Channel depth at exit d_B / r_2	Pitch to cord ratio PC	Non-dim channel inlet area A_{in} / r_2^2	Non-dim channel exit area A_{out} / r_2^2	Channel area ratio A_{in} / A_{out}
S1	0.0484	0.0314	0.287	0.0283	0.0240	1.179
S2	0.1696	0.135	0.287	0.0577	0.0489	1.179
S3	0.0908	0.0532	0.287	0.0386	0.0295	1.309
S4	0.0908	0.0908	0.287	0.0386	0.0386	1.0
S5	0.0908	0.0532	0.418	0.0386	0.0295	1.309
S6	0.15	0.055	0.461	0.105	0.0892	1.179
S7	0.06	0.022	0.4	0.0168	0.0142	1.179

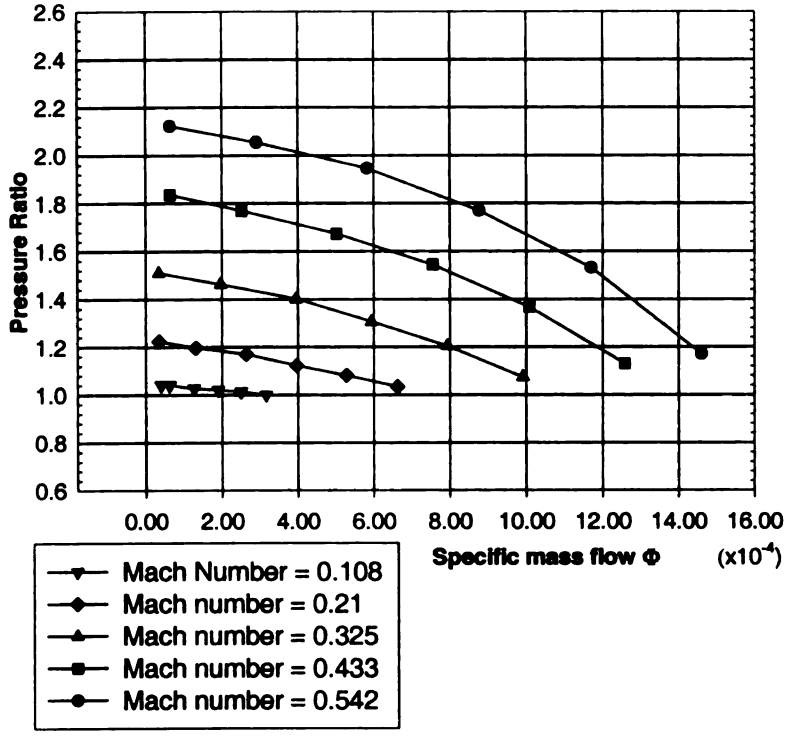

Figure 4.4 Pressure ratio vs. specific mass flow rate at various tip Mach numbers for configuration S1

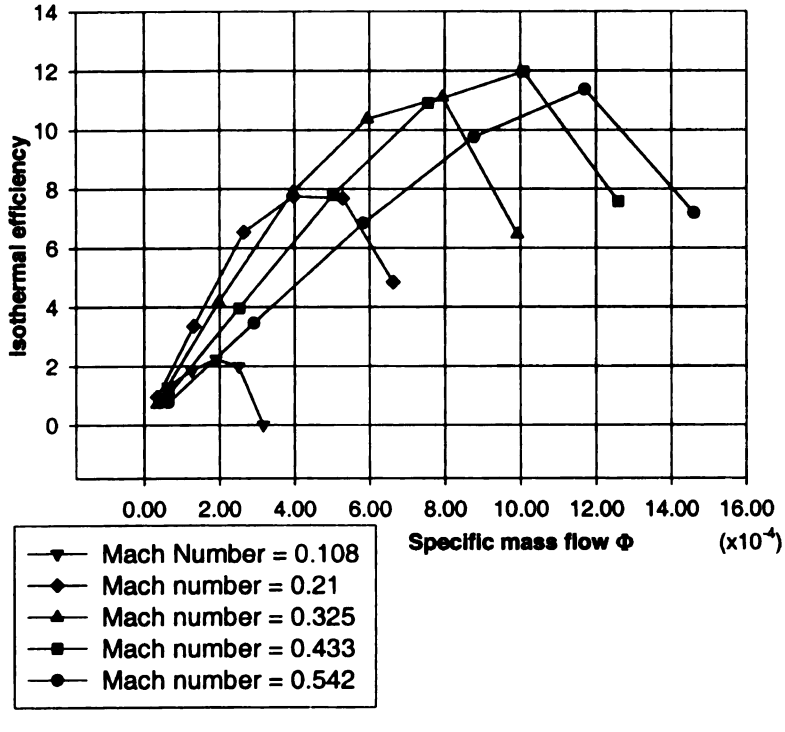

Figure 4.5 Isothermal efficiency vs. specific mass flow rate at various tip Mach numbers for configuration S1

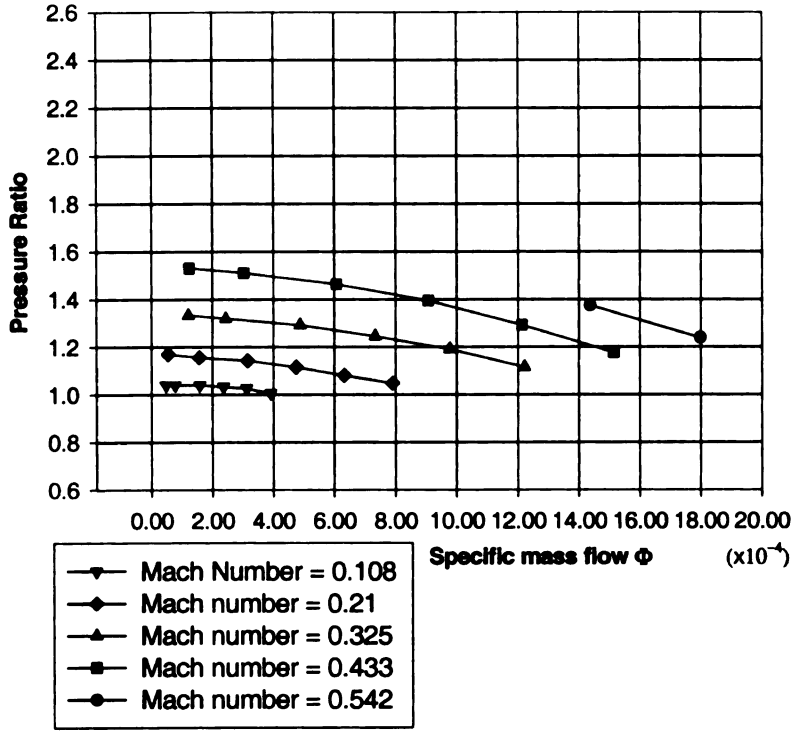

Figure 4.6 Pressure ratio vs. specific mass flow rate at various tip Mach numbers for configuration S2

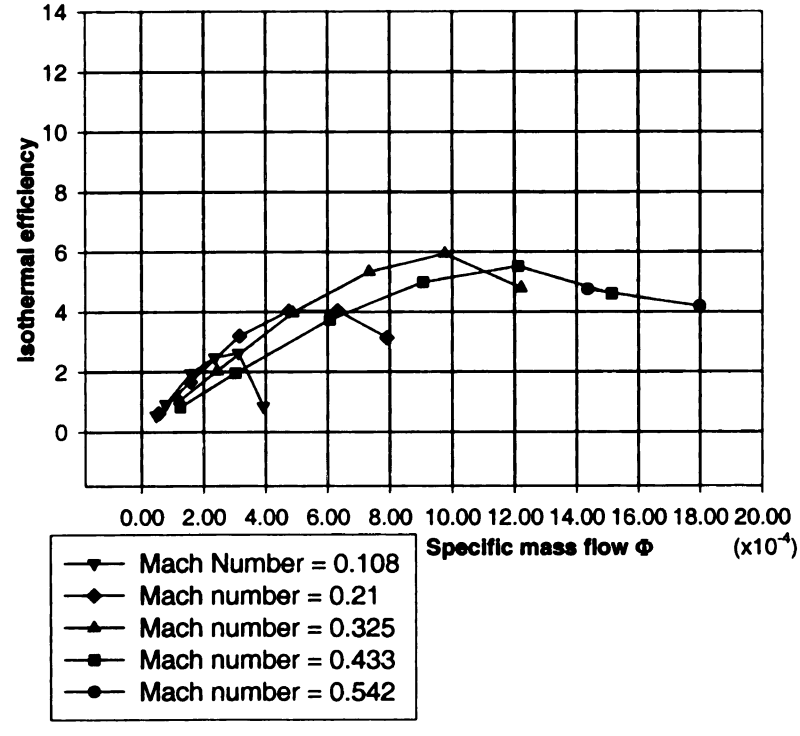

Figure 4.7 Isothermal efficiency vs. specific mass flow rate at various tip Mach numbers for configuration S2

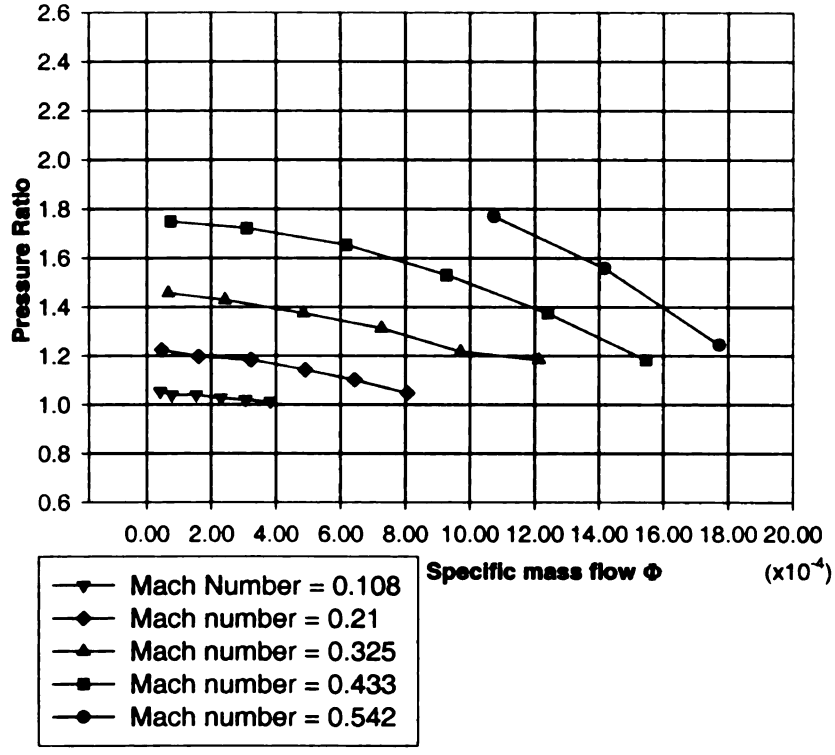

Figure 4.8 Pressure ratio vs. specific mass flow rate at various tip Mach numbers for configuration S3

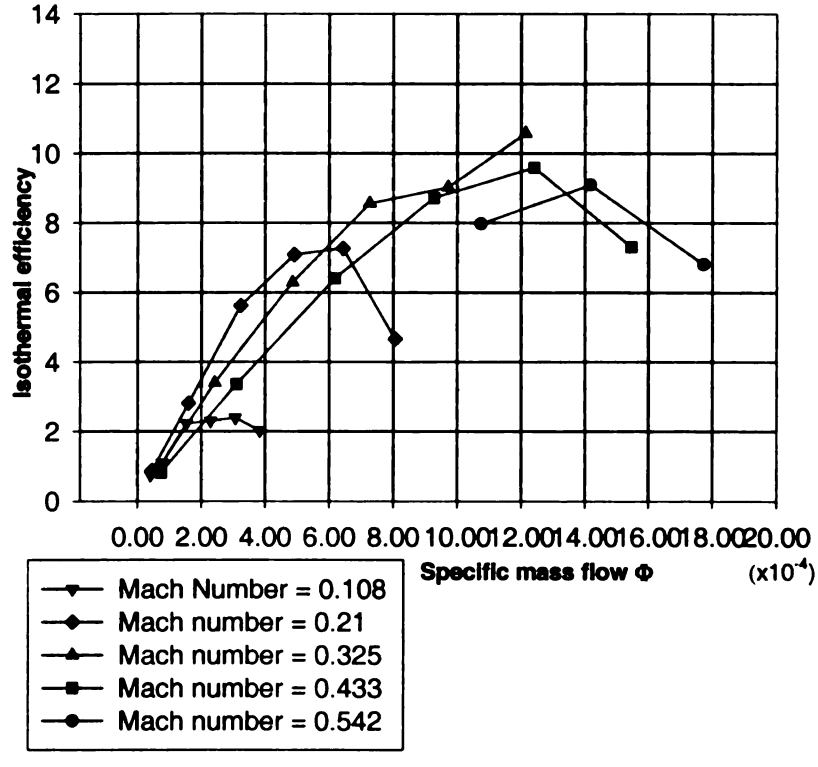

Figure 4.9 Isothermal efficiency vs. specific mass flow rate at various tip Mach numbers for configuration S3

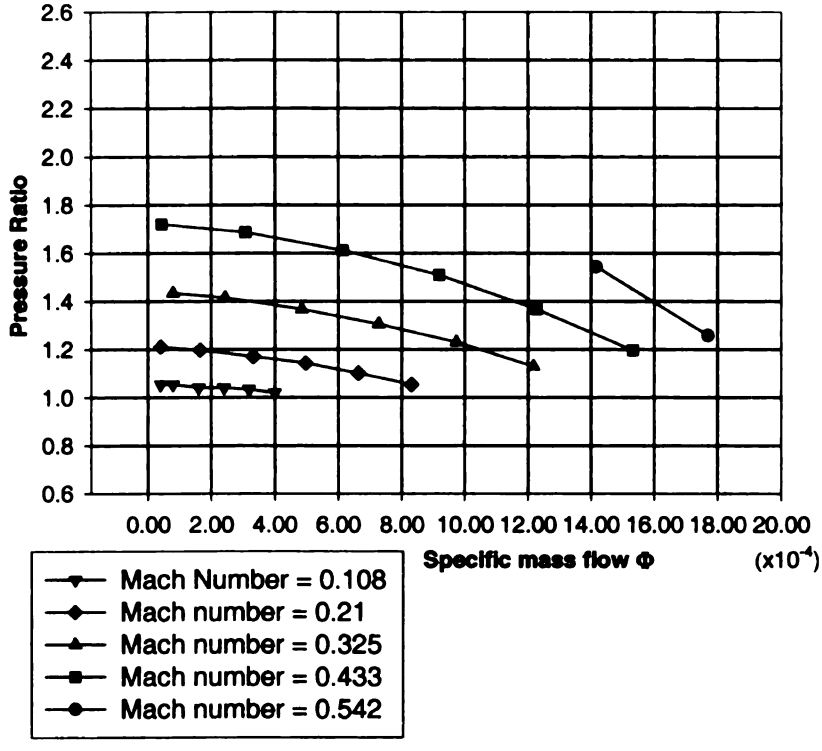

Figure 4.10 Pressure ratio vs. specific mass flow rate at various tip Mach numbers for configuration S4

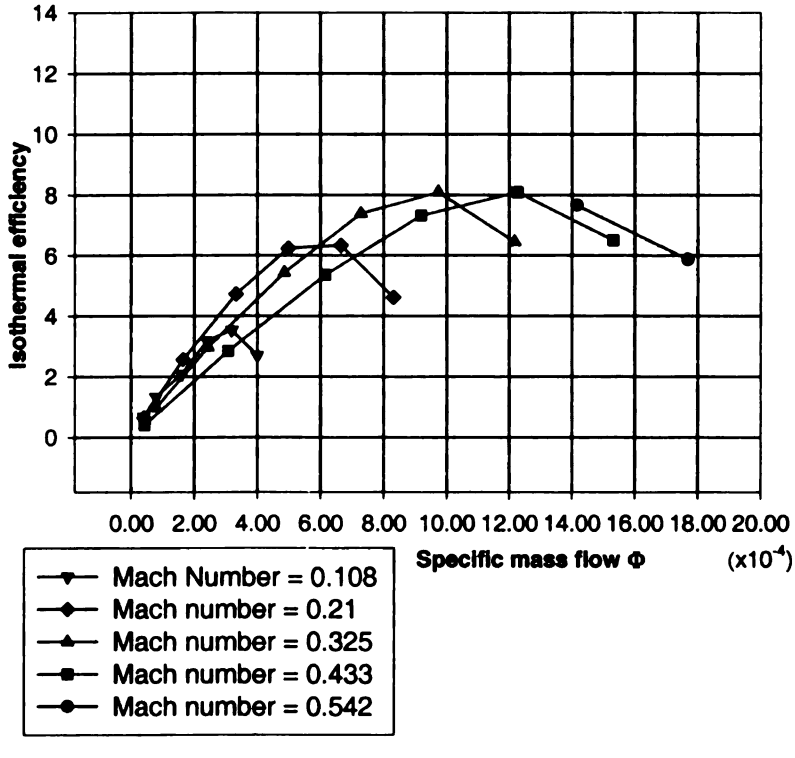

Figure 4.11 Isothermal efficiency vs. specific mass flow rate at various tip Mach numbers for configuration S4

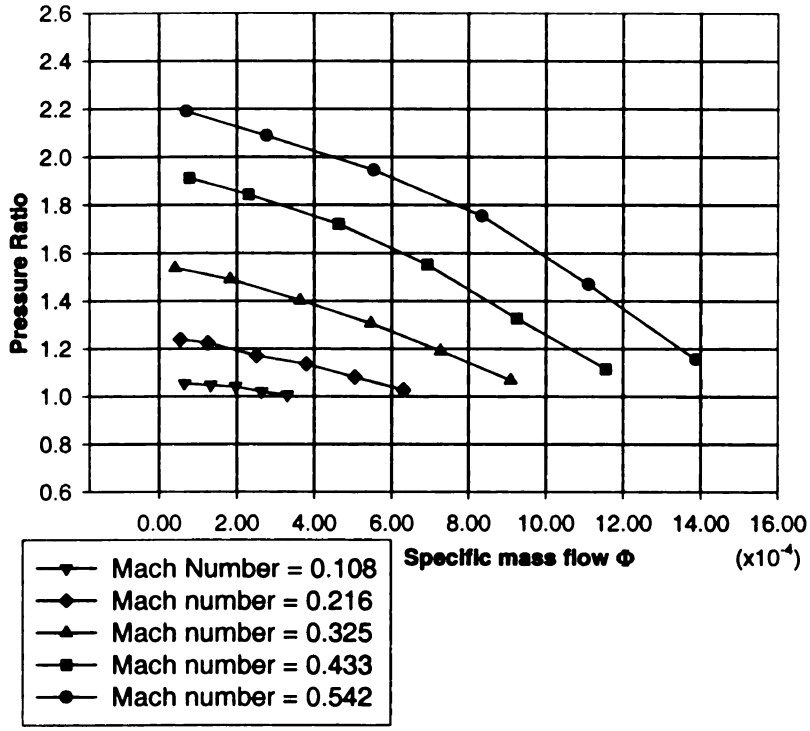

Figure 4.12 Pressure ratio vs. specific mass flow rate at various tip Mach numbers for configuration S5

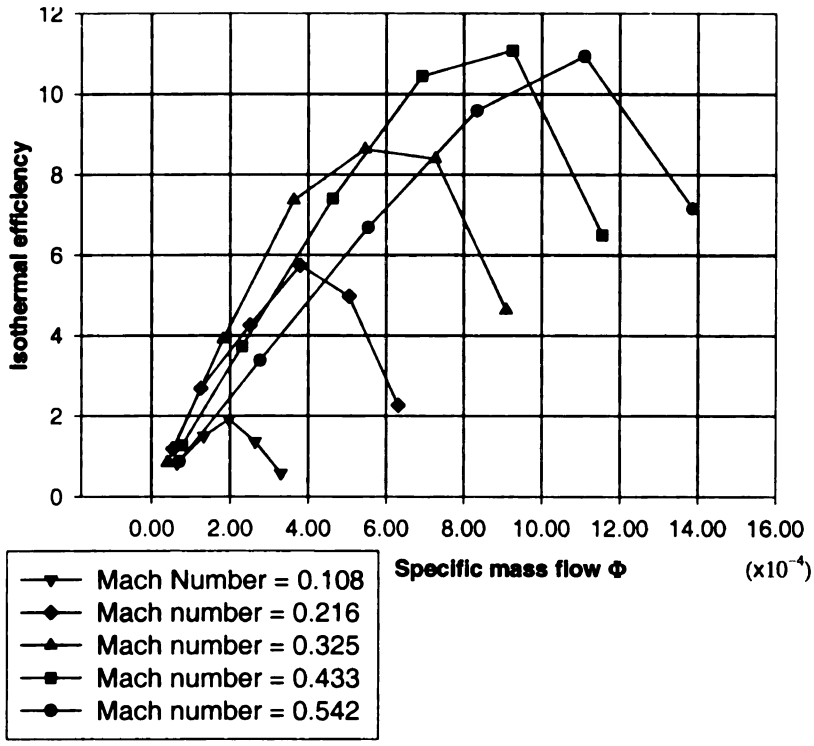

Figure 4.13 Isothermal efficiency vs. specific mass flow rate at various tip Mach numbers for configuration S5

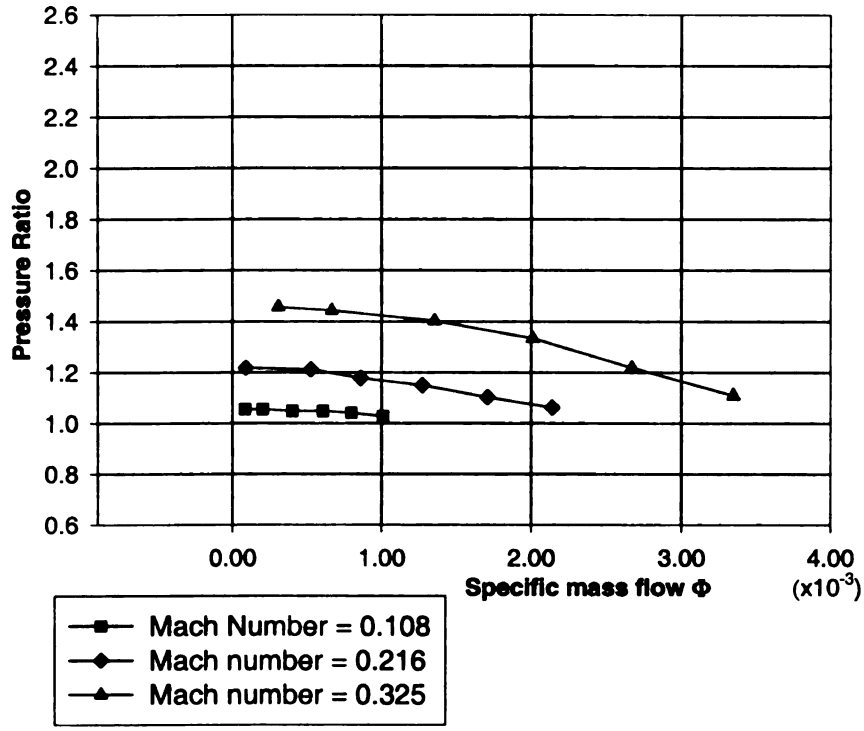

Figure 4.14 Pressure ratio vs. specific mass flow rate at various tip Mach numbers for configuration S6

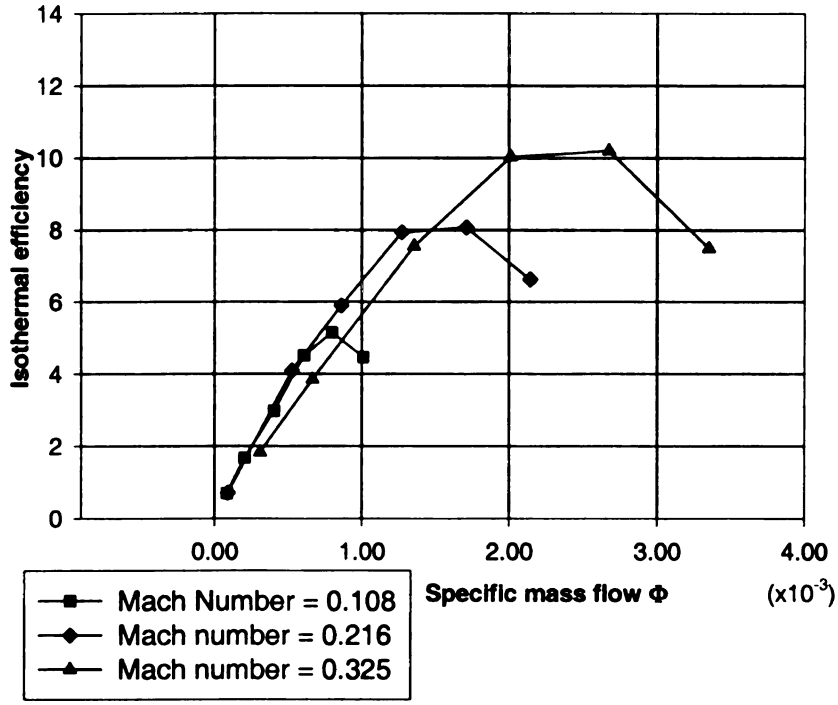

Figure 4.15 Isothermal efficiency vs. specific mass flow rate at various tip Mach numbers for configuration S6

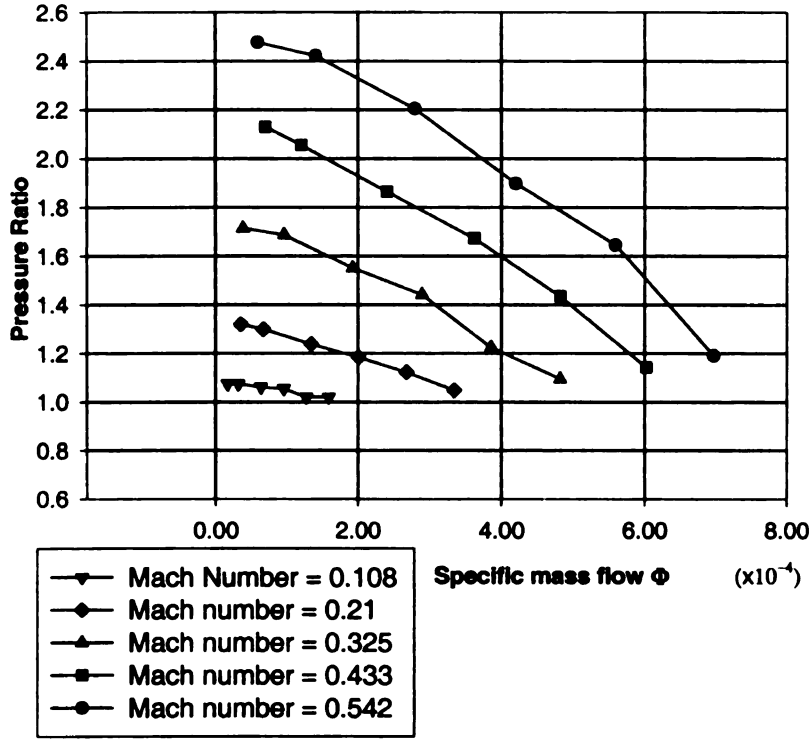

Figure 4.16 Pressure ratio vs. specific mass flow rate at various tip Mach numbers for configuration S7

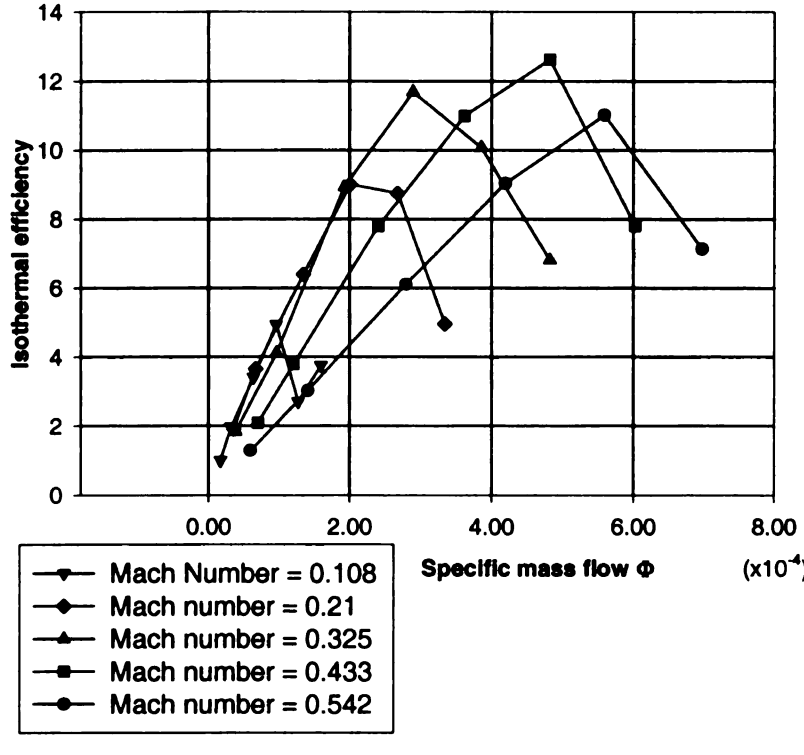

Figure 4.17 Isothermal efficiency vs. specific mass flow at various tip Mach numbers rate for configuration S7

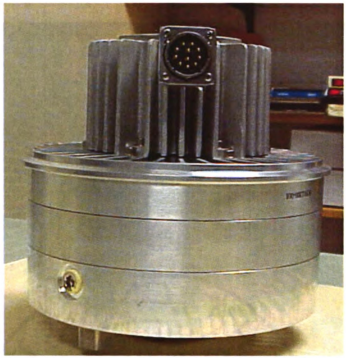

Figure 4.18 Four stage RFC full assembly

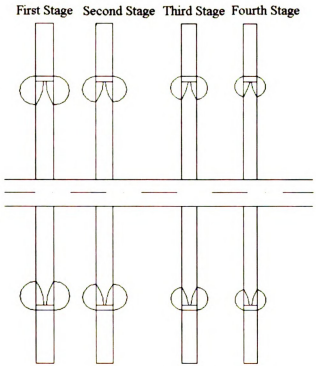

Figure 4.19 Sketch of four stage RFC

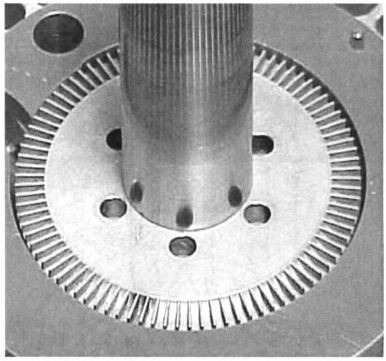

Figure 4.20 1st stage impeller of four stage RFC

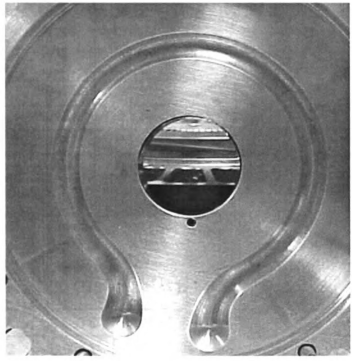

Figure 4.21 1st stage channel of four stage RFC

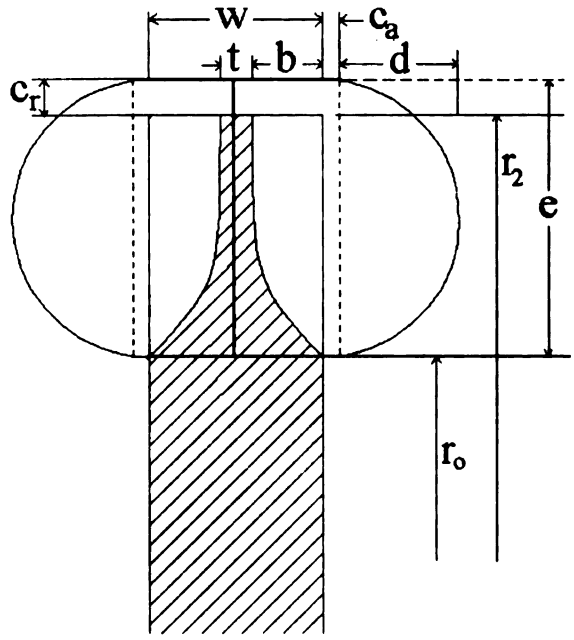

Figure 4.22 Schematic of blade and channel geometry

Table 4.2 Geometry of individual stages of four stage RFC

RFC Stage	Radius Ratio r_o / r_2	Non-dim Blade Depth b/r_2	Non-dim Blade Height e/r_2	Non-dim Radial Clearance c_r/r_2	Non-dim Blade thickness t/r_2	Non-dim Axial Clearance c_a/r_2
1st	0.828	0.0477	0.200	0.0286	0.0151	0.00310
2nd	0.849	0.0429	0.174	0.0238	0.0145	0.00310
3rd	0.866	0.0381	0.155	0.0226	0.0145	0.00286
4th	0.888	0.031	0.131	0.0193	0.0151	0.00286

Contd

RFC Stage	Channel depth at inlet d_A / r_2	Channel depth at exit d_B / r_2	impeller width $(2b+t)/r_2$	Channel inlet area A_{in} / r_2^2	Channel exit area A_{out} / r_2^2	Channel area ratio A_{in} / A_{out}	Pitch to cord ratio PC
1st	0.107	0.0878	0.1104	0.0172	0.0134	1.281	0.406
2nd	0.0932	0.0763	0.1004	0.0130	0.0101	1.286	0.463
3rd	0.0818	0.0672	0.0909	0.0100	0.00789	1.279	0.525
4th	0.0689	0.0563	0.0770	0.00723	0.00562	1.286	0.619

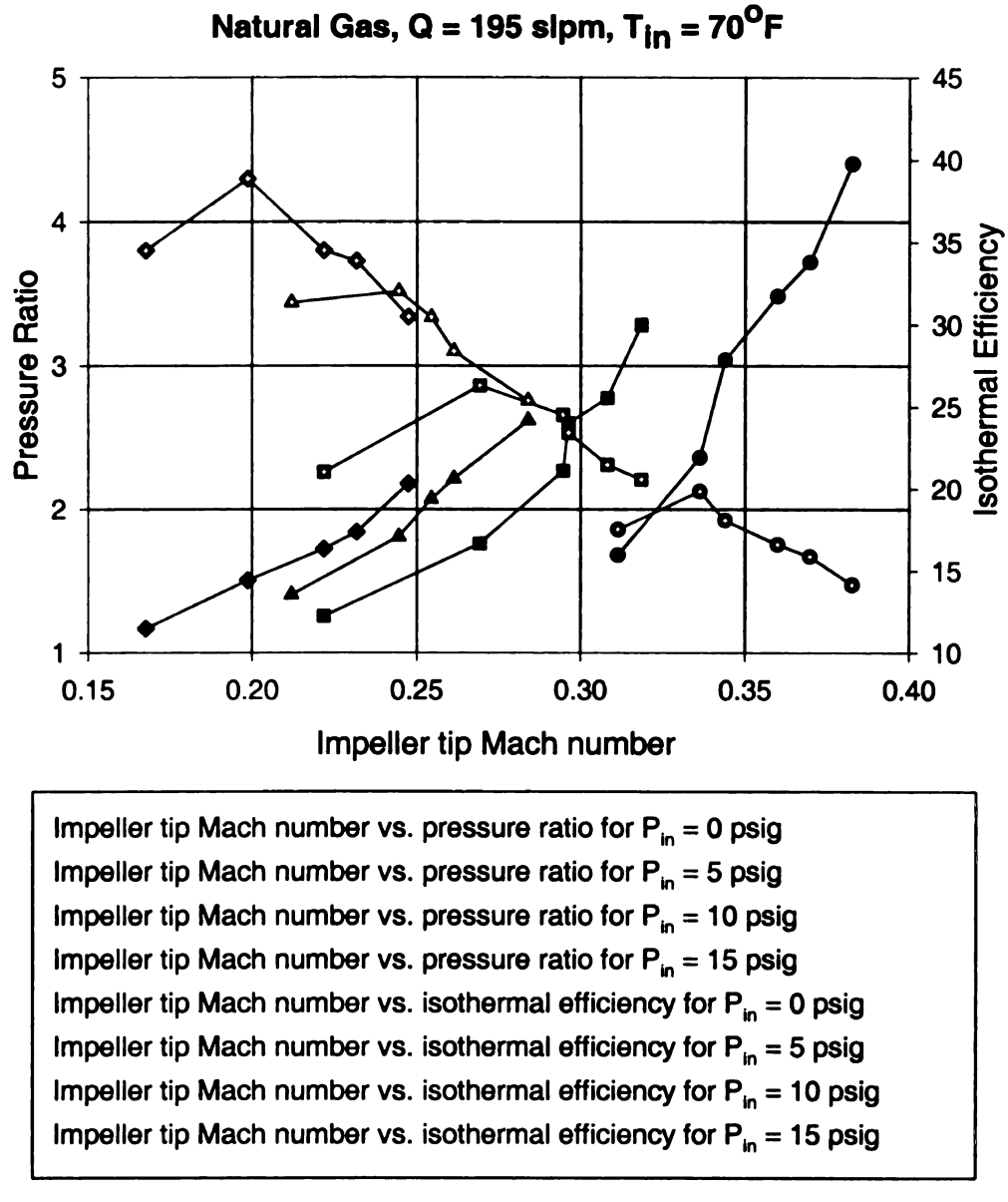

Figure 4.23 Pressure ratio and isothermal efficiency vs. impeller tip Mach number for various inlet pressures

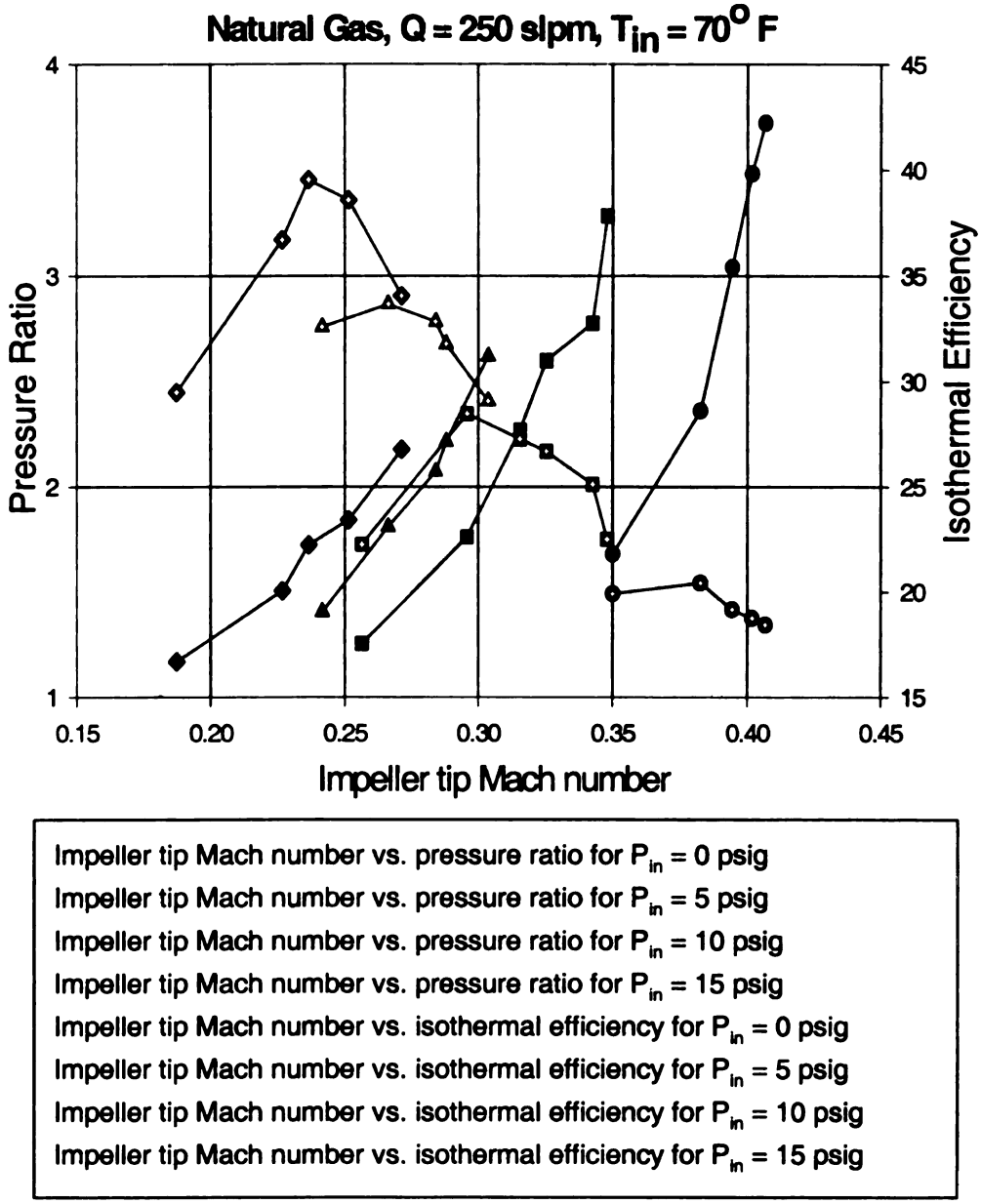

Figure 4.24 Pressure ratio and isothermal efficiency vs. impeller tip Mach number for various inlet pressures

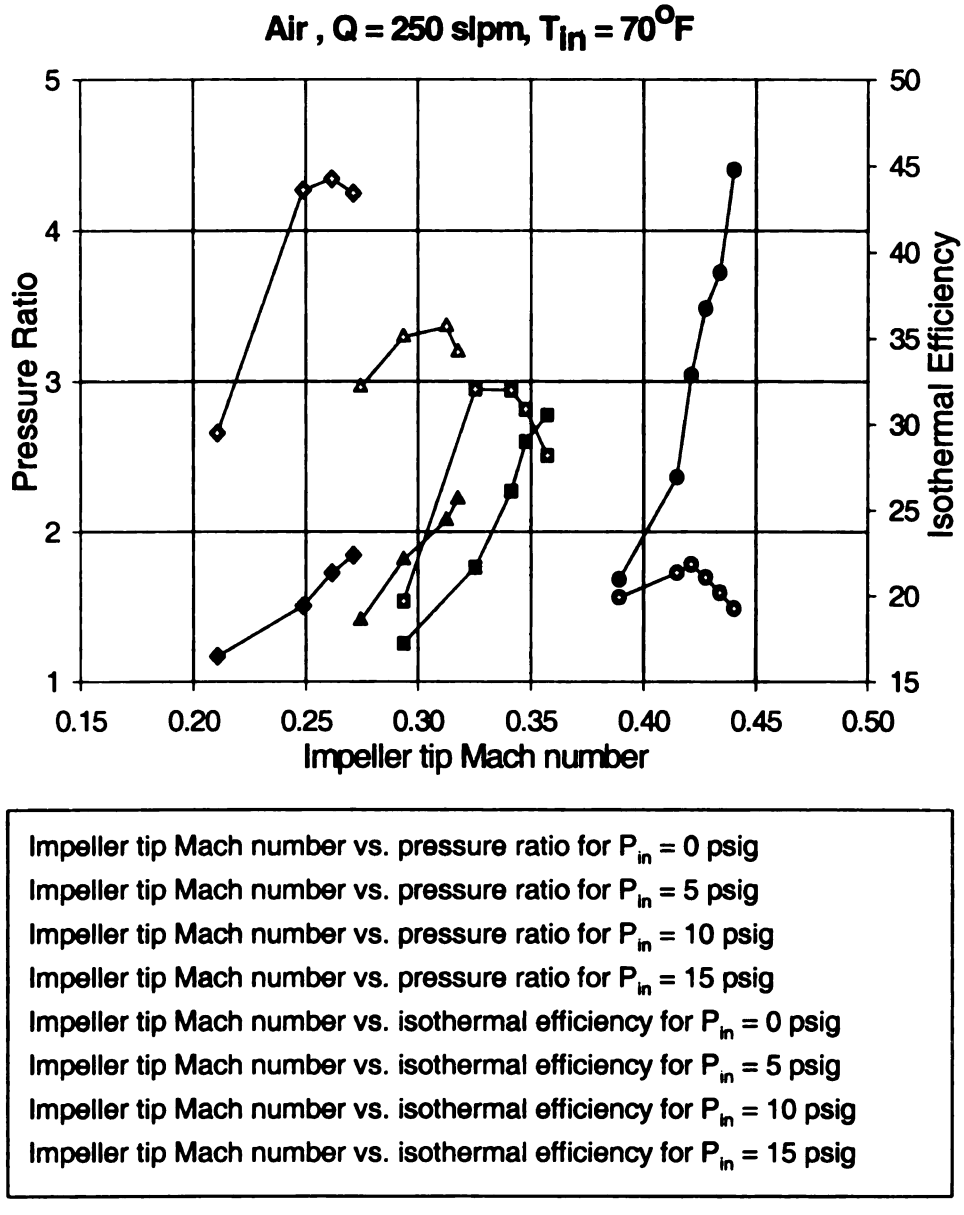

Figure 4.25 Pressure ratio and isothermal efficiency vs. impeller tip Mach number for various inlet pressures

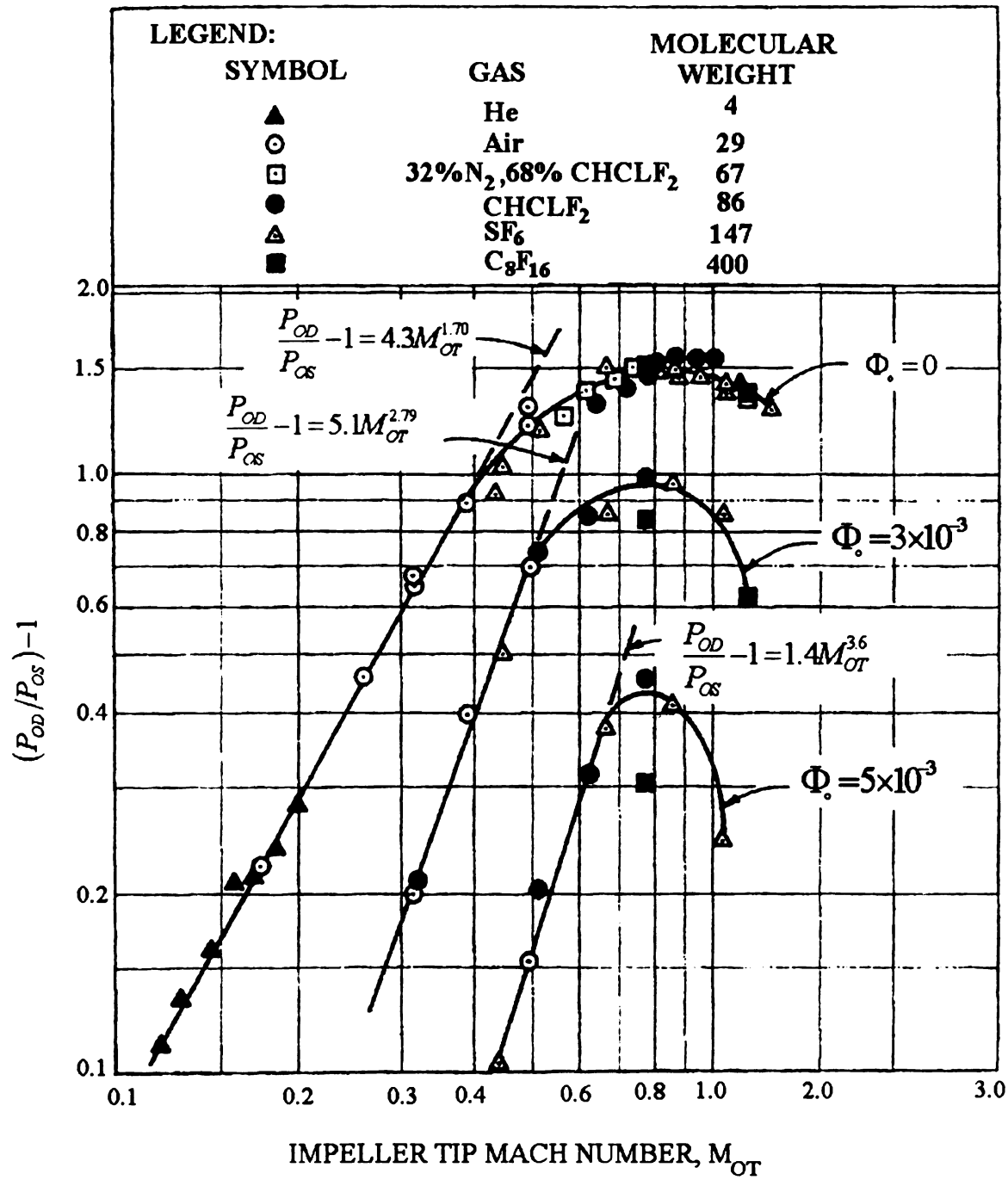

Figure 4.26 Pressure ratio vs. impeller tip Mach number (after Cates, 1964)

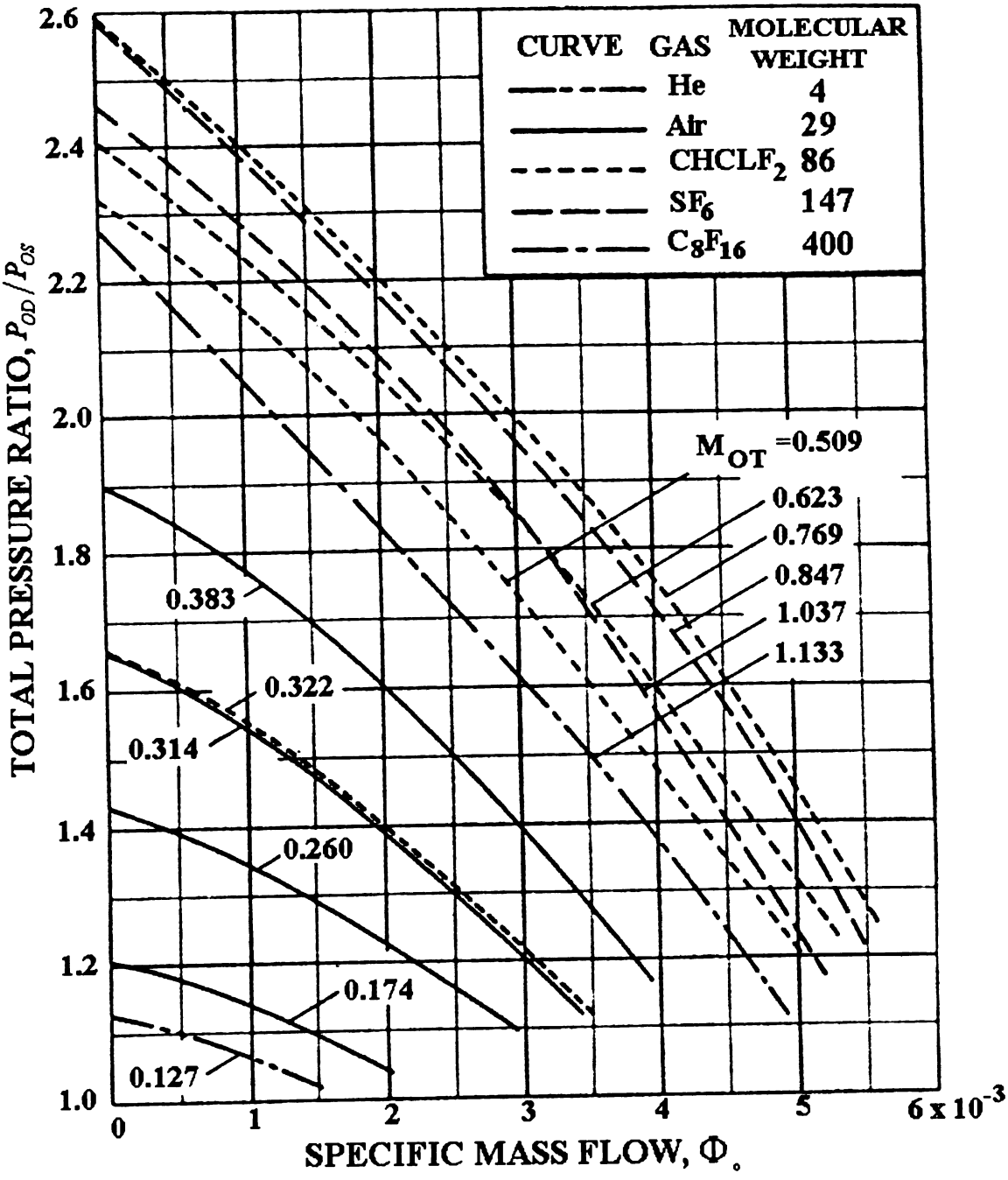

Figure 4.27 Performance map of the ORGDP-1 regenerative compressor (after Cates, 1964)

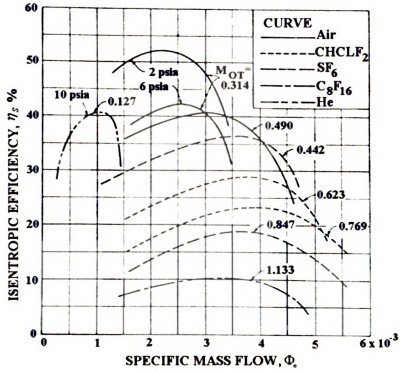

Figure 4.28 Efficiency of the ORGDP-1 regenerative compressor (after Cates, 1964)

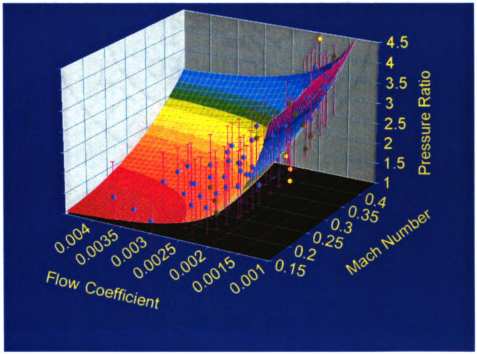

Figure 4.29 Pressure ratio vs. impeller tip Mach number and flow coefficient for four stage RFC

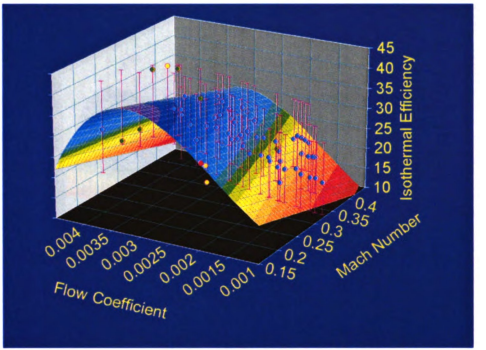

Figure 4.30 Isothermal efficiency vs. impeller tip Mach number and flow coefficient for four stage RFC

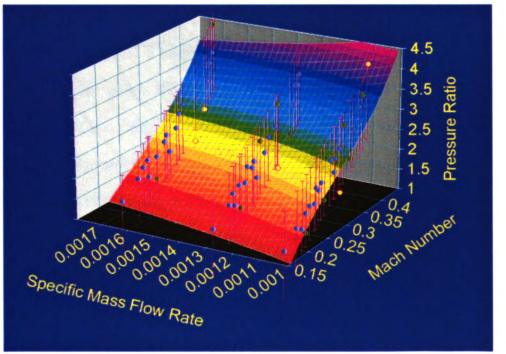

Figure 4.31 Pressure ratio vs. impeller tip Mach number and specific mass flow rate for four stage RFC

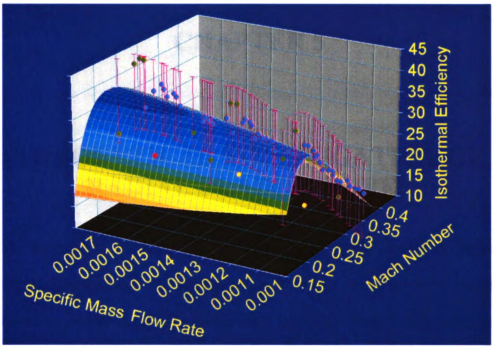

Figure 4.32 Isothermal efficiency vs. impeller tip Mach number and specific mass flow rate for four stage RFC

CHAPTER 5

THEORETICAL INVESTIGATION OF RADIAL BLADE RFC/RFP

There are very few mathematical models in literature which explain the behavior of regenerative turbomachines and predict the performance. Most of these models need extensive experimental support for performance prediction. Hence, it is very interesting from an industrial stand point of view to find efficient theoretical means which are able to forecast the regenerative turbomachine performances using easy to find geometric and fluid dynamic parameters.

Wilson et al [69] presented a theoretical analysis of the three-dimensional fluid motion inside a regenerative pump. Basic model developed by Wilson was to represent the phenomenon in the linear region as shown in Figure 2.10. He made several assumptions and applied fluid dynamic equations to arbitrary control volumes of the pump. The entire pump flow was characterized by tangential velocity V_t and circulatory velocity V_c along a mean streamline. Dimensionless performance characteristics for STA-RITE TH 7 regenerative pump were tested and reported in Wilson et al [69]. Experimental plots of flow versus head were obtained at seven different speeds with air as working fluid. Calculated and experimental performance curves were compared and excellent agreement was observed. Qualitatively, the relations presented by Wilson satisfied the major details of the observed flow phenomena, but they needed extensive experimental support to

predict performance. Moreover, his model assumed incompressible flow, thus unable to predict performance of compressors producing high pressure ratio. Moreover, Wilson model lacked in correlation of losses with geometric and aerodynamic parameters. Wilson's work is extended here to incorporate compressible flow to predict the performance characteristics of Capstone multistage RFC. Moreover, 1-D loss modeling is done to correlate various losses with geometric and aerodynamic parameters, thus eliminating need of experimental support.

5.1 Mathematical Model

Mathematical formulation is based on an arbitrary element of depth $dX_G = r_G d\theta$ in the peripheral direction of compressor as shown in Figure 5.1. Equations of motion can be derived by considering these arbitrary small elements of one side blade and channel. Dimensions of the impeller and flow channel are given symbolically in Figure 5.2 where points 1 and 2 denote the locations at which assumed streamline enters and leaves the impeller respectively. For simplicity in the presentation of the analysis, wall friction and other irreversibility are introduced as head losses.

5.1.1 Assumptions

Following assumptions are made to develop the mathematical model.

- Fluid is assumed incompressible locally within a control volume. In the case of a pump, the fluid is assumed incompressible throughout the pump operation and there is no variation in density from one control volume to the other. However, in the case of a compressor, density changes from one control volume to the other. Thus density is incremented from one control volume to the next using a

correlation which is developed from experimental data. This correlation is generic because it is expressed in terms of non-dimensional parameters. It can be used for the analysis of geometrically similar RFC. Details of this correlation can be found in Appendix B.

- Fluid shear is assumed negligible in the model, however it is considered later in the calculation by assuming a model for tangential head loss.
- Steady flow without any leakages is assumed. Leakages are considered in a separate model to avoid complexity in mathematics. Thus leakages are assumed zero in the basic model.
- Characteristic flow is one-dimensional in which major direction is radial, tangential, and axial. The actual path traversed by a streamline is shown in Figure 5.2.
- There are no end effects of suction, discharge and stripper carryover. The inlet and exit losses are considered in a separate model.
- Tangential pressure gradient is independent of radius. Literature and experimental studies have confirmed that this assumption is quite valid.
- Although, tangential pressure gradient around the periphery is not perfectly linear, however for simplicity, assumption of linear pressure rise across the periphery is reasonable.

5.1.2 Governing Equations

The tangential components of velocity at points 1 and 2 can be given as

$$V_{\theta 1} = \alpha U_1 \tag{5.1}$$

$$V_{\theta 2} = \sigma U_2 \tag{5.2}$$

where σ is the slip factor and α is a shock loss parameter introduced at blade entrance to quantify shock losses. More details on calculation of slip factor and shock loss parameter are provided later in this chapter.

Circulatory velocity at point 1 and 2 is assumed to be equal. Thus,

$$V_{c1} = V_{c2} = V_c \tag{5.3}$$

Circulatory flow rate can be approximated by

$$dQ_c = c_r V_c dX_G \tag{5.4}$$

Applying angular momentum equation to the impeller control volume of Figure 5.1, we get

$$dT = \rho dQ_c \left(r_2 \sigma U_2 - r_1 \alpha U_1 \right) + r_G A_b \frac{dp}{d\theta} d\theta \tag{5.5}$$

Last term on the right hand side in the above equation represents the work done in raising the pressure of the fluid between the impeller blades. This pressure rise is utilized across the stripper to perform a turbine work. Therefore this term is ignored. Power input to the differential control volume can be given as

$$dP = \omega dT \tag{5.6}$$

Thus we can write,

$$dP = \rho dQ_c \left(\sigma U_2^2 - \alpha U_1^2 \right) \tag{5.7}$$

Applying Bernoulli's equation to the impeller control volume of Figure 5.1, we get

$$dP = \rho dQ_c \left(\frac{\sigma^2 U_2^2}{2} + \frac{V_{c2}^2}{2} + \frac{p_2}{\rho} - \frac{\alpha^2 U_1^2}{2} - \frac{V_{c1}^2}{2} - \frac{p_1}{\rho} \right) \tag{5.8}$$

Equations (5.7) and (5.8) yield,

$$\frac{p_1}{\rho} + \frac{V_{c1}^2}{2} + \frac{\alpha^2 U_1^2}{2} + \sigma U_2^2 = \frac{p_2}{\rho} + \frac{V_{c2}^2}{2} + \frac{\sigma^2 U_2^2}{2} + \alpha U_1^2 + g H_{cb} \tag{5.9}$$

where gH_{cb} is the head loss of circulatory velocity through the impeller region.

Applying continuity equation to the channel control volume of Figure (5.1).

$$\rho(V_{\theta m}+dV_{\theta m}/2)(A_c+dA_c/2)+\cancel{\rho dQ_{c1}}=\rho(V_{\theta m}-dV_{\theta m}/2)(A_c-dA_c/2)+\cancel{\rho dQ_{c2}} \quad (5.10)$$

or

$$d(V_{\theta m}A_c)=0 \quad (5.11)$$

where $V_{\theta m}$ is mean tangential velocity which can be obtained as

$$V_{\theta m}=\frac{Q}{A_c} \quad (5.12)$$

Angular momentum equation in the tangential direction yields

$$\begin{aligned}&\rho R_G(V_{\theta m}+dV_{\theta m}/2)(A_c+dA_c/2)dV_{\theta m}=R_G(P-dP/2)(A_c-dA_c/2)\\&-\rho dQ_c(R_1V_{\theta 1}-R_2V_{\theta 2})-R_G(P+dP/2)(A_c+dA_c/2)+R_GPdA_c-\textit{wall friction term}\end{aligned} \quad (5.13)$$

By using continuity equation, the above equation can be reduced to the following equation.

$$dgH=dQ_c/Q_s(U_2V_{\theta 2}-U_1V_{\theta 1})+V_{\theta m}^2dA_c/A_c-dgH_L \quad (5.14)$$

where $Q_s=\omega R_G A_c$ is flow rate based on solid body rotation.

In the right side of the above equation, the first term refers to head rise caused by momentum exchange of blade, the second term gives head rise caused by the deceleration of the mean tangential velocity and the last term gives head loss caused by the friction and the contraction or expansion of the tangential velocity.

Applying Momentum equation in the circulatory direction, we get

$$\cancel{\rho dQ_{c1}V_{c1}}-\cancel{\rho dQ_{c2}V_{c2}}+\rho QdV_c=p_2HB_2dX_2-p_1HB_1dX_1-\textit{wall friction term} \quad (5.15)$$

$$\frac{QV_cdV_c}{dQ_c}=\frac{p_2-p_1}{\rho}-gH_{cc} \quad (5.16)$$

where gH_{cc} is the head loss of circulatory velocity through the impeller region.

Energy equation applied to channel control volume of Figure 5.1 after some simplifications yields

$$\frac{p_2}{\rho}+\frac{V_{c2}^2}{2}+\frac{\sigma^2U_2^2}{2}=\frac{p_1}{\rho}+\frac{V_{c1}^2}{2}+\frac{\alpha^2U_1^2}{2}+gH_{cc}+\frac{Q}{dQ_c}(dgH+dgH_L-V_{\theta m}^2dA_c/A_c+V_cdV_c) \quad (5.17)$$

If equation 5.9, equation 5.14 and equation 5.16 are used in equation 5.17, the first order nonlinear ordinary differential equation can be obtained for the circulatory flow as follow.

$$\frac{QV_cdV_c}{dQ_c}=(1-\frac{Q}{Q_s})(\sigma V_{\theta 2}^2-\alpha V_{\theta 1}^2)-gH_c \quad (5.18)$$

where $gH_c=gH_{cb}+gH_{cc}$ is the sum of head losses related to the circulatory velocity, also called circulatory head losses.

5.2 Slip Loss

Tangential pressure gradient in regenerative turbomachines enhances the slip factor considerably. Pressure difference between any two adjacent blades of an impeller causes a tendency for a secondary circulation about each blade such that the fluid leaving the impeller deviates from the path prescribed by the blade surface, backwards with respect to the positive direction of impeller rotation. The result is that the fluid tangential velocity at exit is less than that which would be expected from the velocity triangle based on the outlet blade angle. In order to allow for the reduction in the ideal tangential velocity, a slip factor is usually introduced which is defined as ratio between actual tangential velocity and that obtained with the assumption that the flow angle and blade angle are identical.

Slip factor is one of the vital items of design information because of its direct effect on energy transfer. A number of methods have been developed by various investigators for the assessment of the effect of slip. Noteworthy are the contributions from Stodola, Busemann, Fergusons and Stantiz. However, these and other authors published methods for the cases where there is essentially no tangential energy gradient. Hence, formulations suggested by these authors are not applicable to regenerative turbomachines in which the sole purpose is to develop tangential pressure gradient.

El-Hag [22] developed a method of analysis of the flow in regenerative turbomachines. He suggested that slip factor for regenerative turbomachines should be viewed as a function of the circumferential gradient of pressure as well as flow variables, impeller speed and dimensions, the angle and number of impeller blades.

i.e.

$$\sigma = f\left(r_2, \omega, \beta_2, Z, W_2, \frac{\partial H}{\partial \theta}\right) \tag{5.19}$$

El-Hag extended the expression proposed by Stodola and proposed a slip factor correlation given below for computing a first order estimate of the slip factor in regenerative turbomachines.

$$\sigma = 1.0 - \frac{U_2 \pi \sin \beta_2}{V_{\theta 2} Z}\left[1 + 2\left(\frac{\omega r_2}{W_2}\right)\frac{\Psi}{\theta_p}\right] \tag{5.20}$$

This relation however needs velocities to be determined experimentally. In this work, authors have proposed an alternative slip factor correlation for regenerative compressors given below.

$$\sigma = \frac{1}{1 + SP \dfrac{2.6}{Z\left(1 - \left(\dfrac{r_o}{r_2}\right)^2\right)}} \tag{5.21}$$

where SP is a factor to incorporate the effect of tangential pressure gradient on slip factor. The term SP is correlated with impeller tip Mach number and specific mass flow rate. This correlation is valid for all stages of Capstone multistage RFC.

$$SP = 1.38 - 0.00317 \frac{\ln(M_{OT})}{(M_{OT})^2} + 8.163 \times 10^{-10} \frac{\ln(\Phi)}{\Phi^2} \tag{5.22}$$

5.3 Shock loss

Shock or incidence losses are caused by difference between blade angle and flow angle when fluid enters the blades. Wilson [69] introduced a shock loss parameter α to quantify such losses. He related shock loss with various geometric and aerodynamic parameters. Although Wilson's model was based on rectangular channel geometry, however still it can be used for Capstone multistage RFC channel geometry. The channel shape and dimensions used by Wilson for his shock loss model can be seen in Figure 5.3. Wilson related the through flow rate with shock loss parameter and known geometry. Following relation was proposed in Wilson [69].

$$Q = \frac{1}{2}\left(\frac{r_2}{r_G}\right) Q_s \left(K_1 \sigma + \frac{r_1^2}{r_2^2} K_2 \alpha\right) \tag{5.23}$$

where, $Q_s = r_G A_c \omega$ denotes the flow associated with solid body rotation and K_1, K_2 and K_3 are dimensionless coefficients depending only on the geometry of the open channel. These coefficients are given as:

$$K_3 = \frac{r_2}{r_G}\left[\begin{array}{l}\dfrac{(A_3+A_4)^2}{A_c^2} - \dfrac{(A_1+A_2)^2}{A_c^2} + \dfrac{cA_1A_2}{r_3A_c^2} \\ -\dfrac{1}{3r_1d}\left(A_3 + A_4 - bd\dfrac{r_3}{r_1}\right)\end{array}\right]$$

$$K_1 = K_3 + 2\frac{(A_1+A_2)}{A_c} - \frac{cA_2}{r_3A_c} - \frac{cA_1}{2r_2A_c}$$

$$K_2 = -K_3 + \frac{2r_2(A_3+A_4)}{r_1A_c} - \frac{A_3^2r_2}{3A_cr_1^2d}\left(5 - 2\frac{r_3}{r_1}\right)$$

where

$$A_1 = \frac{bC_r}{2},\quad A_2 = \left(\frac{b+d}{2}\right)C_r,\quad A_3 = (r_3 - r_1)d$$

$$A_4 = \frac{bd}{2} \text{ and } A = A_1 + A_2 + A_3 + A_4$$

5.4 Circulatory head losses

Circulatory head losses have two contributions.

- Head loss of circulatory velocity through the impeller region is referred as gH_{cb}.
- Head loss of circulatory velocity through the channel region is referred as gH_{cc}.

The sum of these two head losses is the total circulatory head loss given as:

$$gH_c = gH_{cb} + gH_{cc}$$

Circulatory head losses arise from many sources. Following sources of circulatory head loss are quantified.

5.4.1 Channel turning losses (k_t)

These losses are due to 180° turn of the fluid through the channel. Flow pattern is similar to flow patterns in 180° turn without guide vanes. Channel turning losses can be simulated using the following equation.

$$\Delta P = \frac{1}{2}\rho K_t V_c^2 \tag{5.24}$$

where k_t is channel turning loss coefficient and V_c is the circulatory velocity. The channel turning loss coefficient is correlated with channel geometry to study effect of channel geometry on channel turning losses while doing design sensitivity analysis. k_t is a function of channel geometry. It is correlated with two geometric parameters of channel, which are "d" and "e" as shown in Figure 5.4. Correlation of k_t with the ratio $x = d/e$ is given below.

$$k_t = a + bx^2 + cx^4 + dx^6 + ex^8 + fx^{10} + gx^{12} + hx^{14} + ix^{16} + jx^{18} + kx^{20}$$

where $x = d/e$, a = -4.58, b = 335.31, c = -9.87×10^3

d = 1.63×10^5, e = -1.68×10^6, f = 1.14×10^7, g = -5.20×10^7

h = 1.56×10^8, i = -2.97×10^8, j = 3.25×10^8, k = -1.55×10^8

5.4.2 Channel and Blade Mixing Losses

Fluid after passing through blade makes a 90° turn and enters the channel. Circulating fluid mixes with incoming stream of flow and thus it encounters channel mixing loss. Moreover, there is also a loss encountered in the blade passage due to this mixing and we call it blade mixing loss. These losses are simulated by procedure followed in literature to simulate losses in merging streams of flows. It can be assumed that this mixing process takes place at 45° with the incoming stream as shown in Figure 5.5.

Two non-dimensional geometric and aerodynamic parameters are introduced to quantify the mixing losses encountered in the side branch (flow going out from the blade towards channel).

$$C_1 = \frac{Q_c}{Q}, \quad C_2 = \frac{A_c}{A_{circulation}}$$

where,

Q_c is the circulatory flow through one blade passage

Q is the through flow through the channel

$A_{circulation}$ is the area through which flow circulates from blade towards channel

A_c is the channel through flow area

The mixing losses which occur at the exit of blade region when flow takes 90° turn and mixes with the incoming stream of through flow can be simulated by introducing a loss coefficient k_s given by,

$$k_s = \frac{\left(1+(C_1C_2)^2 - 2(1-C_1)^2 - 1.41C_2C_1^2\right)}{(C_1C_2)^2}$$

Blade mixing losses can be determined from,

$$\Delta P_s = \frac{1}{2}\rho k_s V_c^2 \tag{5.25}$$

Mixing losses in the peripheral branch (through flow in the channel) result in pressure drop in the peripheral direction and they can be simulated by introducing a loss coefficient k_{ch} given by,

$$k_{ch} = \frac{1-(1-C_1)^2 - 1.41C_1^2C_2}{(1-C_1)^2}$$

Channel mixing losses can be determined from,

$$\Delta P_{ch} = \frac{1}{2}\rho k_{ch} V_{\theta m}^2 \tag{5.26}$$

Thus the mixing losses are correlated to aerodynamic parameter C_1 and geometric parameter C_2.

5.4.3 Blade turning loss (k_b)

Blade turning losses can be simulated using the following equation.

$$\Delta P = \frac{1}{2}\rho k_b V_c^2 \tag{5.27}$$

where k_b is blade turning loss coefficient. It is a function of channel geometry. It is been correlated with two geometric parameters of channel, which are radial clearance "c_r" and blade width "b" as shown in Figure 5.6. The correlation helps to study the variation of radial clearance and blade width on blade turning loss while doing the sensitivity analysis. Ratio $x = c_r / b$ and peripheral distance dX_G which fluid takes to complete turn through the blades are the inputs for the correlation. Peripheral distance dX_G is estimated by

$$dX_G = r_G \theta_i \tag{5.28}$$

k_b is given as

$$k_b = 0.322 - 0.053\left(\frac{c_r}{b}\right) - 0.00863\, dX_G$$

5.4.4 Sudden expansion (k_{se})

This loss is caused by the increase in flow area when fluid flows from blades to channel. Sudden expansion loss coefficient is related to blade blockage factor given as

$$k_{se} = \left(\frac{BF}{1-BF}\right)^2$$

Sudden expansion loss can be quantified by

$$\frac{1}{2}\rho k_{se} V_c^2 \tag{5.29}$$

Consequently, model for the circulatory head loss can be arranged as follows.

$$gH_c = \frac{1}{2}k_t V_c^2 + \frac{1}{2}k_s V_c^2 + \frac{1}{2}k_b V_c^2 + \frac{1}{2}k_{ch} V_{\theta m}^2 + \frac{1}{2}k_{se} V_c^2 \tag{5.30}$$

5.5 Tangential Head Losses

Head losses caused by channel friction are referred as tangential head losses denoted by dgH_L. They involve the channel curvature effect and can be determined by applying the classic pipe-loss formula.

$$dgH_L = \frac{\lambda_f V_{\theta m}^2 dX_G}{2D_h} \tag{5.31}$$

where

$$\lambda_f = \lambda_o \left(1 + 0.075 \,\mathrm{Re}^{0.25} \left(\frac{D_h}{2r_2} \right)^{0.5} \right) \tag{5.32}$$

λ_o is defined for straight channel as,

$$\lambda_o = 0.316 \,\mathrm{Re}^{-0.25} \tag{5.33}$$

where Re is given based on hydraulic diameter as,

$$\mathrm{Re} = \frac{D_h V_{\theta m}}{\nu} \tag{5.34}$$

5.6 Leakage Losses

Total leakage flow rate can be estimated by the following equation suggested by El-Hag [22].

$$Q_{leak} = \frac{\omega r_2}{2}\left(c_r b + \frac{c_a r_2}{2} \right) + 2C_D \omega r_2 \sqrt{\frac{2\frac{d\Psi}{d\theta}}{Z_s}} \left(c_r (b + c_a) + c_a (r_2 - r_o) \right) \tag{5.35}$$

5.7 Losses in Ports

Losses in inlet and discharge ports are estimated by

Inlet port $$\Delta P_{in} = \frac{1}{2} k_{in} \rho V_{in}^2 \tag{5.36}$$

Outlet port $$\Delta P_{out} = \frac{1}{2} k_{out} \rho V_{out}^2 \tag{5.37}$$

The two loss coefficients K_{in} and K_{out} need to be correlated with the nozzle geometries and flow rates to study the effect of inlet and discharge ports on performance. Discharge nozzle of Capstone multistage RFC is contoured and has very complicated geometry, while the inlet manifold is a straight through hole. Effect of inlet and discharge manifold is not primary aim of this work, so port loss coefficients are not correlated with aerodynamic parameters. Instead, reasonable values of these coefficients are assumed and held constant.

5.8 Performance prediction and comparison with test data

Based on proposed mathematical model and loss correlations, a performance prediction code is developed to predict Capstone multistage RFC performance. Mathematical formulation is based on some geometrical parameters which are assumed to be known from multistage RFC drawings. A high level flow chart of the code is provided in Figure 5.7. Performance prediction code predicts pressure ratio for the entire operating range. Results are compared with test data for Capstone multistage RFC. Excellent comparison is observed as seen from Figure 5.8 and 5.9. These figures represent theoretical and test data overlapped for natural gas as working fluid at four different inlet pressures of 0 psig, 5 psig, 10 psig and 15 psig at inlet temperature of $70^{\circ}F$. To condense the

presentation, Figure 5.8 represents results at 195 slpm and Figure 5.9 represents results at 250 slpm flow rate. The close agreement in theoretical and experimental results led the researcher to carry out extensive sensitivity analysis on various design parameters of RFC to improve performance. In chapter 6, results from design sensitivity analysis are presented along with suggestions for improvement. Moreover, a design procedure for radial and non-radial blade RFC is suggested which can be very useful for designers and engineers.

5.9 Conclusions

To assist in improving efficiency of Capstone multistage RFC, governing equations for the blade and channel region are developed and loss modeling is done to develop correlations of losses with geometric and aerodynamic parameters. The presented mathematical model is useful to predict performance of regenerative pumps and compressors with radial and non-radial blades. A performance prediction code based on governing equations and loss models is developed and performance results are compared with test data on Capstone multistage RFC. Excellent agreement between theoretical and test data is observed which motivated to carry out an extensive design sensitivity analysis to improve RFC performance. Findings of sensitivity analysis are discussed in chapter 6.

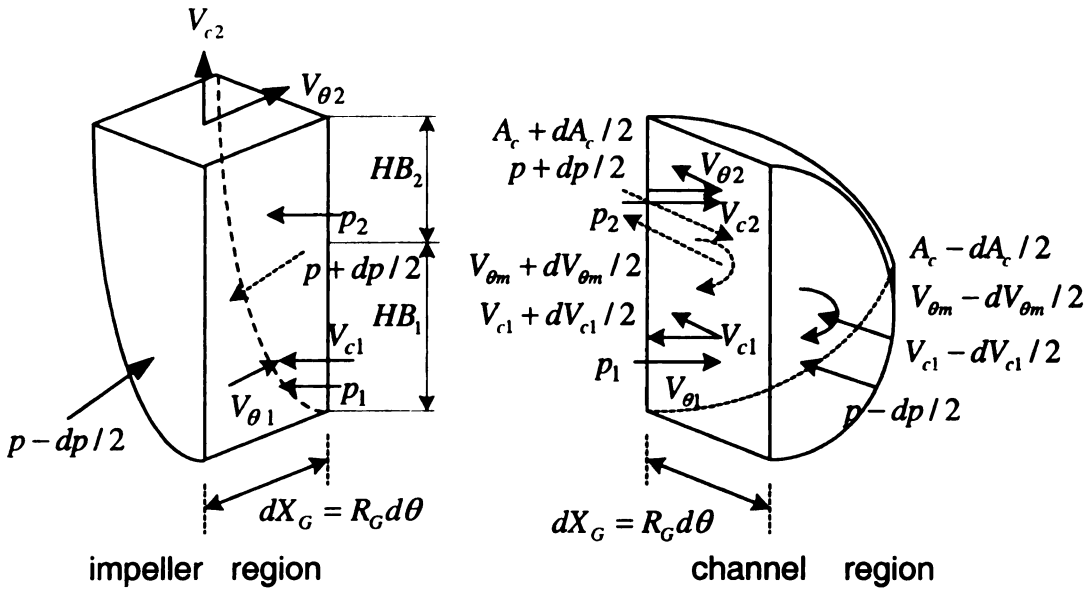

Figure 5.1 Control volumes representing section $d\theta$ of open channel and impeller

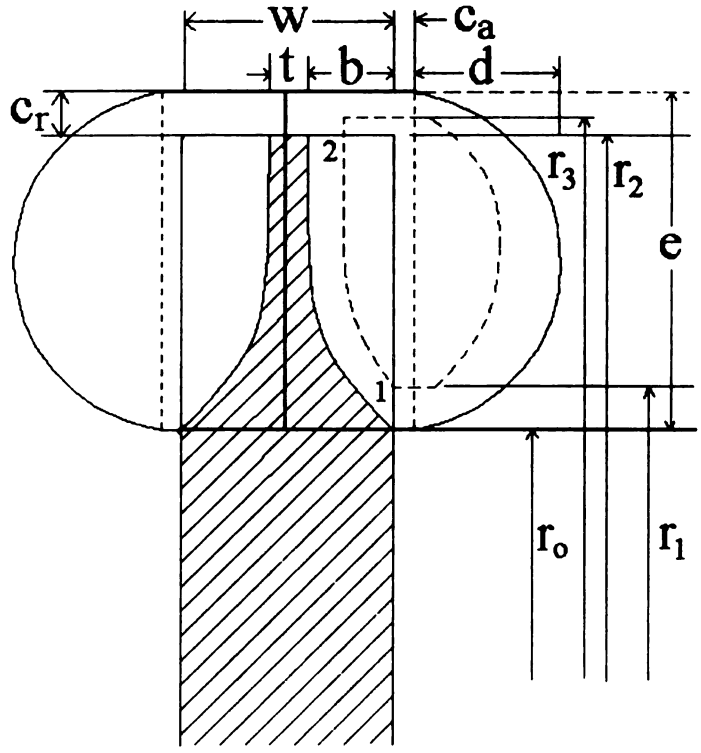

Figure 5.2 Schematic of blade and channel geometry

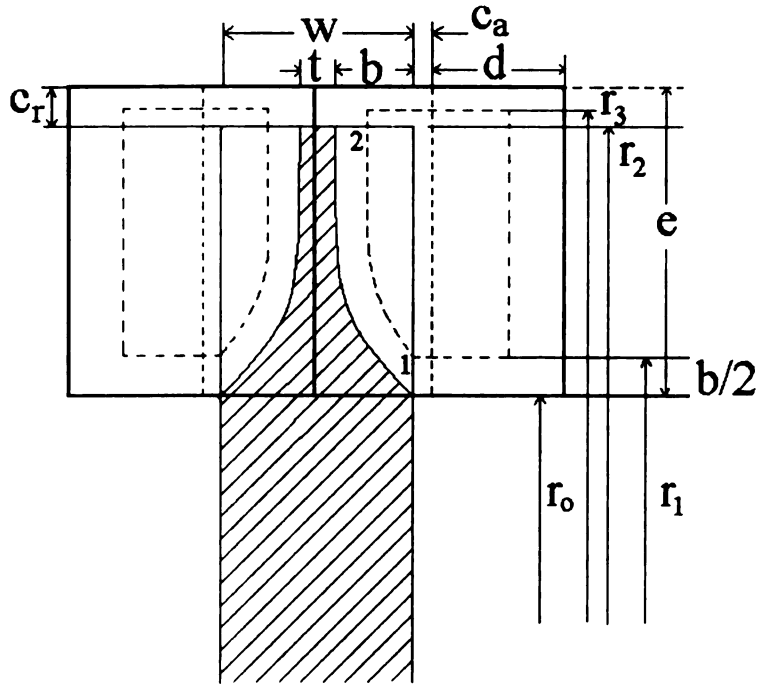

Figure 5.3 Geometry for shock loss model

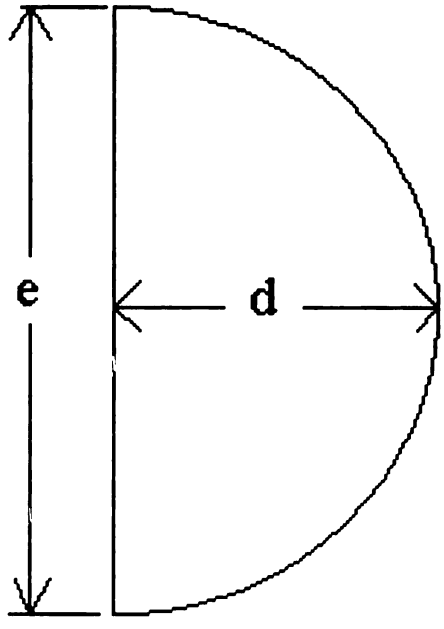

Figure 5.4 Geometric parameters governing channel turning loss coefficient

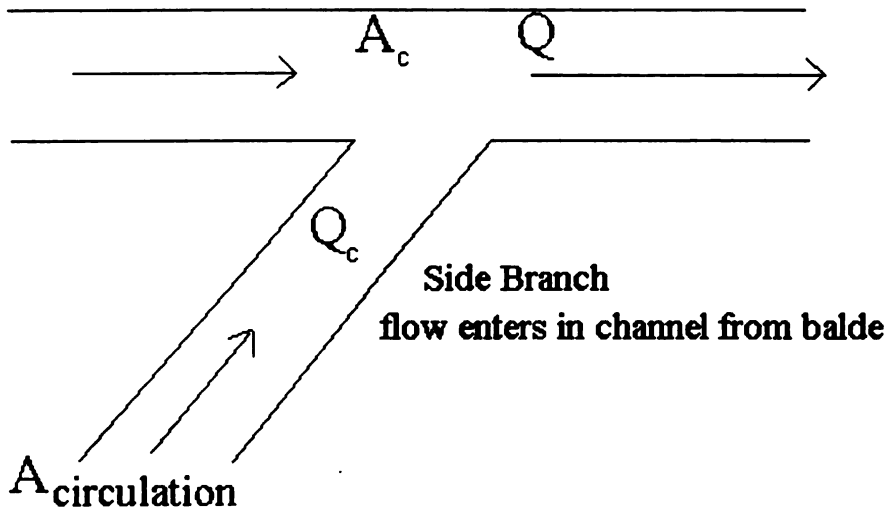

Figure 5.5 Mixing process of flow entering channel through blades

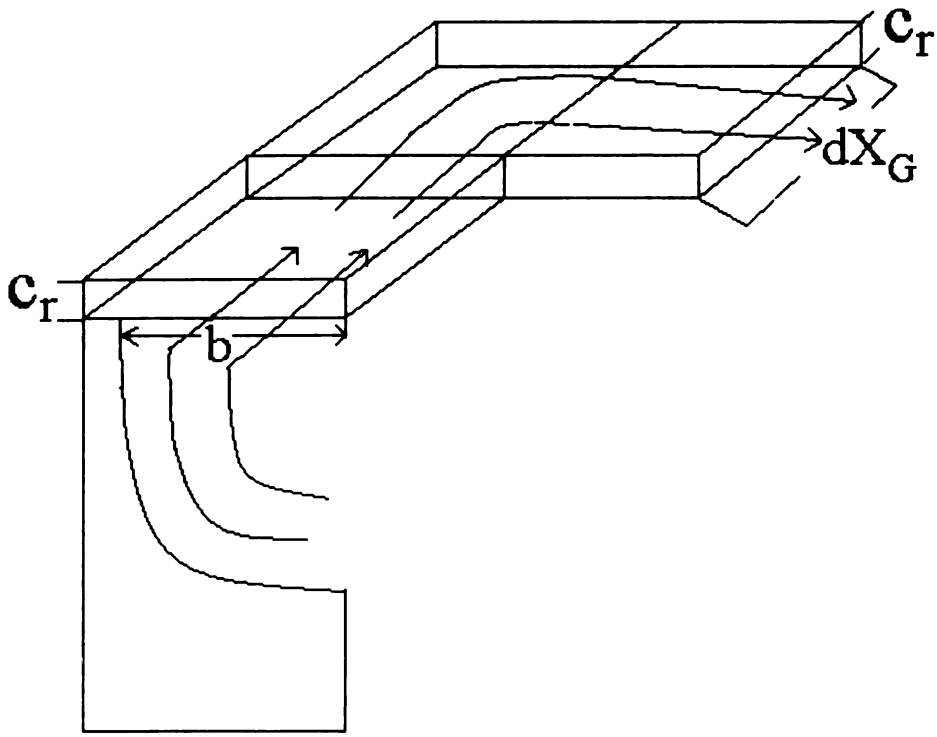

Figure 5.6 Geometric parameters governing blade turning loss coefficient

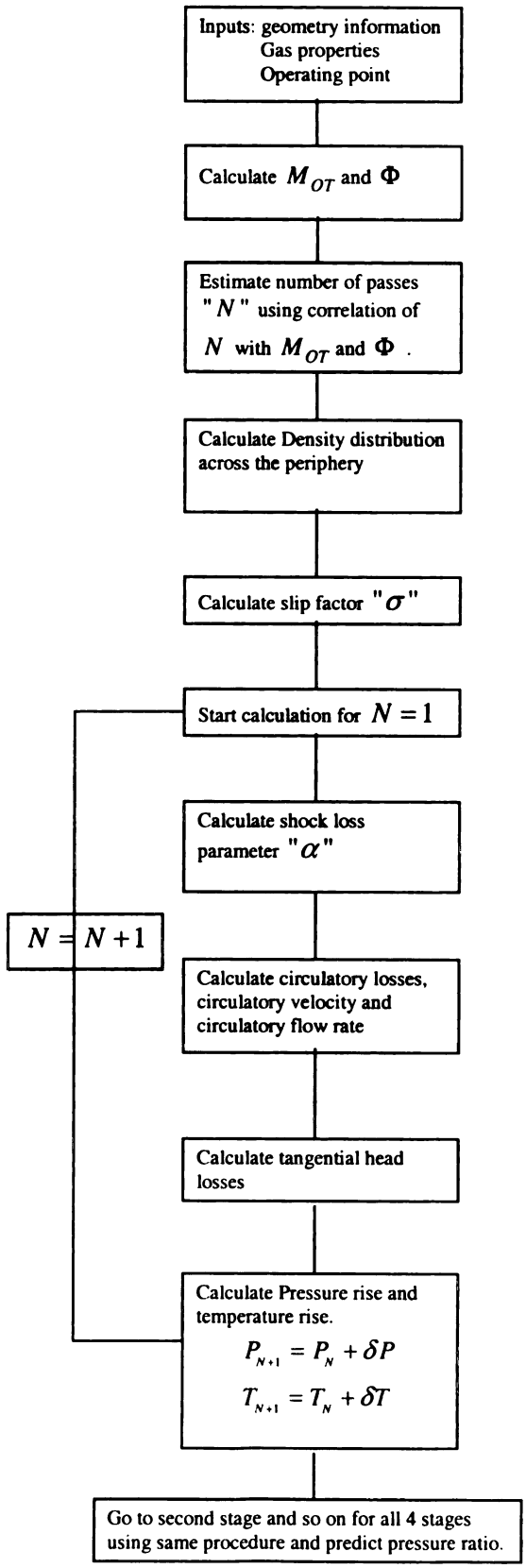

Figure 5.7 Flow chart of performance prediction code

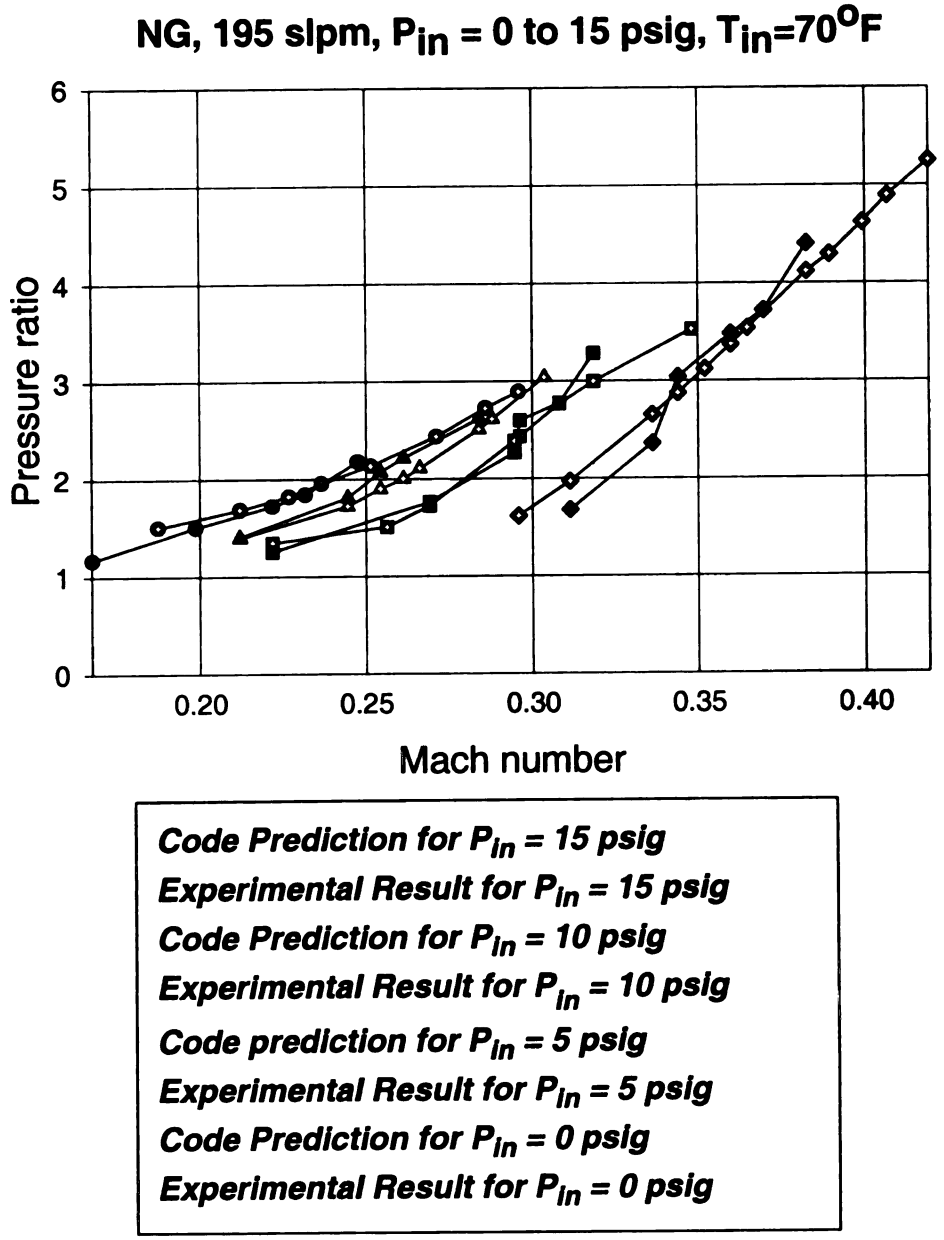

Figure 5.8 Theoretical and test data overlapped for flow rate 195 slpm

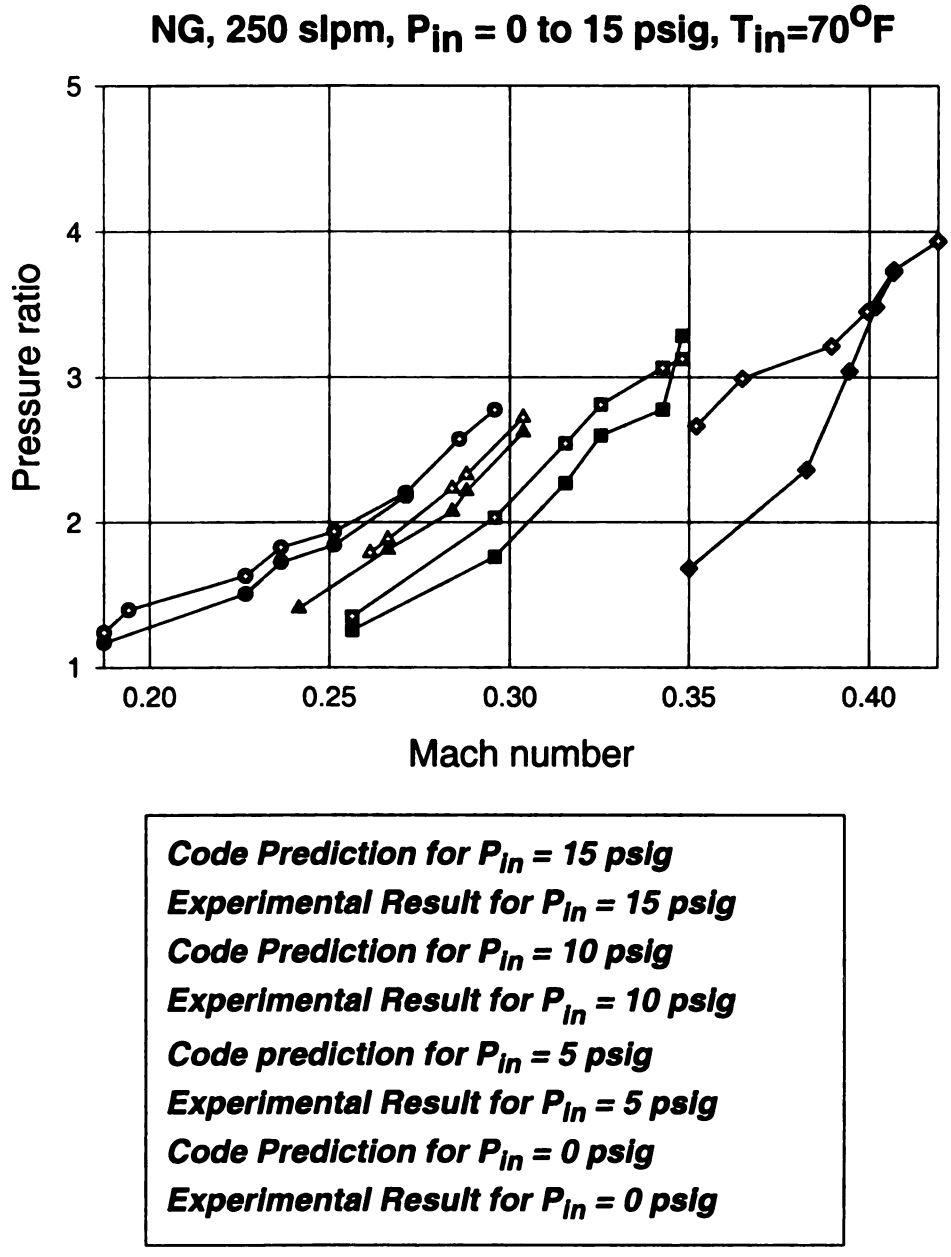

Figure 5.9 Theoretical and test data overlapped for flow rate 250 slpm

CHAPTER 6

DESIGN SENSITIVTY ANALYSIS

Performance prediction code predicts the pressure ratio, however isothermal efficiency is the parameter which designers usually want to maximize. To predict the isothermal efficiency, power draw needs to be predicted as well, which requires heat transfer calculations. An alternate method is adopted here to perform design sensitivity analysis. Pressure ratio and power coefficient are directly proportional to impeller tip Mach number. Moreover, in order to maximize isothermal efficiency of RFC, higher pressure ratio is desired for a given impeller tip Mach number. Usually, it is difficult to optimize the design for all operating points. Therefore, it is a standard practice in turbomachinery to select a design point where designer intends to achieve peak efficiency. Design point selected to perform sensitivity analysis yielded impeller tip Mach number of 0.369 and specific mass flow rate of natural gas equal to 1.04×10^{-3}. RFC builds the required pressure ratio for microturbine operation, however very low isothermal efficiency levels $(15-20\%)$ are achieved. When comparing efficiency to historical test results, it appears that significant improvements to efficiency could be achieved. The idea of sensitivity analysis lies in the fact that if higher pressure ratio is obtained at $M_{OT}=0.369$ keeping $\Phi=1.04\times10^{-3}$ by making design changes in the geometry of RFC, it means the isothermal efficiency is improved. Therefore, the code is run at this design point to do an extensive

sensitivity analysis and study various losses and their behavior with different design changes. The trend in pressure ratio is predicted for each design change. Design changes are optimized so that head losses are minimized and for a given tip Mach number and specific mass flow rate, higher pressure rise and better efficiency is obtained. Sensitivity analysis is performed on blade and channel geometry as discussed independently.

6.1 Analysis of channel geometry

Extensive sensitivity analysis is carried out using the code by varying some channel dimensions listed below and trying to maximize head at given tip Mach number and specific mass flow rate. These dimensions are listed below and are also shown in Figure 6.1.

1. Radial clearance "c_r"
2. Channel inlet area "$A_{c,A}$"
3. Channel height "e"
4. Area ratio $A_{c,A}/A_{c,B}$

6.1.1 Radial clearance "c_r"

Radial clearance "c_r" has effect on three types of losses:

- Shock Loss
- Blade turning Loss
- Channel and blade mixing Losses

Shock loss is minimized by increasing radial clearance "c_r". This effect is studied by varying radial clearance. Shock loss parameter inversely affects the pressure ratio. In order to get higher pressure ratio and isothermal efficiency, shock loss parameter should

be as small as possible and actually a negative value is beneficial since it increases the pressure ratio. Usually, at very low flow rates, negative values of "α" are obtained, which mean higher pressure ratios.

Blade turning loss is also minimized by increasing radial clearance "c_r". Effect of radial clearance on blade turning loss coefficient is studied by keeping all other terms constant in correlation of blade turning loss coefficient with channel geometry. The trend in blade turning loss coefficient with variation in radial clearance can be seen in Figure 6.2 in which various loss coefficients are plotted against the ratio "c_r/r_2". It must be noted that the tip radius is held constant while performing sensitivity analysis for radial clearance. This figure shows that increasing radial clearance helps to minimize losses associated with flow turning through the blades.

Channel and blade mixing losses are also affected with the change in radial clearance. The two loss coefficients "k_m" and "k_{ch}" are plotted with ratio "c_r/r_2" as shown in Figure 6.2. Blade mixing loss does not show any trend and it is very hard to conclude anything that either increasing or decreasing radial clearance helps to reduce this loss. However, a definite trend is obvious in the channel mixing loss. Channel mixing loss becomes more and more negative with increasing radial clearance which helps to increase pressure ratio and efficiency. In order to study the cumulative effect of above losses and effect of radial clearance on pressure ratio, the pressure ratio for first stage of Capstone multistage RFC at design point is plotted against ratio "c_r/r_2" as shown in Figure 6.3. It is obvious from Figure 6.3 that pressure ratio is directly proportional to the radial clearance "c_r". Thus it can be concluded that for a given impeller tip Mach number, increasing "c_r" will increase pressure ratio and isothermal efficiency.

Another interesting point which is observed in the sensitivity analysis is that it is not suggested to increase radial clearance indefinitely. After a certain percentage increase in clearance, the pressure ratio actually starts going down as shown in Figure 6.3. It is found that after a 40% increase in radial clearance, the pressure ratio starts to go down. This is detrimental to the efficiency as well. This is illustrated in Figure 6.4 and Figure 6.5 taken from Cates [15], which show a reduction in pressure rise and decrease in efficiency with huge increase in radial clearance. Cates presented the data at two values of tip Mach numbers; 1) Air with $M_{OT} = 0.383$ and 2) SF_6 at $M_{OT} = 1.04$. However, results on air which are at low Mach number should only be considered. Moreover, in air tests, specific mass flow rate range close to operating point of Capstone RFC should be observed. It is reminded again that emphasis is to optimize the geometry at $M_{OT} = 0.369$ and $\Phi = 1.04 \times 10^{-3}$. Thus SF_6 results should be ignored due to the high Mach number.

Cates varied radial clearance from 0.2 to 0.5, which was a huge increase. This proved detrimental to the adiabatic efficiency as shown in Figure 6.5. It must be noted that in Figure 6.5 "h" represents the radial clearance and "b" is the channel depth. This figure shows that increasing radial clearance is harmful to the efficiency, however, still it can be argued that increasing the radial clearance to a small percentage is beneficial to performance. It was only because Cates increased the clearance by 150% during his testing, which made the efficiency to go down. Sensitivity analysis presented here suggests that increasing radial clearance immensely will prove detrimental. However, the mismatch between trends observed by the code and Cates data need more clarification. Thus results presented in Wilson [69] are studied to learn about the exact behavior of

radial clearance. The same effects were observed by Wilson [69] as shown in Figure 6.6 where it can be seen that a small increase in radial clearance was beneficial for head rise, however a huge increase in radial clearance proved detrimental. It is interesting to compare configuration 1, 2 and 4 in this diagram, where it can be seen that as one moves from 2 to 4, which means a small increase in radial clearance, there is an increase in head coefficient. However, when the radial clearance was increased too much as shown in configuration 1, the head coefficient decreased. It is true that configuration 4 has channel area reduction as well in addition to radial clearance change, but still it can be observed from the three configurations that increasing the clearance indefinitely is detrimental as depicted by configuration 1. However, it will be more useful to study the effect of the ratio "c_r/d_A" and try to optimize that parameter. This will be presented later in this chapter. Thus as a guideline, it is recommended that for RFC under consideration, radial clearance should not be increased more than 25-30%. However, generally speaking an increase in radial clearance is beneficial to its performance.

6.1.2 Channel inlet area "$A_{r,A}$"

Channel area at inlet is a function of channel depth "d_A" and channel height "e" as shown in Figure 5.2. Channel depth effects following losses.

- Shock Loss
- Channel turning Loss
- Skin friction loss

Shock loss model is based on rectangular cross sectional area channel, which is also similar to the cross section of Capstone single stage RFC discussed in chapter 4. Figure 6.7 describes the variation of shock loss parameter "α" with ratio of channel depth at

station A and tip radius "d_A / r_2". It must be noted that tip radius is held constant while doing sensitivity analysis for channel inlet area. It is obvious from Figure 6.7 that a higher value of "d_A"minimizes the shock loss. Thus shock loss model suggests that a higher value of "d_A" is beneficial for improved performance. Channel turning loss coefficient k_t is plotted against ratio "d_A / r_2" in Figure 6.8 to see the effect of channel depth on channel turning loss. This figure suggests that when "d_A"becomes greater, turning loss in the channel also increases. Thus this suggests that a smaller "d_A"is suited to minimize the channel turning loss.

Figure 6.8 is plotted keeping channel dimension "e"as constant and varying "d_A"only. However, it was suggested above that radial clearance has to be increased slightly for better performance. This means, dimension "e"has to be increased as well to match the radial clearance. Therefore, it is essential to study the effect of ratio $x = d_A/e$ on the channel turning loss coefficient. Thus, the ratio $x = d_A/e$ is plotted against channel turning loss coefficient as shown in Figure 6.9. It is interesting that a lower value of this ratio is beneficial for more head rise and efficiency. This also suggests that "d_A"must be reduced for better performance.

Another loss which is affected by varying "d_A"is channel skin friction loss. Skin friction head loss is plotted with ratio "d_A/r_2"in Figure 6.10 to see the effect. It is obvious that as we make the channel depth smaller, skin friction effect increases. This is intuitive as well, because a smaller channel depth would mean more interaction of fluid with channel, thus increasing frictional losses. This suggests that a larger channel depth"d_A" is beneficial for performance.

Above analysis on shock loss, channel turning loss and skin friction loss suggested different behavior with varying channel depth. This random behavior led to confusion in determining which loss is more influential to pressure ratio and efficiency in the RFC. Should channel depth "d_A"be decreased or increased? To help this out, Capstone single stage test data presented in chapter 4 and test data in literature on varying channel depth and its effect on performance is consulted. Figures 6.4, 6.5, 6.6 and 6.10 suggest that at low specific mass flow rate values, a smaller value of "d_A" increases the head and efficiency. Figure 6.4 and 6.5 suggest that the effects of geometry are quite different at different Mach number and specific mass flow rate values. With each successive increase in channel dimensions, the air data exhibits a decrease in pressure ratio at shutoff but a considerable increase at high flow rates. The effects of geometry changes on isentropic efficiency are shown in Figure 6.5. Increase in channel depth causes a sharp drop in efficiency. Figure 6.6 adopted from Wilson [69] also suggests that decreasing channel depth helps to improve the performance. Figure 6.10 obtained from Burton [11] also suggests that at low flow rates, it is beneficial to decrease the channel depth. It is obvious from Figure 6.10 that the trend of channel depth depends on flow rate through the RFC. If this figure is carefully analyzed in terms of head and adiabatic efficiency, it shows that for low flow rate applications, decreasing channel depth is beneficial. This analysis from literature hints that the test data cited is based on a rectangular channel cross sectional area. Rectangular channel area does not guide the flow properly and there can be huge mismatch between the blade angle and fluid angle. This means that rectangular cross sectional shape is responsible for more shock loss. It is true for a rectangular cross sectional area channel that increasing "d_A"will enhance performance, because it reduces

the shock loss. However, it is obvious that increasing channel area will increase channel turning loss significantly. Thus, increasing the channel depth does not seem to provide the solution of the problem. It is thought that the circular cross section channel area of multistage RFC helps to minimize the shock loss. Thus, there is no need to increase the channel depth and rather a decrease in the channel depth "d_A" will prove beneficial to enhance isothermal efficiency. A reduction in channel depth will reduce channel turning loss and moreover provide higher through flow velocity, which might lead to more circulations at low flow rates. The more the number of circulations through the impeller means more head at a given impeller tip Mach number. Thus it can be concluded that a smaller channel depth "d_A"is beneficial for multistage RFC or in other words, smaller channel area is beneficial for better performance at least at the design point. A design criterion for selection of channel depth is not addressed at this point. Based on experimental data and sensitivity analysis, some design criteria for channel depth are presented towards end of this chapter.

6.1.3 Channel height "e"

It is obvious from the above discussion that channel height "e"must be increased as a result of increased radial clearance "c_r".

6.1.4 Area ratio $A_{c,A}/A_{c,B}$

Another important parameter effecting the pressure ratio and hence isothermal efficiency is channel area ratio. From sensitivity analysis of the code, it is concluded that higher the area ratio, higher is the pressure ratio and efficiency at a given impeller tip Mach number. This fact was validated by Capstone single stage experimental test data presented in chapter 4. It was found through test data that a higher area ratio is beneficial for improved

pressure ratio and isothermal efficiency. Figure 6.11 shows the increase in pressure ratio obtained by increasing the area ratio. Unfortunately, there is not much information available in literature on varying cross sectional area RFC to compare and validate our conclusion about area ratio. However, it is intuitive to have a higher area ratio for better compression of fluid.

6.2 Design changes in channel geometry

Performance prediction code suggests which design changes in channel geometry are beneficial for RFC performance. However, it does not provide any precise idea about what percentage variation in each design variable is optimal for performance. It is essential to study the existing multistage RFC geometry and analyze it with other geometrically similar regenerative compressor designs available in literature to get further insight. Thus, an analysis is conducted based on non-dimensional parametric study using available geometric data in literature, geometry of various configurations of Capstone single stage RFC (presented in chapter 4) and geometry of individual stages of multistage RFC. Based on this study, some design criteria for each variable are established as discussed below. Design criteria for sizing the radial clearance and channel depth of RFC is suggested below.

$$0.2 < c_r / d_A < 0.65 \tag{6.1}$$

$$0.03 < c_r / r_2 < 0.05 \tag{6.2}$$

Some authors did experimental sensitivity analysis on channel dimensions in the past. Their analysis is also presented in this work for discussion purpose. Table 6.1 gives some of the dimensions of six configurations tested by Wilson [69]. The maximum

dimensionless head at low flow coefficients was obtained from configurations 2. It is interesting to note that the radial clearance and channel depth for configuration 2 lie in the established bounds.

An experimental sensitivity analysis was also performed by Cates [16]. It is found from Cates paper that best performance at design point resulted by keeping ratio $c_r/d_A = 0.4$ and $c_r/r_2 = 0.04$, which lies in the bound established above.

Test data on ORNL CRDT regenerative compressor was also available in Cates [16] and it was calculated that their design used $c_r/d_A = 0.44$ and $c_r/r_2 = 0.044$ which also lie in the established bound. Moreover, data on ORNL FPD design of RFC is also cited and values of $c_r/d_A = 0.25$ and $c_r/r_2 = 0.048$ were used in their design, which also fall in the established criteria.

Capstone single stage test data is another source to validate the established design criteria. As discussed in chapter 4, S3 configuration was found to be the best configuration. Thus it is interesting to find out values for the two design criteria for configuration S3. When it is explored, it is found that for station A, $c_r/d_A = 0.623$ and $c_r/r_2 \approx 0.05$ gives the best performance. For station B, $c_r/d_B = 1.06$ is found. Fortunately, the value for station A falls in the established bound, however the value at station B is very high. The reason for this high value is that the analysis conducted above is based on a constant channel area throughout the periphery of RFC. However, Capstone multistage RFC and Capstone single stage RFC have varying cross sectional areas. Based on the above discussion, it can be concluded that the suggested design criteria in (6.1) and (6.2) are valid and very useful for designers and engineers to size dimensions at inlet station A for regenerative compressors desired to operate at low specific mass flow rate.

The established design criteria motivated the researcher to analyze existing geometry of multistage RFC in the light of established design criteria. The key geometric parameters for all four stages of the multistage RFC are reproduced in Appendix C. After analyzing the four stages and checking for the established criteria, it was concluded that it is possible to increase radial clearance "c_r" of individual stages by a certain percentage, but it must be noted that it should not be increased too much so that it violates the design criteria in (6.1) and (6.2). A 25-30% increase might be possible without violating the criteria. However, increasing the clearance would imply an automatic increase in channel height "e" as shown in Figure 5.2. Thus channel inlet area and the channel area ratio will have to be established properly by controlling the channel depth d_A and d_B. Another important finding from this analysis is that it might be beneficial for performance improvement to increase the inlet cross sectional area by 10-15% and reduce the exit cross sectional area by 5-10%, so that the channel area ratio can be increased slightly and inlet cross sectional area is increased as well. The logic behind increasing inlet cross sectional area is that as the flow enters from the inlet port, a higher inlet cross sectional area will help the flow to settle and form helical flow pattern. Moreover, the carryover fluid coming from stripper seal (blocking the outlet port pressurized fluid to mix with inlet low pressure fluid) will mix with incoming stream of fluid and extreme turbulence could be reduced by the larger cross sectional area at inlet. Moreover, by this modification, the acceleration region as shown in Figure 2.10 might be reduced and linear region might be increased, which means more head rise can be obtained. This calls for slightly enlarged inlet port as well. It is learnt from literature that higher diameter of inlet and discharge nozzles helps to produce higher heads and better efficiency by reducing

losses in the ports region. Based on the above discussion, following design changes to channel geometry are suggested to improve Capstone multistage RFC performance.

- Increase radial clearance "c_r" by 25-30%.
- Adjust channel height "e" accordingly.
- Increase inlet channel area at station A "$A_{c,A}$" by 10-15%
- It is been proven by many authors and even sensitivity analysis that a smaller value of d_A is beneficial for isothermal efficiency. However, still it is suggested to size d_A based on "e" and value of inlet channel area at station A. d_A can be calculated to produce required inlet cross sectional area at station A.
- Decrease discharge channel area at station B "$A_{c,B}$" by 5-10% or rather little less so that the channel area ratio must be less than 1.35 or maximum 1.40. However, to fit the values and make it look realistic, the increase in "$A_{c,A}$" can also be moved around from 10-15% value to a lower value as desired.
- Based on "e" and "$A_{c,B}$" it is very easy to calculate d_B to produce required discharge cross sectional area at station B.
- Keep a linear area distribution from station A to B.
- Inlet nozzle cross sectional area should be increased 10-15% in order to reduce losses in the inlet port.
- Discharge nozzle is tapered and it should be modified to match with the discharge area at each stage.

6.3 Analysis of blade geometry

First set of design changes focused on relatively simple modifications to channel dimensions. In this phase of sensitivity analysis, focus is on making some design changes to impeller radius ratio to study that how this will effect performance. Impeller tip radius is a very important geometric parameter for performance. It controls overall size of the machine and also the impeller tip Mach number. Impeller tip radius affects two most important sources of losses, i.e., slip and shock. It is found from the code that shock and slip losses are minimized by increasing the tip radius. Moreover, it is found that slip and shock losses can be reduced by making impeller hub radius smaller. To see the cumulative effect, a non-dimensional parameter called radius ratio is introduced which is defined as r_2/r_e. It dictates that what sort of radius ratio will be beneficial for the performance of RFC. Slip factor, shock loss parameter and pressure ratio are plotted against impeller radius ratio in Figures 6.12 and 6.13.

It is very obvious that increasing radius ratio is helpful for better performance. However, after a certain radius ratio, the pressure ratio starts to go down. In order to establish some design criteria for radius ratio, literature is cited to see what sort of radius ratios were used in other RFC designs. The two important non-dimensional parameters to be investigated are r_2/r_e and $A_{c.A}/r_2^2$.

Wilson [69] used values,	$r_2/r_e = 1.48,\ A_{c.A}/r_2^2 = 0.068$
Cates [15] used	$r_2/r_e = 1.428,\ A_{c.A}/r_2^2 = 0.077$
ORNL CRDT used	$r_2/r_e = 1.56,\ A_{c.A}/r_2^2 = 0.0896$
ORNL FPD used	$r_2/r_e = 1.66,\ A_{c.A}/r_2^2 = 0.186$

Capstone single stage RFC configuration S3 used

$$r_2/r_1 = 1.32,\ A_{c.A}/r_2^2 = 0.0128$$

Capstone multistage RFC for all 4 stages

Stage 1. $r_2/r_\circ = 1.2074,\ A_{c.A}/r_2^2 = 0.0172$

Stage 2. $r_2/r_\circ = 1.176,\ A_{c.A}/r_2^2 = 0.0130$

Stage 3. $r_2/r_\circ = 1.153,\ A_{c.A}/r_2^2 = 0.010$

Stage 4. $r_2/r_\circ = 1.126,\ A_{c.A}/r_2^2 = 0.007$

When these designs are compared, it is observed that for individual stages of Capstone multistage RFC, a slight increase in radius ratio is suggested. However, no firm criteria could be established for $A_{c.A}/r_2^2$. It is believed that making other design changes to geometry automatically establishes the ratio $A_{c.A}/r_2^2$. Moreover, establishing a bound for $A_{c.A}/r_2^2$ might as well make the problem over constrained. Therefore, it is suggested that a 5-7% increase in impeller tip radius and 5-7% reduction in impeller hub radius for each stage will be helpful to improve performance of Capstone multistage RFC.

Number of impeller blades is being investigated by many researchers in literature, noteworthy of which is Iverson [34]. Blade number has an obvious effect on slip factor as shown in Figure 6.14. Slip losses are increased immensely when blade number is reduced, which implies very detrimental effect to pressure ratio and efficiency. Experimental sensitivity analysis on Capstone single stage RFC showed that blade number between 75 and 90 seems reasonable for RFC design. Further increase in blade number might prove detrimental, because it will make angle between blades less than 4°, which might not allow enough circulations through the impeller. Instead impeller will look like a rough

surface to the fluid and there will be reduced number of circulations, which is detrimental to performance. Moreover frictional losses can increase due to too many blades in the impeller. Figure 6.15 shows improvement in pressure ratio with increasing blade number.

6.4 Performance improvement by rotor blade chevroning

It has been suggested by many authors that rotor blade shaping or chevroning as shown in Figure 6.16 benefits RFC performance. A sensitivity analysis is carried out based on the code to see how blade angle affects the performance. Basically, the slip losses can be minimized by rotor chevroning. To study the effect of blade chevroning on the slip factor, the blade angle is varied from purely radial 90° blade to chevroned blade with angle of150°. The geometry described in Figure 6.16 results from chevroning the blades of the impeller in the direction of rotation. It is believed that better guidance and circulation is provided to the flow by chevroning the blades. This helps to reduce the slip losses as shown in Figure 6.17. The effect of blade chevroning on pressure ratio is shown in Figure 6.18. There is a clear advantage in chevroning the impeller blades by a certain angle. It must however be noted that the chevron angle should not be more than150°, because doing that might bring in extra retardation to the flow. Mathematical formulation proposed in this thesis does not include the effect of blade chevroning on shock loss. However, the literature suggests that shock losses are minimized by making the chevron angle close to150° as shown in Figure 6.19. It must be noted that the60° angle shown in Figure 6.19 is same as 150° according to our convention. The variation of head coefficient with rotor blade chevroning is compared with test data published in literature. It is found consistent as shown in Figure 6.20 by the increasing trend in head coefficient

obtained with blade chevroning. Moreover, it is also believed that chevroning the blades will help to increase the number of circulations of the flow through the impeller blades, which means more head rise for a given impeller tip Mach number. Such a concept of rotor blade chevroning is employed to develop a regenerative fuel pump for automotive fuel pumping by Delphi Automotives, MI. This design is very promising and yields very good performance as discussed in chapter 7.

6.5 RFC Design Guidelines

So far the discussion is focused on trying to improve the geometry of Capstone multistage RFC. However, to make this discussion more meaningful, it is essential to propose a design procedure for radial and non-radial blade RFC design. There is no evidence available in literature about the existence of any design criteria and guidelines for radial and non-radial blade RFC design. A design procedure is proposed below, which can be followed for sizing dimensions of impeller and channel of radial and non-radial blade RFC.

To avoid the compressibility effects, it is suggested to choose impeller tip Mach number to be less than 0.8, thus

$$M_{OT} < 0.8 \tag{6.3}$$

Using the design criteria in (6.1) and (6.2), the radial clearance and channel depth at station A can be established. The channel area at station A can be found by

$$A_{in} = \frac{\pi d_A^2}{2} \tag{6.4}$$

The impeller hub radius can be calculated using

$$r_o = r_2 + c_r - 2d_A \tag{6.5}$$

A design criteria for the area ratio at station A and station B is proposed

$$1.15 < A_{c,A}/A_{c,B} < 1.35 \tag{6.8}$$

Moreover, it is suggested that the number of impeller blades must be selected using the following design criteria

$$75 < Z < 90 \tag{6.9}$$

For best performance, the blade chevron angle must be selected using the following design criteria

$$45^{\circ} < \beta < 60^{\circ} \tag{6.10}$$

6.6 Conclusions

Extensive design sensitivity analysis is performed on impeller and channel geometry using the performance prediction code. Sensitivity analysis results from the code are collaborated with published test data in literature to propose some design guidelines. Various suggestions pertaining to design improvement of Capstone multistage RFC are laid down. In order to make this discussion more meaningful, a design procedure for radial and non-radial blade RFC is suggested. There is a need to refine the proposed design procedure by incorporating more design criteria. Moreover, CFD analysis must be performed to validate the established design criteria. The performance prediction code takes geometric data and operating point as input and predicts the performance. The next step is to extend the code to work in the design mode, i.e., taking the operating point and desired performance as input, it should be able to design the compressor geometry.

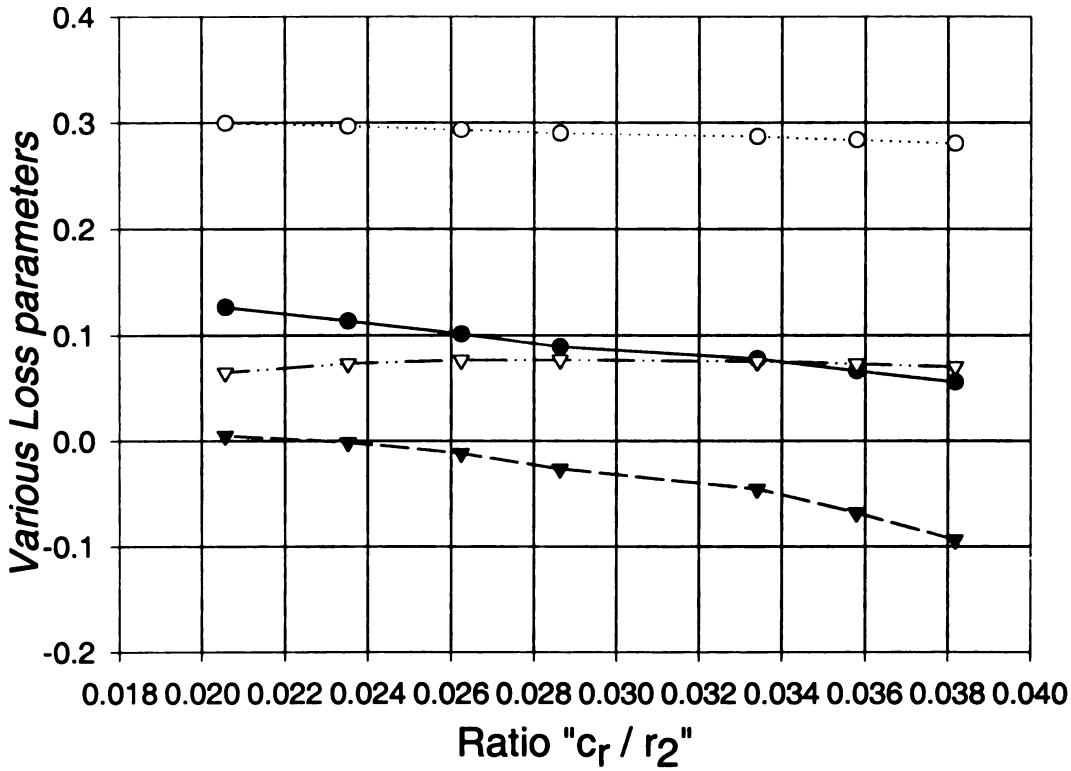

Figure 6.1 Various loss parameters vs. ratio "c_r / r_2"

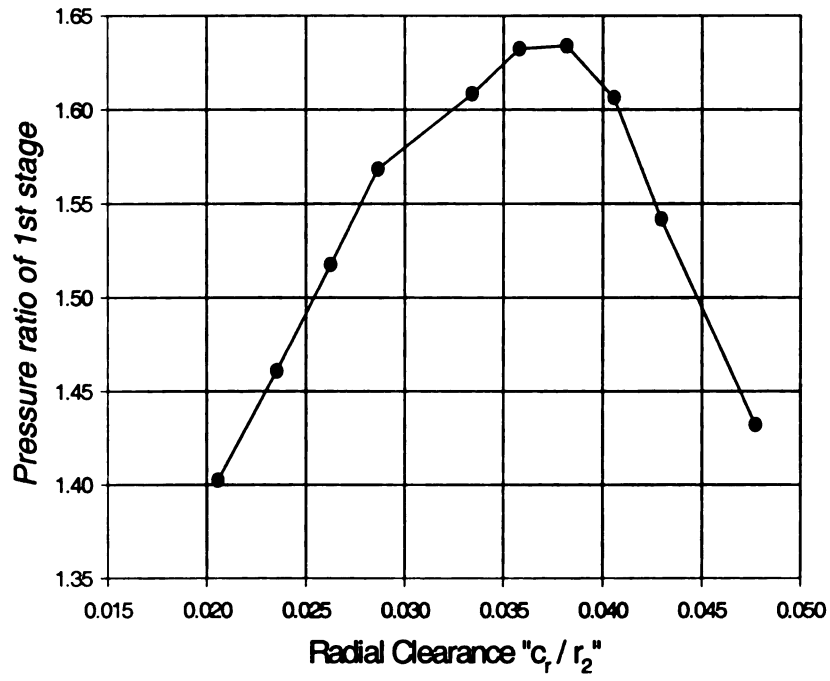

Figure 6.2 Radial clearance vs. pressure ratio for first stage

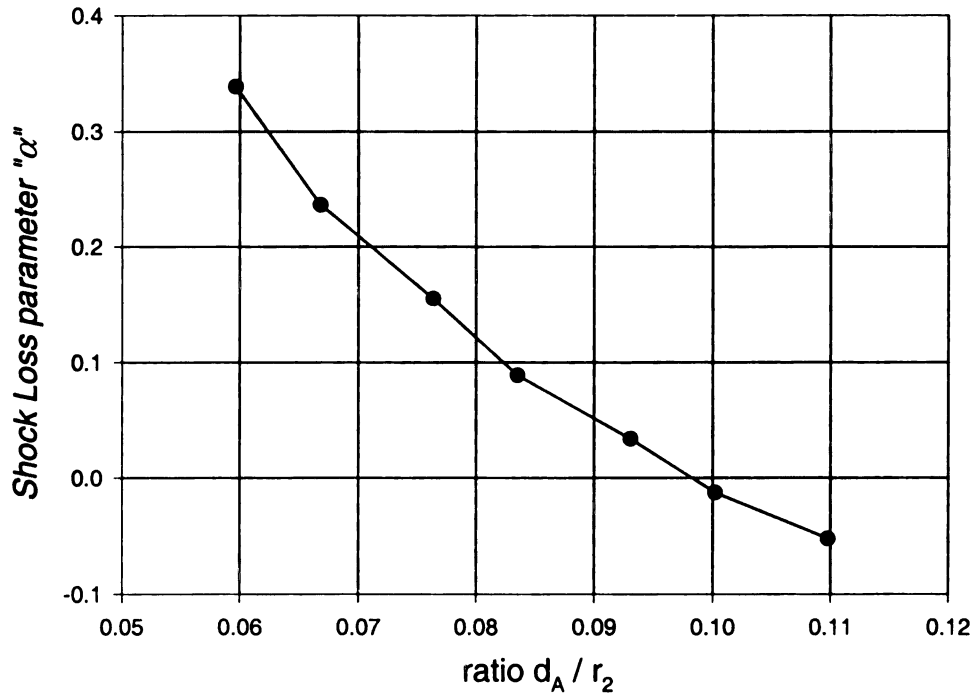

Figure 6.3 Ratio "d_A / r_2" vs. shock loss parameter "α"

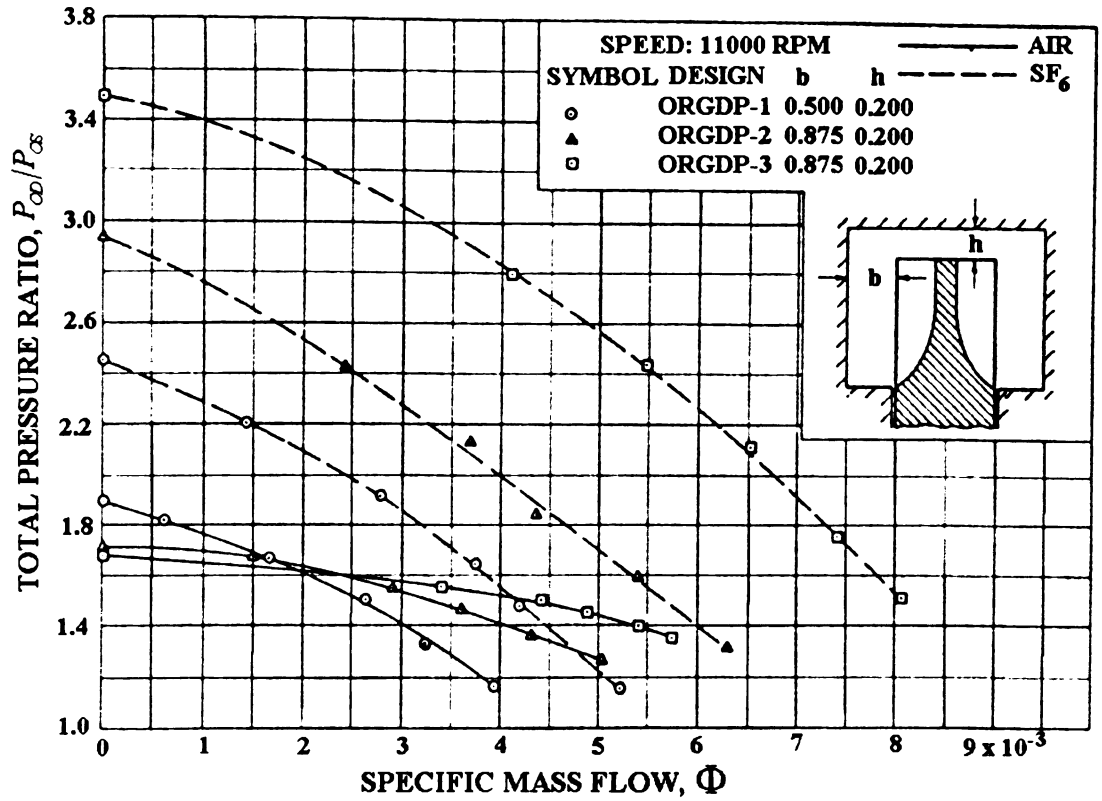

Figure 6.4 Influence of channel geometry on pressure ration (after Cates [15])

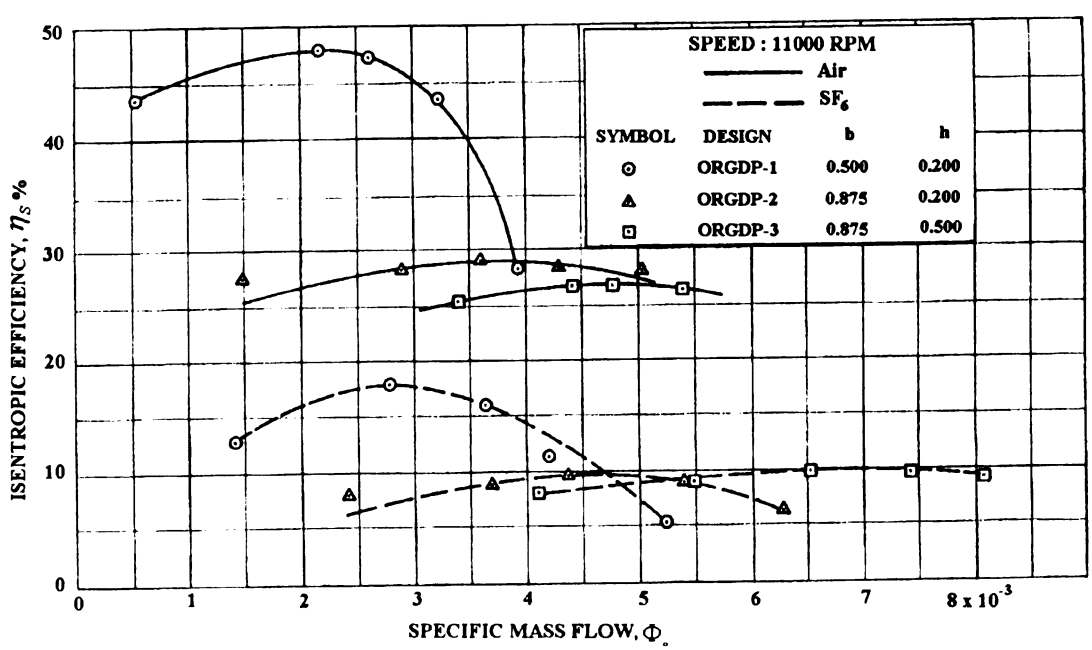

Figure 6.5 Influence of channel geometry on adiabatic efficiency (b=channel depth, h=radial clearance, after Cates [15])

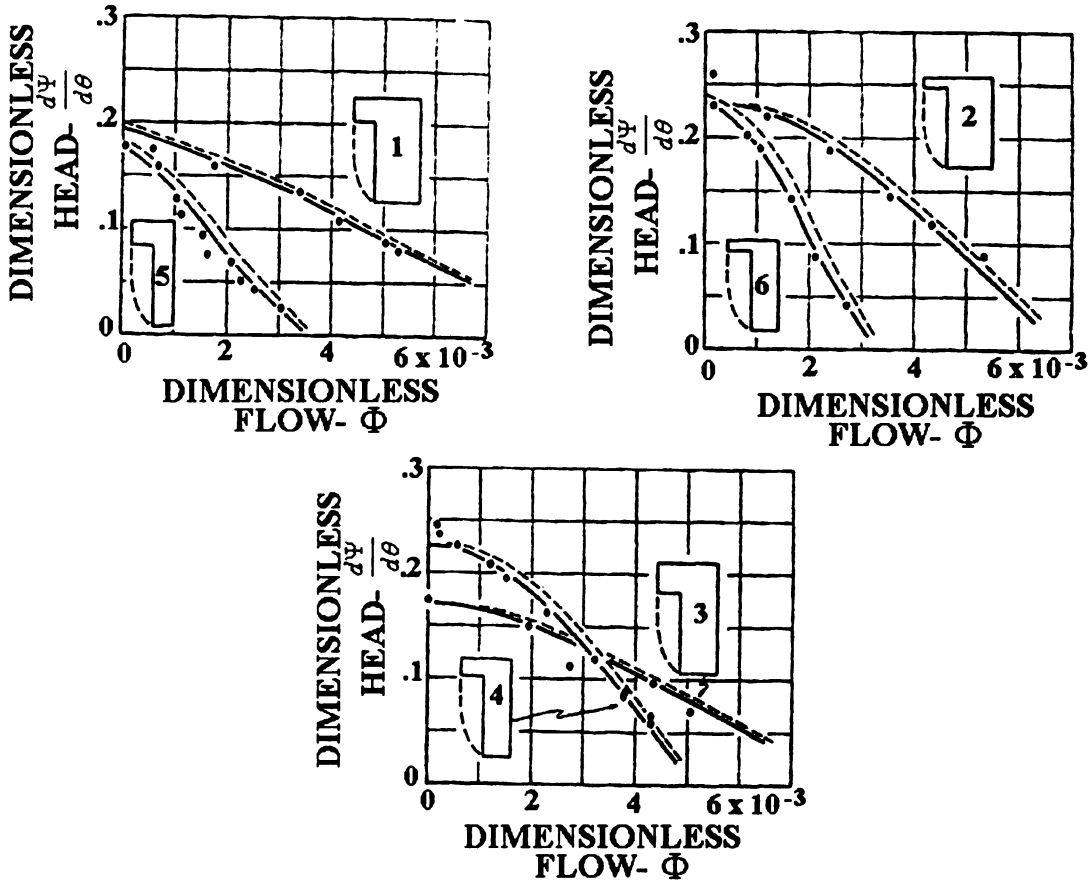

Figure 6.6 Effect of channel geometry on head coefficient (after Wilson [69])

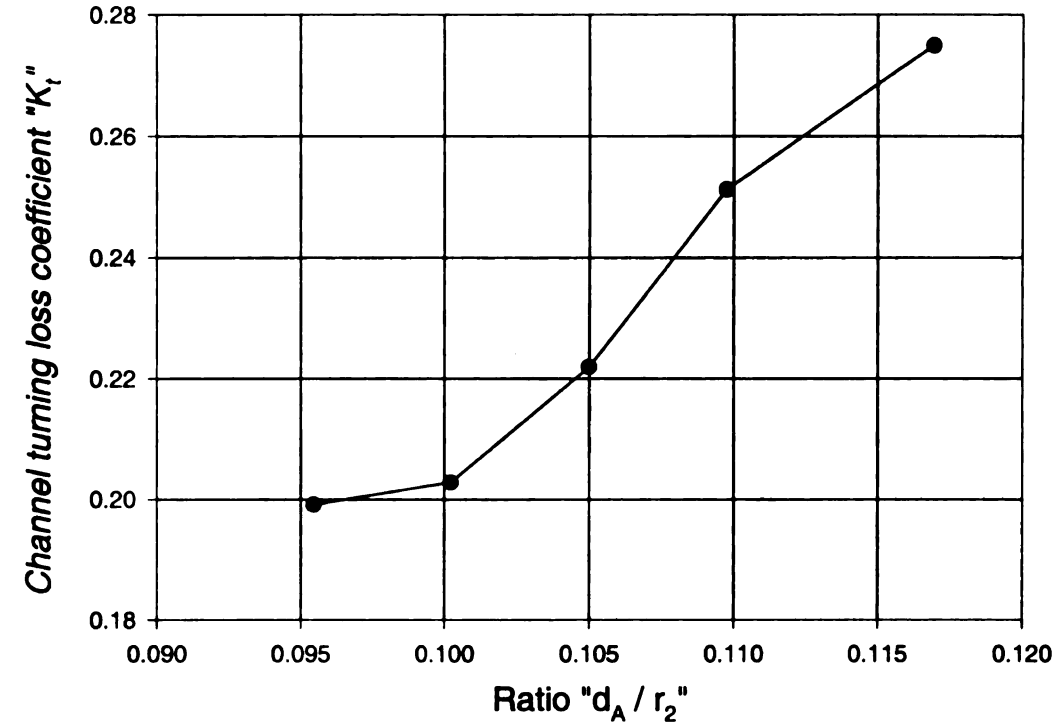

Figure 6.7 Ratio "d_A / r_2" vs. channel turning loss coefficient

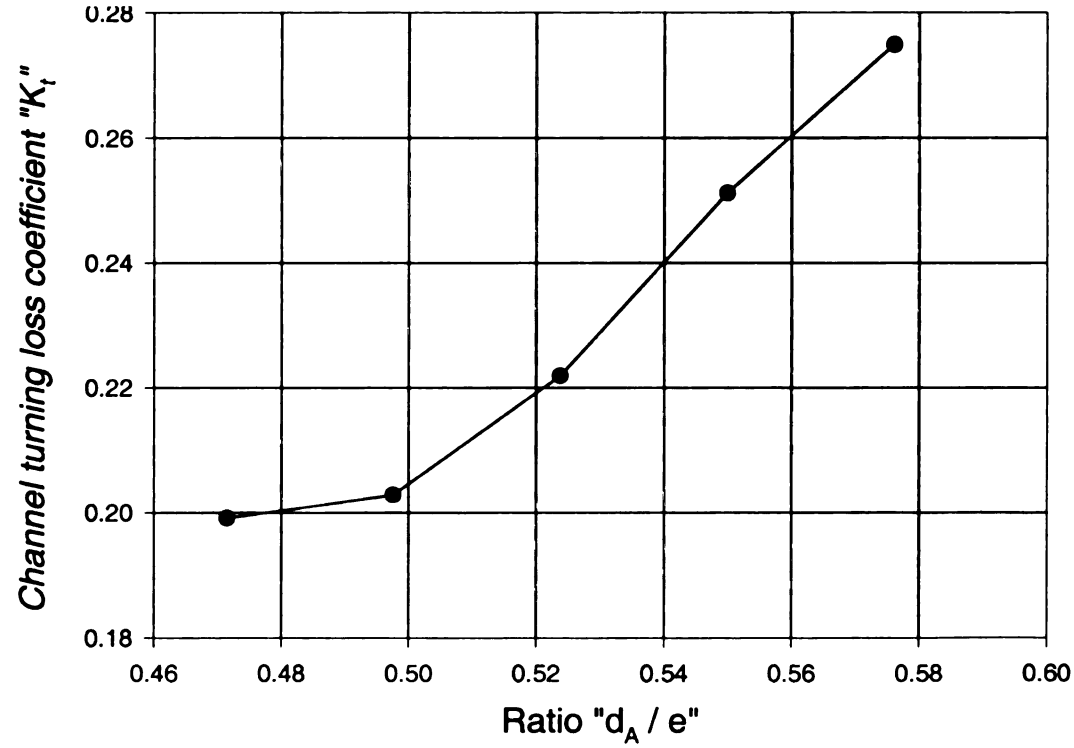

Figure 6.8 d_A/e vs. channel turning coefficient

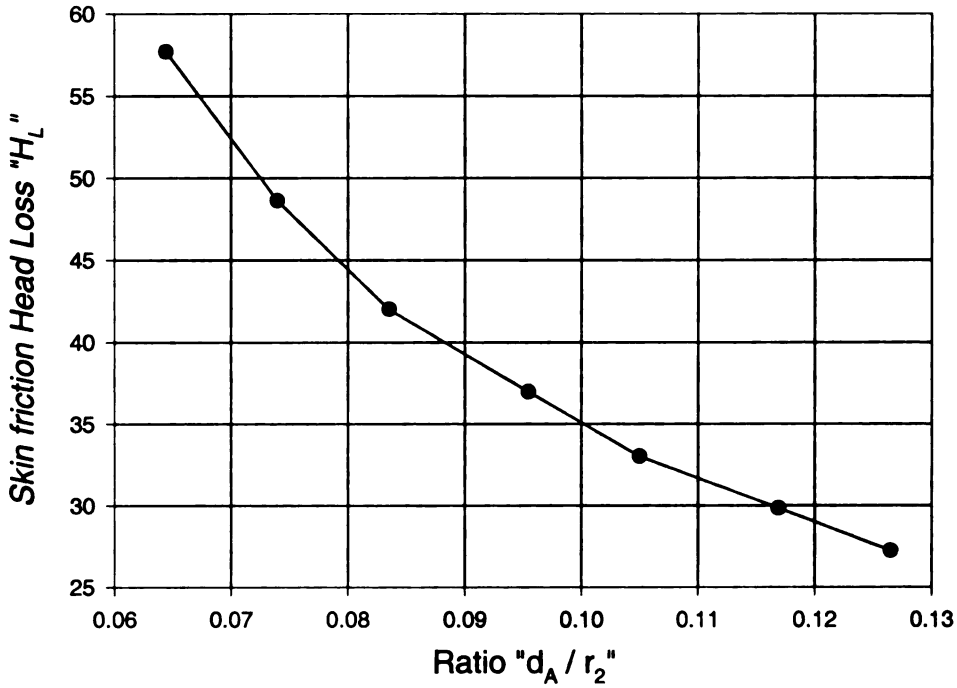

Figure 6.9 Ratio "d_A/r_2" vs. skin friction loss

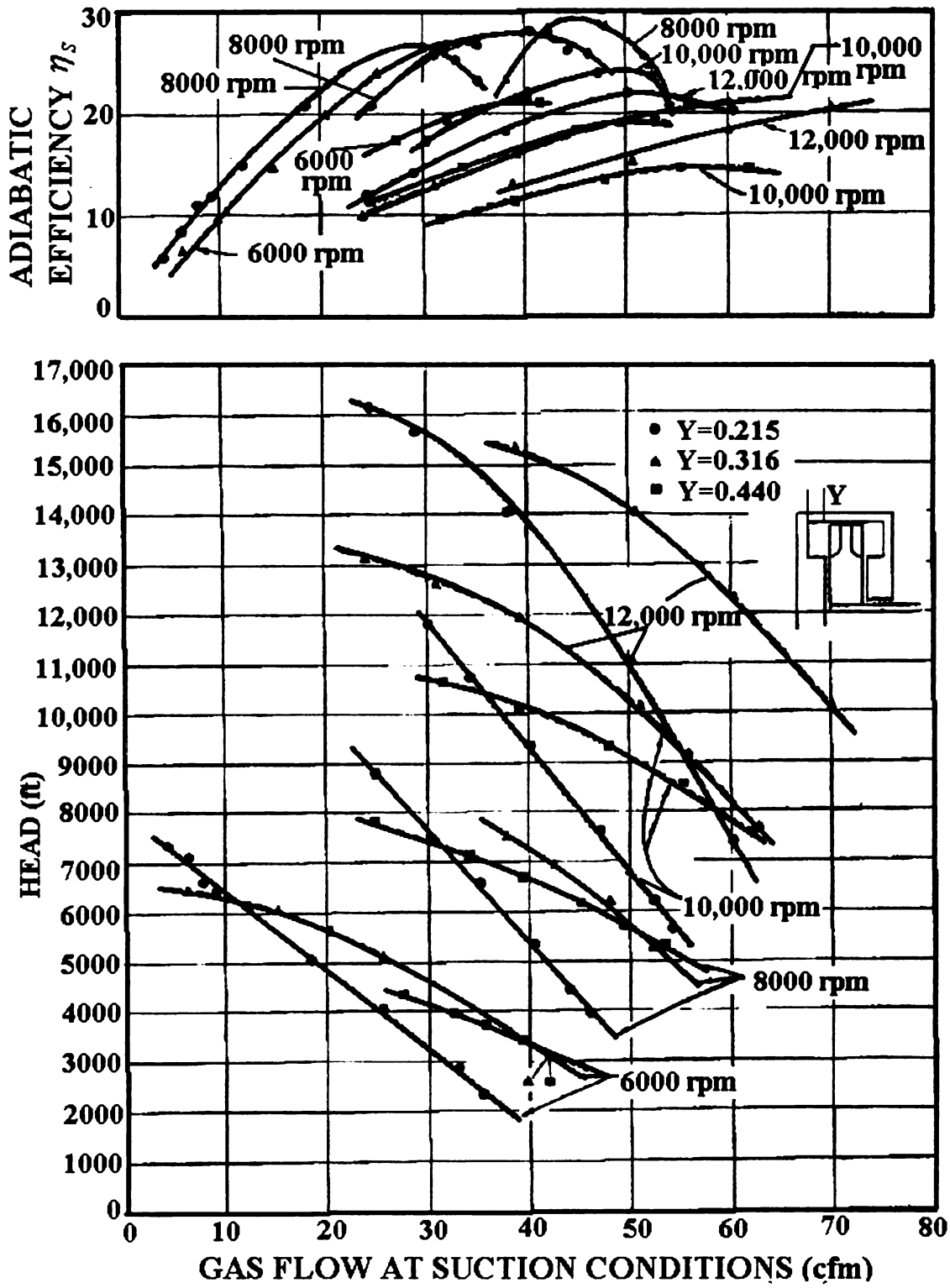

Figure 6.10 Effect of channel dimensions on performance, (after Burton [11])

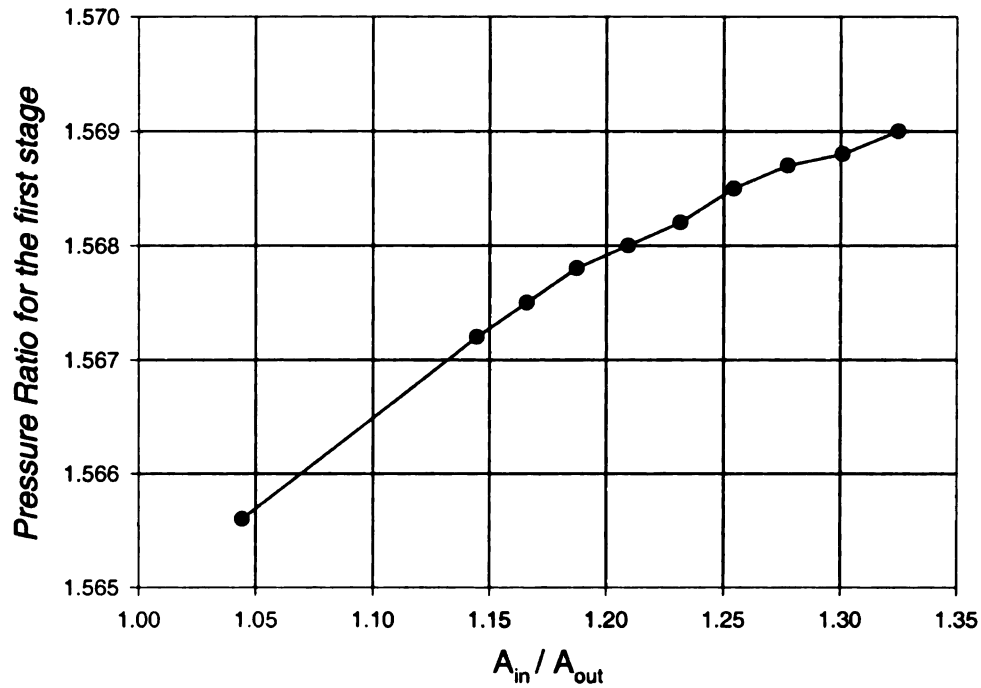

Figure 6.11 Pressure ratio vs. channel area ratio

Table 6.1 Various configurations tested by Wilson for experimental sensitivity analysis

Config #	Radial clearance "c_r" *inch*	Channel depth "d_A" *inch*	Ratio $\frac{c_r}{d_A}$	Ratio $\frac{c_r}{r_2}$	Channel Area, "A" $inch^2$
1	0.875	1.7	0.515	0.092	7.38
2	0.365	1.7	0.215	0.038	6.12
3	1.130	1.41	0.802	0.119	6.80
4	0.620	1.06	0.585	0.065	4.39
5	0.875	0.76	1.15	0.092	3.68
6	0.365	0.76	0.480	0.038	2.89

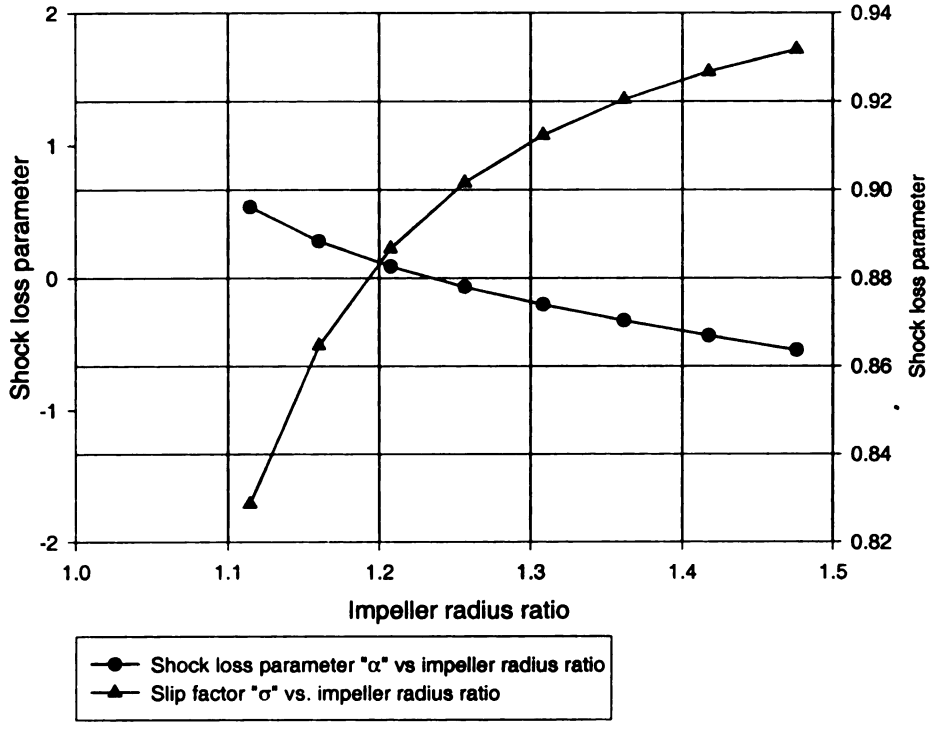

Figure 6.12 Slip and shock loss parameter vs. impeller radius ratio

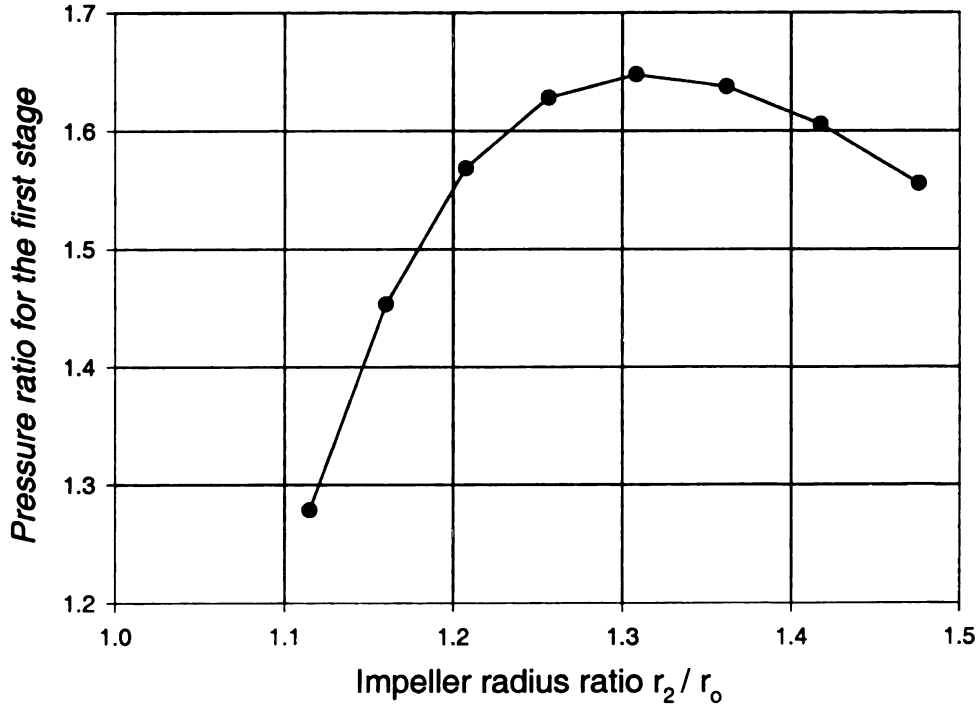

Figure 6.13 Pressure ratio vs. impeller radius ratio

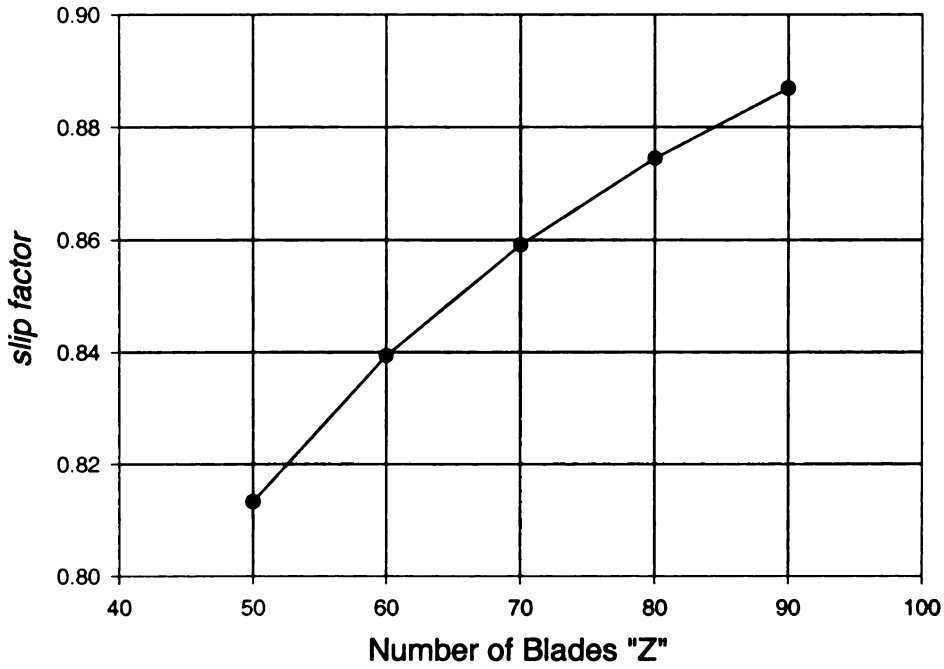

Figure 6.14 Slip factor vs. number of blades

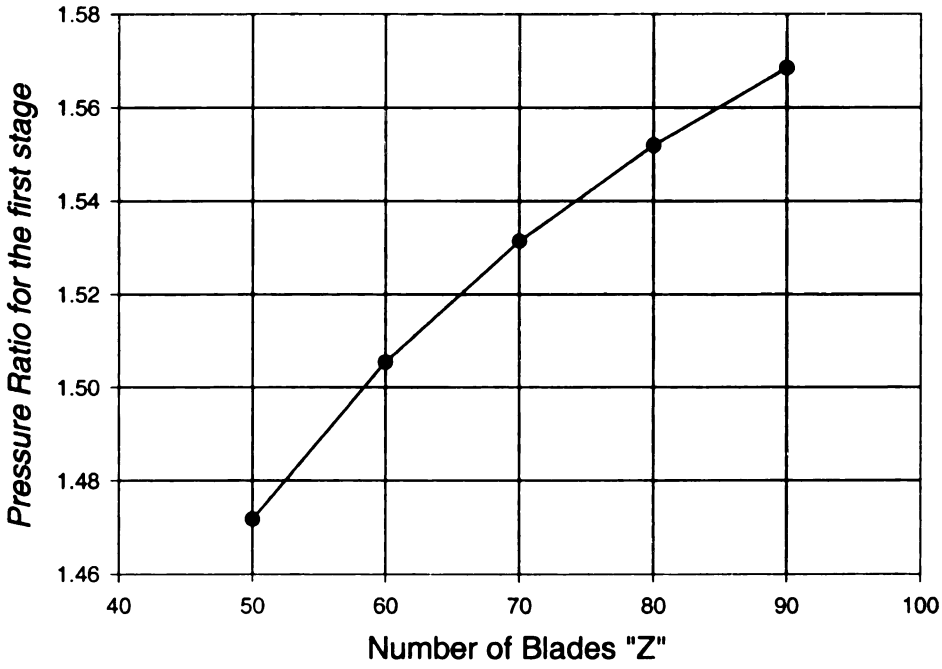

Figure 6.15 Pressure ratio vs. number of blades

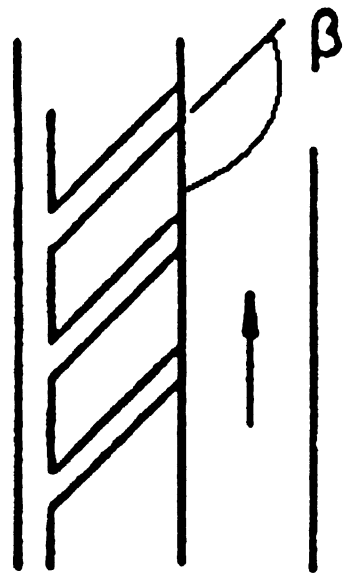

Figure 6.16 Blade chevroning

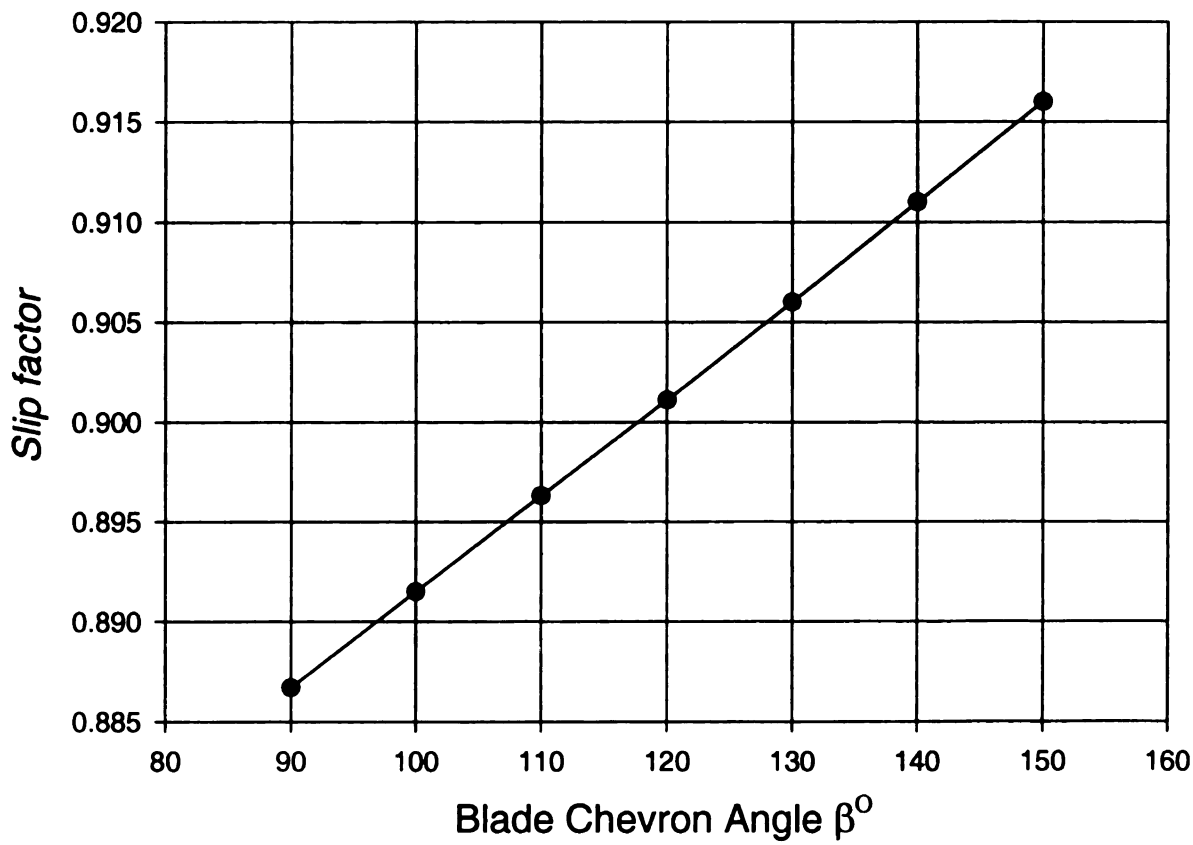

Figure 6.17 Slip factor vs. Chevron angle

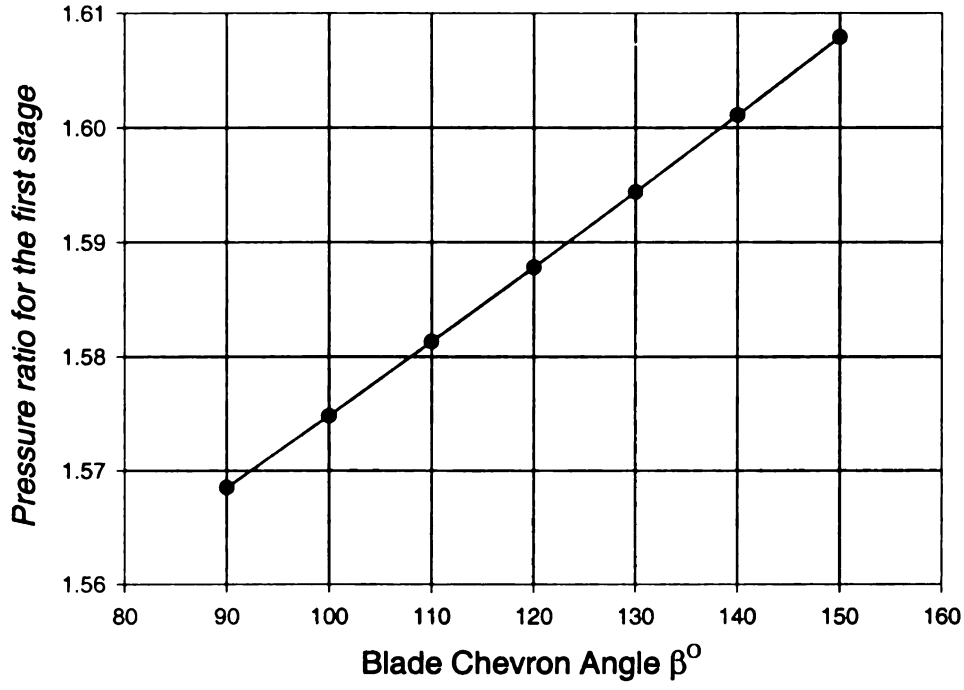

Figure 6.18 Pressure ratio vs. Chevron angle

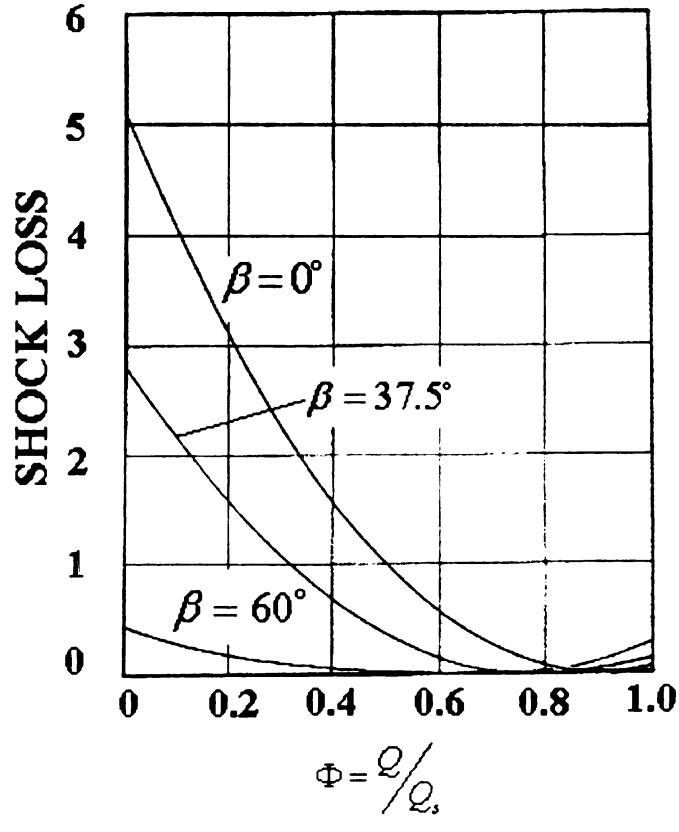

Figure 6.19 Variation of shock loss with chevron angle (after Dewitt [21])

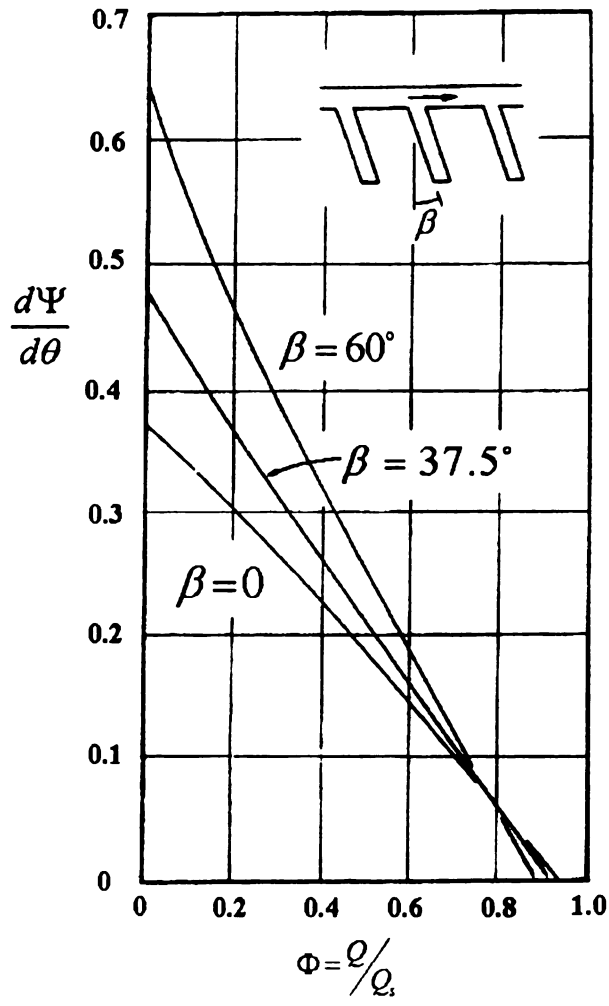

Figure 6.20 Effect of Blade chevroning on head coefficient (after Dewitt [21])

CHAPTER 7

REGENERATIVE AUTOMOTIVE FUEL PUMP

A typical automotive fuel system consists of a gasoline tank, a fuel pump, fuel filter and connecting lines. Schematic of an automotive fuel system is shown in Figure 7.1. Fuel pump is a device which draws the fuel in the fuel tank through the fuel lines to the carburetor or injectors of the engine. Gasoline is stored in the tank under the rear floor in the front-engine automobiles. To function correctly, the fuel pump must move the gasoline in the fuel system from the tank to the carburetor or fuel injection system in sufficient volume and pressure. The sufficient pressure of gasoline in the line between the carburetor and the pump can keep the fuel from boiling and prevent the vapor lock. This gasoline transfer keeps the carburetor bowl full of clean gasoline, regardless of vehicle speed or maneuvering. The fuel pump has to lift against a head of 0.6 m from the tank or more to the carburetor or fuel injection. The fuel metering and atomization system is located higher in the vehicle than the fuel tank. A mechanical or electrical fuel pump is employed to draw the fuel from the tank and deliver it to the carburetor or fuel injectors. It must have sufficient capacity to supply the engine with fuel under all operating conditions. The fuel pump should also maintain sufficient pressure in the line to the carburetor to keep the fuel from boiling and causing vapor block due to high engine temperature under the hood. Fuel pumps for automotive applications have requirements for very high pressure rise at very low volumetric flow rates. In order to achieve this,

regenerative fuel pumps are found to be more useful than any other available pumps. Regenerative pumps achieve very high pressure rise and typically operate around hydraulic efficiency of 20-30%. Due to their low specific speed, regenerative pumps allow high heads at low flow rates and present performance curves with very stable features. In Figure 7.2, a complete pump-motor group similar to those directly inserted in the vehicle fuel tank is schematically presented. The fuel enters through the inlet port as shown in the bottom part of Figure 7.2 and goes through the pump. Impeller of RFP is visible in this figure. The attached motor rotates this impeller and fluid circulates through the blades and discharges out from the outlet at high pressure. There are many reasons for the competitive advantage enjoyed by regenerative pumps over its competitor pumps as discussed below.

7.1 Advantages of a regenerative automotive fuel pump

- The biggest advantage offered by a regenerative pump is its extremely compact design. Typical regenerative fuel pumps employed in automotives are less than 40 mm in diameter which makes the pump motor assemble very compact. This feature is very attractive in automotives because of space limitations.
- Self priming capability offered by regenerative automotive fuel pump makes it very attractive. They have an ability to purge out vapors at start of pump operation and draw liquid fuel inside the impeller, something which other fuel pumps lack. Regenerative pumps are known to have excellent priming behavior.
- Operation at high fuel temperature is another huge advantage offered by these pumps. The fuel coming back from the injection system through the return line is

very hot and thus requires the pump to operate at higher temperature. This is something possible only by using a regenerative pump.

- Simplicity in construction is another huge advantage offered by these pumps.
- They are very cheap to manufacture. A regenerative pump can be manufactured and sold to the market as cheap as $ 20 - $ 50.
- Ignition safety is another advantage offered by regenerative pumps.
- Regenerative automotive fuel pumps are very durable. They have been tested to operate up to 10,000 hours without any problems.
- Low noise level is another highly desired attribute in automotives. RFP are very quiet and present a huge advantage over other fuel pumps.
- No wearing problems in RFP like those found in positive displacement machines.

Over the past few years, regenerative pumps have been subject to more and more interest in the automotive field as injection pumps in spark ignition engines. Badami [7] presented a hypothesis for the evaluation of the circulatory flow rate and based his theory on the consideration of the centrifugal force field in the side-channel and in the impeller vane grooves. He used momentum exchange theory to predict head-flow curves and presented a comparison between theoretical and experimental data. He constructed two innovative regenerative pumps and tested them. Badami attempted to find some new technical solutions for the design of periphery pumps with the aim of enhancing their performance and simplifying their construction. The first pump designed by Badami was a double stage regenerative pump as shown in Figure 7.3. It presented better performance characteristics than those obtained using a traditional regenerative pump with same

overall dimensions. The second pump designed by Badami offered a particular technical solution which allowed some interesting features for the construction of the motor-impeller group. With this solution, the vane grooves were machined directly on to the external periphery of the electric motor, thus reducing the number of parts.

7.2 Delphi Automotive Fuel Pump

Delphi Automotives, MI has designed regenerative fuel pumps with non-radial blade and semicircular channel geometry. Several pump designs have been made for different applications. The pump and motor assembly is very compact as shown in Figure 7.4. The assembly is disassembled and various components are shown in Figure 7.5. The impeller has channels on both sides as shown in Figure 7.6. These channels are built is the casing and help to promote the circulatory flow around the blades. Blade and channel geometry of typical Delphi fuel pump can be seen in Figure 7.7. The blades are non-radial with an angle of 45° in an attempt to provide better guidance to the flow. Channel shape is made semi-circular for better circulation of flow and minimize circulatory losses.

Non-dimensional experimental data of head and hydraulic efficiency versus non-dimensional flow rate is presented in Figure 7.8 and 7.9 using viscor as working fluid. Viscor has properties very close to gasoline, but it is less combustible and better suited for testing. Test data is obtained at different speed (rpm) of the impeller. It is interesting that non-dimensional test data for head and efficiency falls on the same curve. The hydraulic efficiency graph shows that a peak efficiency around 40% can be achieved using regenerative automotive fuel pump. This efficiency does not include the power lost in motor. When motor efficiency is also considered, the net efficiency comes out to be very low, approximately 18% at design point. Figure 7.10 shows the flow rate, current

drawn and overall efficiency versus pressure. Most automotive fuel pumps operate between 12 Volts - 13.5 Volts. The current drawn and voltage can be multiplied to get the power drawn by the pump. Typically the power drawn by this type of pump is around 50-60 Watts. It is very important to make this pump efficient because when the engine is turned on, the pump keeps on operating and draws the power from the battery. If there is a large amount of power drawn from the battery, it can be harmful to life of the battery. Due to unique operational features and advantages offered by regenerative pump, it is of great interest to industry that these pumps operate with better efficiency.

To assist in improving regenerative fuel pump efficiency, the mathematical formulation presented in chapter 5 is used to predict the performance of Delphi regenerative fuel pump. Blade and channel geometry data of two test pump designs can be found in Table 7.1. Hydraulic power (P_{hyd}) transferred from impeller to fluid is consumed by both power required for head rise (P_h) and circulatory power (P_c). The circulatory power keeps the flow circulating through the blades. It is this circulatory power which makes the regenerative pump less efficient than the centrifugal pump.

Hydraulic efficiency can be determined by

$$\eta_{hyd} = \frac{\rho Q g H}{P_{hyd}} \tag{7.1}$$

Including the power lost in motor and other mechanical parts, the overall efficiency is given by

$$\eta_{overall} = \frac{\rho Q g H}{\left(P_{hyd} + P_{disk}\right)} \tag{7.2}$$

The performance prediction code is used to predict the performance of the fuel pump and then carry out a sensitivity analysis on various design variables to see which changes can increase the efficiency. Figure 7.11 shows that the theoretical results of head rise vs. flow are in good agreement with the experimental results at high flow rates. The comparison is good at the design point; however, it has some deviations at off design flow rates. Figure 7.12 however does not show good agreement between efficiency vs. flow rate. The predicted efficiency–flow rate curve is higher than that of experimental data. The reason for this trend is that if the predicted head is higher than the experimental head, it makes the predicted efficiency higher than experimental efficiency. It is obvious that the flow rate at which predicted hydraulic efficiency (η_{hyd}) is maximum is slightly higher than the flow rate at which the predicted maximum efficiency (η) occurs. The reason for this trend is that the ratio of the disk friction power to hydraulic power is considerably increased at higher flow rates. An explanation of this is that disk friction power is independent of flow rate, however, the hydraulic power of a regenerative pump reduces as the flow rate increases.

After predicting the performance, an extensive sensitivity analysis is performed in which it is observed that hydraulic efficiency is largely influenced by R_{tip}, A_c and R_{hub}. The main conclusions from the sensitivity analysis are that if R_{tip} and A_c are increased and R_{hub} is reduced by 10%, efficiency can increase 3-7%. Of course the pressure rise of that point is different from that at design point. The prediction from the code and design suggestions mentioned above need to be validated by CFD analysis on a full pump model before prototype pump with the new design can be made.

7.3 CFD Analysis on regenerative automotive fuel pump

A CFD analysis is performed on a complete pump model to study its internal flow mechanism and performance characteristics at design point. The CFD analysis takes a long time to complete the simulation, thus only selected design points are used to perform CFD. Therefore, it is not easy to get CFD results for the full operating range of the pump. Figure 7.13 shows the complete pump model with inlet and discharge ports, non radial blades on both sides and the flow channels. The pump model is generated in UNIGRAPHICS, while the grid is generated in GAMBIT using hexahedral (Brick) elements. The element count for the full model comes out to be nearly 200,000. A transient analysis is performed with a time step $\Delta t = 2.083\times10^{-5}$ sec for half degree impeller revolution. The simulation is run for two complete revolutions of the impeller. This implies that for 720° impeller rotation, the simulation uses 1440 time steps.

Flow enters the impeller through the inlet port and is divided into two sides of the impeller. Figure 7.11 describes the shape of non-radial blades on both sides of the impeller. Figure 7.12 shows the web between any two blades, which serves to promote the circulatory flow pattern. The fluid coming from the channel circulates through this web and gets entrapped between the blades, which hit the flow. The blades add energy to the fluid until it gets out of the blades and circulates through the channel. After passing through the channel, flow enters the blade row for next circulation. It is this repetitive action of blades on the flow, which makes it possible to produce high heads at very low flow rates in regenerative turbomachines.

Pressure boundary conditions at both inlet and discharge ports are applied and rest of parameters are calculated by the simulation. The reason for applying pressure boundary

condition at inlet and outlet is that since there is a pressure regulator downstream of the pump which maintains a constant pressure of 400 Kpa , it is an automatic choice to apply the known pressure boundary condition at the discharge. Similarly, the inlet port draws fluid from the fuel tank which is at ambient pressure (zero gauge pressure), thus again making it convenient to apply pressure boundary condition at the inlet. With the pressure at inlet and discharge known, CFD analysis calculates the mass flow rate. The fuel pump runs at 5000 rpm when 12 V is applied to it. Torque applied to the impeller is also calculated by CFD, which gives power consumed after multiplying by rpm. The CFD simulations take a very long time to produce the results, therefore it is usual practice to choose a design point to perform CFD analysis. The design point for CFD analysis was chosen to be 5000 rpm and discharge pressure of 400 Kpa .

Figure 7.13 describes the total pressure variation across the periphery of the pump. It can be seen that the pressure gradually builds up as the flow circulates through the blades. The pressure at discharge port is the highest as indicated in the legend. Figure 7.14 shows the circulatory flow pattern in a cross section. The absolute velocity vectors show the circulation in the blades and channel, which is a characteristic of these turbomachines. The CFD model works very well and helps to understand the flow mechanism inside the pump. So far, the suggested design changes from theoretical analysis are not validated by CFD analysis. Instead, the set up of CFD model and flow analysis is completed till now to convince ourselves that this complex fluid flow inside RFP can be modeled by CFD. Currently work is in progress to make suggested design changes in the pump geometry and verify the results by CFD analysis and see if design changes suggested by the performance prediction code can increase the efficiency by 3-7%.

Although current Delphi RFP design performs well and it is currently best design available in automotive industry. However, after doing research on existing design of non-radial blade RFP, need was felt to make fundamental changes to this design to create significant improvement. Therefore, aerodynamically designed aerofoil blades are investigated in next two chapters for RFP/RFC design. Unfortunately, there is almost no information available in open literature about aerofoil blade RFP. However, Sixsmith and Altmann [60] did extensive research on aerofoil blade RFC. This motivated us to carry out a detail investigation on RFC with aerofoil blading in a hope to produce regenerative turbomachines with better efficiency. A compressible flow theory for aerofoil blade RFC is presented in the next chapter.

7.4 Conclusions

The application of regenerative pumps for automotive fuel pumping is discussed in detail. Various advantages of regenerative fuel pumps are explored. Proposed mathematical model is used to predict the performance of Delphi automotive fuel pump. Excellent agreement between theoretical and experimental data is observed at the design point. A sensitivity analysis is performed and it is suggested that if R_{tip} and A_c are increased and R_{hub} is reduced by 10%, hydraulic efficiency can increase 3-7%. A CFD analysis on Delphi fuel pump is presented. Currently, work is in progress to make proposed design changes in the Unigraphics model and perform a CFD analysis. Such an analysis will help to validate the effect of proposed design changes on performance.

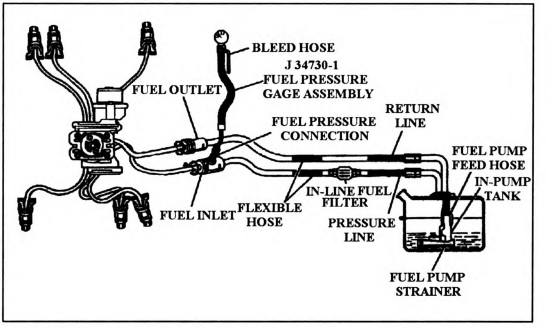

Figure 7.1 A typical automotive fuel system (Courtesy of Delphi Automotives, MI)

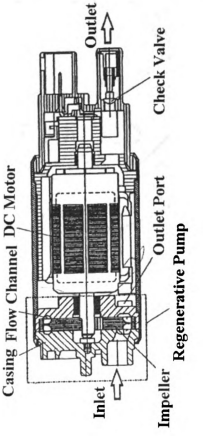

Figure 7.2 A Regenerative automotive fuel pump (after Hubel [32])

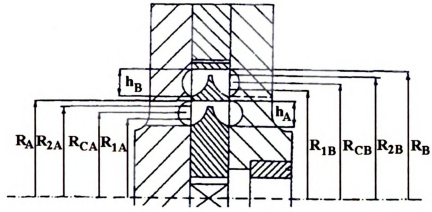

Figure 7.3 Schematic view and geometric symbols of a two stage periphery pump (after Badami [7])

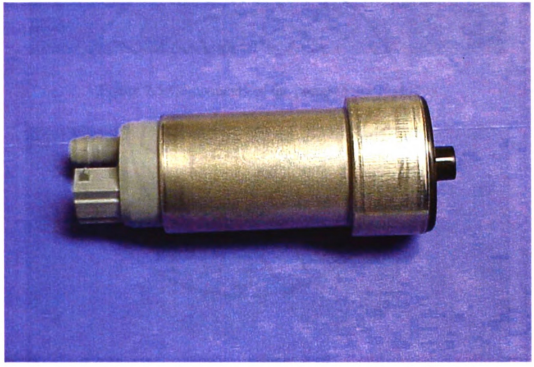

Figure 7.4 Pump and motor assembly of Delphi automotive fuel pump

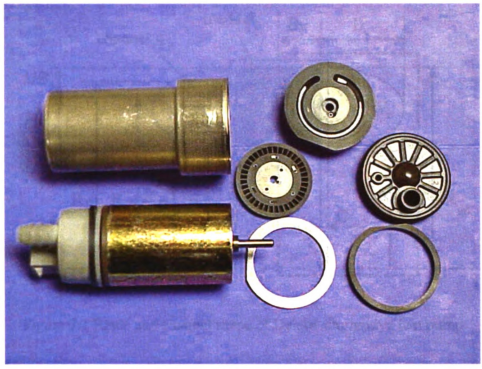

Figure 7.5 Components of the pump-motor assembly

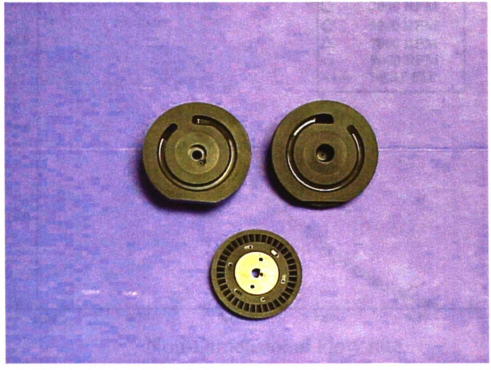

Figure 7.6 Impeller with both side channels

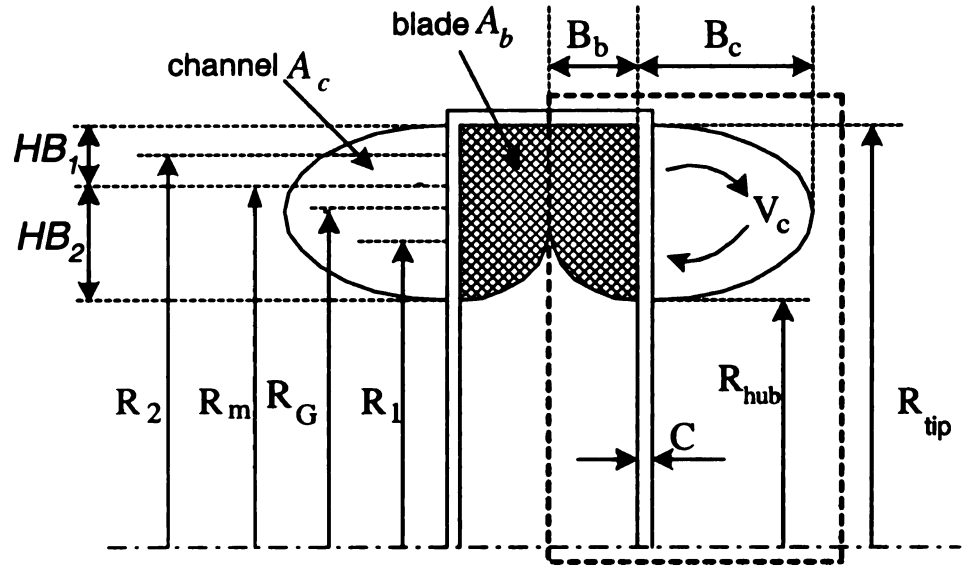

Figure 7.7 Blade and channel shape of Delphi automotive fuel pump

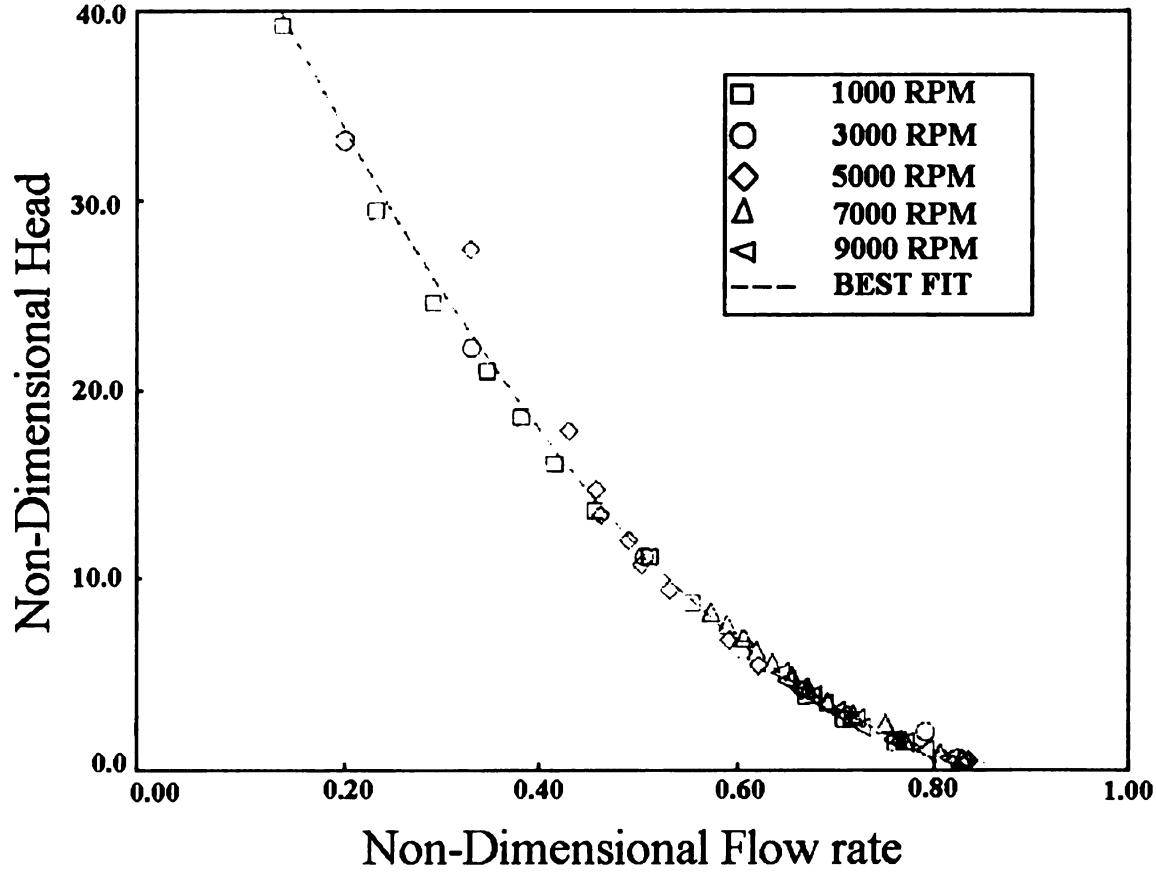

Figure 7.8 Non-dimensional experimental data of head vs. flow rate for Delphi RFP

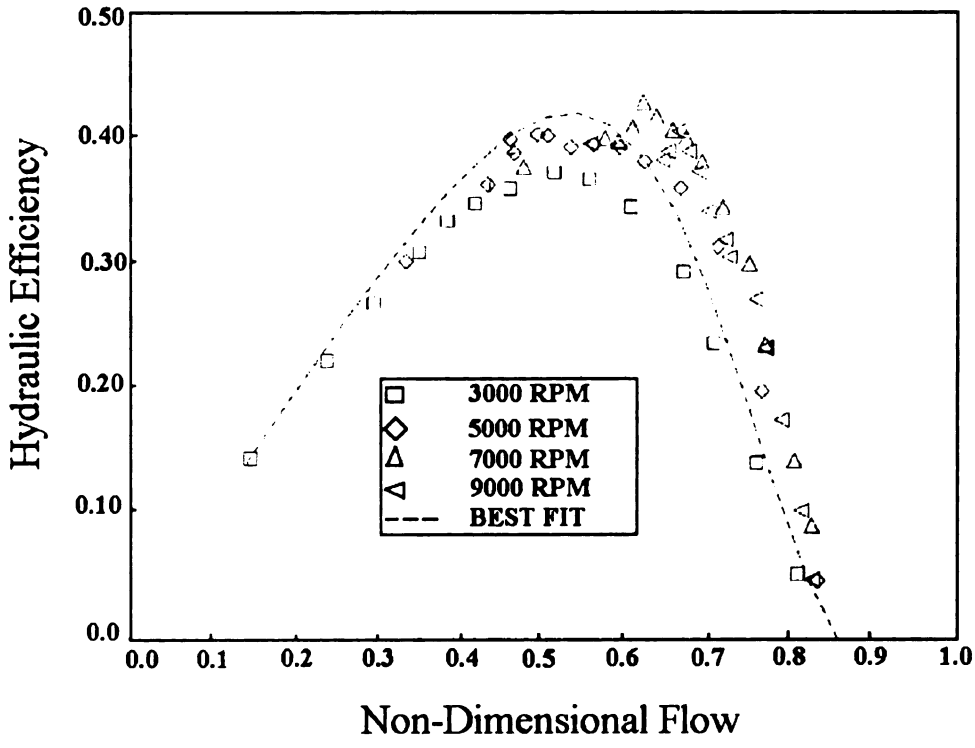

Figure 7.9 Efficiency vs. flow rate for Delphi RFP

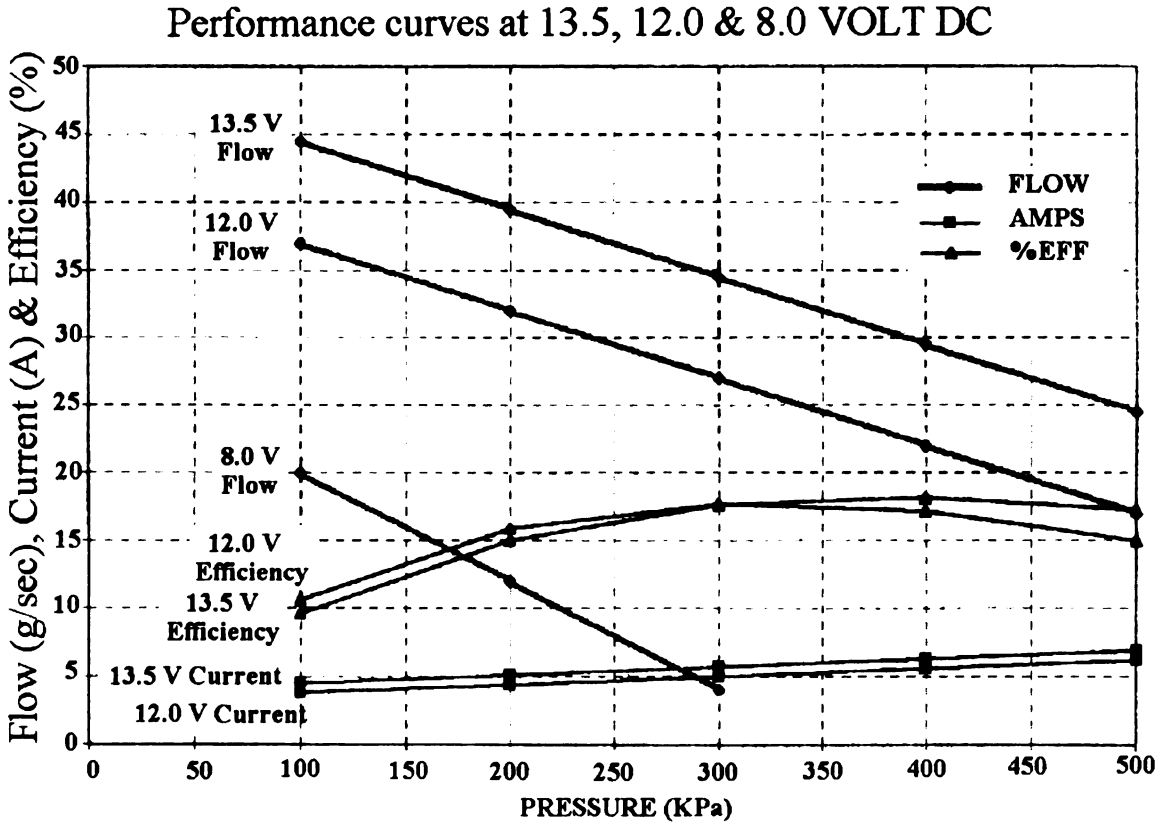

Figure 7.10 Flow, current drawn and efficiency vs. pressure for Delphi RFP

Table 7.1 Geometric data for two RFP designs (Length (mm) and Area (mm^2))

	Test 1	Test 2
R_{tip}	16.375	18.1
R_{hub}	13.125	14.9
R_2	15.608	17.33
R_1	13.984	15.73
A_c	3.27	3.20
B_b	2.1	2.1
β	45°	45°
Z_b	37	41
C	0.01	0.01
BF	0.08	0.08
θ_p	255°	255°

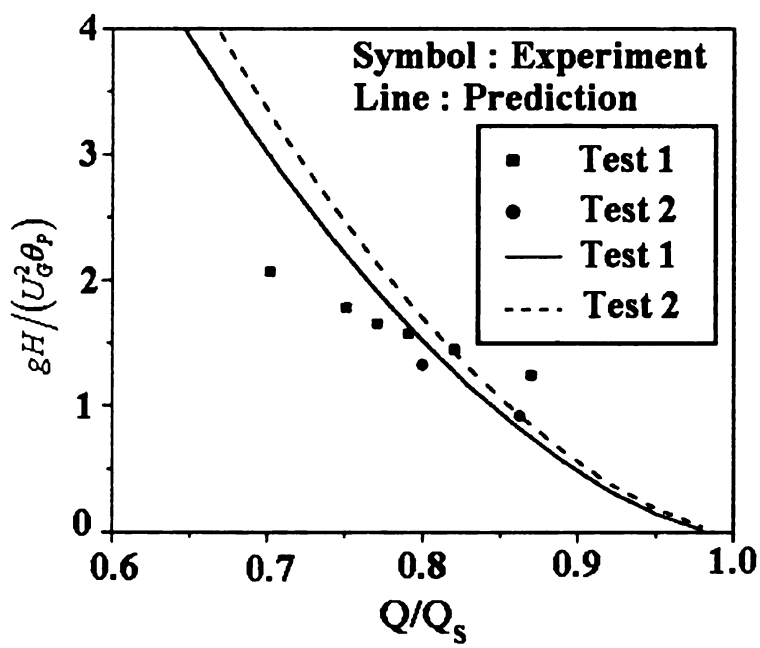

Figure 7.11 Theoretical and experimental non-dimensional head vs. flow

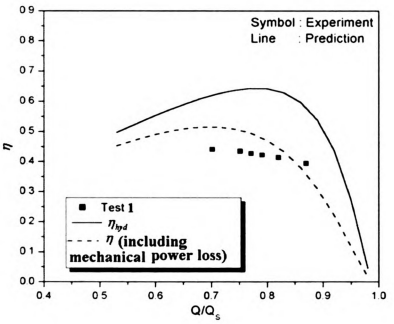

Figure 7.12 Theoretical and experimental efficiency vs. flow

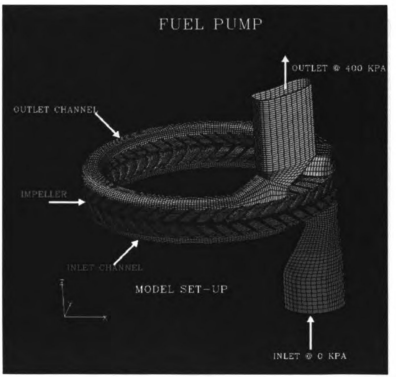

Figure 7.13 UNIGRAPHICS model of regenerative automotive fuel pump

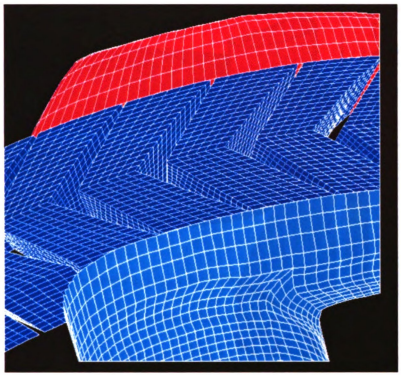

Figure 7.14 Non-radial blades in impeller of RFP

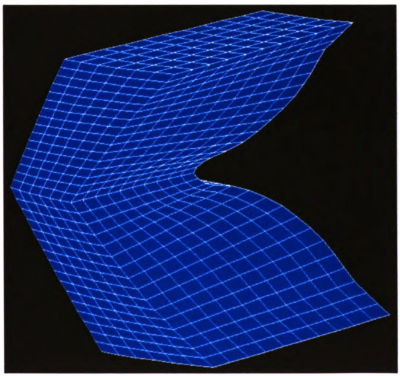

Figure 7.15 Web between two blades of RFP

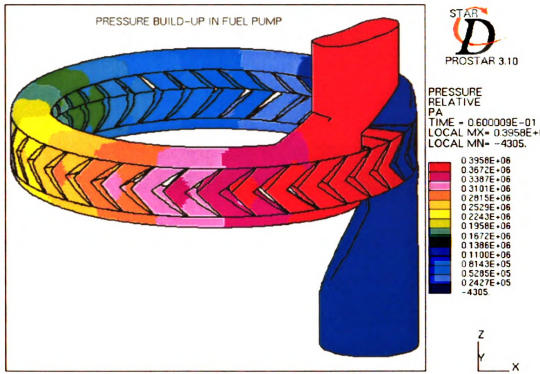

Figure 7.16 Head distribution across periphery of regenerative automotive fuel pump

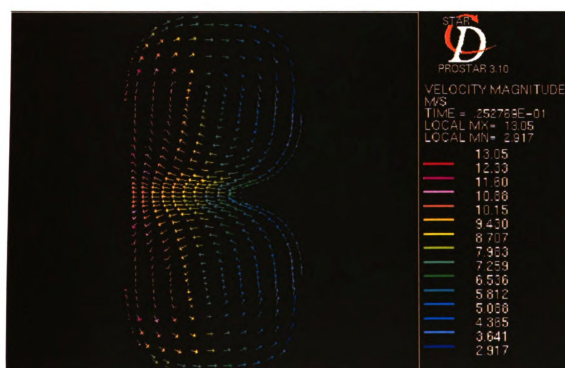

Figure 7.17 Circulatory velocity in the twin channels

CHAPTER 8

COMPRESSIBLE FLOW THEORY FOR AEROFOIL BLADE RFC

Theories for the flow of compressible fluid in regenerative turbomachines are rarely found in literature. Burton [11] made an effort in this direction and reported a simplified theory, which took account of area change and compressibility effects in RFC. However it was unable to explain the circulatory flow pattern in RFC because it was based on Iverson's shear stress theory [34]. Cates [15] investigated performance of RFC with radial blades experimentally using various gases covering a wide range of molecular weight and observed compressibility effects at Mach number greater than 0.8. Burton [12] investigated these compressibility effects and related them to mass flow rate through the stripper, which were ignored by other researchers in incompressible flow analysis. Sixsmith and Altmann [60] introduced a new type of RFC with aerofoil blades and decompression ducts to increase the efficiency. In chapter 5, Wilson's regenerative theory was extended to incorporate compressible flow to predict performance of RFC/RFP with radial and non radial blades and semicircular channel shape. In this chapter, the aim is to predict performance of RFC/RFP with aerofoil blade design by incorporating compressible flow in Wilson's momentum exchange theory. Governing equations for fully compressible flow are developed and loss models are introduced to make performance prediction independent of experimental support. Based on new

formulation, a performance prediction code is developed to predict performance of aerofoil blade RFC. Geometries of MK1 and MK2 regenerative compressors tested by Sixsmith and Altmann [60] are used as input to the code and theoretical prediction is compared with the test data. An extensive sensitivity analysis is performed to determine which geometric parameters affect the performance. After carrying out the sensitivity analysis, suggestions for design improvement are laid down.

8.1 Aerofoil Blade RFC

Most designs of regenerative turbomachines in literature retain a fairly basic geometrical configuration with simple vanes either machined or cast into the impeller. However, the addition of a core in the flow channel to direct the circulating flow together with the provision of aerofoil blades was first shown by Sixsmith and Altmann [60]. They replaced the radial vanes by blades with an aerofoil section. Blades were designed to transfer momentum to the fluid with a minimum of turbulence and friction. They were designed to turn the fluid through a definite angle, which preferably should be about 90°. The annular channel had the core to assist in guiding the fluid such that it circulates through the blading with a minimum of loss. The core also acted as a shroud to reduce losses due to formation of vortices at the tips of the blades. A typical RFC/RFP with aerofoil blades is shown in Figure 8.1.

These authors tested two regenerative compressors with aerofoil blading by blowing air through them. First design was MK1 regenerative compressor designed to run up to 10,000 rpm and deliver 250 liter/sec at a pressure of 2 atm. It had an impeller of 300 mm diameter with a single row of blades. The performance characteristics resembled those of a positive displacement compressor and efficiency was maintained over a wide range of

operating conditions. The torque was almost directly proportional to the back pressure and the compressor could be operated from maximum to zero flow without surging or stalling. The authors also tested MK2 regenerative compressor with the same basic layout but with two blade rows. Main features of MK2 compressor compared to MK1 were the increased peak efficiency to 52% , the lower pressure ratio at which this efficiency occurred, the gentler slope of pressure-volume curves, the lower efficiency at high pressure ratio and the large volume flow at low pressure, i.e., approximately 2.5 times greater than before. The authors retested the MK2 regenerative compressor by making the blading symmetric and found improved performance characteristics. The gain in efficiency was particularly marked at high pressure ratios. For example, at 4000 rpm the efficiency increased by 10 percent at a pressure ratio of 1.5.

8.2 Compressible flow theory

The analysis presented here is a mean line analysis, which represents the helical flow pattern inside a regenerative turbomachine by a streamline. Because of helical flow pattern, this analysis is based on coordinates composed of radial (R), circulatory(ϕ) and tangential direction (θ) as shown in Figure 8.2. Regenerative compressors found in literature have different meridional geometries. The meridional geometry chosen in this analysis is also shown in Figure 8.2, which shows the projected area and length of circulatory flow path in blade and channel region. The existence of a core, which is fixed to the channel helps to guide the fluid such that it circulates through the blade with a minimum loss.

8.2.1 Assumptions

Following assumptions are used in the analysis:

1. Steady and compressible flow
2. Fluid is considered as ideal gas $(p = \rho R_{gas} T)$
3. Helical flow can be described by a mean streamline with tangential velocity (V_θ) and circulatory velocity (V_ϕ) at any position.
4. Circulatory velocity, density, pressure and temperature are considered to vary only along the tangential direction i.e.

$$V_\phi, \rho, T, p = f(\cancel{R}, \cancel{\phi}, \theta)$$

5. Each decompression process is a quasi-equilibrium process.
6. All pressure losses can be categorized into losses related to circulatory and tangential velocity.
7. The effects of inlet and exit regions on performance are not considered in the model, rather they are considered separately.

8.2.2 Derivation of the governing equations

The equations of motion can be derived for an arbitrary small control volume comprising of blade and channel regions as shown in Figure 8.3.

Velocity triangle relation between V, W, and U at location R_2 can be obtained on the basis of the velocity triangle shown in Figure 8.4.

$$V_{\theta 2b} = U_2 + V_{\phi 2} Tan(\beta_{2b}) \tag{8.1}$$

$$W_{\theta 2} = V_{\phi 2} Tan(\beta_2) \tag{8.2}$$

$$V_{\theta 2} = \sigma V_{\theta 2b} \tag{8.3}$$

Similar relation can be obtained at locations R_1. These relations are useful in developing the governing equations.

Continuity

Ignoring flow leakages, it can be assumed that total mass flow rate in tangential direction remains constant. The total mass flow rate can be calculated by adding mass flow rates through channel and blade cross sectional areas. Moreover, total mass flow rate is also equal to the summation of mass flow rate entering the compressor through the inlet port and mass flow rate carried over by the blades through the stripper to the flow channel, referred as carryover mass flow rate denoted by $\dot{m}_s$. Thus we can write,

$$\dot{m}_c + \dot{m}_b = \rho V_{\theta m} A_c + \rho U_b A_b = \dot{m} + \dot{m}_s \tag{8.4}$$

Where, the mean tangential velocity $(V_{\theta m})$ in the channel region is calculated as the average of tangential velocities at R_1 and R_2.

Differentiating equation 8.4, the relation between channel mass flow rate and blade mass flow rate can be expressed as follows

$$d\dot{m}_c = -d\left(\rho U_b A_b\right) \tag{8.5}$$

In addition, it can be assumed that circulatory mass flow rate at inlet and exit of the blade region stays same. Thus,

$$d\dot{m}_\phi = d\dot{m}_{\phi 1} = d\dot{m}_{\phi 2} \tag{8.6}$$

$$d\dot{m}_\phi = \rho V_\phi H_b \tag{8.7}$$

Assuming constant density at an arbitrary tangential location and constant flow areas for incoming and outgoing circulatory flow, it can be concluded that the circulatory velocity also stays same at an arbitrary tangential location. Thus,

$$V_{\phi} = V_{\phi 1} = V_{\phi 2} \tag{8.8}$$

Momentum

Applying the angular momentum equation to channel region in tangential direction,

$$\left[\left(\dot{m}_c + \frac{d\dot{m}_c}{2}\right)\left(V_{\theta m} + \frac{dV_{\theta m}}{2}\right) - \left(\dot{m}_c - \frac{d\dot{m}_c}{2}\right)\left(V_{\theta m} - \frac{dV_{\theta m}}{2}\right)\right] r_G + d\dot{m}_{\phi}\left(r_1 V_{\theta 1} - r_2 V_{\theta 2}\right)$$
$$= r_G\left(p - \frac{dp}{2}\right)\left(A_c - \frac{dA_c}{2}\right) - r_G\left(p + \frac{dp}{2}\right)\left(A_c + \frac{dA_c}{2}\right) + r_G p dA_c - \int_{A_r} r\tau dA_r$$

Simplifying and using equation 8.5, we get

$$dp = \frac{d\dot{m}_{\phi}}{U_G A_c}(U_2 V_{\theta 2} - U_1 V_{\theta 1}) - \rho V_{\theta m} dV_{\theta m} + d\rho \frac{A_b}{A_c} U_b V_{\theta m} - dp_L$$

Dividing by dX and using equation 8.7, we get

$$\frac{dp}{dX} = \frac{\rho V_{\phi} H_b}{U_G A_c}(U_2 V_{\theta 2} - U_1 V_{\theta 1}) - \rho V_{\theta m}\frac{dV_{\theta m}}{dX} - \frac{dp_L}{dX} + \frac{d\rho}{dX}\frac{A_b}{A_c} U_b V_{\theta m} \tag{8.9}$$

Where, $\left(U_G = \omega R_G\right)$ refers to the velocity associated with solid rotation.

In R.H.S. of equation 8.9, first term refers to the pressure rise caused by momentum exchange of the blade; second term represents pressure gradient caused by the deceleration of mean tangential velocity; third term gives pressure loss related to tangential velocity caused by friction or other irreversibilities and the last term represents the deceleration of tangential velocity caused by the increment in density.

Applying momentum equation in the circulatory direction and simplifying, we get

$$\left(\dot{m}_\phi + \frac{d\dot{m}_\phi}{2}\right)\left(V_\phi + \frac{dV_\phi}{2}\right) - \left(\dot{m}_\phi - \frac{d\dot{m}_\phi}{2}\right)\left(V_\phi - \frac{dV_\phi}{2}\right) + \cancel{d\dot{m}_{\phi 1} V_\phi} - \cancel{d\dot{m}_{\phi 2} V_\phi}$$
$$= (p_2 - p_1)\, dA_\phi - \Delta p_{\phi c}\, dA_\phi$$

$$V_\phi\left(\dot{m}_\phi dV_\phi + V_\phi d\dot{m}_\phi\right) = \frac{p_2 - p_1}{\rho} dA_\phi \rho V_\phi - \frac{\Delta p_{\phi c}}{\rho} dA_\phi \rho V_\phi$$

where, $\Delta p_{\phi c}$ is the pressure loss related to circulatory velocity in the channel region.

After some manipulations, we get the governing equation for circulatory velocity which can be expressed as,

$$\frac{dV_\phi^2}{dX} = 2\frac{V_\phi H_b}{V_{\theta m} A_c}\left(\frac{p_2 - p_1}{\rho} - \frac{\Delta p_{\phi c}}{\rho}\right) + 2\left(\frac{V_\phi}{V_{\theta m}}\right)^2 \frac{1}{\rho}\frac{d\rho}{dX}\frac{A_b}{A_c} U_b V_{\theta m} \qquad (8.10)$$

Equation 8.10 represents a highly non-linear differential equation for circulatory velocity.

Angular momentum equation in the blade region can be given as,

$$d\dot{P}_{hyd} = \omega dT$$

$$d\dot{P}_{hyd} = d\dot{m}_c\left(U_2 V_{\theta 2} - U_1 V_{\theta 1}\right) + \left(\rho + \frac{d\rho}{2}\right) U_b A_b U_b^2 - \left(\rho - \frac{d\rho}{2}\right) U_b A_b U_b^2$$
$$+ \left(p + \frac{dp}{2}\right) U_b A_b - \left(p - \frac{dp}{2}\right) U_b A_b$$

Simplifying we get,

$$d\dot{P}_{hyd} = d\dot{m}_c\left(U_2 V_{\theta 2} - U_1 V_{\theta 1}\right) + d\rho U_b A_b U_b^2 + \cancel{dp U_b A_b}$$

Dividing by dX and ignoring the last term in above equation because of negligible pressure rise in the blade region, we get

$$\frac{d\dot{P}_{hyd}}{dX} = \rho V_\phi H_b\left(U_2 V_{\theta 2} - U_1 V_{\theta 1}\right) + \frac{d\rho}{dX} U_b^3 A_b \qquad (8.11)$$

If last term is ignored in R.H.S. of the above equation, first term refers to power consumed in momentum exchange of blade and the second term represents increment in power caused by increment in density.

Energy

The energy equation is applied to channel and blade region at two thermodynamic conditions where regenerative compressors operate. These conditions are

- Adiabatic condition
- Isothermal condition

Equations for the two thermodynamic conditions are developed separately.

- **Adiabatic condition**

Under the adiabatic condition, there is no channel heat transfer. Thus, we can say

$$d\dot{Q}_c = 0$$

The energy equation applied to channel control volume of Figure 8.3 yields

$$\left(\dot{m}_c + \frac{d\dot{m}_c}{2}\right)\left(h_0 + \frac{dh_0}{2}\right) + d\dot{m}_{\phi 1} h_{01} = \left(\dot{m}_c - \frac{d\dot{m}_c}{2}\right)\left(h_0 - \frac{dh_0}{2}\right) + d\dot{m}_{\phi 2} h_{02}$$

Simplifying above equation yields,

$$d\dot{m}_{\phi 2} h_{02} - d\dot{m}_{\phi 1} h_{01} = \dot{m}_c dh_0 + h_0 d\dot{m}_c \qquad (8.12)$$

Similarly for the blade region,

$$d\dot{Q}_b = 0$$

Total enthalpy in blade region can be expressed in terms of enthalpy in the channel region as,

$$h_0 = h + \frac{1}{2}V_\phi^2 + \frac{1}{2}V_{\theta m}^2$$

$$h_{0b} = h + \frac{1}{2}V_\phi^2 + \frac{1}{2}U_b^2$$

Thus,

$$h_{0b} = h_0 + \frac{1}{2}U_b^2 - \frac{1}{2}V_{\theta m}^2$$

The energy equation applied to blade control volume of Figure 8.3 yields

$$d\dot{P}_{hyd} = d\dot{m}_{\phi 2}h_{02} - d\dot{m}_{\phi 1}h_{01} + \left(h_0 + \frac{1}{2}U_b^2 - \frac{1}{2}V_{\theta m}^2 + \frac{dh_0}{2} - \frac{1}{2}d\left(\frac{1}{2}V_{\theta m}^2\right)\right)\left(\rho + \frac{d\rho}{2}\right)U_b A_b$$
$$-\left(h_0 + \frac{1}{2}U_b^2 - \frac{1}{2}V_{\theta m}^2 - \frac{dh_0}{2} + \frac{1}{2}d\left(\frac{1}{2}V_{\theta m}^2\right)\right)\left(\rho - \frac{d\rho}{2}\right)U_b A_b$$

Simplifying, we get

$$\begin{aligned} d\dot{m}_{\phi 2}h_{02} - d\dot{m}_{\phi 1}h_{01} &= d\dot{P}_{hyd} - \rho U_b A_b dh_0 + \rho U_b A_b V_{\theta m} dV_{\theta m} \\ -h_0 U_b A_b d\rho &- \frac{1}{2}\left(U_b^2 - V_{\theta m}^2\right)U_b A_b d\rho \end{aligned} \tag{8.13}$$

From equation 8.12 and 8.13, we get

$$\dot{m}_c dh_0 + h_0 d\dot{m}_c = d\dot{P}_{hyd} - \rho U_b A_b dh_0 + \rho U_b A_b V_{\theta m} dV_{\theta m} - h_0 U_b A_b d\rho - \frac{1}{2}\left(U_b^2 - V_{\theta m}^2\right)U_b A_b d\rho$$

$$\left(\dot{m}_c + \rho U_b A_b\right)dh_0 = d\dot{P}_{hyd} + \rho U_b A_b V_{\theta m} dV_{\theta m} - \frac{1}{2}\left(U_b^2 - V_{\theta m}^2\right)U_b A_b d\rho$$

$$C_p \frac{dT_0}{dX} = \frac{1}{(\dot{m}_c + \dot{m}_b)}\left[\frac{d\dot{P}_{hyd}}{dX} + \rho U_b A_b V_{\theta m}\frac{dV_{\theta m}}{dX} - \frac{1}{2}(U_b^2 - V_{\theta m}^2)U_b A_b \frac{d\rho}{dX}\right] \tag{8.14}$$

Operating under adiabatic condition, equation (8.14) can be used to calculate total temperature distribution.

- **Isothermal Condition**

Another thermodynamic condition in which RFC usually operates is the isothermal condition. The compressor work can be reduced by maintaining the temperature of the gas as low as possible during compression. The isothermal condition is given by

T=constant

The energy equation applied to channel control volume under isothermal conditions yields

$$-d\dot{Q}_c + \cancel{d\dot{P}_{hyd}} + d\dot{m}_{\phi 2}h_{02} - d\dot{m}_{\phi 1}h_{01} - \dot{m}_c dh_0 - h_0 d\dot{m}_c = 0$$

$$d\dot{Q}_c = d\dot{m}_{\phi 2}h_{02} - d\dot{m}_{\phi 1}h_{01} - \dot{m}_c dh_0 - h_0 d\dot{m}_c$$

$$d\dot{m}_{\phi 2}h_{02} - d\dot{m}_{\phi 1}h_{01} = d\dot{Q}_c + \dot{m}_c dh_0 + h_0 d\dot{m}_c \qquad (8.15)$$

Energy transfer process in the blade region happens rapidly, so it can always be assumed an adiabatic process. Thus, we can equate equation 8.15 with equation 8.13 to calculate the heat transfer from the compressor as

$$-d\dot{Q}_c = \dot{m}_c dh_0 + h_0 d\dot{m}_c - d\dot{P}_{hyd} + dh_0 \rho U_b A_b - V_{\theta m} dV_{\theta m} \rho U_b A_b$$
$$+ h_0 d\rho U_b A_b + \frac{1}{2}\left(U_b^2 - V_{\theta m}^2\right) d\rho U_b A_b$$

$$d\dot{Q}_c = \left(\dot{m}_c + \dot{m}_b\right) dh_0 - \left[d\dot{P}_{hyd} + \rho U_b A_b V_{\theta m} dV_{\theta m} - \frac{1}{2} d\rho U_b A_b \left(U_b^2 - V_{\theta m}^2\right) \right] \qquad (8.16)$$

In order to calculate pressure difference between incoming and outgoing flow in a control volume of blade region, Bernoulli equation along the streamline is applied and static pressure rise in the blade region is obtained as

$$\frac{p_2 - p_{1'}}{\rho} = (U_2 V_{\theta 2} - U_1 V_{\theta 1}) - V_{\theta m}(V_{\theta 2} - V_{\theta 1}) - \frac{\Delta p_{\phi b}}{\rho} \tag{8.17}$$

where, $\Delta p_{\phi b}$ is the pressure loss due to circulatory velocity through the blade region.

Some researchers assumed that mean streamline enters and exits the blades rows at same tangential location (θ). However, it is referenced in Krishnan et al [37] that there is a slight difference in tangential location (θ) between the location where the mean streamline enters the blade row and the location where mean streamline exits the blade row $\theta_{1'}$. This slight difference in tangential locations is denoted by $\Delta\theta_{2-1'}$ and is also shown in Figure 8.4. It is believed that the larger the stagger angle of blades, greater is $\Delta\theta_{2-1'}$. It is due to this $\Delta\theta_{2-1'}$ that the pressure difference in equation 8.17 needs to be supplemented by a correction term, so that resulting equation can be compared with equation 8.10.

Under the assumption that the relative tangential velocity within the blade is linearly distributed, the distances traveled in the circulatory and tangential directions can be expressed in the relative frame along the streamline as,

$$\frac{W_\theta dt}{V_\phi dt} = \frac{R d\theta}{\Gamma d\phi}$$

We can say approximately,

$$\frac{W_{\theta mb}}{V_\phi} = \frac{R_b \Delta\theta}{l_b} \tag{8.18}$$

Referring to Figure 8.4, we can say

$$p_1 - p_{1'} = \frac{\partial p}{\partial \theta} \Delta\theta_{2-1'}$$

At an arbitrary tangential position, pressure difference across the blade is given by

$$p_2 - p_1 = (p_2 - p_{1'}) - (p_1 - p_{1'})$$

$$p_2 - p_1 = p_2 - p_{1'} - \frac{\partial p}{\partial \theta}\Delta\theta_{2\text{-}1'} \tag{8.19}$$

Substituting equation 8.19 in equation 8.17, we get

$$\frac{p_2 - p_1}{\rho} = (U_2 V_{\theta 2} - U_1 V_{\theta 1}) - V_{\theta m}(V_{\theta 2} - V_{\theta 1}) - \frac{\Delta p_{\phi b}}{\rho} - \frac{\partial p}{\partial \theta}\Delta\theta_{2\text{-}1'} \tag{8.20}$$

Equating equation 8.10 and 8.20, a first order nonlinear ordinary differential equation for circulatory velocity (V_ϕ) is obtained as

$$\frac{dV_\phi^2}{dX} = \frac{2V_\phi H_b}{V_{\theta m} A_c}\left((U_2 V_{\theta 2} - U_1 V_{\theta 1}) - V_{\theta m}(V_{\theta 2} - V_{\theta 1}) - \frac{\Delta p_\phi}{\rho} - \frac{dp}{dX}\Delta X_{2\text{-}1'}\right) + \left(\frac{V_\phi}{V_{\theta m}}\right)^2 \frac{2}{\rho}\frac{d\rho}{dX}\frac{A_b}{A_c} U_b V_{\theta m} \tag{8.21}$$

where, $(\Delta p_\phi = \Delta p_{\phi b} + \Delta p_{\phi c})$ is sum of pressure loss related to the circulatory velocity.

8.3 Pressure Loss Models

There are two contributions to pressure losses:

- Tangential pressure loss
- Circulatory pressure loss

8.3.1 Tangential pressure loss

The skin friction pressure loss in tangential direction causes reduction of tangential pressure rise and is given by applying the classic pipe loss formula using the concept of hydraulic diameter (D_h).

$$\frac{dp_L}{dX} = \frac{\lambda_f}{D_h}\frac{1}{2}\rho V_{\theta m}^2 \tag{8.22}$$

Where, the friction factor is estimated by correlation used for straight channels given in [20].

$$\lambda_f = 0.316 Re^{-0.25}$$

8.3.2 Circulatory pressure loss

The pressure loss related to circulatory velocity is categorized into several pressure losses as follows. Loss models discussed in chapter 5 were used in the formulation.

Consequently, by summing circulatory pressure loss models, we get,

$$\frac{\Delta p_\phi}{\rho} = \left(k_{in}(Tan\beta_1 - Tan\beta_{1b})^2 + \frac{k_{blade}}{Cos\beta_{1b}^2} + k_{channel} \right)\frac{1}{2}V_\phi^2 \tag{8.23}$$

where k_{blade} and $k_{channel}$ represent all circulatory losses in blade and channel region.

8.4 Inlet port and decompression duct

High pressure gas enclosed by each blade pocket is delivered to the inlet region through the stripper. Stripper carryover fluid is mixed irreversibly with the incoming flow entering the compressor from inlet port as shown in Figure 8.5. This causes an increase in inlet temperature. Moreover, there is a blockage effect for the incoming flow because of the expansion of high pressure gas in the inlet region. This causes lower pressure rise and proves detrimental to the efficiency of RFC. Burton [12] suggested a possible way to increase the efficiency by extracting some of the compressed fluid entrapped in the blades and feeding it either to less harmful regions of the flow channel or to an ejection slot placed around the inlet port. Assuming adiabatic condition and neglecting the

leakage flow rate, Burton considered process in the inlet region as expansion and mixing. The total temperature at the inlet region was calculated by

$$T_{01} = \frac{\dot{m}}{\dot{m}+\dot{m}_s} T_{00} + \frac{\dot{m}_s}{\dot{m}+\dot{m}_s}\left(\frac{\gamma-1}{\gamma}\frac{p_1}{p_s}+\frac{1}{\gamma}\right)T_s + \frac{\dot{m}_s}{\dot{m}+\dot{m}_s}\frac{\gamma-1}{2}M_u^2 T_{00}\left(1-\frac{\rho_1}{\rho_s}(1-(\frac{V_{\theta m1}}{U_b})^2)\right) \tag{8.24}$$

Therefore, the total temperature can be reduced by either reducing temperature (T_s) or reducing carryover mass flow rate ($\dot{m}_s$) through the stripper. Sixsmith and Altmann [60] adopted Burton's idea and introduced decompression ducts to decrease total temperature and hence improve RFC efficiency. Compressed fluid entrapped in the stripper blades was fed through decompression ducts to various positions in the channel as shown in Figure 8.5.

The use of decompression ducts helps to reduce the power input to the compressor by transferring power entrapped in stripper blades to the channel. In this analysis, the decompression process is simulated by assuming flow from a high pressure rigid pocket opened to channel conditions in a quasi-equilibrium manner. Thus, it is expected from this assumption that power transferred by decompression process becomes maximum.

The governing equation for decompression is given by

$$m_{s_i} C_v T_{s_i} - m_{s_{i+1}} C_v T_{s_{i+1}} = (m_{s_i} - m_{s_{i+1}}) C_p T_{i+1} \tag{8.25}$$

$$\frac{m_{s_i} T_{s_i}}{p_{s_i}} = \frac{m_{s_{i+1}} T_{s_{i+1}}}{p_{s_{i+1}}} \tag{8.26}$$

8.5 Efficiency

Power transferred to impeller of RFC can be obtained by summation of hydraulic power and power caused by disk friction. Input power is reduced by the power transferred from decompression ducts to the channel. Power loss caused by the leakage flow through radial and axial clearances is ignored. Therefore, isothermal efficiency can be determined by

$$\eta_{iso} = \frac{\dot{m} R_{gas} T_{00} \ln\left(p_{03} / p_{00} \right)}{\dot{P}_{hyd} - \dot{P}_{decomp} + \dot{P}_{disk}} \tag{8.27}$$

Also, adiabatic efficiency is given by

$$\eta_{adi} = \frac{\dot{m} C_p T_{00} \left[\left(p_{03} / p_{00} \right)^{(\gamma-1)/\gamma} - 1 \right]}{\dot{P}_{hyd} - \dot{P}_{decomp} + \dot{P}_{disk}} \tag{8.28}$$

After circulatory velocity distribution along the channel is obtained, the pressure rise and hydraulic power can be calculated by integrating equation (8.9) and equation (8.11).

$$p = \int_X dp \tag{8.29}$$

$$\dot{P}_{hyd} = \int_X d\dot{P}_{hyd} \tag{8.30}$$

Power transferred through the successive quasi-equilibrium decompression processes is expressed using equation (8.25) as,

$$\dot{P}_{decomp} = \sum (\dot{m}_i C_v T_{s_i} - \dot{m}_{i+1} C_v T_{s_{i+1}}) = \dot{m}_{b2} C_v T_2 - \dot{m}_s C_v T_s \tag{8.31}$$

Some of the input power is lost by friction between rotating impeller disk and stationary casing wall. This disk friction power can be calculated using experimental correlations of Daily [20].

$$\dot{P}_{disk} = \frac{C_{disk}}{2} \rho U_{tip}^3 R_{tip}^2 \tag{8.32}$$

Where, C_{disk} is suggested in Daily [20] as function of clearance and Re_{tip}.

8.6 Regenerative Number (N)

Regenerative number refers to the number of circulations of fluid from inlet to discharge port of RFC. In order to calculate the regenerative number, the magnitude of tangential angle corresponding to one cycle must be calculated. Figure 8.6 shows the distances traveled in the circulatory and tangential directions along a streamline. Moreover, it shows that at the tip of the impeller blade, the ideal possible velocity is $V_{\theta 2b}$. However, it is reduced due to slip losses to a lower value denoted by $V_{\theta 2}$ which represents the actual fluid velocity at the impeller tip. Similarly at the entrance of the blade, the maximum gas velocity is $V_{\theta 1}$, however, due to the incidence losses, this velocity reduces to $V_{\theta 1b}$. The horizontal axis in this diagram describes the angular displacement with $\Delta\phi_c$ representing the angle traversed by the fluid in circulatory direction while passing through the channel region and $\Delta\phi_b$ represents the angle traversed by the fluid in circulatory direction while passing through blade. Thus $(\Delta\phi_c + \Delta\phi_b)$ represents circulatory angle traversed by the fluid in one cycle.

If absolute tangential velocity is assumed to be linearly distributed within blade and channel region, it can be expressed,

$$\frac{V_\theta dt}{V_\phi dt} = \frac{Rd\theta}{\Gamma d\phi}$$

$$\frac{V_{\theta m}}{V_\phi} = \frac{R_G \Delta\theta_c}{l_c} \tag{8.33}$$

Similarly,

$$\frac{U_b}{V_\phi} = \frac{R_b \Delta\theta_b}{l_b} \tag{8.34}$$

Therefore, the regenerative number can be given as,

$$N = \frac{2\pi - \theta_s}{\Delta\theta_b + \Delta\theta_c} \tag{8.35}$$

8.7 Performance prediction

Based on proposed mathematical formulation for compressible flow and loss models, a performance prediction code is developed and numerical results are compared to published experimental data. The non-linear ordinary differential equation for circulatory velocity is solved using predictor-corrector technique for each control volume. The code takes geometric and inlet flow conditions as input and predicts pressure rise, power input, efficiency and other thermodynamic properties.

Geometric data and inlet flow conditions for MK1 and MK2 regenerative compressors tested by Sixsmith and Altmann [60] is used as input to the code. Table 1 reproduces fundamental geometric data of MK1 and MK2 regenerative compressors as suggested in [60]. Moreover, Table 8.1 also contains values of some constants used in calculation.

Air is the working fluid with ambient inlet conditions. A linear distribution of all geometric parameters and loss coefficients is assumed across the periphery between inlet and exit. Blade and channel turning loss coefficient are calculated in a similar way as described in chapter 5. There is no slip loss model available in literature for aerofoil blade RFC. The shape and arrangement of blades in RFC is very similar to axial cascades. Therefore, the deviation correlation of axial cascades for accelerated flow suggested by Howell [31] is chosen to calculate slip factor for MK1 and MK2 compressors. The value of slip factor for MK1 was found to be 0.92, whereas symmetric MK2 design blade yielded slip factor of 0.9 as shown in Table 8.1.

Performance prediction results from the code are superimposed on experimental data for the two compressors as shown in Figures 8.7 – 8.10. These figures include the effect of water-cooling jacket and decompression ducts on performance. Water-cooling jacket was used in the experiment to extract heat from the compressor. The magnitude of extracted heat was not mentioned in Sixsmith and Altmann [60]. Therefore, performance at two thermodynamic conditions, adiabatic and isothermal is predicted in this work. In order to investigate the effect of decompression ducts, comparison with or without decompression ducts is performed. The symbols in each figure mean the combination of two effects, adiabatic vs. isothermal and with decompression duct vs. without decompression ducts. For example, symbol (ISO:3) means isothermal condition with three decompression ducts.

Figure 8.7 and 8.8 show pressure ratio of MK1 and MK2 compressors at different rpm. It can be seen that the pressure ratio at isothermal condition is much larger than at adiabatic condition. This trend is obvious because at same input power and mass flow rate, pressure rise should be maximum at isothermal conditions and minimum at isentropic

conditions. An interesting finding is that most of the experimental data lies between the two thermodynamic conditions, indicating that experimental process is polytropic. Moreover, both compressors show that at low speed (3000 rpm), the results in isothermal condition are in very good agreement with experimental data excluding the low flow rate region. At higher speed, there is a large difference between isothermal prediction and experimental result. Moreover, it is observed that at higher speed there is a smaller difference between adiabatic prediction and experimental data. There can be two possible reasons to explain these trends. Firstly, the compressibility effects can be regarded as a reason for this mismatch and secondly, it can be explained in terms of inadequate compressor cooling. Cates [15] suggested that compressibility effects start to appear when the value of Mach number is larger than 0.4. However, the operating machine Mach number for both MK1 and MK2 ranges from 0.14 to 0.23, which is much smaller than 0.4. Therefore, the mismatch cannot be explained based on compressibility effect. The other possible explanation could be that the compressor did not operate under isothermal condition at higher rpm because of the lack of capacity in water-cooling jacket. Figure 8.11 shows the theoretical magnitude of heat transfer required to be extracted in order to maintain the isothermal condition. The extracted heat increases with decrease in flow rate and increase in speed. Especially, because MK2 is composed of two parallel channels and it needs to extract almost twice amount of heat than MK1. This makes it more difficult to maintain constant temperature than in case of MK1. Therefore in Figure 8.8, it seems that MK2 running 5000 rpm is operating under the adiabatic condition. Figures 8.7 and 8.8 also show that the existence of decompression has little influence on pressure ratio.

Figures 8.9 and 8.10 give comparison of predicted and experimental efficiency under different thermodynamic conditions. Since each decompression process is assumed as a quasi-equilibrium process, decompression power calculated by equation 8.31 is maximum possible power to be extracted from decompression. Therefore, the lines ISO:3 in MK1 and ISO:4 in MK2 represent the line of maximum obtainable efficiency. Moreover, as expected, lines ADI:0 in MK1 and MK2 give minimum efficiency lines as shown in each figure. The maximum efficiency and corresponding flow rate become smaller when changed from isothermal condition to adiabatic condition. These figures show that all experimental data exist between two ultimate thermodynamic conditions. The maximum obtainable efficiency for MK1 and MK2 is similar and lies around 60%. However, a difference of about 7% in the maximum efficiency of line ISO:0 is observed, which represents the effect without decompression ducts. It can be explained by the fact that the power expelled through the stripper in MK1 is greater than that in MK2 compressor because of larger carryover mass flow rate in MK1. Figure 8.10 shows that the overall results for MK2 compressor are in very good agreement with experimental data. Prediction at isothermal condition for 3000 rpm and adiabatic condition at 5000 rpm are good just as in the case of pressure ratio comparison.

Figure 8.12 shows that the ratio of decompression power to hydraulic power, which can be theoretically obtained from quasi-equilibrium equations, is greater in MK1 than in MK2 compressor in spite of less decompression ducts. The reason is that carryover mass flow rate and decompression power are larger as known from equation 8.31 in case of MK1 compressor with larger ratio of blade area to channel area. Therefore, it can be seen from the comparison between line ISO:3 (or ISO:4) and Line ISO:0 in Figure 8.9 and

8.10 that theoretically MK1 can achieve 18% increase in efficiency and MK2 can achieve an increase up to 10% using decompression ducts. However, it must be noted that the complete decompression does not happen in actual compressor when tested experimentally. In particular, since the space surrounded by blades in MK1 is larger than in MK2, the possibility of quasi-equilibrium process is reduced in MK1 than MK2 while rotating at same speed. Due to this reason, in case of MK2 compressor, there is little difference between predicted ISO:4 line and experimental data in Figure 8.10, but a big difference between predicted ISO:3 line and experimental data as shown in Figure 8.9 in case of MK1 compressor. More explanation of this can be given by the fact that although MK1 has three decompression ducts, but physically it can only obtain the effect of one or two decompression ducts. Figure 8.13 shows the variation of regenerative number in MK1 and MK2 with respect to flow rate under the condition ISO:3 and ISO:4 using equation 8.34. The regenerative number at maximum efficiency in MK1 is about 7 and that in MK2 at maximum efficiency point is 5. This can help to explain experimental results showing that pressure ratio at maximum efficiency in MK1 is 1.2 times larger than that in MK2.

8.8 Sensitivity Analysis

There are many design variables which influence performance of RFC. These variables depend on each other, thus making the design process difficult. It is important to investigate all design variables initially and then short list important design variables, which have maximum effect on performance. The idea is to reduce number of controlled design variables to make the design process easy. Therefore, while performing sensitivity analysis, the effect of design variables on head coefficient, efficiency, regenerative

number etc is investigated. A $\pm 20\%$ variation in the base value of each design variables A_c, R_p, R_G, β_b, l_b, k_{tc}, and σ is investigated. While performing sensitivity analysis for one variable, other variables are kept constant. Geometry of MK2 compressor with no decompression duct operating in adiabatic condition with a slip factor of 0.9 is chosen as starting point for sensitivity analysis.

Figures 8.14 represents sensitivity analysis of head coefficient (ψ_{adi}) with respect to design variables. Steep variations in head coefficient with respect to all design variables can be observed with the exception of almost no variation in gradient in case of chord (l_b). It shows a significant rise in head coefficient with increasing blade angle. However, this rise in head coefficient becomes gradual at very high values of blade angle. It can be observed that decreasing A_c and increasing R_p causes an increase in shut-off head (φ_0=0). Conversely, increasing A_c and decreasing R_p decreases shut-off head (φ_0=0) and makes the slope of $(\psi - \varphi)$ less steep. This means that if the compressor is operating at higher flow coefficient, it is better to decrease tip radius and increase channel area. However, close to lower flow coefficients, it is beneficial to decrease A_c and increase R_p. The reason is that at high flow rate, A_c must be increased to reduce the friction loss and because circulatory velocity increase at the same time, it is not needed to increase R_p. Defining a ratio R_p^2/A_c, it can be said that the designer should strive to minimize this ratio at higher flow coefficients and maximize it at lower flow coefficients. Various authors verified this trend experimentally. Cates [15] did an experimental sensitivity analysis and he concluded that at low specific mass flow rate, a decrease in channel area is beneficial for RFC performance and vice versa. The theoretical and experimental

analysis on Capstone single and multistage RFC also suggest that at low specific mass flow rate values, it is beneficial to decrease channel area and increase tip radius and vice versa.

Figure 8.15 shows that maximum efficiency increases with decreasing channel area and increasing tip radius because the circulatory velocity and hydraulic power decrease. It is interesting that the flow range, where compressor can operate effectively, is reduced in spite of the increase in maximum efficiency. However, the decrease in centric radius increases efficiency without changing the overall flow range and the flow rate at which maximum efficiency occurs. In addition, it can be seen that the variation in chord length causes a little effect on efficiency.

8.9 Conclusions

A compressible flow theory for analysis of helical flow in regenerative compressors is put forward for the first time. The continuity, momentum and energy equations are developed for differential control volume containing blade and channel region. The idea of decompression ducts is utilized and governing equations for quasi-equilibrium decompression process are developed. Loss models are introduced in the formulation to predict head rise and efficiency. A performance prediction code is developed based on mathematical formulation and loss models. Geometries of MK1 and MK 2 regenerative compressors are used as input to the code. The code predicts performance characteristics of these compressors. Excellent agreement is seen in comparison with experimental data on these compressors. The idea of decompression ducts proves beneficial to the efficiency. It is found theoretically that 18% increase in efficiency can be achieved using

decompression ducts in case of MK1 design and 10% efficiency can be increased in case of MK2. This conclusion still needs to be validated by introducing decompression ducts in an actual compressor design and test it.

Design sensitivity analysis is performed on important variables effecting RFC performance. It is concluded that at low flow coefficient, an increase in tip radius and decrease in channel area is beneficial to performance and vice versa. A significant rise in head coefficient is achieved with increasing blade angle, however this rise in head coefficient becomes gradual at very high values of blade angle. Observed trends are compared with other published data in literature and found consistent.

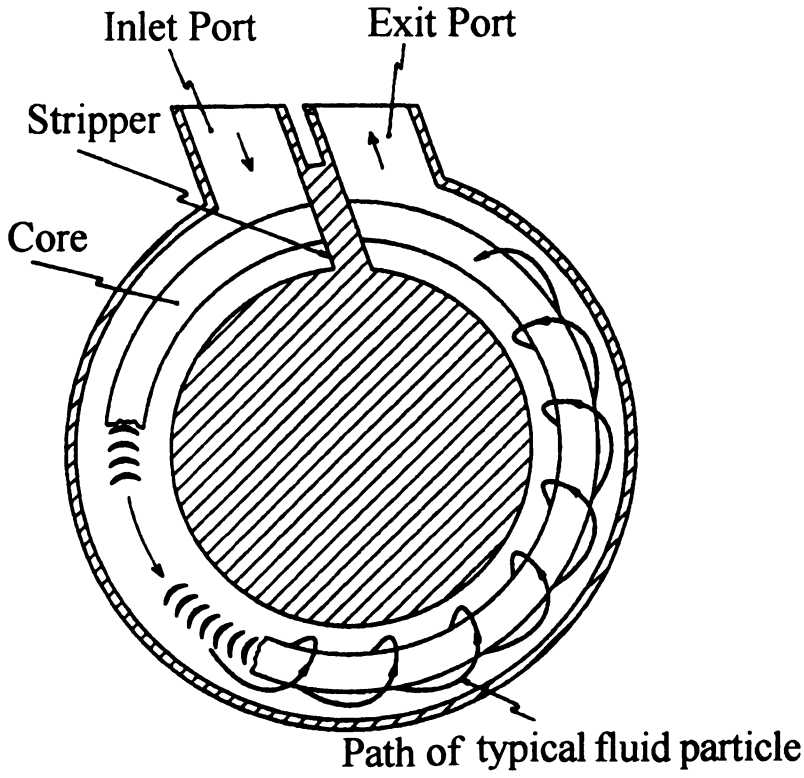

Figure 8.1 Regenerative compressor with aerofoil blades (after Andrew [2])

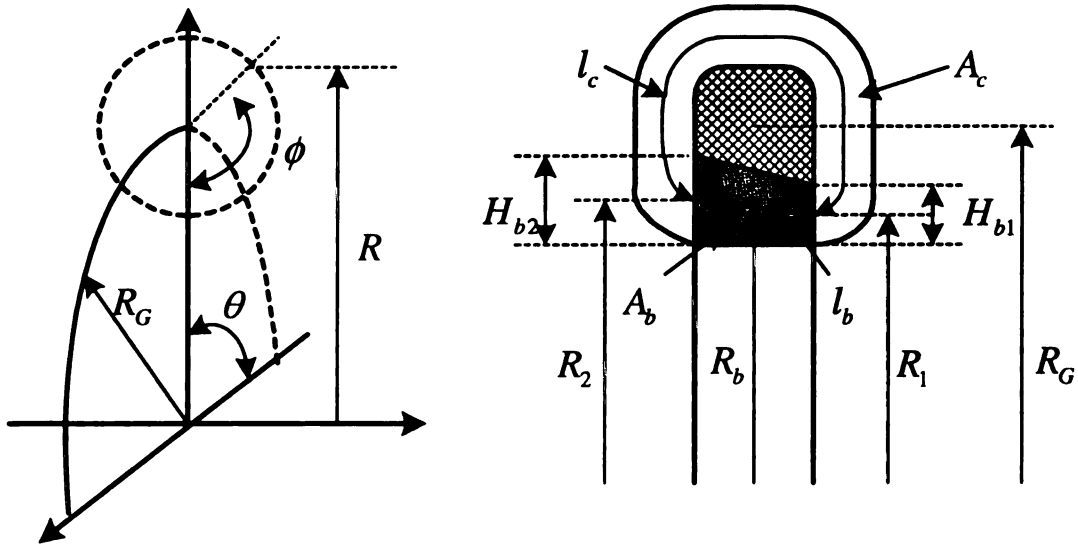

Figure 8.2 Coordinate and meridional geometry

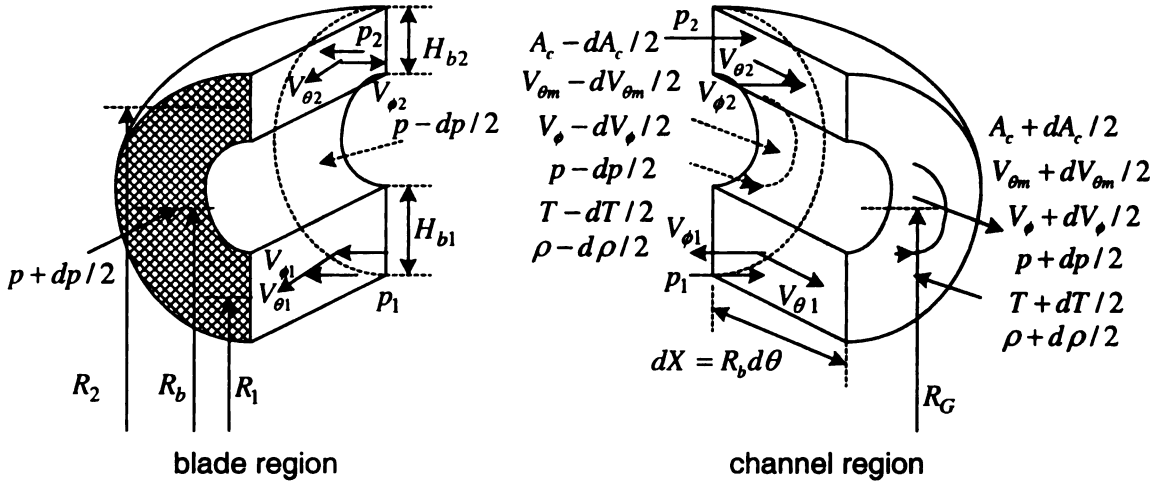

Figure 8.3 Arbitrary small control volume

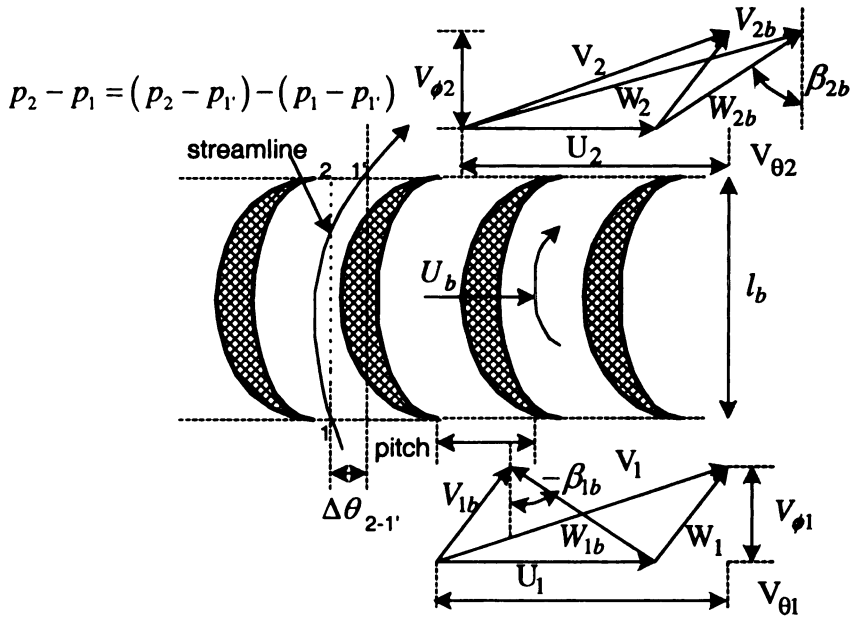

Figure 8.4 Velocity triangles at R_1 and R_2

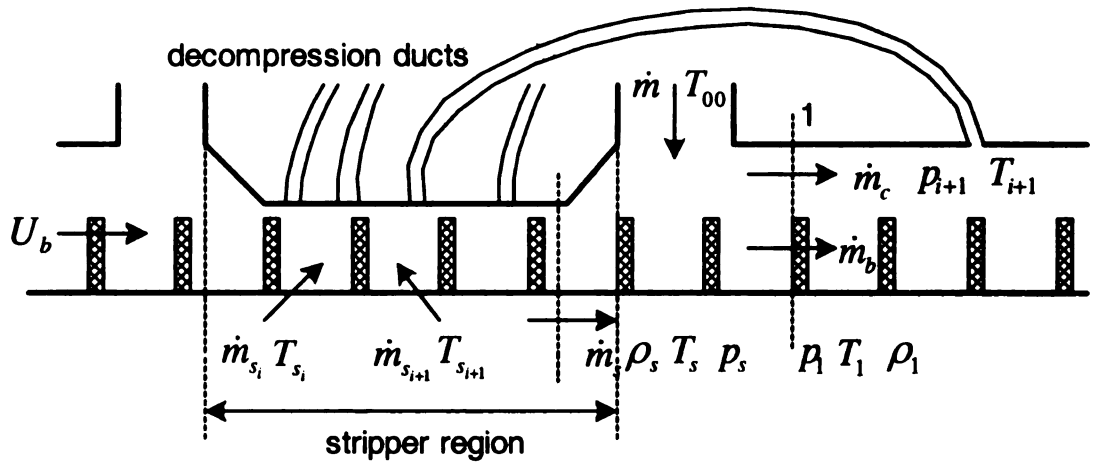

Figure 8.5 Schematic diagram for inlet region and decompression duct

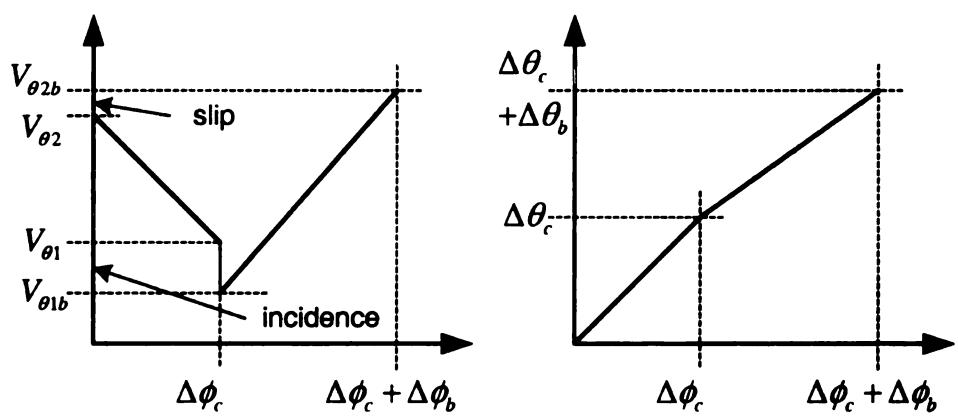

Figure 8.6 Tangential velocity and angle distribution per cycle

Table 8.1 Geometric data and some parameters used in calculation

blade region	R_1	R_2	H_{b1}	H_{b2}	A_b	l_b	Z_b	β_{1b}	β_{2b}	k_{tb}	duct	σ
MK1	141	140	18	15	330	20	120	-50°	40°	0.35	3	0.92
MK2	141	141	18	18	270	15	150	-48°	48°	0.36	4	0.9

Contd

channel region	Inlet					Exit					$\frac{A_{c\,Inlet}}{A_{c\,Exit}}$
	A_c	$\frac{A_c}{A_b}$	l_c	R_G	k_{tc}	A_c	$\frac{A_c}{A_b}$	l_c	R_G	k_{tc}	
MK1	2553	7.7	155	172	1.0	1501	4.6	95	154	1.0	1.7
MK2	2774	10.3	159	175	1.0	2135	7.9	122	166	1.0	1.3

Length (mm) and Area(mm^2)

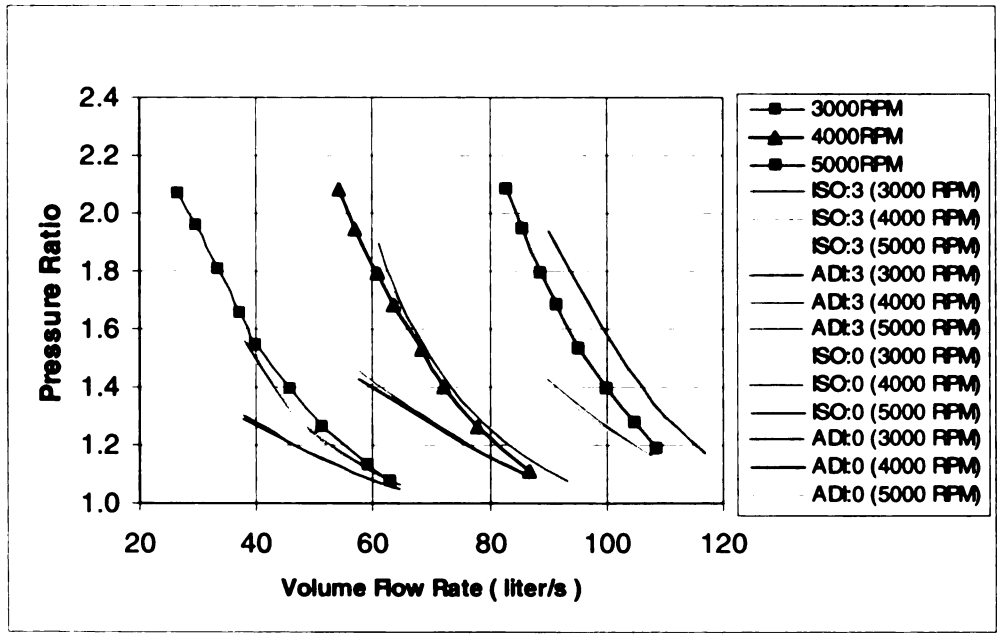

Figure 8.7 Comparison of pressure ratio of MK1 compressor

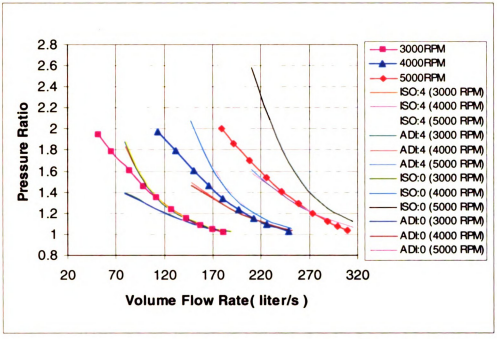

Figure 8.8 Comparison of pressure ratio of MK2 compressor

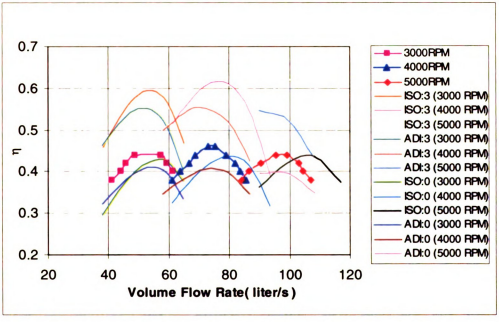

Figure 8.9 Comparison of efficiency of MK1 compressor

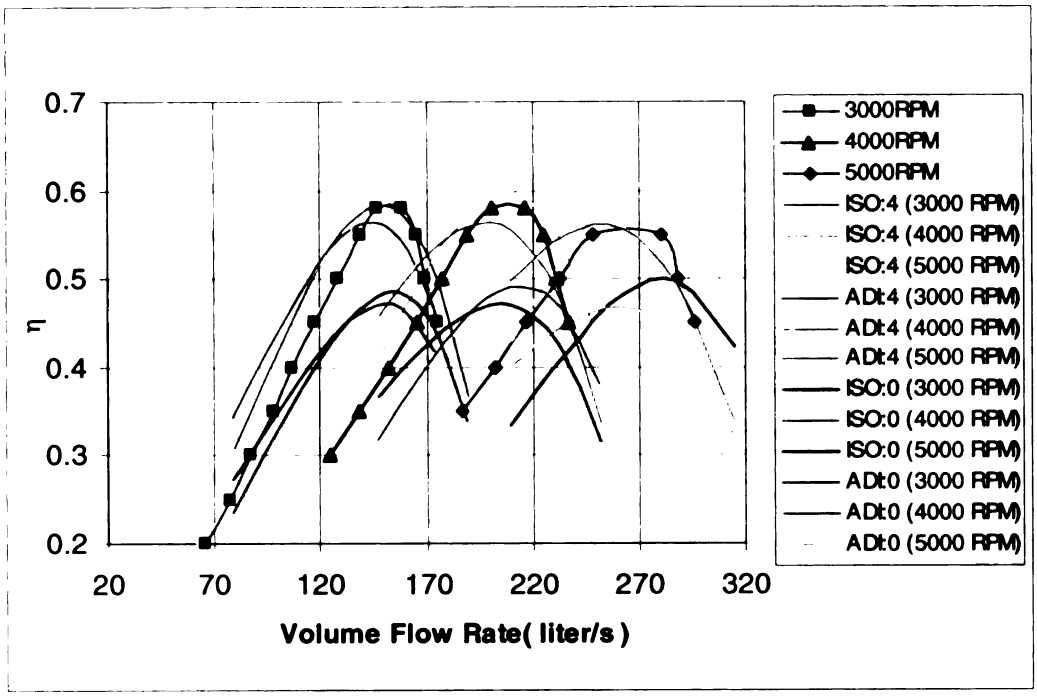

Figure 8.10 Comparison of efficiency of MK2 compressor

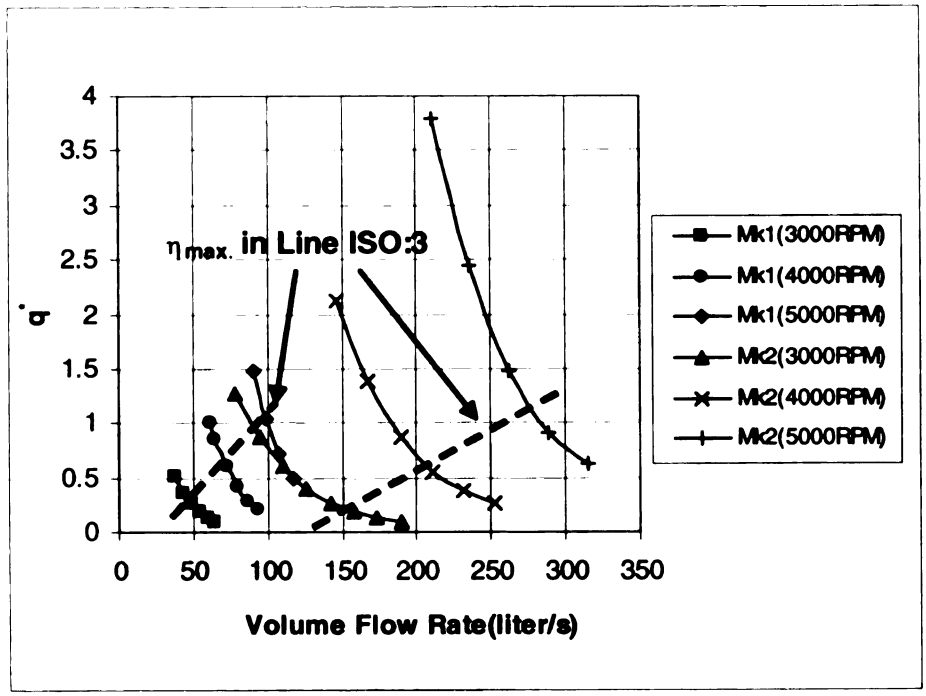

Figure 8.11 Theoretical heat transfer ratio in MK1 and MK2

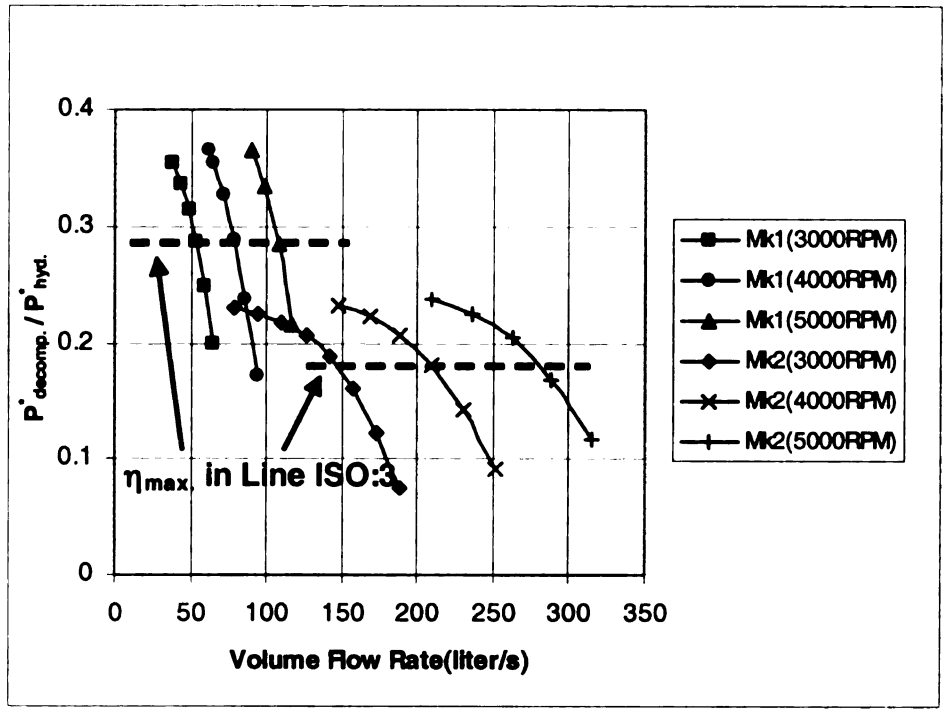

Figure 8.12 The ratio of Decompression power to Hydraulic power

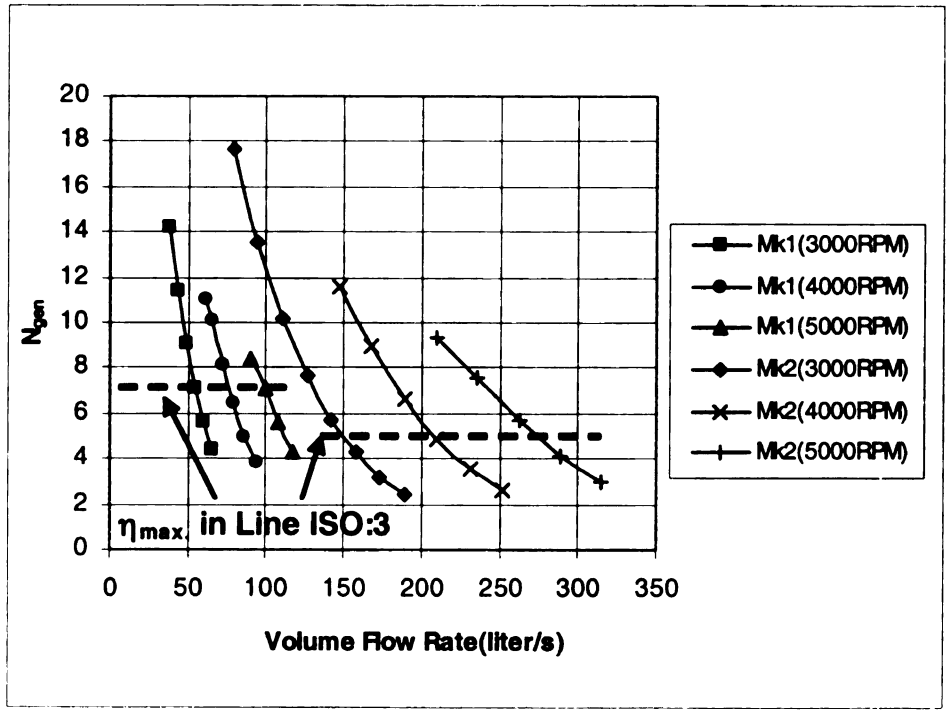

Figure 8.13 The variation of regenerative number vs. Flow rate

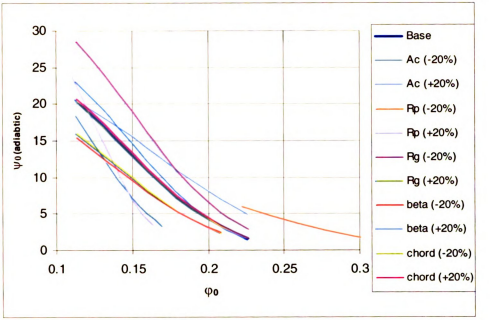

Figure 8.14 Head coefficient vs. flow coefficient

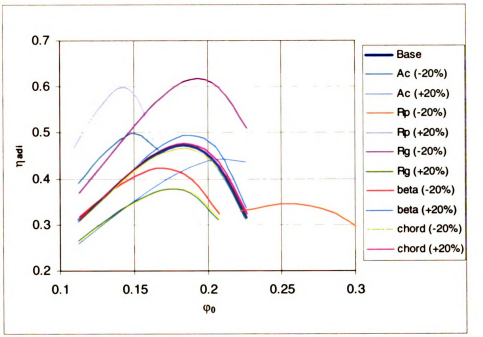

Figure 8.15 Efficiency vs. flow coefficient

CHAPTER 9

CFD ANALYSIS ON AEROFOIL BLADE RFC

Theoretical performance prediction of two aerofoil blade RFC with the inclusion of decompression ducts was discussed in chapter 8. Design sensitivity analysis on these compressor designs suggested a potential improvement in efficiency by making various design changes. The theoretical investigation motivated to perform a CFD analysis on aerofoil blade RFC to validate the effects of design changes on performance. Computational Fluid Mechanics (CFD) has been widely used for the flow analysis in various turbomachines during the last few years. However, there is not much evidence available in literature discussing the utilization of a commercial CFD code to solve flow details in a RFC/RFP. CFD seems to be an attractive tool to analyze and calculate the complex three dimensional flow in regenerative turbomachines to validate the likely effects of design modifications prior to constructing the prototype compressor. Moreover, CFD helps to optimize the geometry for the best performance. The inlet and discharge ports can be designed for minimum losses.

For this purpose, a compressor model is generated in UNIGRAPHICS based on blade geometry of MK2 RFC provided in Table (8.1). The dimensions of aerofoil blades used in the model are provided in Figures 9.1 and 9.2. Symmetric aerofoil blades with 48° angle are used in the model. Blade profiles are drawn using two arcs for simplicity. Channel and blade geometry is shown in Figure 9.3. It can be seen that there is a channel

on each side of the impeller. The top portion represents geometry at a section near the inlet and the bottom portion describes geometry at a section near the outlet. The channel area decreases linearly from inlet to outlet with an area ratio of 1.3. The cores promote circulatory flow in the channel as shown by the arrows in Figure 9.3. A full model of the compressor can be seen in Figure 9.4. Flow goes in the compressor through two inlet manifolds. The twin blade impeller has channel on each side shown by red and green colors. Blades are shrouded by a core on each side around which a helical toroidal flow path is established. Mesh is generated on the Unigraphics model using GAMBIT to perform CFD analysis as shown in Figure 9.5. Mostly hexahedral (Brick) elements are used for meshing, however near the outlet port due to complicated geometry, triangular elements are used. Element count for the full RFC model is 568900 cells. The green and red portions represent the flow in the channel, whereas blue portion represents the flow in the blades.

The inlet manifold of RFC is shown in Figure 9.6. Flow is injected in the impeller blades above the core and then it passes through the blades and goes through the channel for first circulation. It must be noted that that there are two inlet manifolds, one for each channel and blade side. Some RFC are designed with single inlet manifold with a mechanism to divert half of the fluid to each blade and channel geometry. However, this causes lot of turbulence and mixing losses, which led the researcher to design separate inlet manifolds for both sides. In order to explain the path of fluid through the blades and circulation in the channel around the core, Figure 9.7 is presented. The flow goes through the two blades shown on each side in this figure and then goes in the two corresponding channels. There are many circulations of the flow from the inlet port to the discharge ports. Figure

9.8 is a section of the compressor containing few blades, core and channel showing meshing in the cut section.

9.1 CFD Analysis

In order to perform CFD analysis, it is general practice to select a design point where the compressor is likely to operate. Following design point is chosen for analysis.

Working fluid: Air

$Q_{total} = 0.225 \text{ m}^3/\text{s}$
$RPM = 4000$
$\rho_{in} = 1.205 \text{ kg/m}^3$

The total volume flow rate of $0.225 \text{ m}^3/\text{s}$ is divided equally to the two sides. Thus, $0.1125 \text{ m}^3/\text{s}$ goes into the compressor from each inlet manifold. Inlet velocity is obtained by dividing the flow rate by inlet manifold area. The inlet port area is 0.00187 m^2, which yields an inlet velocity of 60.133 m/s from each inlet manifold. This is selected as the inlet boundary condition. Moreover, at the discharge, pressure boundary condition is specified. The pressure ratio at design point is obtained from experimental data to be 1.2. Assuming ambient inlet pressure of 100000 pa, a pressure of $100000 \times 1.2 = 120000$ pa is applied at the discharge port.

CFD simulation is run in commercial CFD software STAR CD. A transient analysis is performed with a time step $\Delta t = 2.083 \times 10^{-5}$ sec for half degree impeller revolution. The simulation is run for two complete revolutions of the impeller. This implies that for 720° impeller rotation, the simulation uses 1440 time steps.

After running the simulation, it was expected that a pressure close to 100000 pa at the inlet should be obtained to verify that pressure ratio of approximately 1.2 is obtainable through this design. However, unexpected trends are observed and desired pressure ratio cannot be achieved. The observed trends are discussed below based on absolute velocity vector diagrams. Preliminary results of the simulation are shown in Figure 9.9 which shows absolute velocity vectors representing the flow direction. It can be seen that all the flow is going in the peripheral direction with almost no circulatory flow. Ideally, some flow should circulate in the channels as it was in case of regenerative fuel pump shown in Figure 7.17. These circulations are actually responsible for pressure rise because the impeller hits the flow and adds energy to it which is recovered as pressure rise. Figure 9.10 represents a cross section of impeller, core and channel and it can be seen that all the flow is coming out without any circulation. Due to this predominantly straight through flow direction, the compressor model is unable to generate required pressure ratio. Thus, the fluid sees the impeller blades as a rough surface and instead of building any pressure, the flow goes through the flow channel without passing through the blades. This implies that the model is not acting as a compressor. After observing these unexpected trends, flow mechanism at the inlet port is investigated to find out the reason of no circulation through the blades.

9.2 Lack of circulatory flow

It is thought by many researchers that the circulatory flow pattern in regenerative turbomachines is set up by the inlet manifold. Fluid entering the inlet from the piping has no circulatory velocity component associated with it. Thus, the inlet manifold has to be designed such that for the very first circulation, it forces the fluid to circulate through the

blades and then for the second circulation, fluid uses its circulatory velocity component and keeps on circulating through the periphery.

The inlet design shown in Figure 9.6 is not good enough to provide the desired circulation. Figure 9.11 indicates that after passing through the inlet manifold, the flow enters the blade from both sides thus eliminating the possibility of any circulation through the blades. Therefore, the flow is pushed through the compressor in the peripheral direction, making it impossible to build pressure. Typically, it is desired that the inlet port directs the flow straight at the inlet edges of the blading so as to get the flow circulating. The inlet port is arranged so that most of the inlet flow has to go through the blading. Without this feature, it is very difficult for the compressor to build up any pressure. This motivated the researcher to modify the inlet port to improve the flow guidance.

9.4 Modified Inlet Design

In order to direct the flow at the inlet edges of the blading, the inlet manifold is modified as shown in Figure 9.12. A 2D view of this inlet design is shown in Figure 9.13. The new design has a constriction (nozzle effect) at entrance of RFC which accelerates the flow before it enters the blade row. This design prevents the flow being fed from both sides of blades, which hindered the circulatory flow pattern in the previous inlet design. A CFD analysis is performed on aerofoil blade RFC using the modified inlet design. Results from this CFD analysis show that flow circulates through the blades, however, the new compressor design is also unable to build desired pressure ratio. There is a marked improvement in pressure ratio in the modified design compared to the previous design, however, still it is less than the pressure ratio obtained from experimental data. The

circulatory flow pattern can be observed in Figure 9.14, which shows that the flow is injected from only one side of the blades, thus forcing it to circulate through the blades. The constriction (nozzle) helps the flow to establish the circulatory motion which is key for pressure build up in regenerative turbomachines. The flow pattern in the blade and channel region at two peripheral locations is shown in Figures 9.15 and 9.16. Figure 9.15 represents a section taken close to the inlet describing the circulatory flow pattern close to inlet. Figure 9.16 represents a section taken at $\theta = 180^{\circ}$ away from the section shown in Figure 9.15. It is interesting to note that there is much higher circulatory velocity close to inlet as compared to somewhat lesser circulatory velocity at a larger peripheral angle. The flow pattern depicted in these figures resembles to that reported in Sixsmith and Altmann [60].

The modified inlet has a constriction (nozzle) which accelerates the flow at entrance producing a huge velocity. The high velocity imparted by the nozzle shape creates extreme turbulence and does not permit enough circulations through the blades. A higher velocity implies that the fluid skips many blades before it becomes fully developed. It is only after settling down that the fluid really starts to circulate through the blades and creates some pressure rise. Thus the flow becomes developed after $\theta = 90^{\circ}$ and initial turbulence is somehow reduced resulting in good pressure rise from $\theta = 90^{\circ}$ to 360°. Currently, work is in progress to further modify the inlet to remove the nozzle effect and inject the fluid with proper guidance and minimum turbulence. The inlet should be designed to direct all the flow through the blades. It should be wide enough to carry the flow and at the same time to accelerate the flow velocity through the blade passages up to the velocity of circulation. CFD analysis is being performed on a proposed "OWL"

shaped inlet as shown in Figure 9.17. Details of this CFD analysis will be reported in a publication to appear shortly.

9.5 Conclusions

An attempt is made to solve flow details in a regenerative compressor using STAR CD. Two inlet designs are proposed, however still the required pressure ratio has not been achieved. The circulatory flow pattern is observed in blade and channel region which is a characteristic of regenerative turbomachinery. Currently research is under way to optimize the inlet manifold so that desired pressure ratio and isothermal efficiency could be achieved. It will be very interesting to implement suggested design changes of chapter 8 in this compressor model to get further improvement in efficiency. Further details on CFD analysis will be reported in a publication to appear shortly.

.

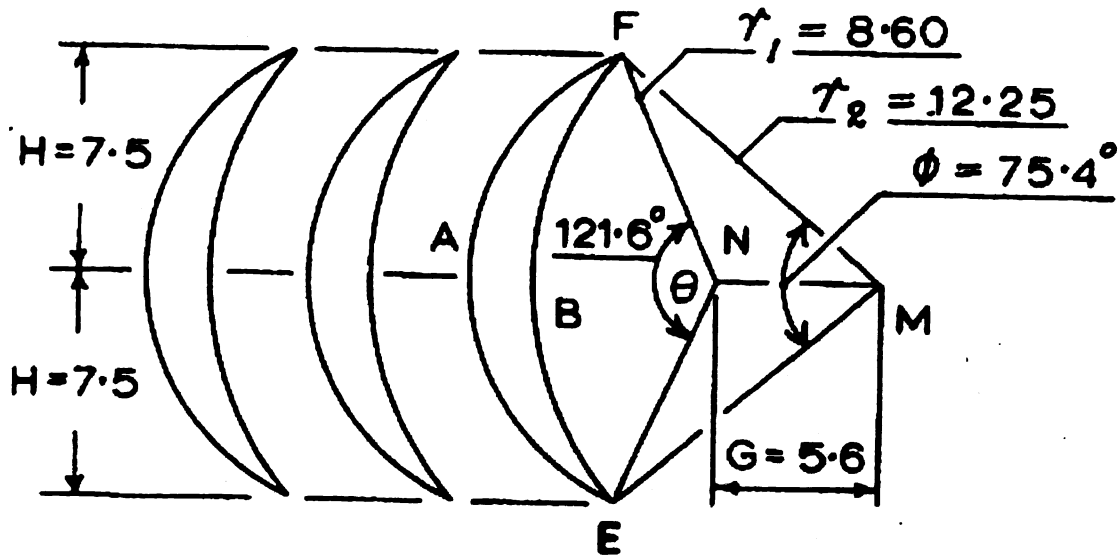

Figure 9.1 Blade dimensions

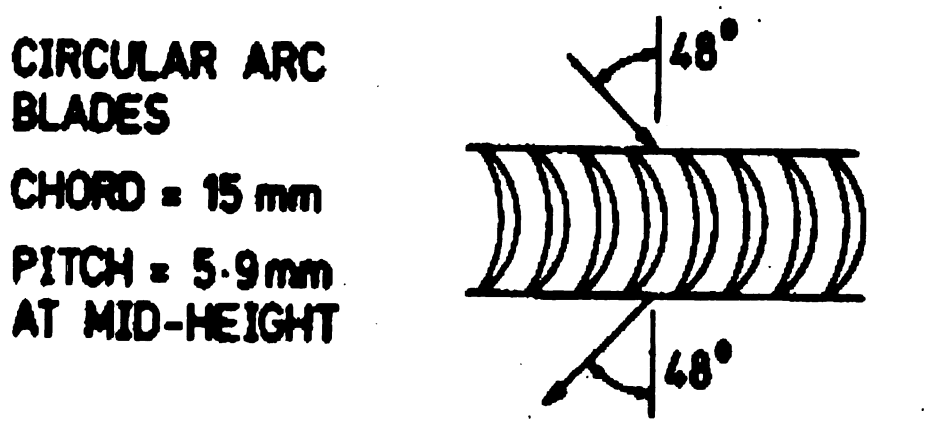

Figure 9.2 Blade design

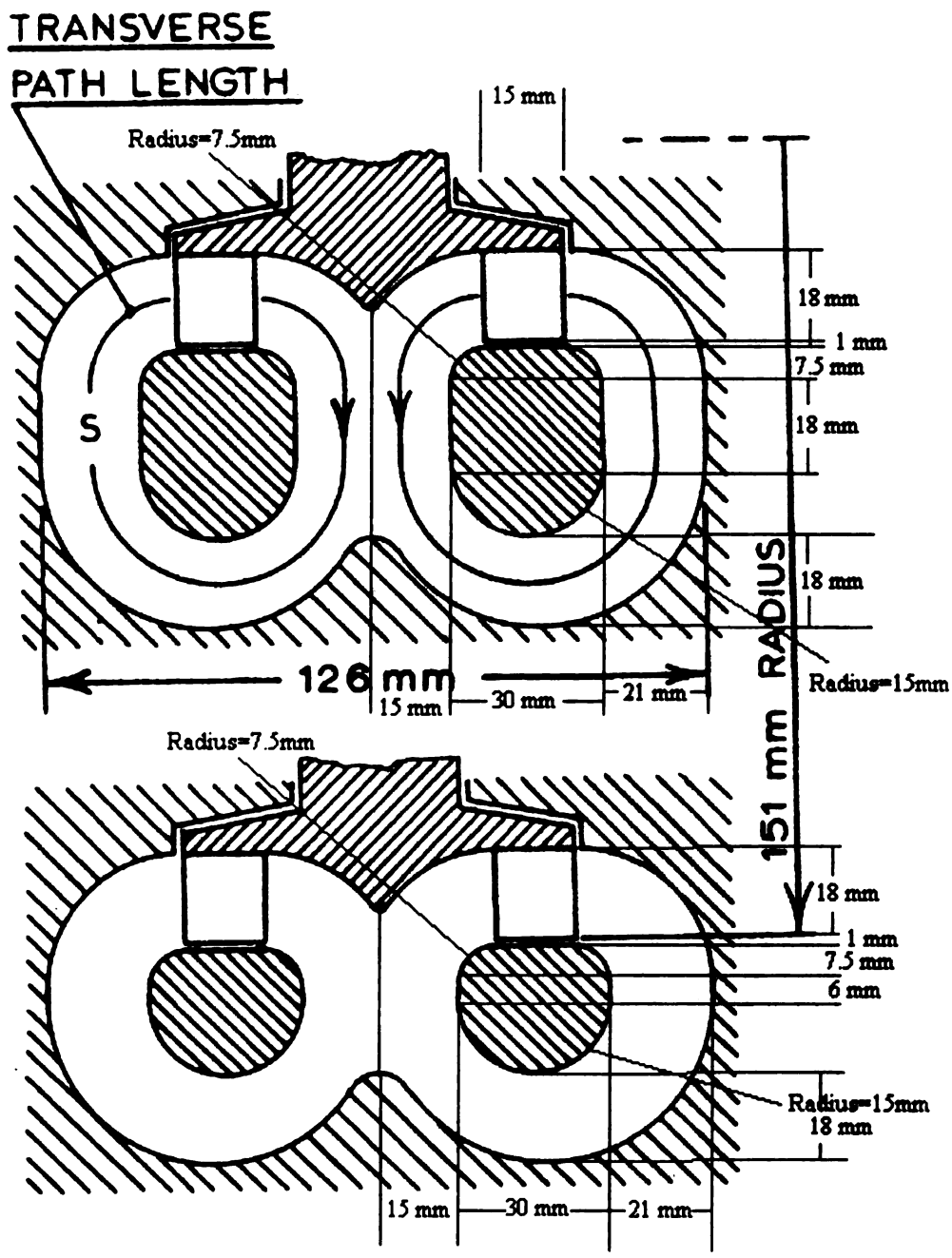

Figure 9.3 Blade and channel geometry

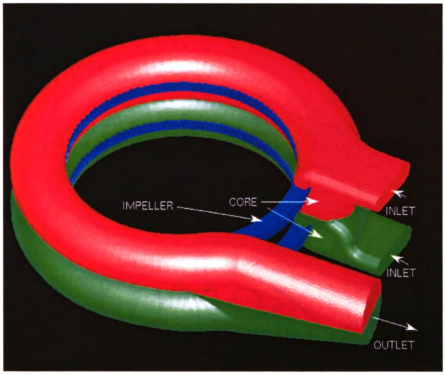

Figure 9.4 Full Assembly of regenerative compressor with aerofoil blades

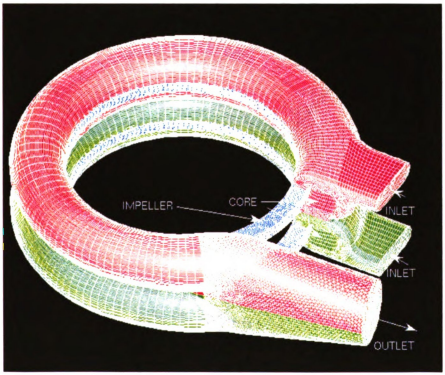

Figure 9.5 Meshing for CFD analysis

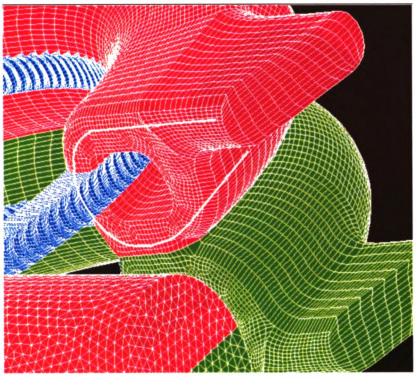

Figure 9.6 Inlet manifold

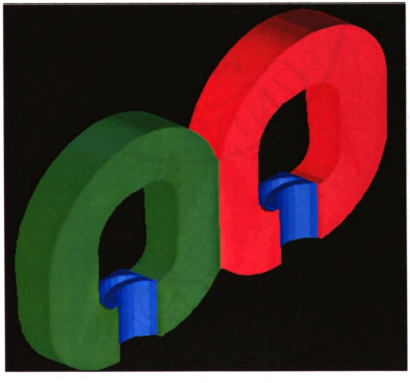

Figure 9.7 cross sectional view of twin blade and channel

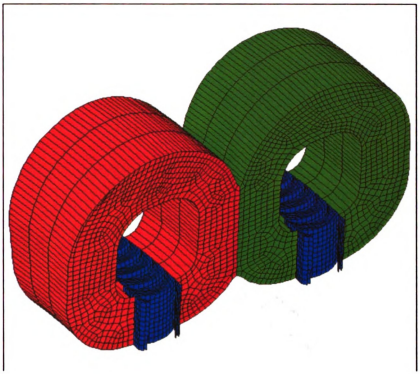

Figure 9.8 Meshing around twin blade and channel

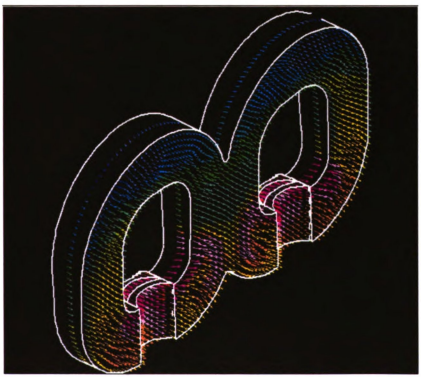

Figure 9.9 Absolute velocity vectors representing the flow direction

Figure 9.10 Absolute velocity vectors representing flow around the core in the channel

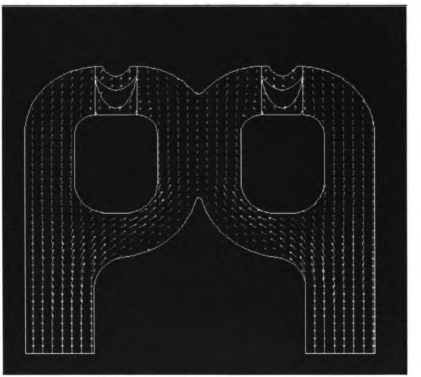

Figure 9.11 Absolute velocity vectors representing flow in the inlet manifold

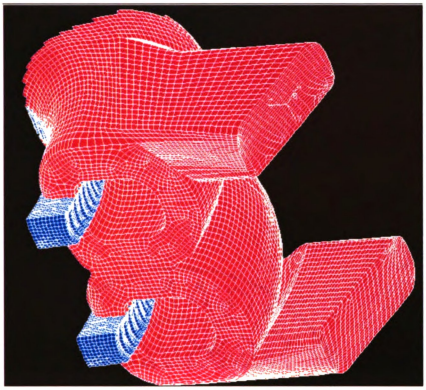

Figure 9.12 Modified Inlet Design (3D view)

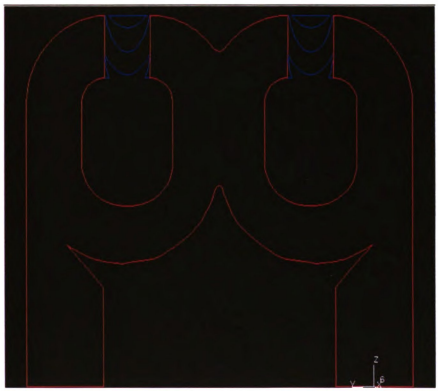

Figure 9.13 Modified Inlet Design (3D view)

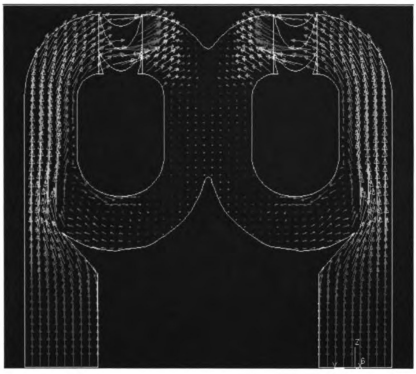

Figure 9.14 Velocity vectors describing circulatory flow pattern through the inlet manifold

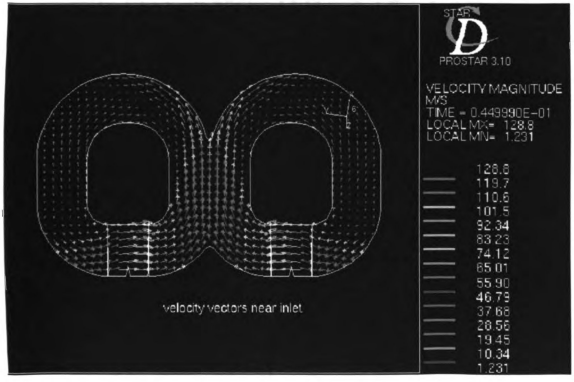

Figure 9.15 Velocity vectors showing circulatory flow pattern near inlet port

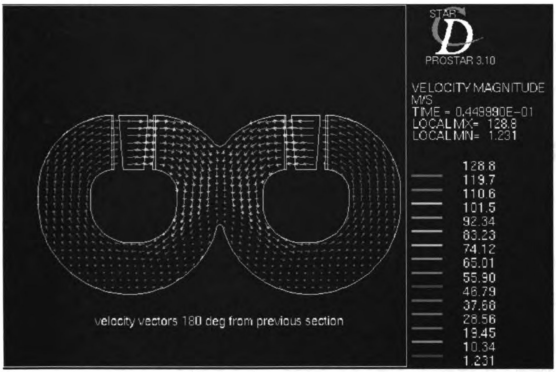

Figure 9.16 Velocity vectors showing circulatory flow at $\theta = 180°$ from inlet port

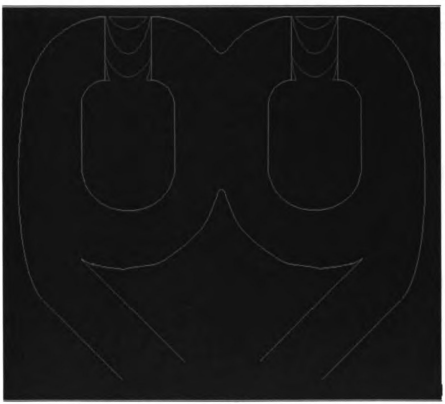

Figure 9.17 Proposed "Owl" shaped Inlet design

CHAPTER 10

CONCLUSIONS AND RECOMMENDATIONS

Performance characteristics of regenerative compressors and pumps are investigated in detail. Regenerative turbomachines have great potential due to their unique design and operational features. There are numerous applications of these turbomachines, specially for duties requiring high heads at low flow rates. Low efficiency and limited range of specific speed are the only drawbacks of these turbomachines. Therefore, this research was started with an aim to improve the performance of RFC/RFP. Several new contributions in this neglected area of research have been made in this dissertation. A thorough explanation of fundamentals and working principle is provided along with various applications. Research is broken down into two main applications of regenerative turbomachines, i.e.

- Application as regenerative compressors for low pressure (0.2-15 psig) natural gas compression for microturbine systems.
- Application as regenerative automotive fuel pump.

Extensive test data on single and multistage RFC with radial blades is presented in terms of various non-dimensional parameters. Test data on multistage RFC was not available in open literature before this dissertation, therefore various correlations between non-dimensional parameters are presented which can prove to be very useful for designers and engineers. A theoretical model is presented to predict performance of radial and non-

radial blade regenerative turbomachines. The model is generic and can be applied to predict the performance of regenerative turbomachines employing compressible media. Various losses are investigated and correlated with geometric and aerodynamic parameters of RFC/RFP. Governing equations and loss models are used to develop a performance prediction code. Excellent agreement between theoretical and test data on multistage RFC is obtained. Based on sensitivity analysis from the code and published test data in literature, design improvement guidelines for multistage RFC are provided. It is believed that these design changes can increase the efficiency of radial blade multistage RFC by 5% or more. However it needs to be validated by CFD and experimentation. To make the discussion more meaningful, a generalized design procedure for radial and non-radial blade RFC is presented in this dissertation.

Automotive fuel pumping is another attractive application of regenerative pumps. Delphi Automotives has developed a regenerative automotive fuel pump with non-radial blades. Proposed theoretical model is used to predict performance of Delphi automotive fuel pump. Performance prediction results are compared with the test data and reasonable agreement is observed. Based on sensitivity analysis from the code, few design recommendations are made. It is believed that such design variations can improve RFP efficiency by 3-7 %. Details of CFD analysis on non-radial blade automotive fuel pump are presented in this dissertation to motivate industry to apply CFD techniques on these turbomachines. A hydraulic efficiency around 40% is obtained from Delphi fuel pump, which is more than any other automotive fuel pump in the market. However, there is still a lot of room for improvement in hydraulic efficiency by employing aerodynamically designed aerofoil blades. Therefore, need was felt to investigate RFC/RFP with aerofoil

blades. There is not much evidence available in literature on aerofoil blade RFP. However, it is found from literature that aerofoil blade RFC can produce isothermal efficiencies in excess of 55%.

In an attempt to further increase the efficiency of regenerative turbomachines, a theoretical analysis on RFC with aerofoil blade is presented. The idea of decompression ducts is utilized to take some of the high pressure fluid entrapped in the stripper blades and feed it to various locations in the channel, thus reducing the power consumed by the compressor. The proposed theory is validated by comparing the obtained results with published experimental data on MK1 and MK2 regenerative compressors with aerofoil blades. The idea of decompression ducts proves beneficial to the efficiency. It is found theoretically that 18% increase in efficiency can be achieved using decompression ducts in case of MK1 design and 10% efficiency can be increased in case of MK2. This conclusion still needs to be validated by introducing decompression ducts in an actual compressor design and testing it. It is concluded from the theoretical analysis that efficiency in excess of 60% can be obtained using aerofoil design RFC.

To further explore the aerofoil blade design applied to a regenerative turbomachine, CFD analysis on a 3D compressor model generated in UNIGRAPHICS is performed. This is a first attempt to perform CFD analysis on aerofoil blade RFC. Preliminary results from the CFD analysis have indicated that the inlet manifold design is very important to RFC performance, a fact which was neglected by almost all researchers in the past. The inlet manifold is responsible for setting up spiral fluid motion in a regenerative turbomachine. Currently work is in progress to design an effective inlet to direct the flow on to the

blades and set up the helical flow pattern with minimum losses. Such an inlet design can create huge effect on efficiency of regenerative turbomachines.

The future direction of research in regenerative turbomachinery should be focused on CFD analysis. The compressor model should be generated in a modeling software like UNIGRAPHICS and CFD analysis should be performed to understand the flow pattern inside these machines. Once the model is generated, various changes in blade geometry, channel geometry, channel area ratios, inlet and discharge ports and stripper design should be performed to optimize the geometry for best performance.

However, such a procedure is very tedious and time consuming, because of complications in grid generation and lengthy CFD simulations. Therefore, theoretical means can help to reduce the CFD work by suggesting important geometries and operating points where CFD analysis needs to be performed.

Once enough work in CFD is performed, there is a need to develop several design criteria in terms of non-dimensional parameters. Such an analysis would lead to development of a generic design code which can take the desired operating point and size the compressor dimensions. The analysis presented in this dissertation was focused on performance prediction and improvement through sensitivity analysis. Thus, tools are developed which take in the geometry data and predict the performance. The next step is to extend such tools to design mode, which mean that the user specifies the desired operating point and the tools should be able to size the compressor dimensions including impeller and channel dimensions, inlet and outlet ports and stripper design etc. Such tools are in huge demand in industry because neither research papers nor text on turbomachinery discusses these design approaches for regenerative turbomachinery. There is a lot of design

information on axial and centrifugal turbomachinery available in literature, however not much work is done in regenerative turbomachinery design. The design tools must be developed after performing a lot of CFD analysis on regenerative turbomachinery to establish more design criteria.

Ongoing research is also focused on building a regenerative flow compressor to be utilized in refrigerators employing water as refrigerant. The compact size and unique features of RFC makes them very attractive for refrigerators.

BIBLIOGRAPHY

[1] Abdalla H.M.M., "A Theoretical and Experimental Investigation of the Regenerative Pump with Airfoil Blades, PhD thesis, September 1981, Applied Mechanics Branch, Royal Military College of Science.

[2] Andrew D.N., "The Calculation of Flow in Regenerative Turbomachines by a Streamline Curvature Method", Proc. Instn. Mech. Engrs., Part A: J. of Power and Energy, Vol. 204, 1990. pp 121-129.

[3] Aoki M., "Studies on the Vortex Pump (1st Report)", Bulletin of JSME, Vol. 26, No. 213, March 1983, pp 387-393.

[4] Aoki M., "Studies on the Vortex Pump (2nd Report)", Bulletin of JSME, Vol. 26, No. 213, March 1983, pp 384-398.

[5] Aoki M., "Studies on the Vortex Pump (3rd Report)", Bulletin of JSME, Vol. 26, No. 216, June 1983, pp 1014-1019.

[6] Aoki M., "Studies on the Vortex Pump (4th Report)", Bulletin of JSME, Vol. 26, No. 216, June 1983, pp 1020-1035.

[7] Badami M., "Theoretical and Experimental Analysis of Traditional and New Periphery Pumps", Proceedings of the 1997 International Congress and Exposition, Feb 24-27 1997, Detroit, MI USA, pp 45-55.

[8] Balje O. E., "Drag-Turbine Performance", Trans. of ASME, August. 1957, pp 1291-1304.

[9] Bicard R., "Investigation on the Inlet Design of the Regenerative Pump", M. I. T. B.S. Thesis, 1957.

[10] Bullough W.A., "A Simple Drag Pump", "Proceedings of the 4th Conference on Fluid Machinery, Akademiai Kiado, Budapest, 1972, p. 211.

[11] Burton D. W., "Review of Regenerative Compressor Theory", Rotating Machinery for Gas-Cooled Reactor Application, TID-7631, April 2-4, 1962 pp 228-242

[12] Burton J. D., "The "Straight Through" Labyrinth Seal as Applied to the Regenerative Turbomachine", 5th International Conference on Fluid Sealing, Paper E1, Warwick England, 30th March-2nd , April, 1971.

[13] Burton J. D., "The prediction and improvement of regenerative turbomachine performance", The British hydromechanics research association, 9th member conference, Cranfield, September 1967

[14] Burton J. D., "A Theoretical and Experimental Analysis of the Flow in Regenerative Pumps and Turbines", PhD Thesis, Southampton University, 1966.

[15] Cates P.S., "Peripheral-Compressor Performance on Gases with Molecular Weights of 4 to 400", A.S.M.E. Transactions 64-WA/FE-25, Meeting November 29-December 4, 1964.

[16] Cates P.S., "Performance Characteristics of a Peripheral Compressor", Technical Division, Oak Ridge Gaseous Diffusion Plant.

[17] Crewdson E., "Water-Ring Self-Priming Pumps", Proceeding of the Inst. of Mech. Engr., Vol. 170, No.13, 1956, pp 407-417

[18] Crowe W. E., Schwarz H., "Development of UHTREX Gas-Bearing Compressors", Rotating Machinery for Gas-Cooled Reactor Application, TID-7690, November 4-6, 1963 pp 253-262

[19] Cundari D., Nuti M., "Appraisal of Regenerative Blowers for Scavenging of Small 2T S. I. Power plants", SAE 920781 pp207-215

[20] Daily J. W., Nece R. E., "Camber Dimension Effects on Induced Flow and Frictional Resistance of Enclosed Rotating Disks", Trans ASME Journal of Basic Engineering, 1960,Vol. 82, pp 217-223.

[21] Dewitt D. P., "Rational Design and Development of the Regenerative Pump", M.I.T. MS thesis, 1957

[22] El Hag, A. I., "A Theoretical Analysis of the Flow in Regenerative Pumps", PhD thesis, University of Bath, England, 1979.

[23] Grabow G., "Influence of the Number of Vanes and Vane Angle on the Suction Behaviour of Regenerative Pumps", Proceedings Conference on Fluid Machinery (5^{th}) Budapest. Hungry, September 15-20, 1975, Vol. 1, pp 351-364.

[24] Grabow G., "Comparison of Radial and Axial Type Regenerative Blower", 1983.

[25] Gessner R.L., "Multistage, Gas-Bearing, Helium Compressor Development", Advances in Cryogenic Engineering, 1966, pp 631-639.

[26] Grindell A.G., "Development of Small Compressor for Gas-Cooled In-Pile Loops", pp 191-199

[27] Hollenberg J. W., Potter J. H., "An investigation of Regenerative Blowers and Pumps", J. of Engineering for industry, Vol. 101, 1979, pp 147-152.

[28] Hollenberg J. W., "Reynolds Number effects on Regenerative pump performance", Trans. of ASME, Vol. 109, No. 4, November 1987, pp 392-395.

[29] Hollenberg J. W., "An investigation of the efficiency of regenerative blowers and pumps", PhD thesis, Stevens institute of technology, 1978.

[30] Hollenberg J. G., "Hydrogen Pipeline Transmission", Stevens Institute of Technology, Hoboken, New Jersey 07030.

[31] Howell A.R., "The present basis of axial flow compressor design: Part I Cascade theory and Performance", ARC R and M. 2095, 1942

[32] Hubel M., Blattel B. and Strohl W., "Investigation of Fluid Mechanics of the Regenerative Pump Used in Gasoline Injection Systems", SAE paper 950077 pp 103-111.

[33] Idelchik I. E., "Handbook of Hydraulic Resistance", 3rd edition, 1994 (CRC Press), Florida, USA

[34] Iversen H.W., "Performance of the Periphery Pump", Trans. of ASME, Jan. 1955, pp 19-28.

[35] Jakubowski M., Kovitz A.A, and Raynor S., "Ideal Fluid Flow in an Enclosure of Toroidal Geometry, Int. J. Non Linear Mechanics, Vol. 6 (1971) pp 101-115 pergamon press.

[36] Khalil M.F., El Shorbagy, K.A., "Thermal Effects on Drag Pump Performance", Proceedings - Canadian Congress of Applied Mechanics, CANCAM 1981, pp 647-649.

[37] Krishnan M.R., Tramm P.C., "Analysis of a Regenerative Pump", Allison Gas Turbine Division, GM corporation, EDR-12381, Indianapolis, Indiana, 1986.

[37] Kupryashin N.N., and Ryazanov S.D., "Analysis of the Operation of Radial-Vortex Type Centrifugal Pumps", Translated from Khimicheskoe i Neftyanoe, No. 4, pp 11-12, April, 1983.

[38] Lentz D. E., "Small Compressors and Vacuum Pumps for stand-alone equipment", 1983.

[39] Mason S. C., "Influence of Internal Geometry upon Regenerative Pump Performance", M.I.T. B.S. thesis, 1957.

[40] Moffat R., "Putting Industrial Vacuum to Work", Hydraulics & Pneumatics, 1987. pp 58-63

[41] Moffat R., "Is there a small Compressor in your Future?", Hydraulics & Pneumatics, pp160-258.

[42] Mugele, United Sates Patent No. 3,973,865, August, 1976.

[43] Ohba H., Nakashima Y., Shiramoto K., Shiramoto K., "A Study on Performance and Internal Flow Pattern of A vertex Pump", Bulletin of JSME, Vol. 21 No.162, 1978 , pp 1741-179.

[44] Ohba H., Nakashima Y., "Studies on the Internal Flow and Performance of the Vortex Pump and Application to Slurry Transporting", Memoirs of the Faculty of Engineering, Kumamoto University, Vol. 29, No. 1, March 1984, pp 1-31.

[45] Oelrich J. A., "Development of an Analysis of a Regenerative Pump", M. I. T. Ph. D Thesis, 1953.

[46] Peterson E. F., Battey R. F., "Soil Vapor Extraction System design Scale-up Consideration" pp113-125

[47] Raheel M., Engeda A., "Current Status, Design and Performance Trends for the Regenerative Flow Compressors and Pumps" (IMECE 2002-39594), Nov 2002, New Orleans, LA.

[48] Raheel M, Engeda A, Hamrin D, Rouse, G "An Investigation of Performance Characteristics of Single-stage and Multi-stage Regenerative Flow Compressors (RFC)", Journal of Mechanical Engineering Science (to appear)

[49] Raheel M, Engeda A, "Performance Improvement Theoretical Investigation of a Regenerative Flow Compressor for Natural Gas Compression Application", (to appear)

[50] Raheel M, Engeda A, "Theory and Design of the Regenerative Flow Compressor (RFC)", International Gas Turbine Congress (IGTC), Tokyo, Japan 2003.

[51] Roppenecker W. F., "New Options in choosing Blowers", Machine Design, pp 66-70

[52] Sasahara T., Yamazaki S. Tomita Y., "Researches on the Performance of the Regenerative Type Fluid Machinery", Bulletin of JSME, December 1980, pp 2047-2054.

[53] Schivley G.P., Dussourd J.L., "An Analytical and Experimental Study of a Vortex Pump", Journal of Basic Engineering, December 1970, pp 889-900.

[54] Senoo Y., "Theoretical Research on Friction Pump", Reports of Research Institute for Fluid Engineering, Kyusku University, Vol.5, No.1, 1948, pp 23-28.

[55] Senoo Y., "A Comparison of Regenerative Pump Theories Supported by New Performance data", Trans. of ASME, Vol. 78, July. 1956, pp 1091-1102.

[56] Senoo Y., "Researches on the Peripheral Pump", Reports of Research Institute for Applied Mechanics, Kyusku University, Vol.3, No.10, July1954, pp 53-113.

[57] Senoo Y., "Influences of the Suction Nozzle on the Characteristic of a Peripheral Pump and an Effective Method of their Removal", Reports of Research Institute for Applied Mechanics, Kyusku University, Vol.3, No.11, August 1954, pp 129-142.

[58] Shimosaka M., Yamazaki S., "Research on the characteristics of Regenerative Pump", Bulletin of JSME, Vol. 3, No. 10, 1960, pp. 185-190.

[59] Shimosaka M., "Research on the characteristics of Regenerative Pump", Bulletin of JSME, Vol. 3, No. 10, 1960, pp. 191-199.

[60] Sixsmith H., Altmann H., "A Regenerative Compressor", Journal of Engineering for Industry, August 1977, pp 637-647.

[61] Sixsmith H., "The Theory and Design of a Regenerative Compressor, Presented at the Institute of Marine Engineers, London, May 7, 1981.

[62] Sixsmith H., Watson M. J., "A Helium Regenerative Compressor", Proceedings of the International Cryogentic Engineering Conference, 1980, pp155-164.

[63] Sixsmith H., "The design of a regenerative compressor for the "ISABELLE" refrigerator" Brookhaven national laboratory, Technical Note No. 31, January, 1977.

[64] Song J.W., Engeda A., Chung M.K., "A modified theory for the flow mechanism in a regenerative flow pump. Proc. Instn. Mech. Engrs., Part A: Journal of Power and Energy, Vol. 217, 2003.

[65] Song J. W., Raheel M, Engeda A., "A Compressible Flow Theory for Aerofoil Blade Regenerative Flow Compressors (RFC)", Journal of Mechanical Engineering Science (to appear).

[66] Swift W. L., Nutt W. E., Sixsmith H., "A helium regenerative compressor", Cryogenic Engineering Conference July 12-16, 1993, Albuquerque, NM

[67] Tomita Y., Yamazaki S., Sasahara T., "The Scale Effect and Design Method of the Regenerative Pump with Non-radial Vanes", Bulletin of JSME, Vol. 16, No. 98, 1973, pp. 1176-1183.

[68] Whitehead D.S., Harrison S., Rose M.G., "A Regenerative Compressor", Cambridge University Engineering Dept, (Technical Report) CUED/A-Turbo, 1982.

[69] Wilson W.A., Santalo M.A., Oelrich J.A., "A Theory of the Fluid-dynamic Mechanism of Regenerative Pumps", Trans. of ASME, Nov. 1955, pp 1303-1316.

[70] Wilson W.E., "Analysis of Turbine Pumps", Product Engineering, Vol. 18, October, 1947 pp 163-166.

[71] Wright, B.C., "Regenerative Turbine Pumps: Unsung Heroes for Volatile Fluids", Chemical Engineering, April 1999, pp 116-121.

[72] Yamazaki S., Tomita Y., "Researches on the Performance of the Regenerative Pump with Non-radial Vanes", Bulletin of JSME, Vol. 14, No. 77, 1971, pp. 1178-1186.

[73] Yamazaki S., Tomita Y., "Researches on the Performance of the Regenerative Pump with Non-radial Vanes", Bulletin of JSME, Vol. 15, No. 81, 1972, pp. 337-343.

[74] Yamazaki S., Tomita Y., "Researches on the Performance of the Regenerative Pump with Non-radial Vanes", Bulletin of JSME, Vol. 17, No. 106, 1974, pp. 459-466.

[75] Yedidiah S., "The Recirculation Theory of Regenerative Pumps", ASME 1993, FED Pumping Machinery, Vol. 154, pp 355-358.

[76] Yedidiah S., "Effect of Energy-Losses on the Head Developed by a Rotordynamics Pump", ASME pumping Machinery Symposium, 1989. FED-Vol. 81, pp 181-186.

[77] Yedidiah S., "Certain Effects of Recirculation on Cavitation in Centrifugal Pumps: Proc.Inst.M.E. Vol. 200, No 4, 1986.

[78] Zozulya I.I., "Effect of the Indentation Profile Shape on the Regenerative-Pump Parameters", Translated from Khimicheskoe i Neftyanoe, No. 6, pp 9 10, June, 1982.

APPENDIX A

- Correlation between impeller tip Mach number (M_{OT}), flow coefficient (λ) and pressure ratio (Π) produced by multistage RFC is given as,

$$\Pi = 0.82 + 21.81 M_{OT}^3 + \frac{3.28 \times 10^{-6}}{\lambda^2} \qquad \text{(A.1)}$$

Regression coefficient $r^2 = 0.766$

- Correlation between impeller tip Mach number (M_{OT}), flow coefficient (λ) and isothermal efficiency (η) produced by multistage RFC is given as,

$$\eta = 20.73 - 34.16 M_{OT} - 4280.08\lambda + 9.7 \times 10^6 \lambda^2 - 1.87 \times 10^9 \lambda^3 \qquad \text{(A.2)}$$

Regression coefficient $r^2 = 0.724$

- Correlation between impeller tip Mach number (M_{OT}), specific mass flow rate (Φ) and pressure ratio (Π) produced by multistage RFC is given as,

$$\Pi = -5.6 + 47.13 M_{OT} - 135.6 M_{OT}^2 + 161.27 M_{OT}^3 + \frac{0.0019}{\Phi} \qquad \text{(A.3)}$$

Regression coefficient $r^2 = 0.724$

- Correlation between impeller tip Mach number (M_{OT}), specific mass flow rate (Φ) and isothermal efficiency (η) produced by multistage RFC is given as,

$$\eta = 2.49 + \frac{26.1}{M_{OT}} - \frac{0.064}{\Phi} - \frac{3.77}{M_{OT}^2} - \frac{1.51\times10^{-6}}{\Phi^2} + \frac{0.0121}{(\Phi)(M_{OT})} \qquad \text{(A.4)}$$

Regression coefficient $r^2 = 0.725$

APPENDIX B

- **Density Distribution across the RFC**

The density has to be incremented by a small value as we move from one control volume to next one to make the fluid behave as compressible. Increment in density depends on many factors such as rotational speed, fluid properties and inlet conditions. An approximate way to find the density distribution across periphery of RFC is to estimate the density at the exit of RFC and then use a linear density distribution from inlet port to discharge port. Density at discharge port is estimated by studying Capstone multistage RFC test data. A correlation for exit density in terms of impeller tip Mach number and specific mass flow rate is developed:

$$\rho_{out} = 0.525 - 5.45(M_{OT})^2 \ln(M_{OT}) + 1.24\times10^8\Phi^3 \tag{B.1}$$

where M_{OT} is impeller tip Mach number and Φ is specific mass flow rate defined as.

$$M_{OT} = \frac{r_2\omega}{\sqrt{\gamma RT_{in}}} \tag{B.2}$$

$$\Phi = \frac{\dot{m}}{4r_2^2 P_{in}}\sqrt{\frac{RT_{in}}{\gamma}} \tag{B.3}$$

The density distribution across the linear region of the compressor can then be obtained using

$$\rho_{n+1} = \rho_n + \left(\frac{\rho_{out} - \rho_{in}}{\theta_p}\right)\times\theta_n + \rho_{in} \tag{B.4}$$

where "n"represents number of control volume.

APPENDIX C

Appendix C provides non-dimensional geometry for all four stages of the Capstone multistage RFC. Figure 4.22 provides some geometry of all four stages, however more detail is provided here which is helpful in design sensitivity analysis performed in chapter 6.

First Stage

Area Ratio = $A_{c,A}/A_{c,B} = 1.2814$
Impeller tip radius = $r_2 = 1.65$ *in*
Impeller hub radius = $r_o = 1.3665$ *in*
Radius ratio = $r_2/r_o = 1.2074$
$A_{c,A}/r_2^2 = 0.0172$
$c_r/r_2 = 0.0293$
$c_r/d_A = 0.274$
$c_r/d_B = 0.334$

Second Stage

Area Ratio = $A_{c,A}/A_{c,B} = 1.2862$
Impeller tip radius = $r_2 = 1.65$ *in*
Impeller hub radius = $r_o = 1.403$ *in*
Radius ratio = $r_2/r_o = 1.176$
$A_{c,A}/r_2^2 = 0.013$
$c_r/r_2 = 0.0257$
$c_r/d_A = 0.275$
$c_r/d_B = 0.337$

Third Stage

Area Ratio = $A_{c,A}/A_{c,B} = 1.279$
Impeller tip radius = $r_2 = 1.65$ *in*
Impeller hub radius = $r_o = 1.431$ *in*
Radius ratio = $r_2/r_o = 1.153$
$A_{c,A}/r_2^2 = 0.010$
$c_r/r_2 = 0.0227$
$c_r/d_A = 0.277$
$c_r/d_B = 0.337$

Fourth Stage

Area Ratio = $A_{c,A}/A_{c,B} = 1.287$
Impeller tip radius = $r_2 = 1.65$ *in*
Impeller hub radius = $r_o = 1.4645$ *in*
Radius ratio = $r_2/r_o = 1.126$
$A_{c,A}/r_2^2 = 0.010$
$c_r/r_2 = 0.0193$
$c_r/d_A = 0.280$
$c_r/d_B = 0.344$